Enhanced station keeping analysis in early desig stage of offshore vessels

Mauro, Francesco

Doctoral thesis / Disertacija

2019

Degree Grantor / Ustanova koja je dodijelila akademski / stručni stupanj: **University of Rijeka, Faculty of Engineering / Sveučilište u Rijeci, Tehnički fakultet**

Permanent link / Trajna poveznica: https://urn.nsk.hr/urn:nbn:hr:190:960798

Rights / Prava: In copyright/Zaštićeno autorskim pravom.

Download date / Datum preuzimanja: **2024-07-14**

UNIVERSITY OF RIJEKA

FACULTY OF ENGINEERING

Francesco Mauro

ENHANCED STATION KEEPING ANALYSIS IN EARLY DESIGN STAGE OF OFFSHORE VESSELS

DOCTORAL THESIS

Rijeka, 2019.

UNIVERSITY OF RIJEKA

FACULTY OF ENGINEERING

Francesco Mauro

ENHANCED STATION KEEPING ANALYSIS IN EARLY DESIGN STAGE OF OFFSHORE VESSELS

DOCTORAL THESIS

Supervisor: Prof. D. Sc. Jasna Prpić-Oršić

Rijeka, 2019.

Sveučilište u Rijeci
TEHNIČKI FAKULTET
Fakultetsko vijeće

KLASA: 030-09/18-01/4
URBROJ: 2170-57-01-18-11
Rijeka, 27. travnja 2018.

Fakultetsko vijeće Tehničkog fakulteta Sveučilišta u Rijeci, na svojoj 7. sjednici u ak. god. 2017./18., održanoj 27. travnja 2018., donijelo je sljedeću

ODLUKU

Sukladno izvješću Stručnog povjerenstva za ocjenu teme doktorske disertacije u sastavu: prof. dr. sc. Roko Dejhalla (predsjednik), prof. dr. sc. Jasna Prpić-Oršić (članica) i doc. dr. sc. Dunja Legović (članica) utvrđuje se da pristupnik **Francesco Mauro, mag. ing. mech.**, ispunjava Zakonom propisane uvjete za izradu doktorske disertacije pod naslovom

Enhanced Station-Keeping Analysis in Early Design Stage of Offshore Vessels (Unaprijeđenje održavanja pozicije pomorskog objekta u ranoj fazi projekta).

Za mentoricu se imenuje prof. dr. sc. Jasnu Prpić-Oršić.

Dekanica

Prof. dr. sc. Jasna Prpić-Oršić

Dostaviti:

1.) Francesco Mauro, mag. ing. mech.
2.) Mentorica prof. dr. sc. Jasna Prpić-Oršić
3.) Služba studentske evidencije
4.) Pismohrana FV

Supervisor: Prof. D. Sc. Jasna Prpić-Oršić

The doctoral thesis was defended on July 2nd 2019 at the Faculty of Engineering of the University of Rijeka.

Committee for the defense of the doctoral thesis:

1. Prof. D. Sc. Roko Dejhalla, University of Rijeka, Croatia, Faculty of Engineering (Sveučilište u Rijeci, Tehnički fakultet) - Committee Chair

2. Prof. D. Sc. Nelida Črnjarić-Žic, University of Rijeka, Croatia, Faculty of Engineering (Sveučilište u Rijeci, Tehnički fakultet)

3. Prof. D. Sc. Nastia Degiuli, University of Zagreb, Croatia, Faculty of Mechanical Engineering and Naval Architecture (Sveučilište u Zagrebu, Fakultet Strojarstva i Brodogradnje)

Acknowledgements

Abstract

In the early design stage, two different approaches are at disposal to perform Dynamic Positioning (DP) predictions: quasi-steady predictions or dynamic simulations. To carry out this kind of calculations, typically the main issues are the thrust allocation and the position error estimation. These topics are more related to control theory rather then to naval architecture. A detailed analysis of the main aspects of DP from the hydrodynamic point of view leads to possible quality improvement of early design stage DP predictions. Besides, evaluating DP ability combined with seakeeping quality of the vessel will lead to a better determination of the real operability of an offshore unit and will allow comparing possible design alternatives with the aim of selecting the better configuration for a ship under design.

The purpose of this thesis is to enhance the standard DP evaluation procedures, giving more importance to the hydrodynamic aspects involved in the determination of the station-keeping ability of an offshore unit. A detailed definition of the environmental loads and the development and implementation of enhanced thrust allocation procedures will allow not only to obtain reliable DP predictions but also to obtain indications how to improve the station-keeping ability of a vessel. The final target of the research is the definition of a combined operability index for an offshore vessel, considering both criteria related to station-keeping and ship motions. The enhancements on environmental forces estimation together with a more detailed focus on the propeller behaviour during DP operations leads to the determination of enhanced thrust allocation procedures, suitable to study different thruster configurations for the same vessel. The evaluation of a global operability index helps designers to rank different solutions, having a multi-criteria vision on the DP thematic, including both station-keeping and seakeeping aspects.

Keywords: dynamic positioning; offshore vessels; thrust allocation; genetic algorithm; propeller modelling; ship motions; operability; early design stage

x

Prošireni sažetak

Za procjenu sposobnosti održavanja pozicije pomorskih objekata na raspolaganju su dva osnovna pristupa: kvazi-statička predviđanja i dinamičke simulacije dinamičkog pozicioniranja. Pri izvođenju ove vrste proračuna obično se nameću dva ključna problema: procjena odstupanja od željene pozicije i optimalna alokacija poriva. Te su teme više odnose na aspekte kontrole nego na samo projektiranje broda te nisu vezane uz analizu njihanja broda na moru o kojoj ovisi operativnost plovnog objekta. Osim toga, tijekom procesa projektiranja pomorskog objekta, odabir lokacije pojedinog propulzora uzduž trupa ne analizira se detaljno, već se određuje temeljem iskustva projektanta i ograničenja unutarnjeg rasporeda. Kako bi se poboljšala kvaliteta preliminarnih izračuna vezanih uz dinamičko pozicioniranje i početna procjena operativnosti broda, u radu se predlaže poboljšanje postupka procjene sposobnosti standardnog sustava dinamičkog pozicioniranja. Pomoću učinkovitijeg alata za izračunavanje sposobnosti održavanja pozicije broda na brodu moguće je istražiti i mogućnost korištenja izračuna parametara dinamičkog pozicioniranja kao alata za projektiranje u ranijoj fazi. U tu se svrhu analiziraju dva moguća problema. Prvo, koristeći izračun parametara dinamičkog pozicioniranja unutar procesa optimizacije, uz ograničenja uvjetovana samom lokacijom, može se odrediti položaj na kojem propulzor ima maksimalnu učinkovitost. Drugo, izračun parametara dinamičkog pozicioniranja kombinira se s izračunom pomorstvenih značajki u cilju definiranja značajki okoliša unutar kojeg plovni objekt djeluje kao i procjene njegove operativnosti s obzirom na aspekte zajedničkog sagledavanja pomorstvenih značajki i dinamičkog pozicioniranja.

Za izvođenje predloženog istraživanja, prvo je bilo potrebno razviti alate za proračun kvazi-statičkih predviđanja kao i onih u vremenskoj domeni. Zatim su se analizirala okolišna opterećenja i ustanovile tehnike proračuna koeficijenata vanjskih opterećanja kao funkcije smjera napredovanja. Razvijene su nove metode optimalne alokacije poriva koje koriste genetske algoritme kako bi se omogućila implementacija učinkovitijih modela za opis karakteristika propulzora. Genetski algoritam koristi se i za optimizaciju položaja propulzora uzduž trupa. Poboljšana

predviđanja sustava dinamičkog pozicioniranja koriste se kako bi se pronašla sprega između graničnih vrijednosti njihanja dobivenih proračunom pomorstvenih značajki i sposobnosti sustava dinamičkog pozicioniranja. Istraživanja su pokazala da su kvazi-statičke metode procjene sposobnosti dinamičkog pozicioniranja, uz adekvatne korekcijske faktore, najpogodniji alat za korištenje u ranoj fazi projektiranja, pogotovo kada je potrebno provesti višestruke izračune. Takvi izračuni mogu projektantu biti brzi pokazatelj sposobnosti sustava dinamičkog pozicioniranja te omogućiti usporedbu različitih rješenja. Usvajanje poboljšanih postupaka za procjenu koeficijenata uslijed opterećenja vjetrom dovelo je do mogućnosti bolje procjene opterećenja na nadvodni dio broda, posebice momenta zakretanja. Postupci koji koriste računarsku dinamiku fluida, validirani na eksperimentima, korisno su sredstvo za određivanje opterećenja uslijed djelovanja struja i omogućuju proučavanje utjecaja parametara oblika trupa na strujna opterećenja. Određivanje sile pomaka teorijom difrakcije daje veću fleksibilnost za određivanje valnih opterećenja na različitim stanjima mora. Razvijen je novi algoritam alokacije poriva temeljen na genetskom algoritmu koji omogućuje razmatranje sustava dinamičkog pozicioniranja u ekstremnim uvjetima i automatski, procjenjujući ukupnu apsorbiranu snagu s detaljnim modelom propulzora, prepoznaje područja međudjelovanja propulzora. Optimalna alokacija propulzora uzduž trupa može se odrediti primjenom genetskog algoritma, pri čemu se za isti pomorski objekt utvrđuje stanje maksimalne sposobnosti s istom instaliranom snagom. Kao konačni rezultat, u radu se predlaže ocjena operativnosti broda s novim razvijenim globalnim indeksom operativnosti, koji se temelji na kritičnim krivuljama dinamičkog pozicioniranja i njihanja koje se nanose na dijagram raspršenja stanja mora. Kritične krivulje dinamičkog pozicioniranja mogu se upotrijebiti za određivanje indeksa operativnosti dinamičkog pozicioniranja koji je alternativa standardnim polarnim dijagramima sposobnosti dinamičkog pozicioniranja koji se uobičajeno koriste u pomorskoj industriji. Ova dva indeksa omogućuju izravnu usporedbu različitih projektnih rješenja u specifičnim radnim okruženjima, što omogućuje projektantima da vrednuju projektne alternative pomoću poboljšanih alata za procjenu sposobnosti dinamičkog pozicioniranja.

Ključne riječi: dinamičko pozicioniranje; pomorski objekti; alokacija poriva; genetski algoritam; modeliranje propulzora; njihanje broda; operativnost; rana faza projektiranja.

List of symbols and abbreviations

The list of symbols gives an explanation of symbols used in different places in this thesis. Symbols only used once are explained close to the equations where they are used in.

Symbols

$\bar{U}$	Mean wind speed at 10 meters above sea level	m/s
$\bar{y}$	Mean value of the data point	various
$\ddot{x}, \ddot{y}, \ddot{\psi}$	Body fixed accelerations	m/s^2,m/s^2,deg/s^2
$\dot{x}, \dot{y}, \dot{\psi}$	Body fixed velocities	m/s,m/s,deg/s
$\bar{\mathbf{x}}$	Minimum norm solution for thrust allocation	N
$\mathbf{A}^+$	Pseudoinverse matrix	
$\mathbf{C}$	Jacobian matrix during optimisations	various
$\mathbf{c}$	Vector of constraints	various
$\mathbf{F_x}$	Vector of longitudinal force components	N
$\mathbf{F_y}$	Vector of lateral force components	N
$\mathbf{g(x)}$	Gradient of the objective function	various
$\mathbf{k}$	Penalty functions vector	
$\mathbf{l}$	Vector of lower bounds	various
$\mathbf{u}$	Vector of upper bounds	various
$\mathbf{X}$	Matrix of variables during GA process and data fitting	various

$\mathbf{x}$	Unknowns thrust components vector	N
$\mathbf{Y}$	Matrix of values to be fitted with regression	various
$\mathrm{d}D$	Wing profile drag force	N
$\mathrm{d}L$	Wing profile lift force	N
A_0	Propeller disk area	m^2
A_E	Propeller expanded area	m^2
A_E/A_0	Propeller expanded area ratio	
A_L	Lateral area of superstructure	m^2
A_T	Transversal area of superstructure	m^2
A_{cp}	Capability plot area	kn deg
a_{ij}	Vessel added mass and moment of inertia for the i,j motions	kg,kg m^2
A_{L_c}	Lateral area of the submerged body	m^2
B	Vessel breadth	m
b	Matrix of the regression coefficients	
B/T	Vessel breadth on draught ratio	
B_S	Mesh base size	m
B_{ij}	Retardation function coefficients for i,j motions	
b_{ij}	Damping coefficients for i,j motions	
B_{S_0}	Initial mesh base size value	m
C_B	Vessel block coefficient	
C_d	Longitudinal drag coefficient for Blendermann regression	
C_h	Height coefficient according to API	
C_M	Midship coefficient	

C_P Prismatic coefficient

C_Q Torque coefficient for four quadrant representation

C_s Shape coefficient according to API

C_T Thrust coefficient for four quadrant representation

C_X Thrust longitudinal component coefficient

C_X^* Thrust longitudinal component coefficient in crossflow

C_Y Thrust lateral component coefficient

C_Y^* Thrust lateral component coefficient in crossflow

C_{cx} Longitudinal current coefficient for API

C_{cy} Lateral current coefficient for API

C_{d_a} Longitudinal drag coefficient for stern directions

C_{d_f} Longitudinal drag coefficient for bow directions

C_{F_m} Frictional coefficient for model scale

C_{F_s} Frictional coefficient for full scale

C_{M_Z} Thruster yaw moment coefficient

C_{mdh} Wave coefficient for API

C_{Mz_c} Yaw moment coefficient for current loads

C_{Mz_g} Yaw moment coefficient for wave loads

C_{Mz_w} Yaw moment coefficient for wind loads

C_{Tn} Nozzle thrust coefficient for four quadrant representation

$C_{W_{aft}}$ Aft waterplane area coefficient

C_{x_c} Longitudinal force coefficient for current loads

C_{x_g} Longitudinal force coefficient for wave loads

C_{x_w}	Longitudinal force coefficient for wind loads	
C_{y_c}	Lateral force coefficient for current loads	
C_{y_g}	Lateral force coefficient for wave loads	
C_{y_w}	Lateral force coefficient for wind loads	
CA_{dyn}	Dynamic allowance coefficient	
D	Propeller diameter	m
D_D	Diameter of the propeller acting withouth interaction	m
D_i	Derivative control coefficient for i motion	
D_M	Maximum thruster diameter	m
D_R	Diameter of the propeller acting in interaction condition	m
e_Q	Correction factor for J in the KQ curve	
e_T	Correction factor for J in the KT curve	
F	Generic force	N
$f(\mathbf{x})$	Objective function	various
f_i	Data fitted with regression analysis	various
F_s	Safety factor	
F_w	Wind force	N
F_x	Longitudinal component of a generic force	N
F_y	Lateral component of a generic force	N
F_{ACT}	Generic actuator force	N
F_{ENV}	Generic environmental force	N
F_{EXT}	Generic external force	N
F_{T_i}	Force delivered by the i-th actuator	N

F_{x_c}	Longitudinal current force component	N
F_{x_G}	Longitudinal force component of a group of thrusters	N
F_{x_g}	Longitudinal wave force component	N
F_{x_w}	Longitudinal wind force component	N
$F_{x_{ACT}}$	Actuators force longitudinal component	N
$F_{x_{ENV}}$	Environmental force longitudinal component	N
$F_{x_{EXT}}$	External force longitudinal component	N
$F_{x_{REQ}}$	Longitudinal force component required by the controller	N
$F_{x_{wL}}$	Lateral wind force according to API	N or ton
$F_{x_{wT}}$	Longitudinal wind force according to API	N or ton
F_{y_c}	Lateral current force component	N
F_{y_G}	Lateral force component of a group of thrusters	N
F_{y_g}	Lateral wave force component	N
F_{y_w}	Lateral wind force component	N
$F_{y_{ACT}}$	Actuators force lateral component	N
$F_{y_{ENV}}$	Environmental force lateral component	N
$F_{y_{EXT}}$	External force lateral component	N
$F_{y_{REQ}}$	Lateral force component required by the controller	N
G	Centre of gravity	
g	Acceleration of gravity	m/s^2
h	Mesh refinement ratio	
h^*	Reference height above sea level	m
h_p	Propeller absolute advance	m

h_w	Height above sea level	m
$H_{1/3}$	Significant wave height	m
I_C	Operability function for motion criteria	
I_i	Integral control coefficient for i motion	
I_{66}	Vessel moment of inertia with respect to G	kg m^2
I_{DP}	Operability function for DP	
I_{TOT}	Global operability function	
J	Advance coefficient	
k_1, k_2	Crossover probability factors	
K_Q	Propeller torque coefficient	
K_T	Propeller thrust coefficient	
k_x	Current form factor for longitudinal force component	
k_y	Current form factor for lateral force component	
k_z	Current form factor for yawing moment	
K_{Tn}	Nozzle thrust coefficient	
L	Generic reference length	m
L/B	Vessel length on breadth ratio	
L/D	Length of nozzle on propeller diameter ratio	
L_d	Nozzle length	m
L_f	Fetch length	m
L_{OA}	Overall vessel length	m
L_{OS}	Length overall submerged	m
L_{PP}	Length between perpendiculars	m

L_{WL}	Length on waterline	m
LCB	Longitudinal centre of buoyancy	% of L_{PP}
M	Vessel mass	kg
M_P	Number of parameters per individual	
M_Z	Thruster yow moment with respect to thruster rotation axis	N
M_z	Generic yaw moment	Nm
M_{ACT}	Generic actuator moment	Nm
M_{ENV}	Generic environmental moment	Nm
M_{EXT}	Generic external moment	Nm
M_{z_c}	Yaw moment due to current loads	Nm
M_{z_g}	Yaw moment due to wave loads	Nm
M_{z_w}	Yaw moment due to wind with respect to O	Nm
$M_{z_{ACT}}$	Actuators yaw moment	Nm
$M_{z_{ENV}}$	Environmental loads yaw moment	Nm
$M_{z_{EXT}}$	External loads yaw moment	Nm
$M_{z_{REQ}}$	Yaw moment required by the controller	Nm
n	Propeller rotation rate	Hz
N'	Non dimensional yaw moment in CFD calculations	
N_G	Number of thrusters inside a group	
N_g	Number of possible wave conditions	
N_h	Number of vessel headings	
N_{ACT}	Number of actuators	
N_{pl}	Number of prism layers	

N_{POP}	Number of individuals	
O	Vessel midpoint	
OP_{DP}	Dynamic Positioning operability index	
OP_{TOT}	Global operability index	
P	Propeller pitch	m
P/D	Pitch on diameter ratio	
p_a	Observed order of accuracy	
p_g	Probability of occurence of a wave according to a scatter diagram	
p_h	Probability associated to vessel heading	
P_i	Proportional control coefficient for i motion	
P_T	Power absorbed by a thruster during DP	W
p_w	Wind pressure	Pa
$P_{T_{MAX}}$	Maximum absorbed power of a thruster during DP	W
p_{w_L}	Wind pressure acting on the lateral superstructure area	Pa
p_{w_T}	Wind pressure acting on the frontal superstructure area	Pa
Q	Propeller torque	Nm
R	Propeller radius	m
R^2	Determination coefficient for regrssion analysis	
r_h	Propeller hub radius	m
R_T	Total resistance	N
R_V	Advance velocity ratio	
R^2_{adj}	Adjusted determination coefficient for regression analysis	
$R_{T_{NS}}$	Total reistance from numerical calculations	N

Re	Reynolds number	
S	Wetted surface	m
S_0	Bare hull wetted surface	m^2
S_ζ	Wave spectral density	m^2/s rad^{-1}
s_H	Height of the centre of A_L on the sea level	m
s_L	Longitudinal centre of A_L measured from O	m
S_w	Wind spectral density	m/s rad^{-1}
S_{APP}	Appendages wetted surface	m^2
s_{L_c}	Longitudinal centre of A_{L_c} measured from O	m
T	Propeller thrust	N
T'	DNV characteristic periods for surge and sway motions	s
T^*	Thrust in crossflow	N
T_k	Charachteristic wave period	s
T_n	Nozzle thrust component of a ducted propeller	N
T_P	Propeller rotational period	s
T_p	Wave peak period	s
T_s	Significant wave period	s
T_x	Generic thrust component in longitudinal direction	N
T_y	Generic thrust component in lateral direction	N
T_z	Wave zero crossing period	s
T_{AV_i}	Available thrust in i direction	N
T_{DES}	Vessel draught	xx
T_{MAX}	Maximum thrust	N or ton

T_{MIN}	Minimum thrust	N
T_{pr}	Propeller thrust component of a ducted propeller	N
U_D	Discretisation uncertainty	
U_E	Experimental uncertainty	
U_I	Iterative solution uncertainty	
U_P	Total uncertainty of the process	
U_{SN}	Numerical uncertainty	
V	Vessel speed	m/s or kn
V_A^*	Advance speed in crossflow	m/s
V_c	Current speed	m/s or kn
V_i	Induced velocity	m/s
V_R	Advance speed in full interaction condition	m/s
V_r	Propeller inflow velocity	m/s
V_t	Effective propeller inflow velocity	m/s
V_w	Generic wind speed	m/s or kn
$V_{W_{MAX}}$	Maximum sustainable wind speed	kn or m/s
X	Thrust longitudinal component on the thruster plane	N
X'	Non dimensional longitudinal force in CFD calculations	
x, y, ψ	Body fixed coordinates	m,m,deg
X_0, Y_0	Earth fixed coordinates	m or deg
X_D	Undisturbed longitudinal thrust component in the thruster plane	N
x_F	Wind yaw moment reduction point	m
x_G	Centre of gravity longitudinal position	m

X_R	Full intraction longitudinal thrust component in the thruster plane	N
x_{T_G}	Longitudinal position of the centre of a group of thrusters	m
x_{T_i}	Longitudinal position of the i-th actuator	m
X_{max_i}	Maximum longitudinal coordinate for a thruster	m
X_{min_i}	Minimum longitudinal coordinate for a thruster	m
Y	Thrust lateral component on the thruster plane	N
Y'	Non dimensional lateral force in CFD calculations	
y^+	Dimensionless wall distance	
Y_D	Undisturbed lateral thrust component in the thruster plane	N
y_i	Data point to fit with regression	various
Y_R	Full interaction lateral thrust component in the thruster plane	N
y_{T_G}	Lateral position of the centre of a group of thrusters	m
y_{T_i}	Lateral position of the i-th actuator	m
Y_{max_i}	Maximum lateral coordinate for a thruster	m
Y_{min_i}	Minimum lateral coordinate for a thruster	m
Z	Propeller blade number	
α	Thrust deviation angle	deg
β	Hydrodynamic pitch angle	deg
β^*	Hydrodynamic pitch angle in crossflow	deg
β_i	Induced hydrodynamic pitch angle	deg
β_p	Propeller pitch angle	deg
β_r	Regression coefficient	
β_{PR}	Hydrodynamic pitch angle in full interaction condition	deg

χ	Generic angle with respect to vessel bow	deg
χ_c	Current encounter angle	deg
χ_c^*	Auxiliary current encounter angle	deg
χ_g	Wave encounter angle	deg
χ_w	Wind encounter angle	deg
χ_w^*	Auxiliary wind encounter angle	deg
Δ	Vessel displacement	ton
δ	angle between incoming flow and propeller plane	deg
δ_c	Cross force parameter for Blendermann regression	
$\Delta_x, \Delta_y, \Delta_\psi$	Errors in the body fixed motions	m,m,deg
δ_C	Comparison error	various
δ_D	Discretisation error	various
δ_E	Experimental error	various
δ_I	Iterative error	various
Δ_{MAX_i}	Maximum sustainable position error in i direction	m
δ_P	Total error of the process	various
δ_{SN}	Numerical error	various
ϵ	Waterline entrance angle according to DNV	deg
ϵ_e	Regression constant in Richardson extrapolation	
ϵ_h	Inverse of the dynamic efficiency of a wing section	
η	thrust loss factor	
η_0	Propeller open water efficiency	
κ	Roughness coefficient for the sea surface	mm

κ_c Heeling moment parameter for Blendermann regression

λ_Q Correction factor for the KQ curve

λ_T Correction factor for the KT curve

$\epsilon_\mathbf{c}$ Tollerances vector on the constraints   various

$\epsilon_\mathbf{r}$ Matrix of errors for regression analysis   various

μ_w Dynamic viscosity of the water   Pa s

∇ Vessel volume m^3

ω Angular frequency   rad/s

ω' Non dimensional wave frequency

ω_p Propeller angular velocity   rad/s

ϕ Roll motion   deg

ϕ_0 Real value according to Richardson extrapolation   various

ψ Vessel yaw   deg

ρ_w Water density kg/m^3

ρ_{air} Air density kg/m^3

τ_i Thrust orientation angle of the i-th thruster   deg

θ Pitch motion   deg

ξ Interaction grade

ζ_0 Streamline direction outside the foremost thruster   rad

Abbreviations

ABS   American Bureau of Shipping

API   American Petroleum Institute

CFD   Computational Fluid Dynamics

CP   Controllable Pitch

CPP   Controllable Pitch Propeller

DARPA Defense Advanced Research Project

DNV Det Norske Veritas

DNV-GL Det Norske Veritas-Germanischer Lloyd

DOE Design of Experiments

DOF Degree of Freedom

DP   Dynamic Positioning

DP2   Dynamic Positioning class 2

DP3   Dynamic Positioning class 3

ECA Emission Controlled Areas

ERN Environmental Regularity Number

FMEA Failure Mode and Effect Analysis

FP   Fixed Pitch

FWD Forward

GA   Genetic Algorithm

GCI   Grid Convergence Index

GPS   Global Positioning System

HLCV Heavy Lift Crane Vessel

IMCA International Maritime Contractors Association

IMO   International Maritime Organisation

ITTC International Towing Tank Conference

JONSWAP Joint North Sea Wave Project

KF   Kalman Filter

KVLCC Kriso Very Large Crude Carrier

MARIN Maritime Research Institute of the Netherlands

MRU   Motion Reference Unit

MSC   Maritime Safety Committee

NPD   Norwegian Petroleum Directorate

NSMB Netherlands Ship Model Basin

OCIMF Oil Companies International Maritime Forum

OSV   Offshore Supply Vessel

PC   Personal Computer

PID   Proportional, Integral and Derivative

PIV   Particle Image Velocimetry

PLCV Pipe Lay Crane Vessel

PLV   Pipe Lay Vessel

PSV   Platform Supply Vessel

QTF   Quadratic Transfer Function

RANS Reynolds Averaged Navier-Stokes

RAO   Relative Amplitude Operator

RMS   Root Mean Square

RSM   Response Surface Method

SIMPLE Semi-Implicit Method for Pressure Linked Equation

SS   Sum of Squares

SSE   Sum of Squared Errors

STBD Starboard side

Contents

Chapter 1

Introduction

The design of a modern offshore vessel requires to investigate from the early design stage many aspects related to naval architecture and marine engineering. Traditionally, issues related to vessels dynamic positioning (DP) capability are also considered according to a predefined operational profile, checking the compliance of the system with dedicated regulations.

Nowadays, with the shifting of exploration and exploitation activities from easily accessible waters into more extreme environments, the number of vessels mounting DP system is continuously increasing, not only in oil and gas fields, but also in other sectors like aquaculture, renewable energy, deep-sea mining activities. Besides traditional offshore sectors, DP system starts to be installed also on board of pleasure yachts and military crafts, spreading the applicability range of the technologies studied for the original application fields.

1.1 Motivation

The continuous increasing of number of vessels equipped with DP systems requires a continuous research in the technologies that have to be installed on board, in such a way to grant a continuous and safe marine operation even in harsh environments. However, the necessity to design modern vessels equipped with DP system requires a more detailed attention to the specific issue from early design stage [145].

Through this work, for *early design stage* it is considered the phase including *conceptual* and *preliminary* design [112, 113], means the design phase that influences over 70 to 80% of the total life-cycle cost of a technical system [147], in this case a ship. For such a reason, being DP an important attribute for a lot of vessels, it is worthy to give much effort to the study of station

keeping ability in early design stage.

Especially in the offshore sector, almost all the vessels that have to operate in deep water are nowadays equipped with a station keeping system. Also the vessels dimensions are increasing, leading to the installation of a higher number of thruster devices on the hull and consequently to higher installed power on board. Offshore vessel operations in deep waters are certainly one of the most challenging aspects of the current marine activities [42] and a good DP capability should be ensured already from the beginning of a new project. At the same time a competitive design should also ensure the optimisation of *seakeeping* behaviour of the vessel, reducing the ship motions with the aim of increasing the ship operability [146, 53] not only during standard operations but also in severe storm conditions. This means that both aspects should be investigated from the preliminary design state, even if nowadays these two characteristics are evaluated separately [98].

To consider both station keeping and seakeeping aspect from an early design stage, it is first necessary to evaluate and study properly the methods that can be used for preliminary station keeping analysis. A particular emphasis should be given on the environmental loads acting on the vessel and its modelling in such a way to ensure homogeneity and coherence between station-keeping and seakeeping calculations. Traditionally the environmental loads considered during a DP calculations are due to wind, waves and current.

Besides environmental issues, particular attention should be given also to the thrust allocation procedures used in preliminary predictions. To solve accurately the thrust allocation problem it is a matter of primary importance, i.e., to determine the orientation of each thruster and the amount of thrust that each device must deliver. Due to the redundancy of any DP system [100], this problem is over-controllable. That means appropriate analysis is needed to establish which kind of allocation procedure is more indicated to cover specific tasks that can rise up during early design stage.

Another focal point is the position of the thrusters. Actually the traditional design approach does not give too much effort to the thruster location on the hull. Typically the thrusters are disposed according to the spaces given by *general arrangements* and propulsive issues, both in case of new constructions and vessels refitting [99, 152]. It is the opinion that by studying with more detail the aspect related to thrusters locations will give advantages in the maximum capability of the vessels under design.

Having defined the main reasons to study more in detail the applications of enhanced methods

for DP predictions during early design stage, it is then necessary to evaluate which is actually the state of the art for the specific mentioned topics.

1.2 Literature review

Prior to start the dissertation it is worthy to consider what is available in the open literature on the main topics that should be covered during the study. At first, the focus will be on the methodologies adopted for *DP predictions* in early design stage. Thereafter the attention will be shifted to the evaluation of *environmental loads*, in the specific for wind waves and current. Then on the possible solutions for *thrust allocation* and *thrusters modelling* finishing with the *combined seakeeping and station-keeping predictions*.

1.2.1 DP predictions during early design stage

The necessity to give more effort to DP predictions since early design stage has been already claimed by designers. In fact van't Veer and Gachet [145] highlight that for offshore units like drill-ships, it is mandatory to consider DP since the beginning of the project.

Once a complex issue like DP has to be treated, several approaches can be considered. According to Smogeli et al. [130] basically two different calculation methods can be used in an early design stage: a quasi-steady approach and a dynamic one. Quasi-steady approach has been widely used for preliminary predictions. Wichers et al. [150] stated that, due to the short computational time, this approach can be used to analyse and compare multiple solutions. In fact quasi-steady calculations are widely used for preliminary assessment of vessel capability [73]. Another approach is given by Lübke [83], proposing a simplified time domain approach in such a way to include directly dynamic effect into early design stage predictions. In fact, in [130] it is noted that quasi-steady prediction are overestimating the vessel capability.

The time domain approach implies a more detailed modelling of the system, which requires for sure more computational time. For such a reason, complete time domain simulations are oriented to more advanced design stages where all the DP systems on board can be simulated as mention by Aalbers et al. [1]. Most of the developments and different procedures developed for time domain solutions are primary devoted to on-board applications, full simulations or model test systems. On this topic, a wide overview is given by Serraris [125] with a specific focus on benchmarking between model tests and DP simulations.

Since no effective standardisation is present for preliminary calculations, Kerkeni et al. [72] proposed a standard procedure to follow for calculations, however the general guidelines reflect what is commonly done by almost all DP users.

1.2.2   Environmental loads

Between the three mentioned main environmental loads, the one that has been most widely analysed and where a lot of literary work can be found is for sure *wind*. In fact naval architects have always be interested on the possibility to evaluate wind loads in early design stage, principally to be able to evaluate the superstructures contribution to ship resistance and for issues related to vessel stability. For such a reason, regression analysis of wind tunnel data have always been performed.

After the basic empirical formulations given by Hughes [61], and modified by Taylor [133], the first multiple regression analysis for wind coefficients, as function of vessel geometrical characteristics, were given by Isherwood [65]. There the wind coefficients for transversal and lateral force, together with yawing moment, were given considering the type of superstructure fitted on the hull. This kind of approach has been also considered by Gould [50], adding more details for the geometry superstructures definition. These kind of procedures are working primary on merchant vessel shape and superstructures, so are not really suitable for offshore vessels.

A different procedure has been proposed by Blendermann [18], where, starting from a database of wind experimental data [21] including also offshore ships, wind loads are analysed as statistical data. An overview of all the above mentioned method is presented in [141].

Besides the approaches based on regressions, other procedure have been investigated also as, for example, the neural networks. On this purpose Haddara and Soares [54] proposed a procedure using in the input layers parameters similar to Isherwood ones, while Valčić and Prpić-Oršić [143] use parameters similar to Blendermann approach. Neural networks are for sure a promising approach, however requires to have at disposal a wide database of experimental data. The development of simple formulations to easily predict wind loads is still active, as the simplified method proposed by Ueno et al. [142] for several kind of vessels derived from more complex analysis carried out by Fujiwara et al. [46, 47].

Also related to wind is the second principal load acting on a vessel during DP operations, means *waves*. According to potential theory, Faltinsen [43] says that the interaction between waves and floating bodies deals both with first and second order effects. As already observed by Remery

and van Oortmersen [121], the components that should be faced by a mooring (and consequently by DP) system are due to low frequency loads. That means only the low frequency contributions of the second order drift forces should be considered and, as described by Lee [80], evaluated by means of potential theory.

As underlined by Cozijn end Frickel [29], the research on hydrodynamic aspects in DP is in continuous development, including also issues related to wave loads, as for example effects of shallow water on the drift forces given by Pessoa [117]. Besides pure wave forces determination, a lot of research has been done on the utilisation of wave drift forces inside DP predictions. For time domain simulations it is necessary also to have a real-time estimation of the total wave drift forces. Pinkster [119] proposed an approach based on the direct relationship between low frequency wave force and relative motion around the ship. This approach has been followed and improved by Aalberts et al. [3, 4] and Quadvlieg et al. [120], however its applicability on board is not easy, due to the complexity of the wave height measurement on the ship. Naajien and Huijsmans [97] proposed to change the wave measurement on board using a radar-based system, however,all these methods and techniques for wave drift force estimation during operations are not applicable in an early design stage. A final overview of possible methods to use for wave loads prediction is given by Temarel et al. [134], where also more complex method related to CFD are discussed.

The last main environmental load to be considered is *current*. In literature there are not a lot of indication regarding regression methods, like Isherwood or Blendermann for wind loads, to determine the current loads coefficients in an early design stage. Most of the methods used to determine current loads are related to CFD. On this purpose the most relevant studies are given by Koop et al. [76, 74, 75], where an overview of the way to determine the loads by means of viscous flow RANS calculation are presented, considering both model and full scale calculations, shallow water effects and multi-body interactions.

Besides all the above mentioned researches over the environmental load and its determination, there are another group of simplified methods that can be used by a designer to have a rough estimate of the environmental loads in an early design stage. Once no detailed information or available data are present for a specified vessel, the simplified approaches given by *Regulation Societies* (like ABS or DNV-GL) or Offshore-related *Associations* (as API or OCIMF) can be used.

1.2.3   Thrust allocation and thruster modelling

Due to the large number of propulsive devices fitted along the hull, the distribution of the total required thrust over the available actuators can be a really complex task.

The overdetermined equilibrium system can be solved by simplification methods, as proposed by Wichers at al. [150], or by more complex optimisation algorithms. First optimisation procedures for thrust allocation are described by Sørdalen [131] and are basically using a Lagrange multiplier approach. A basic optimisation procedure based on pseudo-inverse matrix is used by several authors as Tannuri et al. [132], Millan [95] and Yang et al. [154], however the presence of additional constraints defining the forbidden zones can complicate the solution.

Usually the objective function considered for thrust allocation is regarding the minimum absorbed power. According to Johansen et al. [70] the objective function can be considered to be quadratic, adopting then quadratic programming techniques to solve the equilibrium system.

More advanced methods for thrust allocation could also manage even more complicated objective functions. Van Daalen et al. [35] propose a method able to manage a non-quadratic objective function, by using an iterative Lagrange multipliers-based method. Arditti et al. [14] proposed to consider a further improved method, oriented to time domain calculations, suitable to include thrust rotational rate change between the time steps as a constraint for global optimisation. Arditti et al. [12] propose also to consider thruster-hull interaction to reduce nominal bollard pull thrust coming from propeller open water tests.

Another complication is given by the interaction between thrusters. Prior to consider interactions inside the allocation strategies, attention should be given to the phenomenon modelling. Nowadays, PIV measurements in combination with CFD analysis are a good method to investigate thruster's interactions, both during experiment and autonomous simulations. Cozijn and Hallmann [30, 31, 33, 32] presented a lot of material coming out from PIV measurements during model tests, considering several thruster's configurations and different offshore vessel types. This material is a good support to perform and validate CFD simulations. Ottens et al. [111] performed bollard pull calculations for thruster-hull interactions, comparing the results with both model test and full scale measurements. This highlights that CFD could be a proficient tool to study interactions, because it can be used to study also multiple thruster configurations, as performed by Maciel et al. [84], and figure out useful indications for thruster-hull interaction modelling.

Bulten and Stoltenkamp [26] highlight the possibility to investigate also thruster-thruster in-

teraction by means of CFD computations. However, the procedure to determine a complete overview of the possible interaction areas and its magnitude, requires a lot of computational effort and time. On this purpose some simplified models can be derived from calculations or from model tests to consider thruster-hull interaction (see Nienhuis [102]) or thruster-thruster interaction (Brandner and Renilson [25]).

The results coming from thruster-thruster or thruster-hull interaction studies can be also included into thrust allocation techniques as performed by Arditti et al. [12]. However, the methods implemented inside an optimisation procedure should be simple and quick to execute in such a way not to increase the calculation time.

Another important point is the modelling of the propellers. As mentioned, the trust allocation procedures consider the thrusters as pure thrust generators, just correcting the final outcome with empirical interactions formulas as described by Valčić et al. [144].

In general, the thrusters modelling inside DP prediction programs is not representing the effective behaviour of the propeller. In fact, the currently adopted thrust allocation procedures are not capable to reproduce the real behaviour of a propulsor in waves or under the action of a current. As mentioned only empirical corrections are considered and applied outside the allocation algorithm.

1.2.4 Combined station-keeping and seakeeping predictions

During a preliminary design stage, where not all the details of the vessel to be design are available, it is common practice to consider separately station-keeping ability and seakeeping characteristics. To the best of our knowledge, the examples combining the two aspects in an early design stage do not exist in the literature. On the contrary it is well known that the action of the thrusters influences the dynamic behaviour of the vessel. As example, Jenssen [68] discusses a way to use thrusters to limit low frequency pitch motions on a semi-sub. Jürgens et al. [71] describe some examples for Offshore Supply Vessels (OSV) equipped with Voith-Schneider cycloidal propulsors, used also for roll motion stabilisation. Jin et al. [69] present a DP control, including also roll and pitch motions. It must be noted that all these methods can be applied in time domain simulations, so they cannot be proposed for a preliminary design DP calculation. In conclusion, as stressed by Nabergoj [98], the combined handling of DP and Seakeeping since early stage design should be investigated more in detailed, prior to perform model tests or complex 6-DOF simulations.

1.3   Objectives

From the proposed literature review it is clear that a lot of research has been done and will be performed in the coming future regarding DP systems and hydrodynamics related to station-keeping.

However, it is clear that the main focus of modern research is oriented to improve the performances of onboard DP systems. That relates to developing models and algorithms suitable to perform complex time domain simulations not usable in the early design stage. In this sense, preliminary calculations will not benefit from the continuous research findings, especially for hydrodynamic related topics. Then, the physical models implemented inside DP prediction programs for early design stage are too simplistic, leading the designers to make bad decisions in a crucial step of the project.

On this purpose it is proposed to dedicate more attention to the environmental force determination, to grant the best possible input to DP calculations in early design stage.

Besides loads determination, it is crucial to select the most suitable approaches to be used in early design stage predictions, which means to choose a quasi-steady solution or a time domain one. More in detail, the thrust allocation logic should be analysed with particular detail, having in mind the objective of the calculation. In fact, during a preliminary design stage, different calculation types can be carried out, traditional calculations aimed to determine the maximum wind speed a vessel can face per each heading (vessel DP capability), or more complex analyses related to compare multiple design solutions. On this purpose different kind of allocation strategies can be used, in such a way to optimise calculation times without losing the accuracy needed for the study.

Since no indication is given on the strategy the designers use to locate the thruster devices along the hull, it is proposed to study a method to optimise the location of the thrusters, having in mind the objective to increase vessel's DP capability.

In any case the main lack in literature is the determination of a procedure capable to consider both seakeeping and station-keeping issues in a preliminary design stage. For this reason the main focus of the study will be centred on the determination of a procedure capable to perform a combined prediction, assessing in a preliminary design stage the effective operability of the vessel in terms of motions criteria and DP capability.

The improvement of the environmental forces modelling together with a more detailed focus on the propeller behaviour during DP operation will led to the determination of enhanced thrust

allocation procedure, suitable to study different possible thrusters' configuration for the same vessel. The determination of a global operability index will help designers to rank different solutions, having a multi-criteria vision on the thematic of DP including both station-keeping and seakeeping aspects.

1.4 Organisation of the thesis

The present thesis work is organized to cover the main research topics analysed during the PhD study. The thesis is not following the chronological order of the researches carried out during the study period, but is organized as the proposed enhanced DP analysis should be performed in early design stage.

For this purpose, after the introduction given in the present Chapter 1, Chapter 2 gives an overview of the possible calculations that can be carried out during a preliminary design stage, comparing quasi-steady to time domain approaches and showing the typically adopted representation methods for the obtained results.

In Chapter 3 the focus will be on the environmental loads determination in early design stage, considering wind, current and waves. The main methods available in literature for the preliminary loads estimation will be described. With reference to wind loads, a statistical reanalysis of the Blendermann database has been performed and the results are there presented. Regarding current, the possibility to evaluate the loads by means of CFD is investigated and compared with standard regulation approaches. CFD computations have been used to obtain regression formulas for current loads on a database of 15 vessels. At last, methods to evaluate wave loads are presented, introducing a method to scale diffraction calculations results between vessels of different sizes but having similar hull shapes.

Chapter 4 is dedicated to thrust allocation algorithms and propeller modelling for early design stage. Different approaches are proposed for thrust allocation, traditional methods and enhancements to more complex solutions. Moreover, a newly developed thrust allocation strategy, based on genetic algorithms (GA), is presented as a novel approach for extreme events determination and is compared with the traditional allocation algorithms. Thereafter attention has been given to the modelling of thrusters. First a model for the operation in cross-flow is given, then thruster-thruster interaction is considered. The propeller modelling has been implemented inside different allocation procedure and the comparison with standard prediction is shown.

In Chapter 5 a newly developed procedure to optimise the thruster location on the hull is described. The optimisation is aimed to maximise the vessel DP capability according to the main general constraints given by hull geometry and other constraints that can be derived from vessel general arrangement. The algorithms adopted for thrust allocation inside the optimisation procedure have been selected between the ones studied and implemented in Chapter 4.

In the final section of the thesis, Chapter 6, the integration with seakeeping in early design stage is discussed. First, a newly developed procedure to consider motion limiting environment in DP capability is presented. Then, in the final point of the thesis, a new calculation procedure is proposed, capable to evaluate, for the first time, the effective operability of an offshore vessel considering both traditional motion critical curves and new determined DP ones.

Chapter 2

Dynamic Positioning calculations

Once DP calculations should be faced in a preliminary design phase, several approaches can be followed, according to the number of information at disposal to the designer and, of course, of the specific knowledge and know-how of the design office. Principally the main differences can be determined by the calculation methodology adopted: time-dependent or quasi-steady.

The time dependent calculations are derived from a real simulation of the DP control system mounted on board, where all the vessel dynamics and the on-board mounted systems should be modelled and have an active part in the final simulation. On the other hand, the quasi-steady approach does not require, in first approximation, any dynamic simulation, while it determines a simple static equilibrium to state the capability of the DP system.

Through this section, a description of the two mentioned approaches will be given, together with a comparison between the two methods in terms of final outcomes and total calculation time. To perform the comparison, the self-developed codes for both the quasi-steady and the newly proposed simplified dynamic simulation are developed.

Prior to start with the purely description of the calculation models, a rough introduction on DP will be done, together with the definition of the reference system that will be adopted trough the whole study.

2.1 DP system

The DP system is designed to automatically maintain a vessel in a predetermined position with a specific heading, by using only the actuators (propulsive or auxiliary ones) and steering devices mounted on-board. The system should be able to balance the external loads acting on the vessel
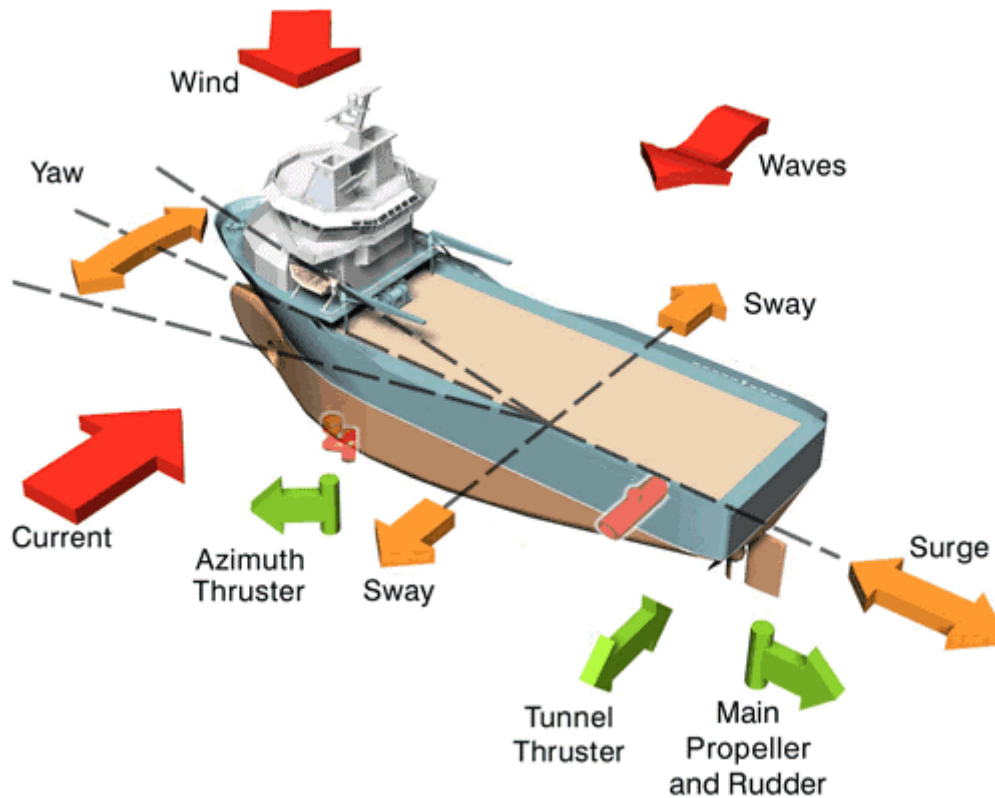
11

Figure 2.1: Dynamic Positioning concept[48]

as schematically reported in Fig. 2.1.

DP system is mostly installed on modern Offshore Units, because it allows the vessel/unit to operate, keeping a certain position, even though a conventional mooring system cannot be used due to the huge sea depth [28], the unfavourable sea bottom conformation or the presence of a lot of installations or pipes on the seabed. By using the same system, the vessel is not only able to keep the desired position, but can also follow a predetermined route with fixed way-points at low speed. Once this second mode is desired, the system can be mounted on-board of other kind of vessels, not directly related to Offshore market. This is the case of cruise ships (for crabbing operations), pleasure crafts or military vessels like mine sweepers. The same control strategy can be also used for slow speed manoeuvring of submersible units. The adoption of DP system to keep a certain course is giving nowadays a huge improvement in the time spent for certain operations like pipe-laying or cable-laying, where a traditional mooring equipment needs a lot of time to complete the whole operations [151], implying also the utilisation of a small fleet of support vessel.

2.1.1 Brief historical outline

The development of first DP systems started around 1960, when the necessity to discover and build new offshore oil and gas fields forced worldwide offshore companies to operate ever in deeper waters. While operating in deep waters, conventional *jack-up* units were no more suitable for drilling operations. Moreover, particular conditions related to an inhomogeneous seabed conformation makes also a conventional mooring system not favourable. However, the first DP-equipped vessel for really deep waters was the drill-ship *CASS I*, adopted for a scientific research program (the Mohole Project [16]) aimed to penetrate the Earth's crust under 3600 meters of water. In the specific, the vessel equipped with four steerable thrusters was able to keep position within a range of 180 meters from target by manual control. The position was determined with radar signals from surface buoys and by sonar signals from sub-sea beacons. After these first applications, the installation of DP system on-board of offshore vessel rapidly increases. However such kind of vessels were prototypes, not considering redundancy criteria, being also really dangerous for the operation safety. Through '70 and '80 decades, no specific regulation and guidelines were written and each improvement was related to the direct test of systems on board of the new designed vessels. This trend has been inverted once the International Maritime Organisation (IMO) produces the well known IMO Maritime Safety Committee (MSC) Circular 645 [64], which established international guidelines for vessels with DP systems, applicable to all the dynamically positioned units or vessels built after 1 July 1994. Thereafter, in 1995 the International Maritime Contractors Association (IMCA) has been formed, with the aim to study all relevant issues related to offshore operations, bringing out guidance and suggestions to tackle new situations and challenging environments. On this purpose IMCA is annually publishing reports related also to DP equipments, presenting a source of information for designers and operators that want to start a DP-related project.

2.1.2 Station keeping strategies

Dynamic positioning is just one of the possible choices suitable to keep an object in a determined position in deep water. In fact, besides DP system, a traditional mooring system can be used, or the structure can be directly led on the seabed. Of course there is also the possibility to adopt hybrid solutions. In the past, it was quite common to find vessels or floaters combining DP and traditional mooring lines. However, in the modern constructions, it is usual to adopt full DP or fully moored solutions.

Table 2.1: Advantages and disadvantages of station-keeping strategies

FIXED STRUCTURE	MOORING	DP
ADVANTAGES		
• No thruster system, extra generators, control system • Impossible to lose position • No danger for operators due to propellers rotating in water	• No thruster system, extra generators, control system • Impossible to lose position • No danger for operators due to propellers rotating in water	• High manoeuvrability of the unit in all conditions • No support vessels • Water depth independent • Quick to start service • No seabed limitations
DISADVANTAGES		
• Impossible to manoeuvre • Limiting water depth	• Limited manoeuvrability • Auxiliary vessels needed • Complexity for deep water • Hours to day time to escape • Seabed limitations	• Complex thruster system and auxiliary generators • High installation costs • High consumption • Possibility to lose position • Danger for operators and ROV • High maintenance costs

It is clear that the main advantages of a DP system is the possibility to operate in really deep sea, however there are many other advantages but also disadvantages for each mentioned station-keeping strategy. In Table 2.1 an overview of the main advantages and disadvantages of the different station keeping strategies is given.

As it can be seen the main advantages of the DP system are related to the flexibility given by the system compared to other solutions. However there are also disadvantages, essentially due to the complications and additional costs that the system implies.

2.1.3 DP system components

A DP control system is composed of a lot of devices that are needed to perform three main tasks: measure the actual unit position and heading, establish the actions needed to keep the desired position and a set of actuators to develop the required forces.

There are different ways to determine the current position of the vessel, the most common one are now based on GPS, radar or hydro-acoustic sensors. However more ancient and simple systems can be adopted, like tensioned wires or systems based on riser monitoring. For the vessel orientation, i.e. to measure vessel's heading, the giro-compass installed on board or a combination of GPS with inertial devices mounted on-board can be used. Besides position and heading, other quantities are monitored, related to the whole vessel operation. The Motion Reference Unit (MRU) is measuring ship motions, while aft and forward immersion is constantly monitored. Wind speed is also measured and can be also used for short terms predictions. Depending on the kind of operation the unit is caring out, other data can be collected, as, for example, the pipe tensioning (pipe-lay operations) or the acceleration on the lift rope (lifting operations).

All these kind of information are sent to the control system which is responsible for the error evaluation with respect to the desired values. Because the interval between two data samplings could be to wide to ensure a stable control, it is necessary to estimate the vessel dynamics and the acting forces in-between the samplings by using,for example, the Kalman filter techniques. The control system is then responsible to evaluate the forces needed to correct the error and to determine how to divide the estimated forces through the different actuators.

The actuators used in DP system for large units are basically azimuth thrusters. However it is possible to find other kind of actuators, such as fixed tunnel thrusters (commonly used for Supply Vessels), the retractile units or the combined action of rudder and propulsive propeller.

2.2 Reference system

As mentioned, DP systems involved the necessity to study several quantities related to environmental forces, vessel dynamics and other additional loads. All these quantities are used to define the state of the vessel during operations.

In the specific case of DP, the quantities involved are not related to the same engineering field, and its determination is sometimes related to conventions and methods being part of different
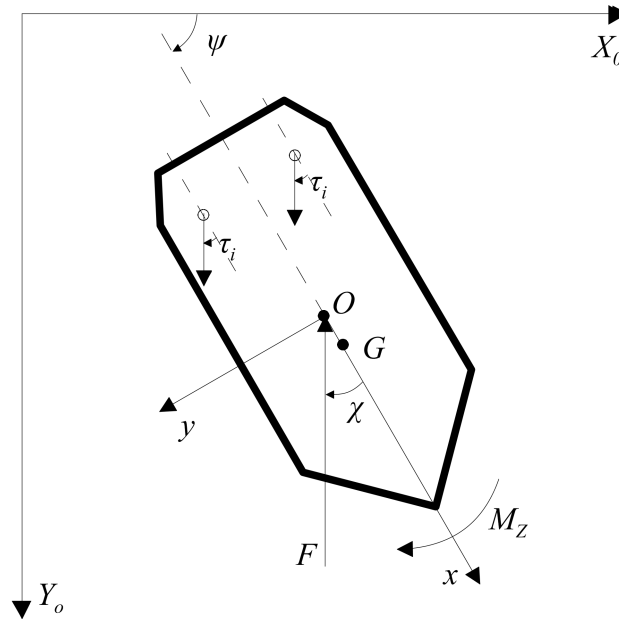
Figure 2.2: Reference systems (*earth-fixed* and *body-fixed*) adopted for DP calculations

knowledge fields. This can lead to a set of inhomogeneous data referring to different conventions especially for the reference system considered. Moreover, performing quasi-steady and dynamic simulations requires the adoption of a ship fixed and an earth fixed reference system.

For this purpose, a common reference system (presented in Fig. 2.2) has been adopted through the whole study, in such a way to have homogeneity between environmental loads, external loads, vessel dynamics and thrusters locations.

To describe the behaviour of a vessel during DP operation in an early design stage, a bi-dimensional approximation can be sufficient. The unit motions can be described limited to the horizontal plane representative of the undisturbed water free surface. On this plane, to establish the vessel position, an earth-fixed reference system $O_0 X_0 Y_0$ has been adopted, then, to consider the vessel dynamics, a body-fixed reference system Oxy has been introduced.

In the specific, for the body-fixed, a right handed Cartesian system has been adopted, having the origin centred in the vessel *midpoint O*, means, in case of a three-dimensional extension of the model, the final z axis will result positive downwards. The *midpoint* is located at the intersection between the ship's waterline plane and the longitudinal one at a distance $L_{PP}/2$ forward from the aft perpendicular, being L_{PP} the length between perpendiculars. Having a reference system centred away from the unit centre of gravity G will result in a formulation of the vessel motion equations, where all the transport terms should be included. The problem is not reflecting to external loads, since, as it will be explained in Chapter 3, environmental loads

are usually expressed with reference to O.

Considering Fig. 2.2 as representative example, the encounter angles of the environmental and external loads (χ) and the thrust direction orientation (τ_i) are defined positive in clockwise directions. In such a way the 0 degrees are representative of the bow and the 90 degrees of the starboard side as suggested by IMO regulations [64].

2.3 Quasi-steady approach

The first approach that can be used for DP calculations is the quasi-steady approach. In this method the dynamics of the vessel and in general of the whole DP operation is not considered. For such a reason the only reference system adopted for the analysis will be the body-fixed one. Since in the quasi-steady approach the time dependence is not considered, the problem reduces to the determination of a global time-independent equilibrium between external forces and on-board actuator ones. The equilibrium of the forces acting on planes parallel to the horizontal one can be written, with respect to the previously described body-fixed reference system of Fig.2.2, in the following form :

$$
\begin{cases}
\vec{F}_{ACT} + \vec{F}_{ENV} + \vec{F}_{EXT} &= \vec{0} \\
\vec{M}_{zACT} + \vec{M}_{zENV} + \vec{M}_{zEXT} &= \vec{0}
\end{cases}
\tag{2.1}
$$

where the subscription index $_{ACT}$ refers to the actuator, $_{ENV}$ to the environmental and $_{EXT}$ to the external forces and moments. (2.1) is written in vectorial form. Moreover, being the DP a system aimed to maintain an equilibrium, generally thruster's forces and moments components have an opposite sign with respect to environmental ones, so that (2.1) can be written component-wise as follows:

$$
\begin{cases}
F_{xACT} &= F_{xENV} + F_{xEXT} \\
F_{yACT} &= F_{yENV} + F_{yEXT} \\
M_{zACT} &= M_{zENV} + M_{zEXT}
\end{cases}
\tag{2.2}
$$

It must be noted that, as the reference system is centred in the origin O, the moment equilibrium has to be evaluated with respect to this point.

Equilibrium equation (2.2) is valid for each incoming direction and magnitude of the external loads. To be more specific, being environmental and external forces variable with the direction, and being an offshore vessel equipped with a certain number of actuators (N_{ACT}), (2.2) can be

rewritten to include these details:

$$
\begin{cases}
\displaystyle\sum_{i=1}^{N_{ACT}} F_{T_i} \cos \tau_i & = \ F_{x_{ENV}}\left(\chi_{ENV}\right) + F_{x_{EXT}}\left(\chi_{EXT}\right) \\[2ex]
\displaystyle\sum_{i=1}^{N_{ACT}} F_{T_i} \sin \tau_i & = \ F_{y_{ENV}}\left(\chi_{ENV}\right) + F_{y_{EXT}}\left(\chi_{EXT}\right) \qquad (2.3) \\[2ex]
\displaystyle\sum_{i=1}^{N_{ACT}} \left(F_{T_i} x_{T_i} \sin \tau_i - F_{T_i} y_{T_i} \cos \tau_i\right) & = \ M_{z_{ENV}}\left(\chi_{ENV}\right) + M_{z_{EXT}}\left(\chi_{EXT}\right)
\end{cases}
$$

where x_{T_i} and y_{T_i} are the actuator's centres of rotation coordinates according to body-fixed reference systems, F_{T_i} are the actuators forces acting on the hull and χ_{ENV} and χ_{EXT} are the environmental and external forces encounter angles. In (2.3) no reference is made to the actuator delivered thrust (T_i), since, as it will better specified in Chapter 4 it differs from the F_{T_i} and cannot be directly used in the equilibrium equation.

To be more precise, it should be stressed that the environmental loads are not only varying with the encounter angle χ_{ENV} but also with the specific environmental condition considered for the calculation. As it has been introduced, the main environmental loads concerns *wind*, *waves* and *current*; each of them can vary in its magnitude according to the analysed condition.

During an early design stage calculation, different conditions can be investigated, referring to specific cases given by classification societies, which are oriented to analyse some sort of maximum environmental loads situations or to evaluate the station-keeping ability on a specific working environment.

In any case, the principal output given by a quasi-steady calculation is a so-called capability plot, which is representing the quantities evaluated during DP predictions according to specific standards. In the following section, the outcome and the conventions adopted for this graphical output will be described.

2.3.1   Capability plots

Once a quasi-steady calculation is performed, it is essential to define a common representation system, able to homogenise the outcomes of different calculation softwares [72]. As mentioned, the nature of a quasi-steady calculation can be different, according to the regulatory framework or due to the possibility to investigate non-standard conditions.

In any case, most of the calculations deals with the study of the DP system with loads coming from several directions, covering the range from 0 to 360 degrees. This kind of consideration suggests to display the obtained results as function of the encounter angle χ in a polar graph.
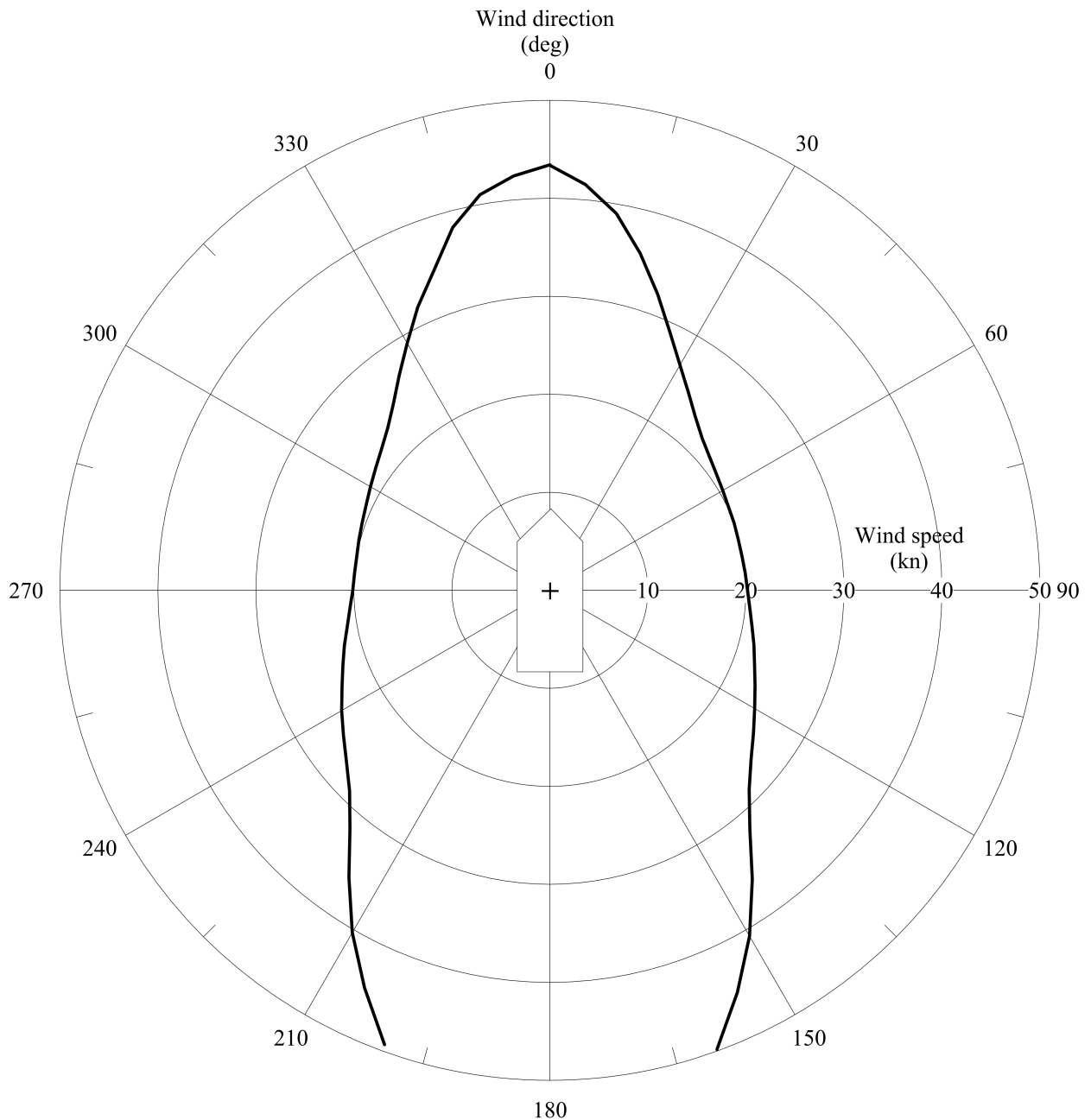
Figure 2.3: DP capability plot representation according to IMCA standards [62]

This lead to the creation of the capability plots diagrams (Fig. 2.3), which are normally referring to standards given in [62].

Here indications are given on the loads that have to be considered on a basic calculation (wind, waves and current), providing simplified methods to evaluate them but stating that more reliable data could be used where available. Besides environmental conditions, indications are given for the actuators modelling, stating that, where more reliable data than the ones given by the recommendation are present, the advanced data should be used.

More important is the part related to *Failure Conditions*, introducing the concept that after the

worst case failure the system should be capable to keep the position within safe limits. The concept of worst case failure depends on the type of vessel and should be identified through a failure mode and effects analysis (FMEA)[63]. In practice this is essentially due to the loss of one engine room or one half of the main switchboard, loosing the use of half of the actuator devices. It must be noted that the worst case may change with heading χ, so the envelope of the worst cases should be considered.

However, the most important part of the recommendation is given by the guidelines on the representation of the obtained results, stating that:

- Plots should be in polar form, with wind speed scale between 0 and 50 m/s in steps of 10 m/s at each 15 mm.

- Wind, wave and current are supposed to be collinear, with a constant current speed of 1 knot constant with depth.

- The limiting wind speed should be plotted at least once every 15 degrees. Linear interpolation between points is admitted.

- Two plots should be provided, one for intact and one for the worst failure case envelopes.

According to the above mentioned guidelines, the capability plot should be reported as shown in Fig. 2.3. As it can be seen, the graph takes almost one page of the thesis format without giving too much informations with respect to the calculations results.

However, in order to obtain graphs that will be more readable and less space consuming, the standard outputs of the capability analysis will be here reported according to a different format, which is similar to IMCA standards, but with some modifications. First of all the dimensions, the capability plots will be modelled in such a way to have wind axis of 4 cm of length and the wind speed (V_W) will be expressed in knots. The wind axis maximum will change according to the analysed vessel capability to maximise the plot area where results are present. During the discussion it will be possible that the loads specifications established by IMCA will change, as e.g. for wind-wave correlation or current speed. In such a case the new settings will be reported in the figure caption.

In any case, once two DP capability diagrams are compared, they will always be representatives of the same representations, so that the obtained solutions could be compared.

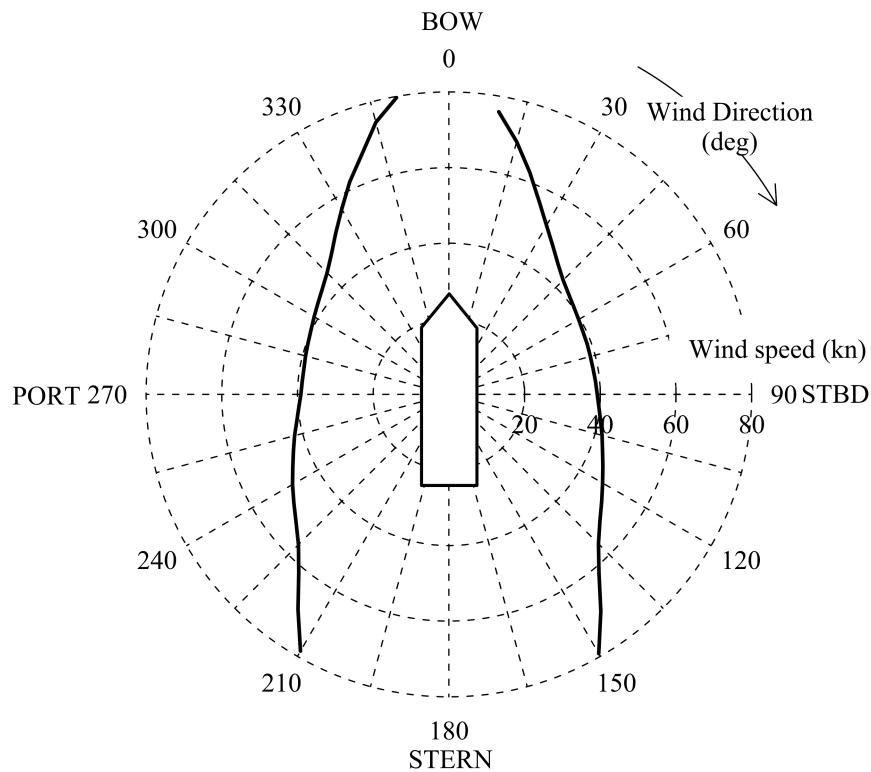An example of the adopted strategy is given in Fig. 2.4, where the comparison between two

Figure 2.4: DP capability plot representation standard adopted for this thesis. In the specific case use has been made of IMCA wind-wave correlation

calculations on the same vessel but with different thruster modelling is presented, adopting a non-IMCA wind-wave correlation. It seems that the adopted graph resolution can be considered as a good standard for the capability plots that will be proposed thereafter.

This is the standard way to adopt a capability plot, however use can be made of the same representation technique for other kind of calculations, or for the representation of different quantities. In fact with the capability plots also the loads acting on a unit in a specific environmental condition can be plotted, the actuators developed force or the absorbed power. In the case when also these other quantities have to be shown, the polar plots defined similarly as in Fig. 2.4 should be constructed.

2.3.2 Calculation results

The outcome of the quasi-steady simulation is basically composed of the maximum sustainable wind speed that the system can face with the active actuators working. As mentioned this kind of analysis should be done also considering the possible failures on the system. In such a case the calculations are aimed to obtain a notation class from dedicated classification societies.

The classification societies give different notations according to their own nomenclature and standards [38, 6, 39, 37], but basically refers to the IMO classification given in [64]. Here the DP vessels can be subdivided in three classes: *class 1*, *class 2* and *class 3*. *Class 1* refers to an automatic position/heading control with all the actuators working. *Class 2* (usually called also DP2) refers to a manual or automatic position/heading control considering a single failure (without losing a compartment), while *class 3* (usually called DP3) is considering the failure case involving one compartment of the vessel, means loosing half of the generating power. In particular, to evaluate with a final value the capability of the DP system, the DNV proposed the calculation of an Environmental Regularity Number (ERN) [38] which is considering also the multiple failure cases (DP2 and DP3).

More recent regulations [40] drastically changed the IMCA standards of representation and the ERN concept, adopting a new standard based on Beaufort scale and giving specific indications regarding the environmental loads modelling and the thrust losses that should be included in the calculations. Since it is really hard to validate a quasi-steady approach [126], because it is impossible to establish a positioning error in a quasi-steady calculation [8], it is common to simply provide compliance with other softwares (as the one provided by classification societies [101] or by DP operators [73]) in such a way to ensure a sufficient confidence level of the solution [148]. As already mentioned, by considering each one of the possible standards, the result of a quasi-steady program is a capability plot, being representative of the maximum sustainable wind the DP system is able to face in certain conditions, under the simplifications and assumptions given by the selected standard. However, from preliminary capability analysis, also other data can be obtained, regarding, as example, the total amount and repartition of the environmental forces or the utilisation of the single thrusters at each desired environmental condition. These kind of data can be really helpful in an initial design stage to verify whether the vessel is able to attend certain standard that cannot be directly evaluated from a maximum sustained wind envelop.

2.4   Dynamic simulations

Another way to determine the capability of an offshore vessel is the use of dynamic simulations. As it can be imagined by the name, this kind of simulations includes the vessel and actuators dynamics and are based on the time-domain simulations.

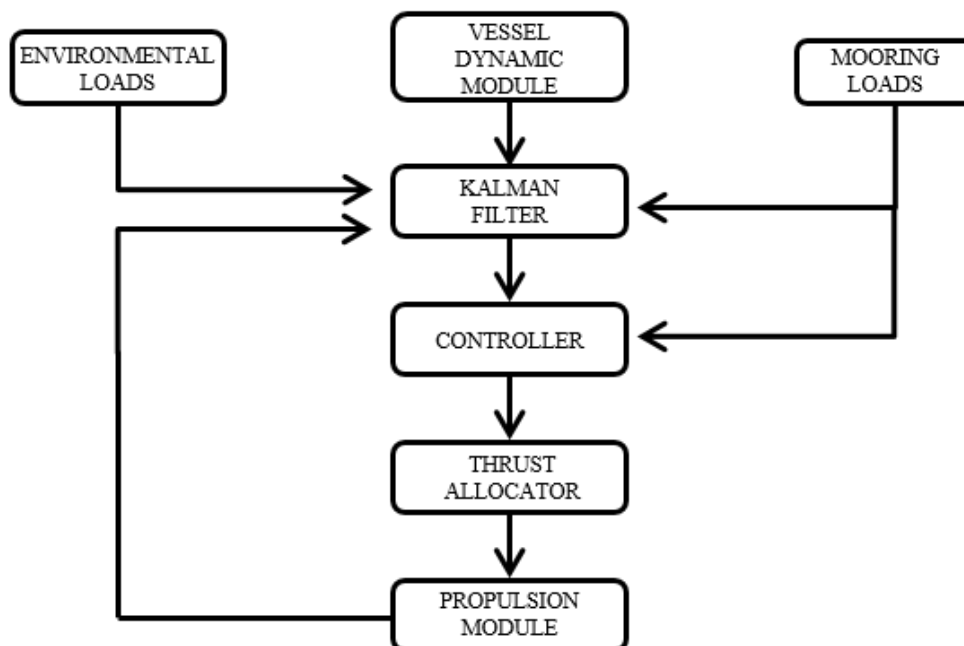The main improvement of a time-domain simulation, with respect to a quasi-steady approach, is

Figure 2.5: Calculation scheme of a complete DP dynamic simulation.

the possibility to simulate the whole DP system [125]. In such a case, it is no more necessary to evaluate a simple static equilibrium between internal and external forces, but a detailed modelling of all the components involved in the system is needed. In certain cases, the dynamic simulations are used to test the algorithms that will be mounted on board, to provide the validation with full scale data [129]. The same is valid for software used in model test [126] also.

As mentioned, the necessity to simulate all the main components of the system mounted on board, requires the knowledge of engineering fields that are outside naval architecture. In fact, the necessity to implement the control system implies specific knowledge of control theory, typical of electrical and system engineering. However, since the system should be mounted on a vessel, there must be a combination of specific knowledge coming from control engineers and some from naval architects. A complete dynamic simulation uses a set of algorithms to evaluate the vessel position and the position error, and then to correct this error in time domain.

As it can be seen in Fig. 2.5, during a dynamic simulation the position is determined by the vessel dynamic module (which can include also the simulation of the measuring system), then position data together with environmental forces (wind) and mooring forces are sent to the Kalman Filter (KF) module [45] (or Extended KF in case of non-linearities) to estimate the low frequency motion and speed of the vessel. The estimated position is then send to a controller estimating the required forces needed to correct error position by means of the actuators.

However, to simplify the implementation of a basic dynamic simulation not oriented to a system

to install on board, the modelling of the observer can be in first approximation neglected.

2.4.1   Simplified dynamic method

As mentioned, in this preliminary study a simplified simulation model has been considered [89], discarding the implementation of KF module, and (with reference to Fig. 2.5) sending directly the dynamics output to the controller.

With the adoption of this dynamic method, the determination of vessel's dynamics is of primary importance. By considering the vessel as a 3-DOF mass-spring system, the response of a floating vessel in waves can be described, considering Cummins equations [34], in the following form with respect to the ship fixed reference system of Fig. 2.2:

$$
\begin{aligned}
(M + a_{11}(\infty))\ddot{x} = {}& Mx_G\dot{\psi}^2 + \int_0^t B_{11}(\tau)\dot{x}(t-\tau)\,\mathrm{d}\tau \\
& + (M + a_{22}(0))\dot{y}\dot{\psi} \\
& - (a_{22}(0) - a_{11}(0))V_c\sin(\chi_c - \psi)\dot{\psi} \\
& + F_{x_{ENV}} - F_{x_{ACT}}
\end{aligned}
\tag{2.4}
$$

$$
\begin{aligned}
(M + a_{22}(\infty))\ddot{y} = {}& (Mx_G + a_{26}(\infty))\ddot{\psi} - \int_0^t B_{22}(\tau)\dot{y}(t-\tau)\,\mathrm{d}\tau \\
& - \int_0^t B_{26}(\tau)\dot{\psi}(t-\tau)\,\mathrm{d}\tau + (M + a_{11}(0))\dot{y}\dot{\psi} \\
& + (a_{22}(0) - a_{11}(0))V_c\sin(\chi_c - \psi)\dot{\psi} \\
& - F_{y_{ENV}} + F_{y_{ACT}}
\end{aligned}
\tag{2.5}
$$

$$
\begin{aligned}
(I_{66} + a_{66}(\infty))\ddot{\psi} = {}& (Mx_G + a_{62}(\infty))\ddot{y} - \int_0^t B_{66}(\tau)\dot{\psi}(t-\tau)\,\mathrm{d}\tau \\
& - \int_0^t B_{22}(\tau)\dot{y}(t-\tau)\,\mathrm{d}\tau + (Mx_G + a_{62}(0))\dot{y}\dot{\psi} \\
& - M_{z_{ENV}} + M_{z_{ACT}}
\end{aligned}
\tag{2.6}
$$

where M is the ship mass, I the vessel moment of inertia, a_{ij} the added masses, B_{ij} the retardation function coefficients, x_G the longitudinal centre of gravity and V_c and χ_c are the current speed and encounter angle respectively. The retardation function coefficients can be determined comparing the solution of motion equations (2.4)-(2.6) for a unitary amplitude harmonic oscillation, with the analytical frequency domain solution for the same motion [106]. This will led to the following formulations:

$$
B_{ij}(\tau) = \frac{2}{\pi}\int_0^\infty b_{ij}(\omega)\cos(\omega t)\,\mathrm{d}\omega
\tag{2.7}
$$

The above described equations should be integrated in the time-domain. Here, a fixed time step approach has been adopted, using a fourth order Runge Kutta integration method, in order to obtain vessel's position and velocities. The selection of the time step Δt depends on the vessel's dimensions and inertias.

In the simplified method the outputs of the vessel dynamics are directly sent to the controller algorithm. The evaluated positions and velocities from the vessel dynamics calculations, should be compared with the required ones. In such a way, it is possible to estimate the errors related to position and speed. The errors need to be corrected by the controller, determining the required thrust magnitude and orientation needed to minimise the error.

There are a plenty of possible solutions to implement a controller, however, the most used is the PID (*Proportional*, *Integral* and *Derivative*) type. By using this kind of implementation, the required thrust and moment needed to correct the position and speed errors can be written in the following form:

$$T_{x_{REQ}} = P_x \Delta x + I_x \int_{\Delta t} \Delta x \mathrm{d}t + D_x \dot{x} \tag{2.8}$$

$$T_{y_{REQ}} = P_y \Delta y + I_y \int_{\Delta t} \Delta y \mathrm{d}t + D_y \dot{y} \tag{2.9}$$

$$M_{z_{REQ}} = P_\psi \Delta \psi + I_\psi \int_{\Delta t} \Delta \psi \mathrm{d}t + D_\psi \dot{\psi} \tag{2.10}$$

the P_i, I_i and D_i ($i \in x, y, \psi$) control coefficients should be set for each application in order to ensure a stable positioning and make an effective use of all the thrusters. The parameters settings are also influenced by the entity of the total load acting on the vessel, leading to different optimal settings at each loading condition.

However, it is possible to adopt some general rules [125] to get the initial guess for the control coefficients. These kind of simplifications lead to the following initial conditions:

$$P_i = \frac{T_{AV_i}}{0.6 \Delta_{MAX_i}} \tag{2.11}$$

$$D_i = 1.2 \sqrt{(M + a)_i P_i} \tag{2.12}$$

$$I_i = 0 \tag{2.13}$$

where T_{AV} is the currently available force/moment and Δ_{MAX} is the maximum sustainable position error. The integral coefficient is usually set to zero since it can be source of instability. It can be, in first approximation, discarded because it represents a mean positioning error with respect to the desired value and DP usually corrects fluctuations around it. Means, once the

settings are not correct, I_i coefficient can insert an additional drift to the vessel that can be source of an undesired loss of position.

Of course, more precise and complex algorithms can be found in literature and could be installed on-board, allowing also to make vessel acting in collaborative operation in a totally autonomous way. However, for a simplified method, an adoption of a more simple algorithm can be accepted, since the position of the vessel and the total acting loads are directly evaluated through the calculations and not estimated by a KF based algorithm.

Regarding the thrust allocation algorithm, several methods and strategies can be adopted, however the effect of those kind of algorithms will be more deeply discussed in Chapter 4.

Really important for a time domain simulation is the definition of the environmental loads. Usually, for a complete simulation, such as for the simulation of the on-board system, the wind load is really important, since it is the only one that can be directly measured on board and enters directly in the KF state estimations. For the simplified method, all the environmental loads can be defined as per a quasi-steady calculations, using the same loads coefficients. However, the necessity to describe a time-varying environment will led to some peculiarities in the modelling. In fact, the dynamics allows to investigate also the direction fluctuations around the mean encounter directions χ_i and also the magnitude fluctuations, leading to an environment modelling composed by non-stationary loads.

In the proposed simulation method, the current is considered constant in speed and direction, however, at each time step, the relative angle and speed are considered according to vessel dynamics. The wind case is different and a dedicated modelling has been implemented to reproduce also the effect of wind gusts. Wind gusts, as well as waves, can be modelled by means of spectra. Several kind of gust spectra can be found in literature [36, 55, 104, 11], some specific for certain sea areas and others more general:

$$S_w(\omega) = \frac{4\kappa L_f^2 \omega}{\left(1 + \left(\frac{L_f \omega}{\bar{U}}\right)^2\right)^{4/3}} \tag{2.14}$$

$$S_w(\omega) = \frac{4\kappa L_f \bar{U}}{\left(2 + \left(\frac{L_f \omega}{\bar{U}}\right)^2\right)^{5/6}} \tag{2.15}$$

$$S_w(\omega) = \frac{320 \left(0.1\bar{U}\right)^2}{\left(1 + \left(172\omega \left(0.1\bar{U}\right)^n\right)^{-0.75}\right)^{\frac{5}{3n}}} \tag{2.16}$$
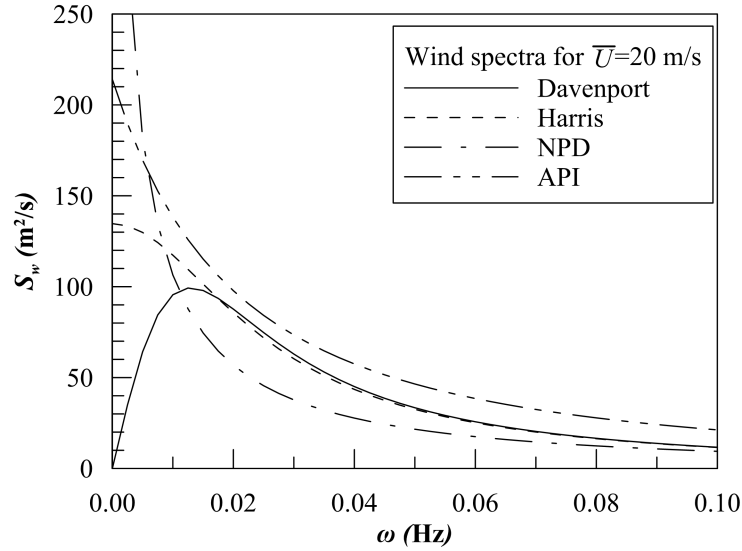
Figure 2.6: Comparison between different wind spectra for a reference wind speed $\bar{U}$ of 20 m/s.

$$S_w(\omega) = \frac{\left(0.15\bar{U}(0.5)^{-0.125}\right)^2}{0.1C\bar{U}}{\left(1 + 1.5\frac{\omega}{0.1C\bar{U}}\right)^{5/3}} \qquad (2.17)$$

where L_f is the fetch length expressed in meters, $\bar{U}$ is the mean wind speed at 10 meters height in m/s, κ is the roughness coefficient set to 0.0025 mm for sea surface, ω is the frequency expressed in Hz and n and C are two coefficients set to 0.468 and 0.025 respectively. Equation (2.14) is representative of the so called Davenport spectrum, which considers value of L of about 1200 meters as default value. Equation (2.15) is the Harris spectrum, considering a standard fetch length of 1800 meters as suggested values. Equations (2.16) and (2.17) are representative of NPD and API spectra respectively. NPD spectrum is usually representative of the North Sea wind and is used jointed to JONSWAP wave spectrum, while API one can be representative of different sea areas according to the parameter selection (C can vary between 0.01 and 0.10). In Fig. 2.6 a comparison is given between all the spectra for a condition considering all the standard input parameters and a common wind speed of 20 m/s. As it can be observed, the spectra have completely different shapes, resulting in different kind of gusts. Davenport spectrum models only the velocity fluctuations that should be than added to a constant wind speed, all the other spectra consider directly the total wind speed. Spectra like the NPD are giving more impact to low frequency fluctuations with respect to the others, so it is more indicated to model environments where the gusts are less frequent but with high velocity change, while other spectra will be more indicated for environments characterised by more recursive low amplitude fluctuations. In any case, since the choice of the spectrum type is depending on the simulated environment, all the

possibilities are implemented in the environmental modelling module, allowing the user to make the most appropriate choice. With this approach it is then possible to determine a time varying wind speed that can be used to evaluate wind loads, adopting the proper wind loads coefficients as in the quasi-steady approach.

The wave loads are modelled as consequence of wind environment. In fact, according to the evaluated wind speed, wave height and period are determined and the mean drift forces evaluated, using the same coefficients as for the quasi-steady calculation.

Since the final aim of the simulation is the determination of a capability plot, it is important to establish a procedure to determine it from time-domain simulations. In fact, a time domain simulation is not suitable to automatically determine a capability plot, but more than one simulation should be performed. Once an environmental setting has been chosen, the simulation should run to cover 3 hours of physical time, than, since the environmental loads are determined by a stochastic process, at least 3 simulations should be carried out for each condition to ensure output consistency. To determine a capability plot, this process should be executed per each vessel heading angle, increasing the mean wind speed. The detailed procedure to determine the final limiting environment is described in appendix A.

Time domain simulations can be used not only for capability plot determination but also to investigate other particular situations, like target approach simulations or specific low speed manoeuvres that needs to be done during certain DP operations.

2.5   Comparison

In order to evaluate which of the two possible approaches is more indicated to proceed further in the rest of the study, a test case has been set up to compare results and computational time of the two procedures.

For the test case, the two before described procedures have been applied on a Drill-ship, having the characteristics reported as in Table 2.2 and a thruster system as described in Table 2.3. The coefficients used for the simulations are the same in both cases, using database values for the wind, waves and current loads. The methods to obtain the coefficients and the non-dimensionalisation techniques adopted will be thereafter described in Chapter 3. In both simulations, Pierson-Moskowitz wind-wave correlation has been applied and a constant current of 1.0 m/s has been considered. All the loads are collinear.

Table 2.2: Main dimension of the test case Drill-ship

	Symbol	Units	Value
Overall length	L_{OA}	m	226.50
Length between perpendiculars	L_{PP}	m	220.00
Design breadth	B	m	55.00
Design draught	T_{DES}	m	12.22
Volume	∇	m^3	114854.6

Table 2.3: Thruster layout and dimensions

No.	Name	x_T (m)	y_T (m)	T_{MAX} (ton)
1	AFT Centreline	-105.00	0.00	91.95
2	AFT Port side	-86.00	-16.50	91.95
3	AFT Starboard side	-86.00	16.50	91.95
4	FWD Port side	60.00	-16.50	91.95
5	FWD Starboard side	60.00	16.50	91.95
6	FWD Centreline	80.00	0.00	91.95

An important aspect of the simulation is given by the selection of the thrust allocation procedure. In quasi-steady simulations and time-dependent ones, not always the same algorithms are adopted, and, as it will be explained in Chapter 4, the allocation algorithm strongly influences the final DP capability.

For this purpose, since this first study is only an investigation of the calculation method that is convenient to use for an early design stage, a simple allocation procedure [150] will be adopted for both quasi-steady and time domain simulations. This choice will ensure that the difference between the two simulations will be representative of dynamic effects.

Under these assumptions the two procedures were applied on the reference test case, resulting in the capability plot reported in Fig. 2.7 for the intact condition, means considering all the thrusters active. As it can be seen, the two capability plots are different, highlighting that the quasi-steady simulation (dotted in the graph) overestimates the vessel capability compared with time domain simulations. This statement can be considered valid since both procedures use the same methods to evaluate loads and thrust allocations, and the differences are mainly due to
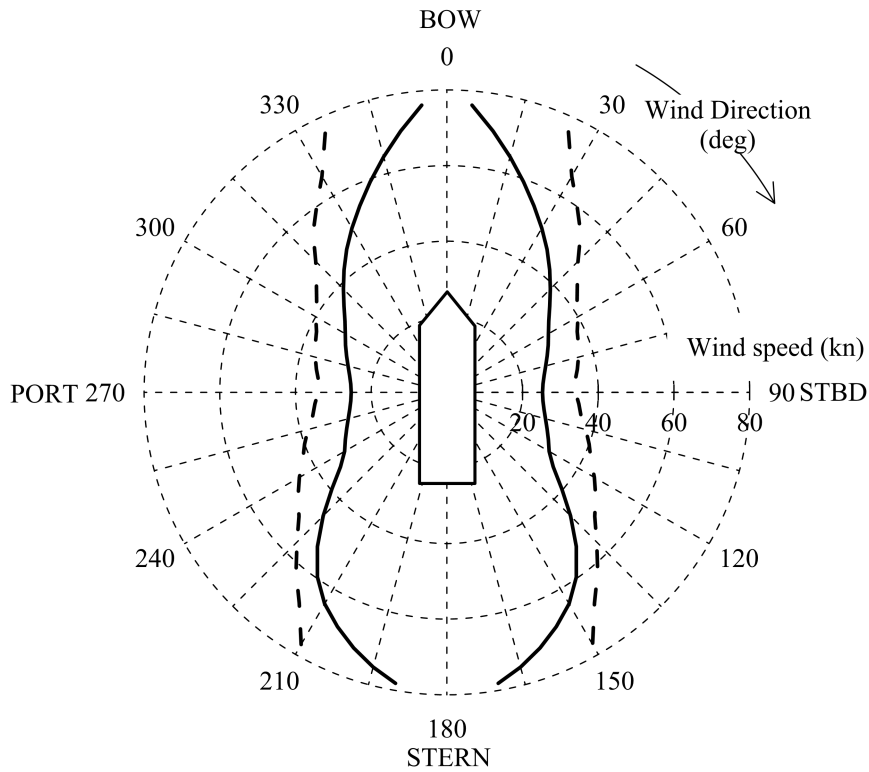
Figure 2.7: Comparison between quasi-steady (*dotted*) and time domain (*continuous*) simulations for the Drill-ship test case, considering Pierson-Moskowitz wind-wave correlation

dynamic effects. This is in line with results obtained in other studies [130, 125], but the results are also influenced by the acceptance criteria selected for the limiting environment detection during time domain simulations. In the specific a maximum position error of 5 meters and a yaw error of ±3 degrees have been considered, being in line with [130] adopted criteria and regulation suggestions [40].

In the specific test case it can be observed that the final maximum sustainable wind is about 30% lower at each encounter angle. This may suggest to consider a proper dynamic allowance coefficient (CA_{dyn}) to correct quasi-steady calculations in order to have a more reliable result compared to time-domain one. The differences between the maximum sustainable wind according to quasi-steady and time domain calculations are not constant at each wind incoming direction. Fig. 2.7 highlights that, for the analysed vessel, the capability reduction is higher for head and stern wind directions than for lateral ones. The CA_{dyn} is than variable with the vessel heading. For such a reason, the determination of CA_{dyn} requires the execution of at least a complete simulation case with a time-domain software. Moreover, the execution of a time domain DP simulation (also in the developed simplified form) requires the availability of data, as the vessel moment of inertia or added masses, that are difficult to accurately estimate during

the early design stage and will increase calculation uncertainties.

Since the whole study will be oriented to the determination of an enhanced prediction method for early design stage, it is essential to evaluate another aspects to compare the two methods: the calculation time. In fact, in an early design stage it is important to have a sufficiently reliable tool able to evaluate and compare multiple solutions in a short time, giving to the designer the preliminary information on how to improve and change his design.

A quasi-steady simulation evaluates a capability plot in few seconds, being really fast and suitable for an early design phase. A time-domain simulation needs to simulate at least 3 times 3 hours of physical time per each angle and wind conditions and each run requires more than 2 minutes of calculation time on a common PC. This is results in more than 1.5 hours to obtain a capability plot. This is acceptable once a final prediction on a vessel should be performed, however, is not acceptable once multiple design variations should be considered. For such a reason, it has been selected to consider the quasi-steady approach for the further investigations that will be carried out during this study.

Chapter 3

Environmental load coefficients

The main loads considered in a DP calculation are for sure the environmental ones. Since a vessel operates in an open sea area, the main causes for external loads are due to *wind*, wind driven *waves* and *current*. Depending on the typical environmental conditions of certain zones, other loads can be considered relevant, e.g. swell waves, extreme waves, exceptional currents or ice. The study of particular conditions goes outside the main goal of this work, since for an early design stage more generic situations are considered or, once operational areas are already known, the environmental modelling can be approximated using specific global statistics for the selected area.

For stated reasons, in this chapter main loads coming from wind, waves and current will be analysed and methods and procedures to estimate the environmental loads coefficients in a sufficiently accurate way for DP predictions in early design stage will be identified.

3.1   Wind loads

One of the most significant loads for an offshore vessel/unit is the one coming from wind action. An accurate determination of the wind loads type is required, not only for DP predictions, but also for the analysis of propulsion, towing, manoeuvring, stability, mooring and deck load capacity [140]. Until the recent years, the most common ways to determine wind loads were model tests or statistical methods derived by experiments. Recently the approach based on CFD is also used with some confidence. In any case, a more precise wind loads estimation can be obtained by using wind tunnel tests, but they are relatively expensive and time consuming for an early design stage. Therefore, commonly statistical methods are used.

There are not precise indication which are the most relevant and reliable methods for wind loads to be used in an early design stage. In fact, also classification societies [40, 6] and associations [62, 105, 9] propose different simplified methods to be used as a starting point for design. These method can be used when no other data are at disposal to designers. As claimed by some authors [72], there is a need to propose some hierarchical guidelines to proceed with wind loads estimation in an early design stage, since besides a plenty of methods for the coefficients estimation, there are also multiple ways to represent and obtain the non-dimensional wind load coefficients. The purpose of this study is not to establish a ranking between the available methods to determine wind loads, but to build up a procedure suitable to give a more reliable result in an early design stage. Moreover, it is important to establish also a standard method to deal with non-dimensionalisation of wind loads. In fact, among the different possible solutions for environmental loads determinations, several reference systems and non-dimensionalisation parameters are used. Here the reference system described in Chapter 2 and reported in Fig. 2.2 will be used. For the non-dimensional parameters, further detail analysis is needed.

3.1.1   Non-dimensional coefficients

There are different methods provided in the literature to determine non-dimensional coefficients from forces and moments obtained from measurements or calculations. The provided coefficients are sometimes dimensional, so that the problems with the effective comparison between different methods/measurements could arise.

Therefore, it has been decided to proceed with a common non-dimensionalisation for all the wind coefficients treated during this study, adopting the following notations:

$$C_{x_w}\left(\chi_w\right) = \frac{F_{x_w}\left(\chi_w\right)}{\frac{1}{2}\rho_{air}V_w^2 A_T} \tag{3.1}$$

$$C_{y_w}\left(\chi_w\right) = \frac{F_{y_w}\left(\chi_w\right)}{\frac{1}{2}\rho_{air}V_w^2 A_L} \tag{3.2}$$

$$C_{Mz_w}\left(\chi_w\right) = \frac{M_{z_w}\left(\chi_w\right)}{\frac{1}{2}\rho_{air}V_w^2 A_L L_{PP}} \tag{3.3}$$

where the wind load forces and moment are referring to the selected reference system and are reported in N and Nm. A_T and A_L are the transversal and lateral projected areas of the vessel superstructures respectively and L_{PP} is the length between perpendiculars of the vessel. V_w is the wind speed expressed in m/s referring to a 10 m height from the water free surface, while ρ_{air} is the air density expressed in kg/m^3. The coefficients are varying with the wind encounter

Table 3.1: Coefficients conversions according to different reference systems

Ref. system	χ_w	C_{x_w}	C_{y_w}	$C_{M_{z_w}}$
Blendermann	$360-\chi_w$	+	-	-
OCIMF	$360-(\chi_w-180)$	-	+	-
API	χ_w	-	-	-
DNV	χ_w	+	-	-

angle χ_w which is compliant with the adopted reference system. Through this study, all the wind coefficients have been directly translated into the selected reference system and non-dimensional form, to be directly comparable within each other.

In Table 3.1 a short overview is given on how to switch from a reference system to the one selected for this study.

3.1.2 Wind coefficients for early design stage

The most precise method to determine wind loads is for sure the execution of model tests. However, it is really hard to perform them at an early design stage. Therefore, a designer should be able to evaluate wind loads using alternative methods from the literature or from the classification societies.

The most commonly adopted methods for wind loads estimations on ships [61, 65] are based on the standard merchant vessel superstructures, which are not fully compliant with offshore vessels [141]. More complex and sophisticated methods, like CFD calculations, require a detailed description of the vessel superstructures, which is not usually known in an early design stage.

API method

One of the most commonly used procedures for wind loads determination in offshore world is the one suggested by the American Petroleum Institution [9], where the wind loads are determined as function of the wind pressure acting on the projected areas of the vessel superstructures. The pressure is expressed as:

$$p_w = \frac{1}{2}\rho_{air}V_w^2 C_h C_s \tag{3.4}$$
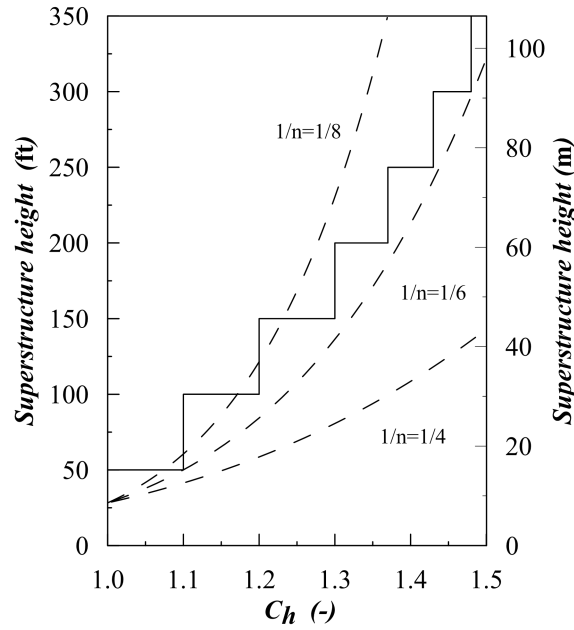
Figure 3.1: Height coefficient C_h proposed by API as a function of superstructure height compared with wind speed profiles

where C_h and C_s are the height and shape coefficient respectively. C_h is the stepped discretisation of a wind velocity profile, which is usually described as:

$$V_w\,(h_w) = V_w^* \left(\frac{h_w}{h^*}\right)^{\frac{1}{n}} \tag{3.5}$$

where V_w^* is the reference wind speed at the reference height h^* and n is varying between 6 and 8. In Fig. 3.1 it is possible to observe the API discretisation with different wind profiles determined according to equation (3.5). As it can be seen, the C_h discretisation is made in steps of 50 ft (about 15 m).

C_s coefficient is related to the superstructure shape, and varies from 0.40 (spheric superstructures) to 1.50 (isolated superstructures). By adopting this method, the vessel superstructure must be divided in different zones in order to evaluate the forces in transversal (F_{x_wT}) and longitudinal (F_{y_wL}) direction, considering the different superstructures shapes and reference areas:

$$F_{x_wT} = \sum_i p_{wTi} A_{T_i} \tag{3.6}$$

$$F_{y_wL} = \sum_i p_{w_{Li}} A_{L_i} \tag{3.7}$$

where p_{wTi} and $p_{w_{Li}}$ are the pressures evaluated according to equation (3.4) for the longitudinal and transversal projected areas A_{L_i} and A_{T_i} respectively.

Starting from these first forces estimates, the variation with χ_w can be determined with simple trigonometric formulations [9] or more complex ones [10] as follows:

$$F_w\left(\chi_w\right) = F_{x_{wT}} \frac{2\cos^2\chi_w}{1+\cos^2\chi_w} + F_{y_{wL}} \frac{2\sin^2\chi_w}{1+\sin^2\chi_w} \tag{3.8}$$

then x and y components can be determined:

$$F_{x_w} = F_w \cos\chi_w \tag{3.9}$$

$$F_{y_w} = F_w \sin\chi_w \tag{3.10}$$

Once [9] regulation is adopted, the components are obtained by substituting F_w with $F_{x_{wT}}$ and $F_{y_{wL}}$. No specific indication is given regarding the yawing moment evaluation, that, in any case, can be derived from F_{y_w} similar to other procedures.

DNV method

With the emission of the new regulations [39, 40], DNV gives new guidelines to determine the wind loads on an offshore vessel in an early stage design. Previously described API method is assuming that the designer knows with a sufficient level of accuracy the shape of the superstructures to fit on the vessel, to be able to determine the C_s accurately.

According to the method proposed by DNV, only the main parameters of the superstructures need to be used, evaluating the wind forces according to the following formulas:

$$F_{x_w} = \frac{1}{2}\rho_{air}V_w^2 A_T\left(-0.7\cos\chi_w\right) \tag{3.11}$$

$$F_{y_w} = \frac{1}{2}\rho_{air}V_w^2 A_L\left(0.9\sin\chi_w\right) \tag{3.12}$$

$$Mz_w = F_{y_w}\left(s_L + 0.3\left(1 - 2\frac{\chi_w^*}{\pi}\right)L_{PP}\right) \tag{3.13}$$

where the air density is equal to 1.226 kg/m^3, s_L is the longitudinal centre of A_L measured from origin O and χ_w^* is defined as follows:

$$\chi_w^* = \begin{cases} \chi_w & \text{if } 0 < \chi_w < \pi \\ 2\pi - \chi_w & \text{if } \pi \le \chi_w \le 2\pi \end{cases} \tag{3.14}$$

By adopting this notation, the method is suitable to reproduce in a better way, compared to API method, the behaviour of the yawing moment due to an incoming wind. The procedure is not giving indications to obtain non-dimensional value, since it is oriented to directly evaluate loads inside a DP capability calculation.

3.1.3   Statistical analysis of Blendermann database

An useful option to determine wind loads coefficients is for sure the adoption of a database. Between the different possible options to use a database, the adoption of regression techniques is one of the most common and reliable solutions.

As mentioned, regarding wind loads, the most wide and complete database available in the literature for ships is the one given by Blendermann [21], where the same author already proposed dedicated regression techniques to determine wind coefficients [17, 18, 19, 20]. In particular, in [18] a regression model based on the classical solution of the mathematical flow on the so-called Helmholtz-Kirchoff plane has been proposed, using the following parametric loading functions:

$$C_{x_w} = C_d \frac{A_L}{A_T} \frac{\cos \chi_w}{1 - \frac{\delta_c}{2} \left(1 - \frac{C_d}{C_q}\right) \sin^2 (2\chi_w)} \tag{3.15}$$

$$C_{y_w} = C_q \frac{\sin \chi_w}{1 - \frac{\delta_c}{2} \left(1 - \frac{C_d}{C_q}\right) \sin^2 (2\chi_w)} \tag{3.16}$$

$$C_{Mz_w} = \left[\frac{s_L}{L_{PP}} - 0.18 \left(\chi_w - \frac{\pi}{2}\right)\right] C_{y_w} \tag{3.17}$$

$$C_{Mx_w} = \kappa_c \frac{s_H L_{PP}}{A_L} C_{y_w} \tag{3.18}$$

where C_{Mx_w} is the heeling moment. The above equations are expressed as function of four primary wind loads parameters: C_d representative of the transverse resistance, C_q for lateral resistance, δ_c as cross-force parameter and κ_c for the heeling moment factor. The only geometrical parameters that need to be known for the vessel are A_L, A_T, s_H and s_L; where s_H and s_L are the lateral area position coordinates with respect to origin O.

The above mentioned regression method is based on the assumption that the rate of change of the moment reduction point x_f is constant for all the vessels. In fact, equation (3.17) can be rewritten as follows:

$$C_{Mz_w} = \frac{x_f}{L_{PP}} C_{y_w} \tag{3.19}$$

where:

$$x_f = s_L + \frac{\mathrm{d}x_f}{\mathrm{d}\chi_w} \left(\chi_w - \frac{\pi}{2}\right) \tag{3.20}$$

In the original studies, according to formulation (3.20) together with (3.17), the authors supposed that for all the vessel types, quantity $\frac{\mathrm{d}x_f}{\mathrm{d}\chi_w}$ is equal to 0.18.

However, considering the different kind of superstructure shapes between each vessel type, it is reasonable to presume that $\frac{dx_f}{d\chi_w}$ will also change with the vessel type. For this purpose, it is proposed to perform an enhanced regression analysis by considering also $\frac{dx_f}{d\chi_w}$ as regression parameter. In this sense, to analyse the new regression parameter, it is necessary to obtain an estimate of the x_f value per each wind direction χ_w. The x_f value is determined by dividing the experimental C_{Mz_w} by experimental C_{y_w} at the same encounter angle. Then it is possible to represent x_f as a function of the vessel heading. Generally, x_f has a linear trend for headings from 20° to 160°. The data became unstable close to 0° and 180°. Here, both C_{Mz_w} and C_{y_w} values tend to zero; consequently, their ratio is no more stable. The analysis is performed toward a reduced interval of headings to avoid the influence of extreme points. Usually, it is sufficient to discard the data value at most for the first and last 30°; however, the adequate heading interval has to be selected ship by ship. By doing that, the x_f data are fitted with linear regression to determine $\frac{dx_f}{d\chi_w}$, which is the angular coefficient of the regression line. An example of the regression analysis is given in Fig. 3.2 for a supply vessel of the Blenderman database. Analysing the data in Fig. 3.2, it can be seen that the regression model proposed by Blendermann is not reproducing really well the behaviour of the moment level x_f, the newly proposed regression model is fitting better the measurements distribution. To further enhance the regression model, it is also proposed to change the regression parameter for the longitudinal direction, instead of C_d, C_{d_a} and C_{d_f} (the drag coefficient for the head and the following winds) have been used, selecting as reference values the mean C_{x_w} at 0° and 180° per each vessel type. The coefficient C_q has been selected as the mean of the C_{y_w} at 90° per each vessel type. For such a reason the newly developed regression procedure is splitting equations (3.15) and (3.16) in two sub-cases for head and following wind. With reference to Table 3.2, it can be seen that, despite for a few vessel types, the regression of $\frac{dx_f}{d\chi_w}$ is giving different results compared to the constant value proposed by Blendermann. In Fig. 3.3 a comparison is given for the C_{Mz_w} on a supply vessel of the Blenderman database, highlighting that the new proposed regression is reproducing better the wind yawing moment with respect to the previous regression. Moreover, the application of two different drag coefficients for the stern and the fore winds, leads to an overall increase of the model accuracy. To evaluate the benefits, it is necessary to evaluate the quality of the regression. In this case use has been made of the determination coefficient R^2 defined as:

$$R^2 = 1 - \frac{SSE}{SS_{tot}} \tag{3.21}$$
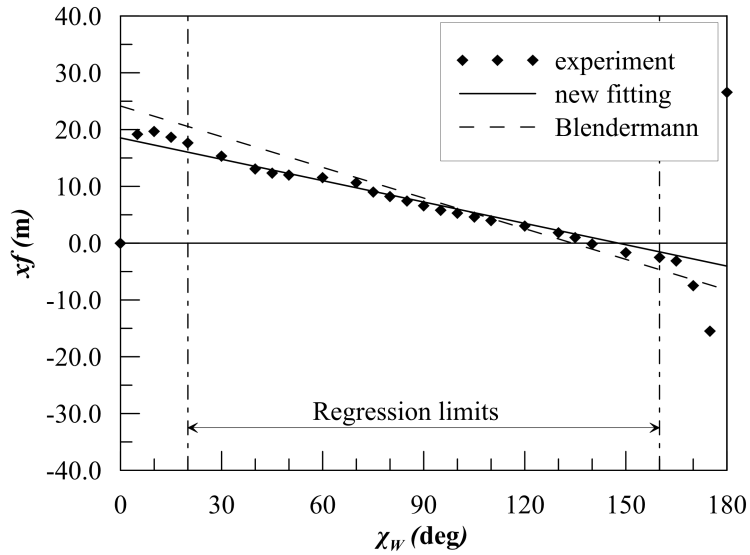
Figure 3.2: Comparison between old and proposed x_f regression analyses for SUP0102BN of the Blendermann database
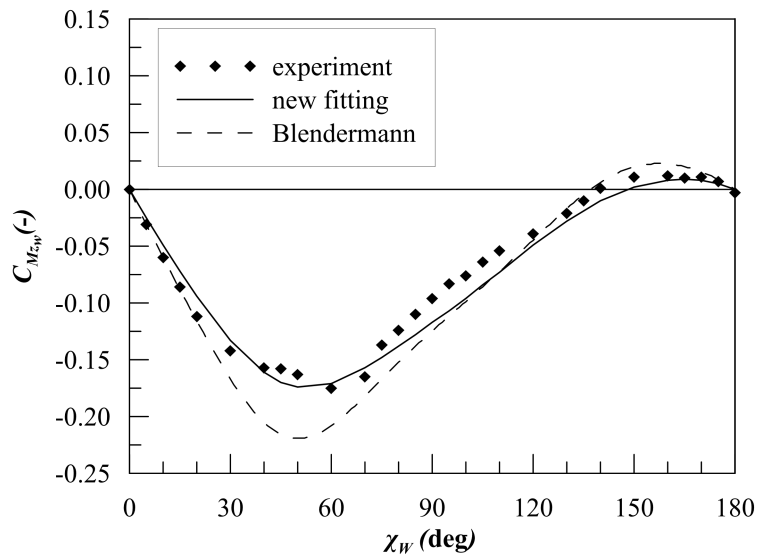
Figure 3.3: Comparison between old and proposed C_{Mz_w} regression analyses for SUP0102BN of the Blendermann database

Table 3.2: Statistical parameters of Blendermann wind model data

Vessel type	C_q	C_{d_f}	C_{d_a}	δ_c	$\mathrm{d}x_f/\mathrm{d}\chi_w$
Car Carrier	1.02	0.59	0.86	0.45	0.52
Diving Vessel	0.90	0.60	0.80	0.55	0.18
Drilling Vessel	0.95	1.36	1.38	0.69	0.12
Passenger Liner	0.90	0.40	0.40	0.80	0.18
Research Vessel	0.85	0.55	0.65	0.60	0.18
Supply Vessel	1.01	0.54	0.84	0.52	0.15
Tanker, laden	0.70	0.90	0.55	0.40	0.18
Tanker, ballast	0.70	0.75	0.55	0.40	0.18
Fishing Vessel, Cutter	0.95	0.70	0.70	0.70	0.40
Yacht	0.90	0.55	0.60	0.60	0.18

where:

$$SSE = \sum_{i=1}^{n} (y_i - f_i)^2 \tag{3.22}$$

$$SS_{tot} = \sum_{i=1}^{n} (y_i - \bar{y})^2 \tag{3.23}$$

$$\bar{y} = \frac{1}{n} \sum_{i=1}^{n} y_i \tag{3.24}$$

y_i are the data point to fit, $\bar{y}$ is the data point mean and f_i are the fitted values coming from the regression.

A comparison has been made between the R^2 values obtained for the new regression and the original one on the supply vessels present inside the Blendermann database. In Table 3.3 it can be seen that the new regression analysis gives a better reproduction of the wind coefficients, due to the better definition of the differences between the fore and the aft part of the coefficients and tanks to the dedicated regression on $\frac{\mathrm{d}x_f}{\mathrm{d}\chi_w}$ for the yawing moment.

3.2   Current loads

Compared with wind, current load is less incisive in the total amount of the environmental causes. However, it remains still a considerable loads and cannot be a priori discarded. In

Table 3.3: Comparison between R^2 values on the supply vessels of Blendermann database

Vessel	C_{x_w}		C_{y_w}		$C_{M_{z_w}}$	
	old	new	old	new	old	new
SUP0101BN	0.956	0.978	0.977	0.988	0.813	0.915
SUP0102BN	0.932	0.958	0.973	0.986	0.821	0.923
SUP0106BN	0.916	0.975	0.971	0.984	0.816	0.917
SUP0107BN	0.923	0.962	0.975	0.988	0.827	0.921
SUP0109BN	0.912	0.937	0.974	0.994	0.825	0.922
SUP0111BN	0.874	0.885	0.969	0.991	0.785	0.896

fact, for particular applications (e.g. operations close to river estuaries), current load can be predominant to the others, so that an accurate estimation of the current coefficient is necessary. The most reliable way to determine current load is for sure using model tests, but, as in the wind case, the costs and design accuracy level required to perform it is too high for an early design stage. Besides model tests, a promising technique is given by viscous flow CFD calculations. In any case, also this approach requires the high computational time and also the high skill level for the designer in order to obtain reliable results from calculations.

Also in the case of current, each hydrodynamic institute, classification society or dedicated association is using its own reference system and non-dimensionalisation method. The reference system presented in Fig. 2.2 will be used here, but for the non-dimensional coefficients more detailed discussion is needed.

3.2.1   Non-dimensional coefficients

In the present work, a common method has been selected to determine the non-dimensionalisation of the current loads. In the literature and analysing research institutes reports and methodologies, several options are available. There are methods that, to be compliant with wind coefficients non-dimensionalisation, use lateral and transverse projected areas of the submerged hull. Other methods use the product $L_{PP}T_{DES}$, having a sort of equivalent rectangle instead of the area projection itself. In such a study the vessel wetted surface S is used and the non-dimensional coefficients are determined in the following form:

$$C_{x_c}\left(\chi_c\right) = \frac{F_{x_c}}{\frac{1}{2}\rho_w S V_c^2} \tag{3.25}$$

$$C_{y_c}(\chi_c) = \frac{F_{y_c}}{\frac{1}{2}\rho_w S V_c^2} \tag{3.26}$$

$$C_{Mz_c}(\chi_c) = \frac{M_{z_c}}{\frac{1}{2}\rho_w S L_{PP} V_c^2} \tag{3.27}$$

where ρ_w is the density of the water. In the case of the moment Mz_c, also the length is considered to obtain a non-dimensional value. Through the study, all the reported current coefficients will follow this standard in order to avoid misunderstandings between different reference systems and non-dimensionalisation techniques.

3.2.2 Current coefficients for early design stage

In an early design stage it is usual to adopt simple methods that are mainly based on classification society indications, or, as second choice adopting coefficients coming from measurements on similar vessels.

Since the second option is something not available in the literature, the most commonly used methods from regulations will be described here.

API method

The method proposed in [9] is a simple approximation. In fact, the document itself states that in case more reliable data are present, those should be used for current force determination. In absence of reliable data, the following formulations should be used to determine the maximum longitudinal and transversal loads:

$$F_{x_{cMAX}} = C_{cx} S V_c^2 \tag{3.28}$$

$$F_{y_{cMAX}} = C_{cy} S V_c^2 \tag{3.29}$$

where the dimensional coefficients C_{cx} and C_{cy} should be 2.89 and 72.37 Ns^2/m^4, respectively. The forces can be thereafter distributed across χ_c with simple sinusoidal rules. No general indication is given for the determination of the yawing moment.

DNV method

In regulation [40] a simplified method to evaluate current loads is presented. As for wind loads, the method is not evaluating coefficients directly, but estimates the forces as function of the

vessels main particulars that are available in an early design stage.

Current forces can be evaluated according to the following formulations:

$$F_{x_c} = \frac{1}{2}\rho_w V_c^2 BT_{DES} \left(-0.07\cos\chi_c\right) \tag{3.30}$$

$$F_{y_c} = \frac{1}{2}\rho_w V_c^2 A_{L_c} \left(0.60\sin\chi_c\right) \tag{3.31}$$

$$M_{z_c} = F_{y_c}\left(s_{L_c} + \max\left(c_c, -0.2\right)L_{PP}\right) \tag{3.32}$$

$$c_c = \min\left[0.4\left(1 - 2\frac{\chi_c^*}{\pi}\right), 0.25\right] \tag{3.33}$$

where the water density ρ_w has to be set to 1026 kg/m^3, s_{L_c} is the centre of the submerged lateral area with respect to origin O. The auxiliary encounter angle to determine the moment is evaluated as:

$$\chi_c^* = \begin{cases} \chi_c & \text{if } 0 < \chi_c < \pi \\ 2\pi - \chi_c & \text{if } \pi \le \chi_c \le 2\pi \end{cases} \tag{3.34}$$

It is also specified that the current method is suitable to evaluate loads once the current speed is low enough to maintain the Froude number evaluated on the vessel breadth B under the value of 0.1.

3.2.3   Regressions of a database of CFD data

An option to evaluate the current loads more accurately is by using the CFD calculations. Such a numerical approach is for sure not indicated to be directly used in a preliminary design stage since it requires a lot of computational effort, not necessary for the complexity of the calculation itself, but for the amount of calculations needed to obtain the current forces on the hull.

In case a current load calculation should be carried out, some simplifications can be considered to decrease the calculation time, without loosing too much accuracy in the final forces estimation. First of all the double-body approximation can be considered, since the current speed is low enough to discard Froude related phenomena. Moreover, despite of the presence of particularly big appendages, the resolution of the equations can be done considering a segregated approach, reducing then the calculation time. In any case, despite a single calculation could converge with sufficient accuracy in a couple of hours on a small cluster, to reproduce the loads curve at least 11 calculations are needed to cover the encounter angles χ_c for a symmetric ship. Moreover, the adoption of a numerical method requires the use of calculation procedure and meshes validated

on experimental results, to prove the reliability of the coefficients.

Once sufficiently reliable and validated meshes are at disposal (see Appendix C), it is possible to adopt this method to build a database of numerical calculations on a hull family, to perform a regression analysis on the obtained coefficients.

Since it is really hard to have a database at disposal with a sufficient number of vessels to build a regression the systematic series is used in this study. As an exploratory study, a family of 15 drillships (see Appendix B) has been created on the base of a Box-Behnken design space [22] in order to investigate the variation of the current non-dimensional coefficients with reference to the hull main parameters. Since the study is based on a systematic series, only certain main parameters have been changed, in this case L/B, B/T and C_B.

On each member of the population, calculation were done in model scale, in order to simulate 8 meter model where was possible to adopt a previously validated mesh. The calculations were executed for 11 angles. As highlighted in Appendix C, the geometrical parameters are influencing the behaviour of the non-dimensional coefficients. Moreover it can be noticed the behaviour of the C_{x_c}, which is more complex with respect to the simplistic assumptions of the methods provided by classification societies. Such kind of behaviour is typical for high C_B hull as drillships and cannot be captured with standard methods.

Since the computations are performed on model scale, it is necessary to find a way to scale the results on full scale. Here, it has been selected to scale the coefficients according to the ITTC 1957 ship model correlation line, so that the coefficients (non-dimensionalised as per equations (3.25)-(3.27)) obtained from calculations have been transformed to reproduce a sort of *current form factor*. The final full scale coefficient are obtained as:

$$C_{x_c} (\chi_c)_S = C_{F_S} (1 + k_x (\chi_w)) \tag{3.35}$$

$$C_{y_c} (\chi_c)_S = C_{F_S} \left(1 + k_y (\chi_w)\right) \tag{3.36}$$

$$C_{Mz_c} (\chi_c)_S = C_{F_S} (1 + k_z (\chi_w)) \tag{3.37}$$

where k values are determined as:

$$k_i (\chi_w) = \frac{C_{i_m}}{C_{F_m}} - 1 \tag{3.38}$$

where C_{F_m} is the frictional coefficient on model scale and C_{i_m} with $i \in x_c, y_c, Mz_c$ are the model scale coefficients determined by CFD computations.

Since the database is derived from a Box-Behnken space, a quadratic model has been selected

as base of the regressions, resulting in the following formulations:

$$k_x(\chi_c) = a_0 + a_1(C_B) + a_2(C_B)^2 + a_3(B/T) + a_4(C_B)(B/T) + a_5(B/T)^2$$
$$+a_6(L/B) + a_7(L/B)(C_B) + a_8(L/B)(B/T) + a_9(L/B)^2 \qquad (3.39)$$

$$k_y(\chi_c) = b_0 + b_1(C_B) + b_2(C_B)^2 + b_3(B/T) + b_4(C_B)(B/T) + b_5(B/T)^2$$
$$+b_6(L/B) + b_7(L/B)(C_B) + b_8(L/B)(B/T) + b_9(L/B)^2 \qquad (3.40)$$

$$k_z(\chi_c) = c_0 + c_1(C_B) + c_2(C_B)^2 + c_3(B/T) + c_4(C_B)(B/T) + c_5(B/T)^2$$
$$+c_6(L/B) + c_7(L/B)(C_B) + c_8(L/B)(B/T) + c_9(L/B)^2 \qquad (3.41)$$

The equations (3.39)(3.40) and (3.41) are representative of the complete regression model, while case by case the non representative coefficients have been discarded according to associated p value. a_i, b_i and c_i coefficients are varying also with χ_c, and dedicated regressions have been made for 11 angles.

In Table 3.4 an example of the obtained coefficients for k_x regression. Here the quality of the regression has been studied not only by means of the determination coefficient R^2 defined in equation (3.21) but also with the R^2_{adj} defined as:

$$R^2_{adj} = 1 - \left(1 - R^2\right)\frac{n-1}{n-p-1} \qquad (3.42)$$

where n is the number of data to fit and p is the number of variables included in the regression model. R^2 can be considered as an unbiased estimator of the R^2 [127] and is considerate an adequate estimator of model fit, especially in the feature selection stage of regression model building. In Table 3.4 also the determination coefficients are reported. It can be noted that, having selected a different regression per each angle is given, the obtained statistical values are quite high, being always above 0.8 for R^2 and above 0.7 for R^2_{adj}. Further improvement could be probably reached by increasing the number of predictors, considering dependences higher than the second order, however that means increase the initial vessel population. In Figs. 3.4, 3.5 and 3.6 the results obtained applying the proposed regressions and the calculation outputs are presented with reference to the 15 drillships. The curves confirm that the proposed regression model is capable to capture the trend of the coefficients obtained by means of CFD calculations. This kind of approach can be followed for other vessel types, leading to the definition of dedicated regressions associated with ship type, being able to capture the peculiarities of the coefficient shapes.

Table 3.4: Regression coefficients for k_x

					χ_c (deg)						
	0.0	7.5	15.0	30.0	60.0	90.0	120.0	150.0	165.0	172.5	180.0
a_0	21.635	21.147	32.868	19.691	366.316	-126.235	-13.227	-31.1138	-1	-29.737	-
a_1	-41.348	-43.347	-66.097	-55.981	-637.374	426.224	-	-	61.548	43.924	82.455
a_2	27.228	28.000	38.403	39.951	266.832	-301.942	-25.950	-24.412	-30.900	-18.596	-40.466
a_3	-2.227	0.0392	1.212	6.594	-73.238	21.254	-	-0.556	3.044	4.357	8.999
a_4	-6.110	-6.567	-5.421	-7.465	71.663	20.579	-	-2.808	-3.499	-2.389	-5.496
a_5	3.543	2.449	1.200	-0.618	-1.819	-42.545	-	0.851	-0.006	-0.737	-1.382
a_6	3.647	4.189	-0.841	10.212	-52.3494	-148.003	-	2.437	-5.845	-0.081	-1.055
a_7	-7.232	-6.013	-3.236	-	45.695	118.840	-1.032	-0.596	-	1.551	7.662
a_8	1.685	1.416	1.714	2.131	12.793	28.525	-	0.523	0.285	-0.507	-1.183
a_9	0.713	-0.046	0.227	0.793	0.923	4.410	4.242	-1.138	-0.803	0.010	-2.203
R^2	0.940	0.925	0.865	0.973	0.906	0.938	0.999	0.998	0.998	0.998	0.997
R^2_{adj}	0.832	0.791	0.822	0.924	0.775	0.818	0.998	0.994	0.995	0.994	0.991
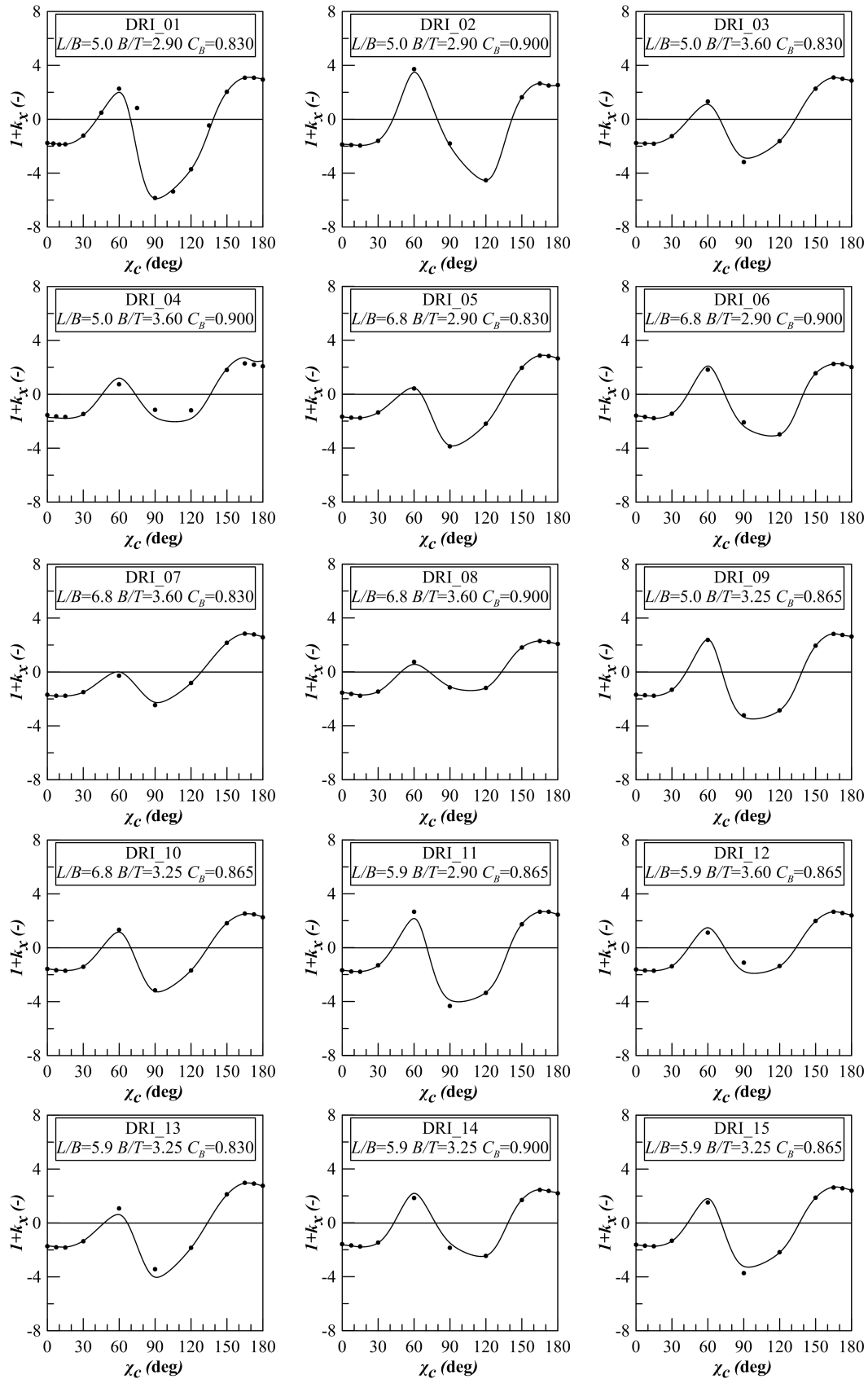
Figure 3.4: Coefficient $1 + k_x$ for the drillship family according to CFD calculations (*dots*) and to proposed regression model (*continuous*)
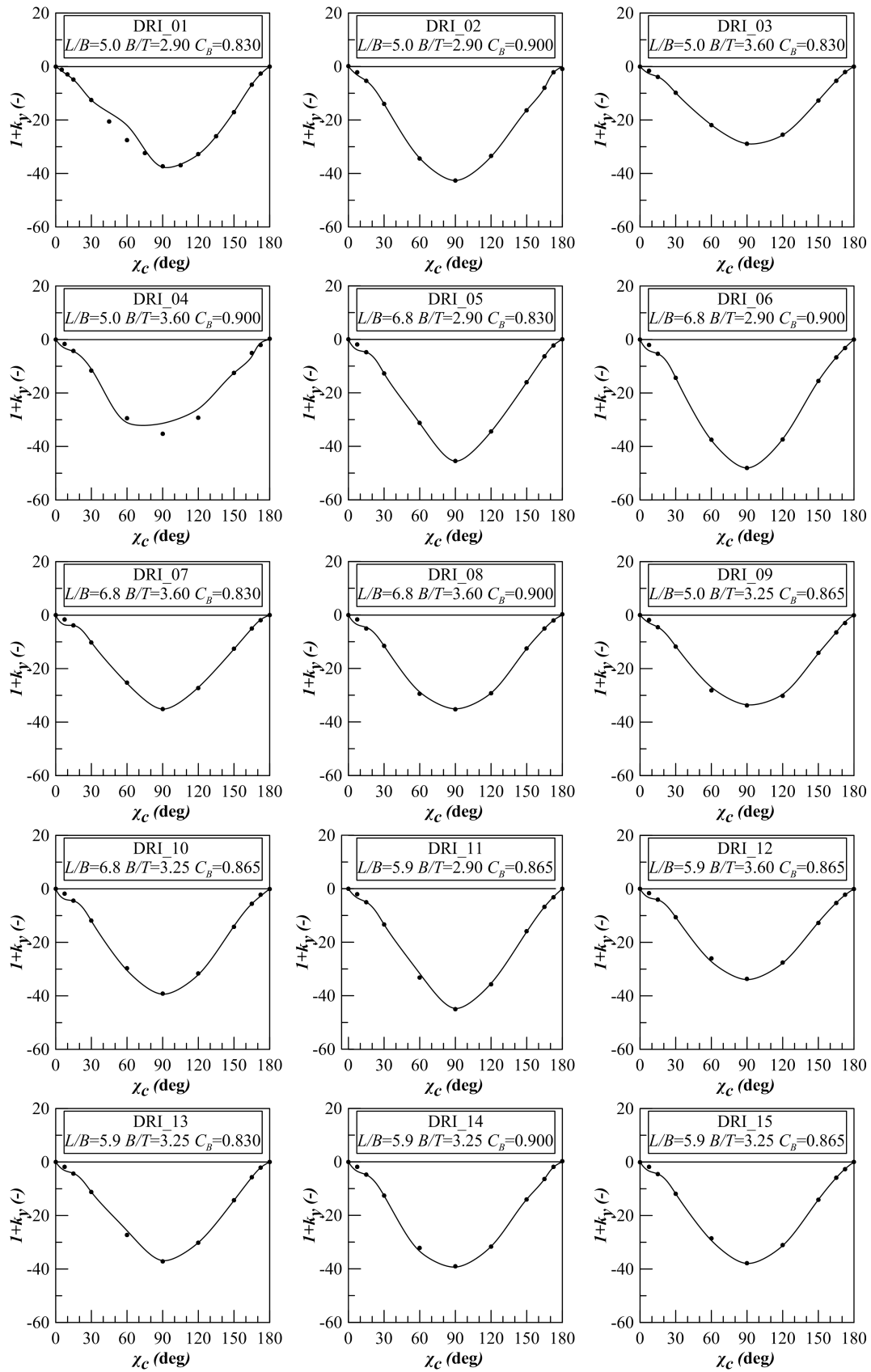
Figure 3.5: Coefficient $1 + k_y$ for the drillship family according to CFD calculations (*dots*) and to proposed regression model (*continuous*)
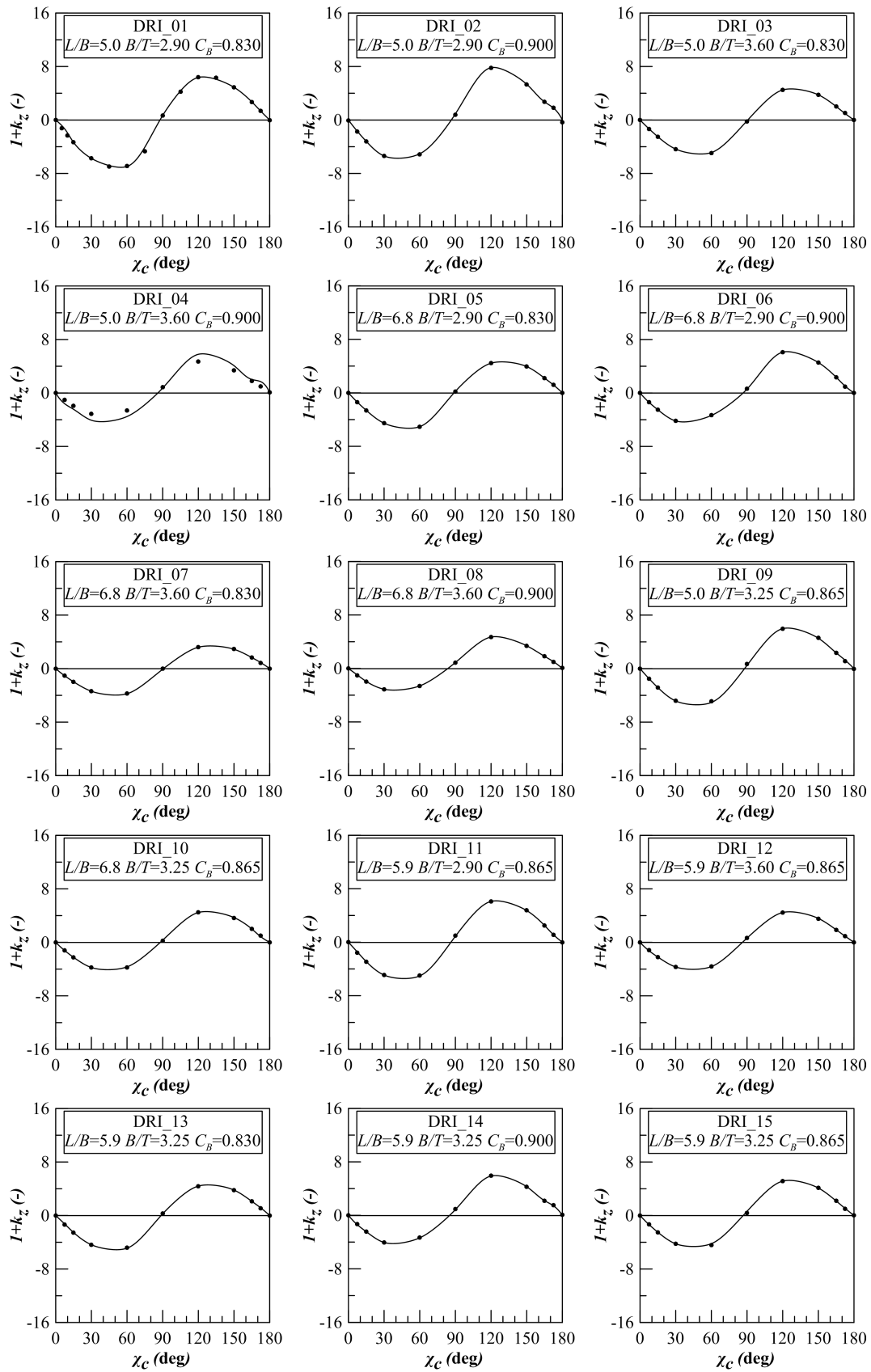
Figure 3.6: Coefficient $1 + k_z$ for the drillship family according to CFD calculations (*dots*) and to proposed regression model (*continuous*)

3.3 Wave loads

The wave loads acting on a floating body are directly correlated with the wind loads. In fact, the waves considered in DP calculations are supposed to be generated by a specific wind. Anyway the determination of the wave loads coefficients is not correlated with the determination of wind once. The two phenomena are related by a determined wind-wave correlation, that varies according to the specific site or to the regulation adopted for DP calculations [40]. According to this correlation, at each wind speed a certain wave height $H_{1/3}$ and wave period T_z or T_p is associated. The wave load is generated by a constant drift component and first and second order variable components. Since DP system faces corrections around a mean values, usually only drift forces are considered.

Having defined the reference wave parameters, the two approaches can be defined: one based on simplified formulations deriving directly the wave forces or spectral integration methods using drift forces quadratic transfer functions (QTF) evaluated by model tests or diffraction calculations.

3.3.1 Non-dimensional coefficients

The non-dimensionalisation of the wave loads is somewhat different with respect to wind and current coefficients. In fact, it is common to insert the wave height as parameter and there is no reference speed to adopt for the process. The adopted formulations result then in the following form:

$$C_{x_g}\left(\chi_g\right) = \frac{F_{x_g}\left(\chi_g\right)}{\frac{1}{2}\rho_w g H_{1/3}^2 \nabla^{\frac{1}{3}}} \tag{3.43}$$

$$C_{y_g}\left(\chi_g\right) = \frac{F_{y_g}\left(\chi_g\right)}{\frac{1}{2}\rho_w g H_{1/3}^2 \nabla^{\frac{1}{3}}} \tag{3.44}$$

$$C_{Mz_g}\left(\chi_g\right) = \frac{M_{z_g}\left(\chi_g\right)}{\frac{1}{2}\rho_w g H_{1/3}^2 \nabla^{\frac{2}{3}}} \tag{3.45}$$

where ∇ is the vessel volume at the considered draught. The presented method is not a standard, since sometimes instead of $\nabla^{1/3}$, L_{WL} is adopted.

3.3.2   Wave coefficients for early design stage

In an early design stage simple formulations are available, so that the methods with certain simplifications should be applied. On this purpose it is not convenient to use coefficients obtained by means of calculations, since they require the knowledge of the hull form and vessel moments of inertia. Those calculations can be used only when a vessel is similar to a previous one already tested or analysed. In case of a really preliminary calculation it is needed to adopt simplified methods that are usually provided by classification society and dedicated associations.

API method

This procedure allows to evaluate the maximum loads acting in the longitudinal and the transversal direction according to the following formulations:

$$F_{x_g MAX} = 0.13 C_{mdh} B^2 L_{WL} H_{1/3}^2 \tag{3.46}$$

$$F_{y_g MAX} = C_{mdh} B^2 L_{WL} H_{1/3}^2 \tag{3.47}$$

where C_{mdh} is a coefficient given in graphical form as function of significant period T_s and the characteristic period T_k defined as:

$$T_k = \begin{cases} 0.64\sqrt{B + 2T_{DES}} & \text{for beam seas} \\ 0.33\sqrt{L_{WL}} & \text{for head and stern seas} \end{cases} \tag{3.48}$$

being T_{DES} the reference draught. T_s is estimated from $H_{1/3}$ from another graph presented in [9]. The coefficients for the other directions χ_g can be derived using the trigonometrical relations. No indication is given for the yawing moment.

DNV method

In this case indications are given to evaluate directly the wave forces and the yawing moment as function of the encounter angle χ_g. The following equations are adopted:

$$F_{x_g} = \frac{1}{2}\rho_w g H_{1/3}^2 B h\left(\chi_g, \epsilon, C_{WLaft}\right) f\left(T'_{surge}\right) \tag{3.49}$$

$$F_{y_g} = \frac{1}{2}\rho_w g H_{1/3}^2 L_{OS}\left(0.09 \sin \chi_g\right) f\left(T'_{sway}\right) \tag{3.50}$$

$$M_{z_g} = F_{y_g}\left(s_L + \left(0.05 - 0.14\frac{\chi_g^*}{\pi}\right)L_{OS}\right) \tag{3.51}$$

where a particular formulation is given for h as a function of the entrance angle ϵ and aft water-plan coefficient C_{WLaft}. The auxiliary encounter angle to evaluate the moment is given with:

$$\chi_g^* = \begin{cases} \chi_g & \text{if } 0 < \chi_g < \pi \\ 2\pi - \chi_g & \text{if } \pi \leq \chi_g \leq 2\pi \end{cases} \tag{3.52}$$

The function of the wave period is defined in the following form:

$$f\left(T'\right) = \begin{cases} 1 & \text{if } T' < 1 \\ T'^{-3}e^{1-T'^{-3}} & \text{if } T' \geq 1 \end{cases} \tag{3.53}$$

being T'_{surge} and T'_{sway} function of the zero crossing period T_z.

In such a way it is possible to reproduce drift forces and moments for each encounter angle in an early design phase.

3.3.3 Coefficients from diffraction calculations

A possible solution to determine the drift forces is to perform diffraction calculations. In such a case, mean wave drift forces and moments are determined starting from quadratic wave drift transfer functions variant with the angle χ_g between the wave incidence angle and the ship's heading and the wave frequency ω. Anyway, a ship never encounters regular waves so this set of data must be associated to an irregular sea state.

The stochastic process of an irregular sea can be described by different types of spectrum, so that forces and moments are determined for a given wave condition by multiplying the regular drift coefficients by the spectrum $S_\zeta(\omega)$ and then integrating the product over a range of frequencies:

$$F_{x_g} = \rho_w g \nabla^{1/3} \int_0^\infty C_{x_g}\left(\omega, \chi_g\right) S_\zeta(\omega)\,\mathrm{d}\omega \tag{3.54}$$

$$F_{y_g} = \rho_w g \nabla^{1/3} \int_0^\infty C_{y_g}\left(\omega, \chi_g\right) S_\zeta(\omega)\,\mathrm{d}\omega \tag{3.55}$$

$$M_{z_g} = \rho_w g \nabla^{2/3} \int_0^\infty C_{Mz_g}\left(\omega, \chi_g\right) S_\zeta(\omega)\,\mathrm{d}\omega \tag{3.56}$$

where the $C_i\left(\omega, \chi_g\right)$ are the coefficients obtained from diffraction calculations in regular waves. It must be noted that the same modelling can be used for coefficients coming from model test in regular waves.
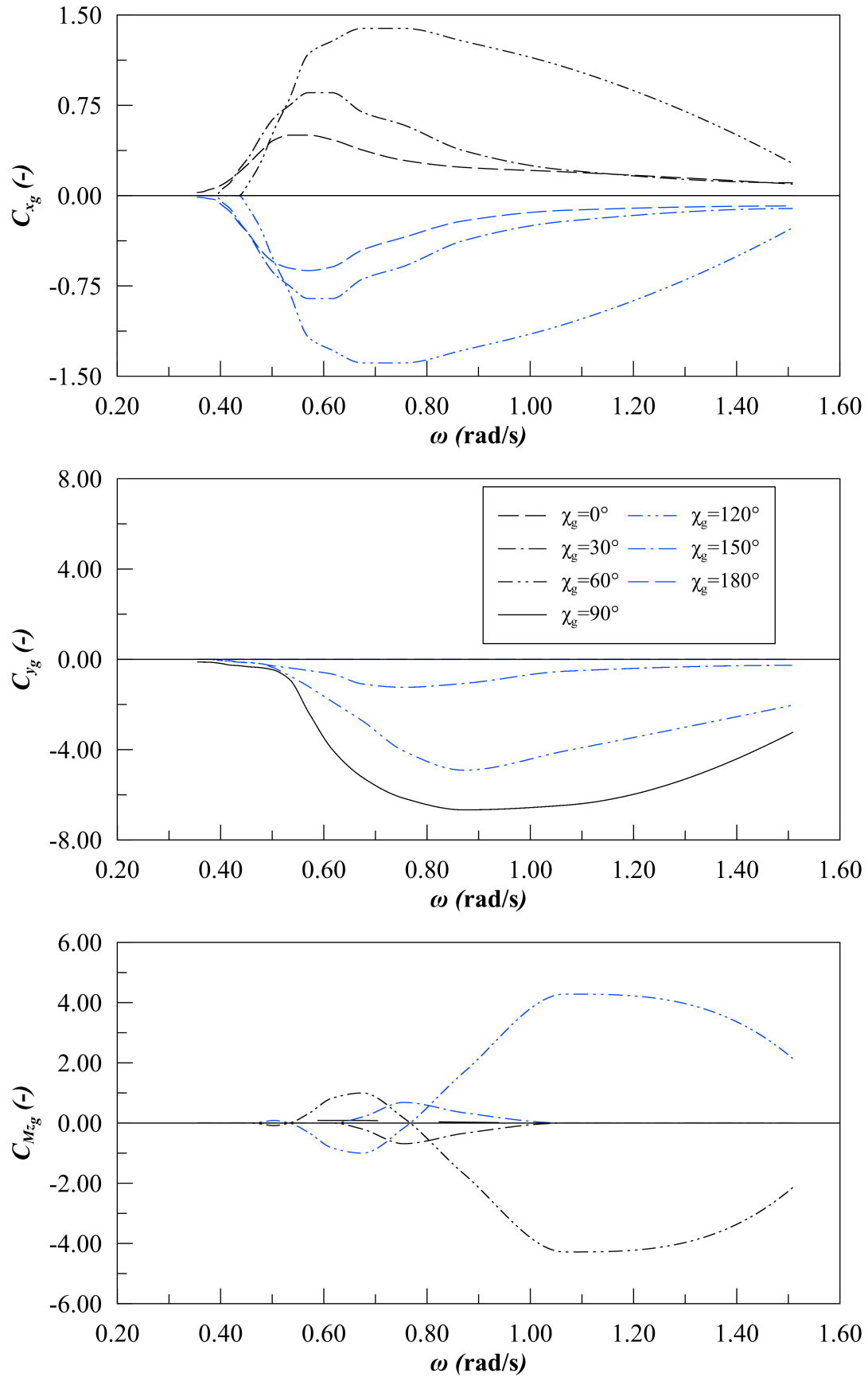
Figure 3.7: Drift force coefficients obtained by means of diffraction calculation for the drillship described in Chapter 2

Table 3.5: Main dimension of the reference PSV

Length between perpendiculars	L_{PP}	55.00	m
Length at design waterline	L_{WL}	55.00	m
Length overall	L_{OA}	60.00	m
Breadth	B	13.30	m
Design draught	T_{DES}	3.80	m
Volume	∇	2110.5	m^3

In case of similar ships, the data can be reported by means of a non-dimensional frequency defined in the following form:

$$\omega' = \omega \left(\frac{\nabla^{1/3}}{g} \right)^{\frac{1}{2}} \qquad (3.57)$$

By means of this transformation, than it is possible to scale the coefficients in frequency range according to the vessel volume. In Fig. 3.7 an example of those coefficients is given for a reference drillship.

As for the previously investigated current loads, here, diffraction calculation can be also used to produce a database of coefficients as starting point for dedicated regression analysis. However, the adoption of the non-dimensional frequency will grant more flexibility and in the evaluation of the wave force for similar vessel types, having more accurate loads with respect to standard regulation calculations.

3.4 Environmental loads effect on capability plots

With different definition of the environmental loads and different methods to determine the coefficients, according to the selected method different total loads will be estimated for a certain vessel. This will, of course, have an impact on the final capability predicted by a DP calculation program. On this purpose a comparison has been made on a platform supply vessel (PSV), adopting loads coming from enhanced methods proposed for wind and wave loads and other coming from standard regulations. The selected PSV has the main dimension as reported in Table 3.5. The vessel is not equipped with azimuth thrusters but is propelled by two conventional ducted propellers. The main propellers in combination with the rudders are used during dynamic positioning. Also two bow tunnel thrusters are installed for DP purposes.
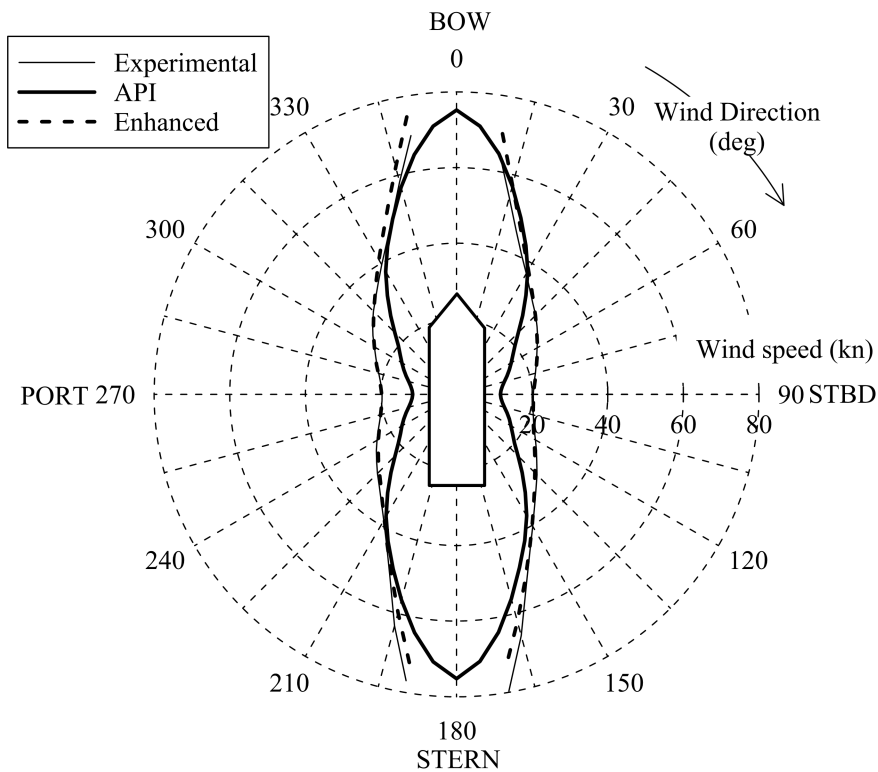
Figure 3.8: Capability plot envelopes according to different environmental loads definition on the selected PSV

In Fig. 3.8 a comparison is made on the reference vessel between the capability plots obtained with environmental loads coming from experiments, loads coming from API regulations (where also moment has been evaluated) and loads evaluated with the wind coefficients coming from Blendermann statistics and wave loads from diffraction calculations on a vessel of the same type. With reference to the wave loads, it was not possible to perform the calculation directly on the same ship because the hull geometry was not at disposal. Therefore the geometry of a comparable supply vessel has been used, scaling the coefficients in frequency according to equation (3.57).

As it can be seen, the capability plots obtained between experimental and API loads are quite different, since API apparently overestimates the total loads especially for lateral force. Once the coefficients coming from the proposed enhanced methods are used instead of traditional preliminary design approach ones, the difference with experimental loads is reduced. This highlights the importance to have a reliable reproduction of the environmental loads during the early design phase.

Chapter 4

Thrust allocation strategies and thrusters modelling

Once a quasi-steady approach is adopted for an early design stage DP prediction, the thrust allocation logic becomes the most important algorithm involved in the vessel capability determination.

In fact, the allocation algorithm is responsible for the balance between external forces, including the environmental loads described in Chapter 3, and the on-board actuator ones. For such a reason, it is relevant to study more in detail the different possibilities that can be adopted to solve the thrust allocation problem. Besides, the fact that the thrust forces are developed by actuators that are mainly steerable or fixed thrusters, it is also important to take care of the thruster modelling, in order to estimate in a better way the effective thrust and absorbed power given by each propeller in working condition.

The aim of this part of the thesis is not to identify an universal allocation algorithm suitable to model all the issues related to the thrust modelling (thrust deduction, interactions with other thrusters or with appendages, ventilation, etc...), but to study the advantages and disadvantages given by possible different solutions in order to identify the best algorithm for each possible design situation that should be faced. In this chapter, after a brief description of simple allocation strategies that can be adopted in a really early design phase, more complex algorithm will be described, including a developed proposal for the so called *booster* allocation strategies aimed to saturate all the thrusters to investigate the effective upper capability limit of the system. All the presented thruster allocation algorithms have been implemented and tested on reference vessels to evaluate the differences between them on the DP capability plots.

Together with the allocation strategies, attention will be paid to the thruster modelling, studying two different approaches to evaluate the thruster behaviours in an effective working environment, considering a complex model based on a propeller working in cross-flow with a 4-quadrant modelling and a more simple method based on the bollard pull working point. For the complex model also thruster-thruster interactions will be modelled, comparing the obtained results with available model test measurements for a reference ship.

In the following sections, at first the propeller modelling methods will be described and then the allocation strategies will be discussed.

4.1   Thrusters modelling

The forces requested by DP system to keep the vessel in position, are usually given by a set of thrusters, which are located along the hull-bottom, according to structural and general arrangements constraints. By knowing the maximum thrust that should be generated for station keeping issues, the most suitable thruster typology can be selected. For big offshore units, the common choice is to use propulsion devices based on ducted propellers, the so called thrusters. The thrusters are not designed ad hoc for a single installation, but are available in standard sizes given by the producers. In Fig. 4.1 an example is given of standard thrusters [149] in Z-drive and L-drive configurations. This distinction has no effect in the modelling, since it is related only to the installation of the electrical or mechanical engine. An important distinction for the modelling is due to the adoption of a fixed pitch (FP) or a controllable pitch (CP) propeller. Another important distinction for the thruster modelling is studying the device as a fixed tunnel thruster or a steerable one, in any case, both of them can by either equipped with FP or CP propellers.

For applications some special devices can be used as actuators, like Voith-Schneider cycloidal propulsors or pump-jets. Also the main propellers, acting in combination with the rudders can be used as actuators, however, in this study, the focus has been given to thrusters only.

4.1.1   Open water characteristics

To consider the behaviour of a thruster, different conditions must be taken into account: the open water condition, the cross-flow condition, the behind hull condition and the interaction condition.
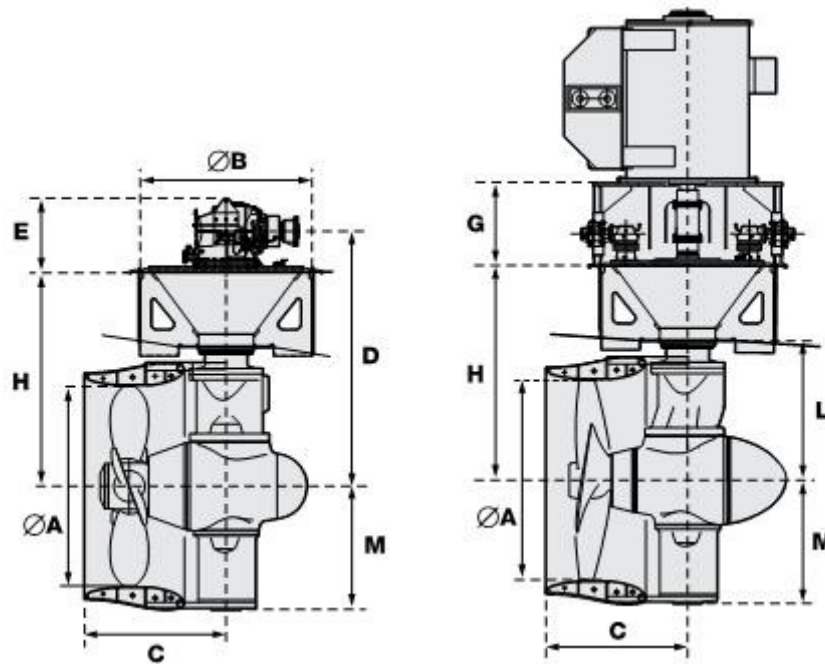
Figure 4.1: Example of steerable thruster in Z-drive (*left*) and L-drive (*right*) configuration
[149]

To evaluate the open water characteristics of a propeller, the numerical/analytical methods or experimental tests in uniform flow can be used. Within the present study, despite cross-flow conditions, the loads acting on the propeller have been considered stationary. This is an essential assumption for any further consideration.

Both for a full scale and for a model scale propeller, the most important characteristics are:

- *Geometric characteristics*: are the principal dimensions and the geometry of the propeller, including also the inclination between propeller axis and incoming flow.

- *Kinematic characteristics*: are the advance speed and the revolutions, including also the non-dimensional coefficients correlated to them and to geometric parameters.

- *Dynamic characteristics*: represent the forces delivered by the propeller (thrust and torque), considered as mean value during one propeller revolution.

A propeller advances in a fluid rotating at the same time; the two movements are independent and simultaneous. The motion along propeller axis occurs at the advance speed V_A while the rotation around the same axis is at an angular velocity $\omega_p = 2\pi n$, where n is the propeller rotation rate expressed in revolution per seconds. If the propeller would advance in the fluid like a screw threaded into the nut, then in a round it would advance of its geometric pitch P.
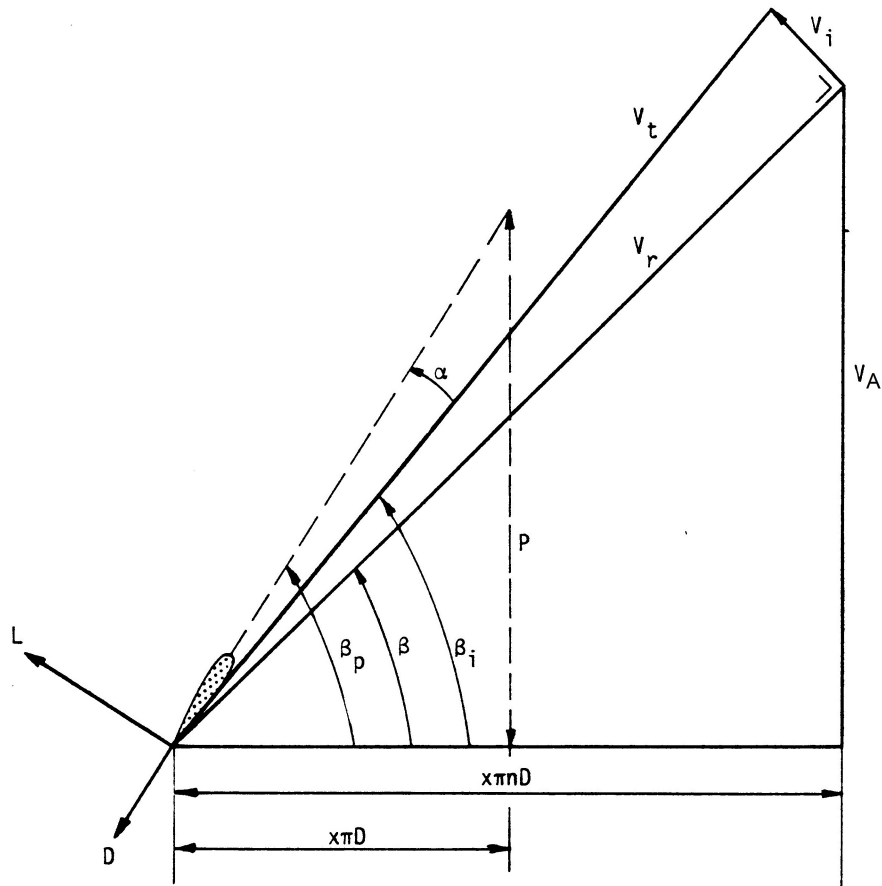
Figure 4.2: Direction of undisturbed inflow at a propeller section [77]

Because of the changes of the flow due to induced velocities V_i (axial u_a, circumferential u_θ and radial u_r components) generating an axial acceleration and a deceleration of the rotational flow behind the propeller, the propeller translates of a smaller amount.

The effective distance covered by the propeller during a single rotation is called linear or absolute advance h_p. This is described by the advance speed V_A and by the propeller rotational period $T_P = 1/n$ according to the following expression:

$$h_P = V_A T_P = \frac{V_A}{n} \tag{4.1}$$

From these considerations, the principal fundamental kinematic parameter of the propeller, the advance coefficient, can be defined:

$$J = \frac{h_P}{D} = \frac{V_A}{nD} \tag{4.2}$$

The relative advance coefficient allows to define the hydrodynamic pitch angle β at a certain blade radius, defining the flow direction on the considered blade element:

$$\tan \beta = \frac{V_A}{\omega_p r} = \frac{V_A}{x\pi n D} = \frac{J}{x\pi} \tag{4.3}$$

where the non dimensional section radius x is defined as r/R, being $R = D/2$. The definition of this angle will be then used for the four quadrant condition.

The propeller section has to act as a wing section relative to the undisturbed inflow. So the blade sections have a certain angle of attack with respect to the inflow velocity V_r, which angle is the propeller pitch angle β_p. The hydrodynamic pitch angle β is proportional to the advance coefficient J, which is a combination of the propeller pitch P and the circumferential distance over one revolution $x\pi D$.

If there were no disturbances, the angle of attack at which the blade section operates will be the difference between β and β_p. However, an important factor for the real inflow angle is the induced velocity V_i (see Fig. 4.2).This velocity, generated by the influence of other blade sections or by other blades and the wake behind the propeller, can be considered, as first assumption for moderately loaded propellers [81], perpendicular to V_r. The actual inflow velocity of the blade section is therefore the velocity V_t at an induced hydrodynamic pitch angle β_i. For thin profiles the lift L of the propeller section is proportional to the angle of attack $\alpha = \beta_p - \beta_i$ (except for cambered sections, where zero lift angle α_0 should be added) and is perpendicular to V_t. The drag is also dependent on the angle of attack, but in a more complicated manner. However, drag is considerably smaller than lift. The combination of lift and drag at the different radii, results in the propeller thrust and torque:

$$T = Z \int_{r_h}^{R} dT dr = Z \int_{r_h}^{R} \frac{1}{2}\rho C_L V_r^2 c \cos \beta_i \left(1 - \epsilon \tan \beta_i\right) dr \tag{4.4}$$

$$Q = Z \int_{r_h}^{R} dQ dr = Z \int_{r_h}^{R} \frac{1}{2}\rho C_L V_r^2 c \sin \beta_i \left(1 - \epsilon \tan \beta_i\right) r dr \tag{4.5}$$

where r_h is the hub radius, $\epsilon_h = dD/dL$ is the inverse of the hydrodynamic efficiency of a wing section and dL and dD are the wing profile lift and drag forces.

It is usual to represent the results of thrust and torque determination (by means of calculation or experiments) in the so called *open water curves*. The form in which open water results are given is conventionally a non-dimensional open water representation, in which thrust coefficient K_T and torque coefficient K_Q are plotted against J. The non-dimensional coefficients are obtained

as follows:

$$K_T = \frac{T}{\rho_w n^2 D^4} \tag{4.6}$$

$$K_Q = \frac{Q}{\rho_w n^2 D^5} \tag{4.7}$$

In the same diagram also the open water efficiency of the propeller can be represented. Open water efficiency is defined as the ratio of power supplied to the shaft and the power delivered by the propeller, resulting in the following formulation:

$$\eta_0 = \frac{T V_A}{2\pi Q n} = \frac{K_T}{K_Q} \frac{J}{2\pi} \tag{4.8}$$

This is the standard way to present the dynamic characteristics of a propeller, however other representations have been used in the past in order to include more propellers in one diagram. This is the case of the systematic series propeller design diagrams, as the famous $B_p - \delta$ and $B - \mu - \delta$ [78] for the Wageningen B-series propellers [139, 79], or the equivalent Papmel diagrams [115].

The thrusters are not conventional propellers but are equipped with a duct, so their behaviour will be similar to ducted propellers. In such a case the total thrust T should be divided into propeller component $T_p r$ and nozzle component T_n [85]. Usually the non-dimensional coefficient of the total thrust is given as per equation (4.6), but, additionally, also the thrust of the nozzle can be separately non-dimensionalised:

$$K_{Tn} = \frac{T_n}{\rho_w n^2 D^4} \tag{4.9}$$

In such a case the efficiency is still evaluated using equation (4.8), considering a K_T for propeller plus nozzle. There are different kinds of nozzles available in literature, however the most commonly used are the accelerating ones and principally the ones named: 19A, 22, 24 and 37. One of the most important parameters is the length ratio, between the nozzle length L_d and the inner propeller diameter D. Another parameter to take into account is the contraction ratio, i.e. the ratio between inflow and outflow areas, represented also as the duct section angle α_d. The mostly used duct is the 19A one, having an L/D ratio of 0.5 and a shape characterised by straight output section. Nozzles 22 and 24 have a L/D ratio of 0.8 and 1.0 respectively, being indicated for applications where bollard pull characteristics are really relevant. However astern performances are poor for these nozzles. Once also the bollard pull in astern condition is of utmost importance, then nozzle 37 can be a suitable solution, having a more symmetrical profile

between inflow and outflow.

Since it has not been planned to develop a calculation method to directly calculate the thrust and torque of a thruster and no model test has been scheduled, a first estimate of systematic series available in literature should be used, where data could be easily adopted inside a DP prediction program.

4.1.2 Polynomials

To overcome the necessity of iterative readings on design diagrams during the propellers selection process, data coming from systematic series have been grouped into regression available in polynomial form [109, 110]. This has been done at first with the B-series propellers, however those propellers are not suitable to simulate a thruster, which means that other series should be used to represent a thruster, distinguish also between the behaviour of a FP or a CP thruster.

Fixed pitch thruster

Systematic series have been developed also for ducted propellers [85][107]. The development by NSMB (now MARIN) was starting from a propeller different from B-series one, differences mainly due to the blade contour, which had a finite length at the tip. The blade contour was typical for designs made by *Kaplan*, consequently the propeller has been named K-propeller. This FP propeller was equipped both with an accelerating and a decelerating duct, leading to the definition of the K_a and K_d propeller. For practical uses the accelerating duct have been widely used, so the K_a series is considered as an extension of the B-series for ducted propellers.

The dynamic characteristics of the K_a series have been presented by means of regression equations [108] in the following form:

$$K_T = \sum_{j=0}^{6} \sum_{i=0}^{6} A_{j,i} \, (P/D)^j \, J^i \tag{4.10}$$

$$K_{Tn} = \sum_{j=0}^{6} \sum_{i=0}^{6} B_{j,i} \, (P/D)^j \, J^i \tag{4.11}$$

$$K_Q = \sum_{j=0}^{6} \sum_{i=0}^{6} C_{j,i} \, (P/D)^j \, J^i \tag{4.12}$$

where the coefficients are only function of pitch ratio P/D and J; $A_{i,j}$, $B_{i,j}$ and $C_{i,j}$ coefficients are function of the nozzle type. That means multiple regressions are needed to describe the
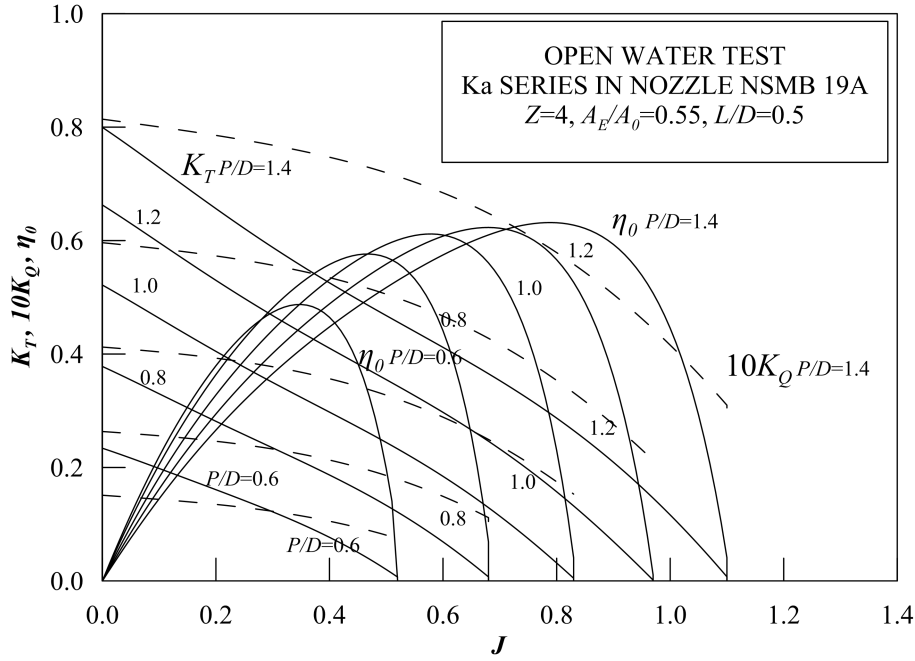
Figure 4.3: Open water diagrams for K_a4-55 sub-series

whole series, while the above equations are valid for a single Z and A_E/A_0. In the NSMB proposal no cross fairing has taken place between the different diagrams as done for B-series regressions. For the same series, another regression model has been proposed [155], resulting more similar to B-series regression model:

$$K_T = \sum a J^p \, (P/D)^q \, (A_E/A_0)^r \tag{4.13}$$

$$K_{Tn} = \sum a_1 J^{p_1} \, (P/D)^{q_1} \, (A_E/A_0)^{r_1} \tag{4.14}$$

$$K_Q = \sum a_2 J^{p_2} \, (P/D)^{q_2} \, (A_E/A_0)^{r_2} \tag{4.15}$$

where the coefficients are also function of the expanded area ratio. Coefficients a, p, q and r are varying also according to the nozzle type. In Fig. 4.3 an open water design charts obtained from regression equation is presented for a sub-series of K_a propellers. However, the reproduction of a steerable thruster requires another step. In fact, the K_a propellers have not been studied and tested as thruster unit but as standard ducted propeller to be fitted on a shaft line. Moreover, the nozzles used on commercial thrusters are not equal to standard ones. That lead to a difference between the open water curve of a single propeller and the open water curve of a thruster. Corrections can be made to the open water characteristics of a ducted propeller [59, 86], to take into account the additional drag given by the thruster housing and the differences in dynamic
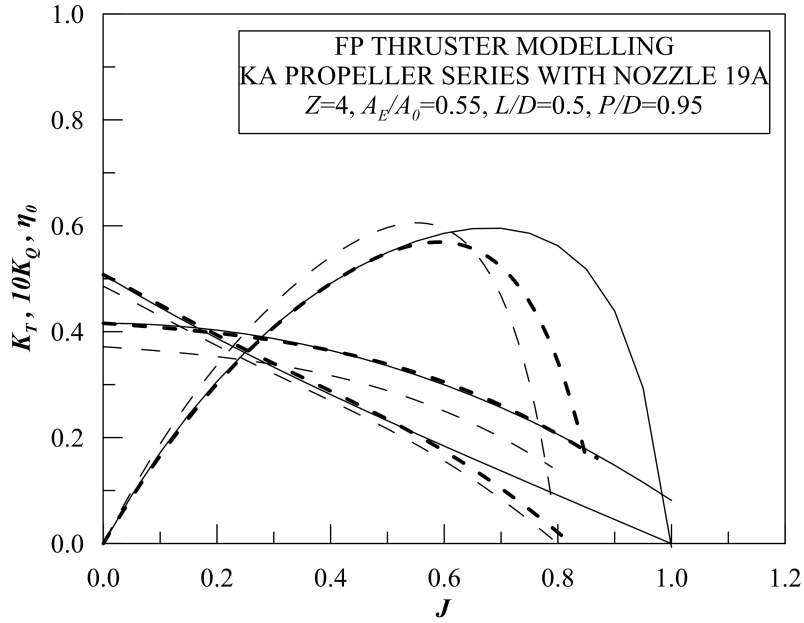
Figure 4.4: Open water curve of a commercial thruster (*continuous*), a K_a propeller (*dotted*)

and a K_a propeller with corrections (*bold-dotted*)

coefficients between units and propeller. The corrections can be written in the following form:

$$\lambda_T = \frac{K_T}{K_{T_0}} \tag{4.16}$$

$$\lambda_Q = \frac{K_Q}{K_{Q_0}} \tag{4.17}$$

$$e_T = \left. \frac{J}{J_0} \right|_{K_T} \tag{4.18}$$

$$e_Q = \left. \frac{J}{J_0} \right|_{K_Q} \tag{4.19}$$

where the terms indexed with $_0$ denote the values related to the systematic series polynomials. λ_T is representative of a correction factor for the bollard pull value of K_T, λ_Q is a correction for the bollard pull value of K_Q, while e_i factors are coefficients used to modify the J range, that can vary between thrust and torque. In Fig. 4.4 an example is given, comparing the open water curve of a commercial thruster with the open water curve obtained applying the before mentioned corrections to a K_a propeller having the same main geometric characteristics of the thruster propeller. As it can be seen, adopting the corrections, it is possible to reproduce quite well the thruster behaviour in the stable part of the characteristic open water curve, which is the part used for traditional powering predictions.

For DP purposes it is proposed to consider, as first approximation, the description of the bollard
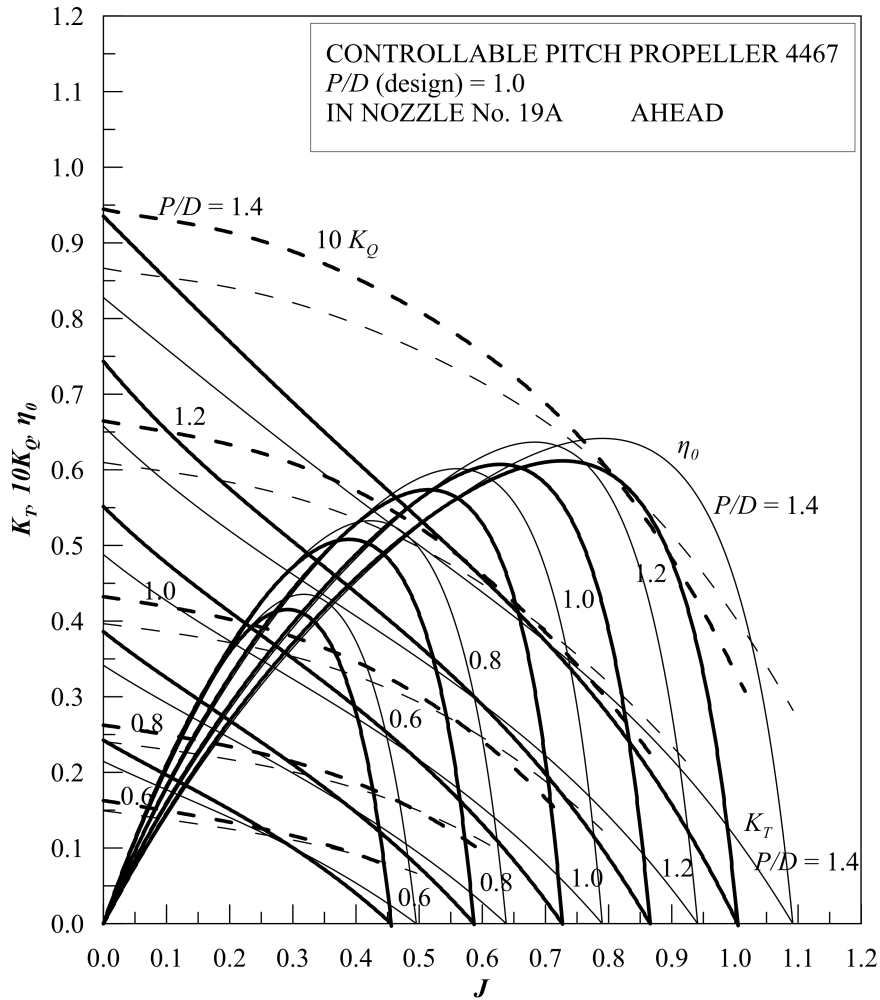
Figure 4.5: Open water curve of K_{cp} propeller (*dotted*) and a K_{cp} thruster (*continuous*) with corrections

pull conditions as significant for station-keeping operations [88]. Then, starting from open water diagram, it is possible to extract the T and Q curves for bollard pull condition and obtain a thrust-power relationship in the following form:

$$P_T = \frac{a}{D} T^b \tag{4.20}$$

where D is the propeller diameter and a and b are regression coefficients for the bollard pull condition.

Controllable pitch thrusters

The modelling of CP thrusters is not equal to FP ones. In the literature there are not many examples on systematic tests for CP propellers. The most suitable one is given by the so called K_{cp} propellers [77], composed by two propellers with a geometry close to that of $K_a 4$-55

propeller. One propeller, named 4467, had a uniform pitch and a pitch ratio of 1.0, the other one (4468) had zero pitch at all radii, suitable to simulate propellers which had to operate in both directions.

Also formulations for K_{cp} polynomials can be obtained from the open water diagrams, in the following form:

$$K_T = \sum_{i=0}^{6} A_i J^i \tag{4.21}$$

$$K_{T_n} = \sum_{i=0}^{6} B_i J^i \tag{4.22}$$

$$K_Q = \sum_{i=0}^{6} C_i J^i \tag{4.23}$$

where A_i, B_i and C_i are polynomial formulations expressed as a function of the P/D. Regarding the modelling of a CP thruster, the same assumptions and corrections described for the FP thruster can be considered valid. In this way, adopting corrections according to equations (4.16)-(4.19) the open water characteristics of a CP thruster can be evaluated. An example is given in Fig. 4.5. In this case regression can be made as for the FP propeller to simulate the bollard pull configuration with equations having the same formulation of equation (4.20).

Moreover, the K_{cp} propellers have also measurements for the behaviour in astern condition. This is particularly indicated to describe the behaviour of a tunnel thruster.

4.1.3 Four quadrants representation

The thrusters, while operating in DP, are not always working in bollard pull condition or in the positive J range as described in the previous section. Due to the presence of a current and considering the different rotation rates of the thruster, all the combinations between the direction of the propeller and the inflow can occur. To study those particular operational conditions, all the possible algebraic combinations between V_A and n must be considered, those kinematic characteristics can be equal, smaller or greater than zero. That means the complete diagrams in the four quadrants are needed, distinguishing between the following four conditions:

- Positive rotation rate and positive inflow speed

- Negative rotation rate and positive inflow speed

- Negative rotation rate and negative inflow speed
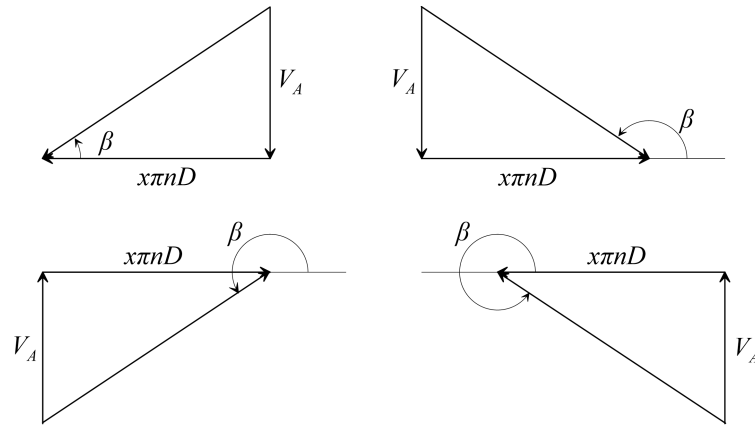
Figure 4.6: Velocity triangles for the first (*top left*), second (*top right*), third (*bottom left*) and fourth (*bottom right*) quadrant

Table 4.1: Operational modes of a propeller in the four quadrants

Quadrant	Advance angle	Advance coefficient	Advance speed	Propeller rotation
I	$0 < \beta \leq 90$	$J > 0$	$V_A > 0$	$n > 0$
II	$90 < \beta \leq 180$	$J < 0$	$V_A > 0$	$n < 0$
III	$180 < \beta \leq 270$	$J > 0$	$V_A < 0$	$n < 0$
IV	$270 < \beta \leq 360$	$J < 0$	$V_A < 0$	$n > 0$

- Positive rotation rate and positive inflow speed

Since both rotation rate and advance speed of the propeller can be zero during the transition from one condition to another, the non-dimensional coefficient used for open water diagrams becomes meaningless. In fact, when rotation rate is zero, then J (eq. (4.2)) and the dynamic coefficients (eqs. (4.6), (4.7)) become infinite. When V_A is zero, then the efficiency becomes zero and has no meaning for the judgement of e.g. the bollard pull. That means other parameters should be used for the judgement of these conditions.

The four mentioned conditions can be expressed as function of the hydrodynamic pitch angle β (eq. 4.3) of the propeller. An overview of the possible situations is given in Table 4.1. With reference to Fig. 4.6, the four quadrant behaviour can be better described. In the top left diagram, both rotation rate and propeller inflow velocity are positive, being representative of the *first quadrant*. In the top right diagram, the speed remains positive, while propeller rotation is reversed. In such cases the β is between 90 and 180 degrees and is usually referred as *second*

quadrant. The left bottom diagram is representative of the *third quadrant* where both rotation and inflow are negative. This condition can be also indicated as *astern* condition [77]. Finally the bottom right diagram represents the *fourth quadrant* with positive rotation rate and negative inflow.

It is usual to adopt as reference the radius corresponding to $0.7R$, evaluating β at this reference:

$$\tan \beta = \frac{V_A}{0.7\pi n D} \tag{4.24}$$

which is defining the angle of the inflow velocity, while its magnitude is given by:

$$V_r = \sqrt{V_A^2 + (0.7\pi n D)^2} \tag{4.25}$$

Adopting this velocity, the thrust and the torque can be non-dimensionalised in the following way:

$$C_T = \frac{T}{1/2\rho V_r^2 A_0} = \frac{8}{\pi} \frac{T}{\rho_w V_r^2 D^2} \tag{4.26}$$

$$C_{Tn} = \frac{8}{\pi} \frac{T_n}{\rho_w V_r^2 D^2} \tag{4.27}$$

$$C_Q = \frac{8}{\pi} \frac{Q}{\rho_w V_r^2 D^3} \tag{4.28}$$

Also the four quadrant representation of the K_a series can be expressed in polynomial forms [108], adopting a 20 terms Fourier polynomial function of β:

$$C_T = \sum_{k=1}^{20} (a_k \cos k\beta + b_k \sin k\beta) \tag{4.29}$$

$$C_{Tn} = \sum_{k=1}^{20} (a1_k \cos k\beta + b1_k \sin k\beta) \tag{4.30}$$

$$C_Q = \sum_{k=1}^{20} (a2_k \cos k\beta + b2_k \sin k\beta) \tag{4.31}$$

where a and b coefficients are given for different P/D, A_E/A_0 and nozzle type. In Fig. 4.7 the four quadrant behaviour of a sub-series is represented, considering also the interpolation between different P/D. It is important to observe that the thrust coefficient is not affected too much by the changes in P/D, but on the contrary, the torque coefficient is strongly influenced by the pitch changes. The nozzle is affected by P/D change mostly between $-20 < \beta < 20$, which is the area of interest for dynamic positioning operations.
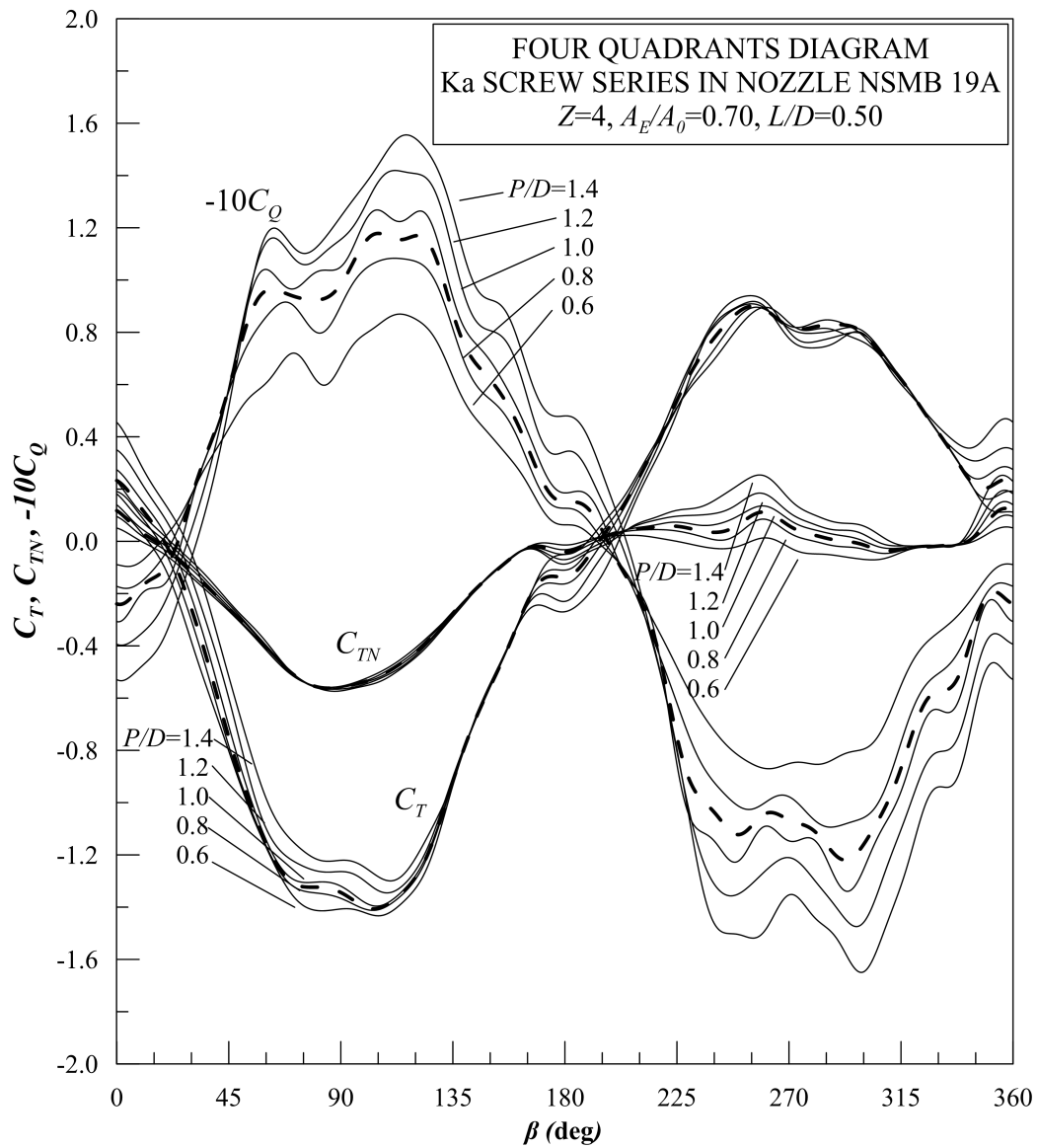
Figure 4.7: Four quadrant representation of Sub-series K_a4-70, with interpolation between P/D (*dotted*)

Cross-flow modelling

Usually, when performing open water test, the advance speed V_A is supposed to be perpendicular to the propeller disc. In such a case the developed thrust is completely oriented in the propeller axis direction. An azimuthal thruster will not always act in this kind of situation, especially during operations in areas characterised by the presence of a strong current.

Being the thrusters oriented in such a way to balance forces and moments acting on the vessel, it is not true that they are always oriented with the current direction. That means the propeller will work in transversal cross-flow, leading to a dis-alignment δ between thruster orientation and current one. In such a way, a transversal force is generated, resulting in a different orientation
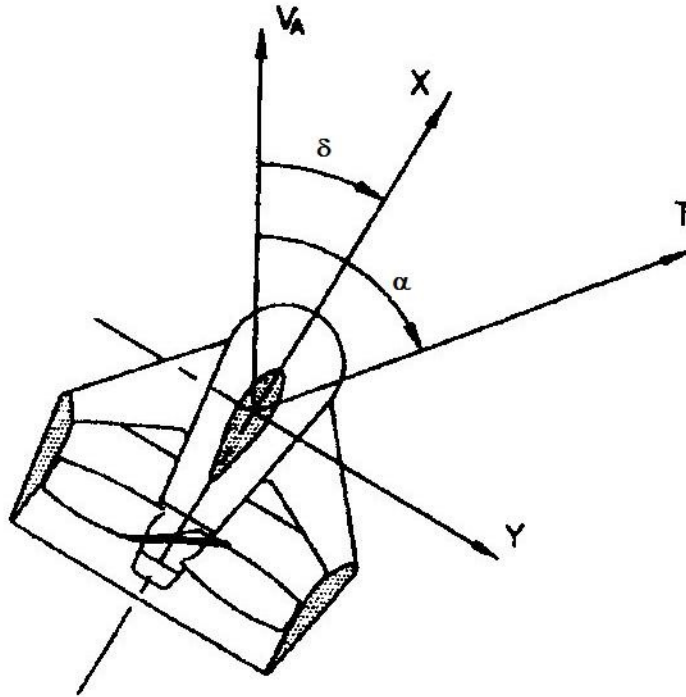
Figure 4.8: Reference system for a thruster in cross-flow [25]

of the generated thrust, which will be no more collinear with thruster axis but is misaligned of an angle α with respect to the main stream direction (see Fig. 4.8), modifying also the thrust intensity.

Considering a thruster rotating clockwise, the following dimensional parameters can be identified as function of the relative orientation δ between thruster and incoming flow:

  - Longitudinal force X acting in thruster axis direction

  - Transversal force Y acting in the thruster axis perpendicular direction

  - Moment M_Z generated on the thruster centre of rotation

  - Absorbed torque Q

Thanks to experimental tests [108], those quantities were measured and published for propeller K_a4-70 with a P/D of 1.00. The results, presented in non-dimensional form, have been reported in the 4 quadrants representation:

$$C_X = \frac{8}{\pi} \frac{X}{\rho_w V_r^2 D^2} \tag{4.32}$$

$$C_Y = \frac{8}{\pi} \frac{Y}{\rho_w V_r^2 D^2} \tag{4.33}$$

$$C_{M_Z} = \frac{8}{\pi} \frac{M_Z}{\rho_w V_r^2 D^3} \tag{4.34}$$

$$C_Q = \frac{8}{\pi} \frac{Q}{\rho_w V_r^2 D^3} \tag{4.35}$$

The obtained coefficients are functions of δ and β. The study was performed specifically to study the behaviour of a ducted propeller, so all the experiments were limited to I and IV quadrants, which are properly the operating fields of a thruster during DP operations. Therefore, the study has been restricted to the β range between -90° and 90°. To evaluate the behaviour of the propeller in cross-flow by means of an analytical solution, it is convenient to consider a variable inflow speed as function of δ [108] as:

$$V_A^* = V_A \cos \delta \tag{4.36}$$

in this case, a fictitious angle of advance β^* can be defined:

$$\tan \beta^* = \frac{V_A^*}{0.7\pi nD} \tag{4.37}$$

Under those assumptions, it is possible to derive formulations for x direction thrust and torque coefficients starting directly form polynomial coefficients expressed in equations (4.29) and (4.31) for C_T and C_Q:

$$C_X^* (\beta^*) = C_T (\beta^*) f \tag{4.38}$$

$$C_Q^* (\beta^*) = C_Q (\beta^*) f \tag{4.39}$$

where f has the following formulation:

$$f = \frac{\tan^2 \beta^* \cos^2 \delta + 1}{\tan^2 \beta^* + 1} \tag{4.40}$$

However, this approach cannot be used to evaluate the transversal force Y and the moment M_Z. Then, this kind of modelling is suitable only when the Y force can be supposed small enough not to influence the total thrust magnitude. This assumption can be considered valid only for small values of δ. The moment M_Z can be considered negligible, since the distance from the propeller disc to the thruster rotation axis is much lower than the moment lever of the thruster with respect to origin O.

If Y force cannot be neglected, then, assuming that the thruster has characteristics similar to a K_a4-70 propeller with P/D close to 1.00, the experimental curves can be directly used, and the total thrust magnitude and direction could be evaluated:

$$T^* = \sqrt{X^2 + Y^2} \tag{4.41}$$
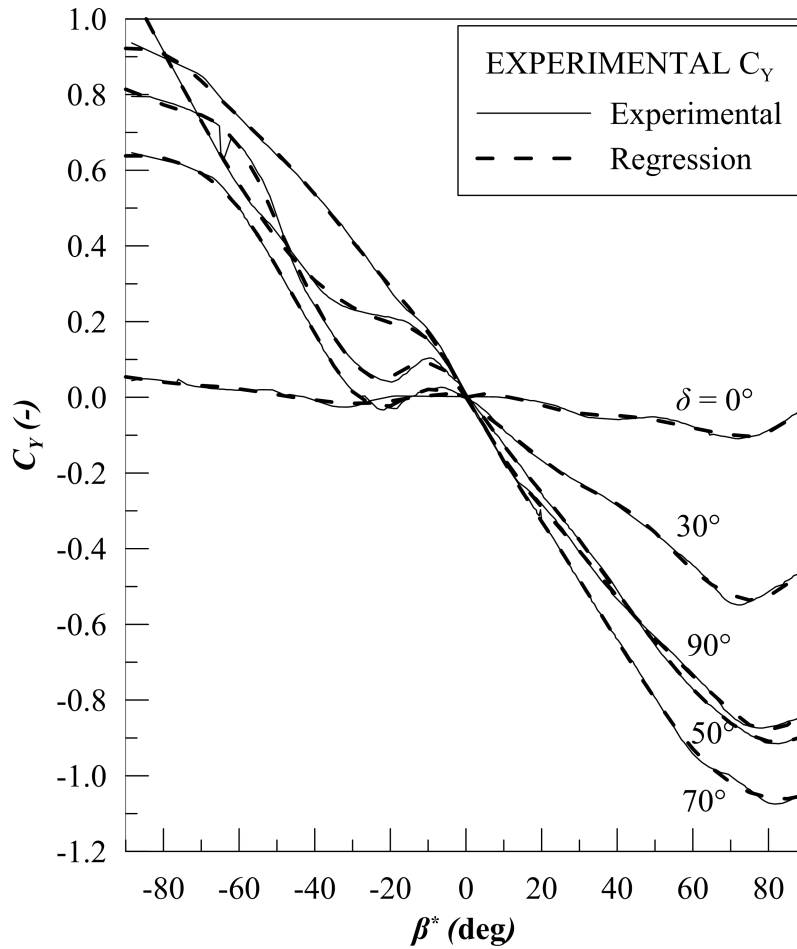
Figure 4.9: Reproduction of experimental C_Y coefficients for K_a4-70 propeller

$$\tan \alpha = \frac{Y}{X} \tag{4.42}$$

As it can be seen in Fig. 4.10, the thrust amount at each fictitious hydrodynamic pitch angle β^* changes its shape compared to standard bollard pull condition ($\beta = 0°$). Moreover, the thrust coefficient changes also with δ angle. The results obtained for α can be visualised in Fig. 4.11, highlighting that the thrust direction can be changed up to 30° during conditions suitable for station keeping problem. The proposed model, due to the simplicity of the analytical formulation, is not adequate for the whole set of β, in all four quadrants. However, the procedure is stable for a β range from -20° to 20°, which can be considered acceptable for DP operations.

4.1.4 Thruster-thruster interaction

The modelling described in the previous sections is supposing that a thruster operates in an uniform inflow. However, since thrusters are disposed also close to each other or in presence of certain appendages (e.g. skegs), it can happen that, for certain orientation angles, they will act
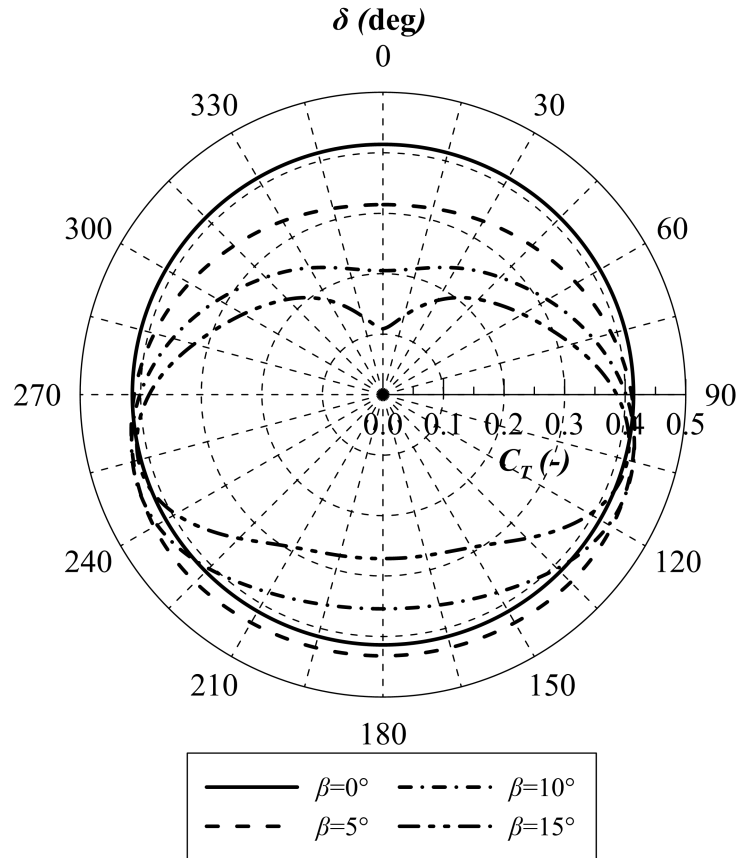
Figure 4.10: C_T at different β angles as function of δ for a K_a4-70 propeller

in a disturbed flow. Then, a propeller acting in a cross-flow disturbed by the action of another device or of a significant appendage could have a drastic reduction in the maximum deliverable thrust with a constant absorbed power.

To model this kind of propeller loss, an analytical model [25] aimed to reproduce the thrust loss between two closely spaced azimuth thrusters will be used. Here the procedure for two thrusters has been reproduced and extended to three thrusters case, which is a realistic case for most the operative offshore vessels, and has been also extended to the evaluation of appendages effect. The method supposes that the foremost thruster is acting in open-water condition, while the thrusters behind it are influenced according to their reciprocal position. Once a thruster is oriented directly in the wake-flow of another one, the inflow velocity can be evaluated as:

$$V_r = \frac{1}{2}\left(V_A \left(2\cos\delta - 1\right) + \sqrt{V_A^2 \left(2\cos\delta - 1\right)^2 + \frac{4kX}{\rho_w A_0}} \right) \tag{4.43}$$
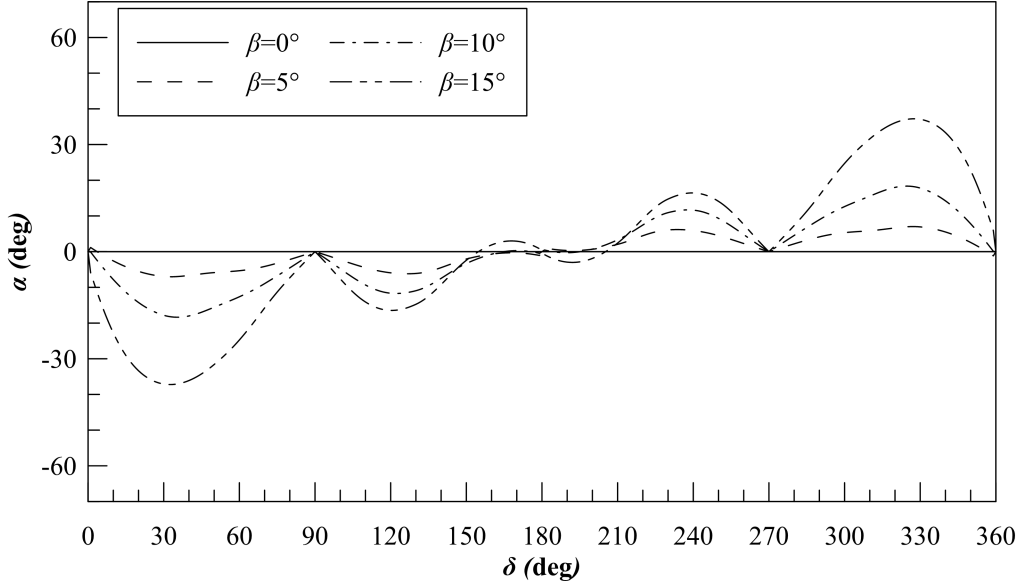
Figure 4.11: Deviation between thrust direction and thruster orientation for a K_a4-70 propeller

where A_0 is the propeller disc area and k is the *run coefficient* assumed equal to 0.43. By changing V_r, also the hydrodynamic pitch angle is changing, resulting in:

$$\tan \beta_{PR} = \frac{1}{2}\left(\tan \beta \left(2 \cos \delta - 1\right) + \sqrt{\tan \beta \left(2 \cos \delta - 1\right)^2 + \frac{2kC_X^*}{\cos^2 \beta}} \right) \tag{4.44}$$

Then a velocity ratio can be defined:

$$R_V = \frac{V_A}{V_R} = \frac{\tan \beta}{\tan \beta_{PR}} \tag{4.45}$$

denoting the ratio between the advance of the thruster acting in open water and one acting in full interaction with the first one. However, if the thrusters are oriented in different directions, the portion of propeller disc area of the in-wake thruster should be determined. This can be done modelling the wake of the first thruster according to a cylindrical model [5] using an auxiliary reference system with origin on the second thruster centre of rotation. Under these assumptions, the wake trajectory can be expressed as:

$$\bar{x}_R = \frac{e^{\bar{y}_R}\left|\tan \frac{\zeta_0}{2}\right|}{2} + \frac{1}{2e^{\bar{y}_R}\left|\tan \frac{\zeta_0}{2}\right|} - \frac{1}{\sin \zeta_0} \tag{4.46}$$

where:

$$\bar{x}_R = -R_V^2 \frac{2C_N}{\pi} \frac{x_R}{D} \tag{4.47}$$

$$\bar{y}_R = -R_V^2 \frac{2C_N}{\pi} \frac{y_R}{D} \tag{4.48}$$
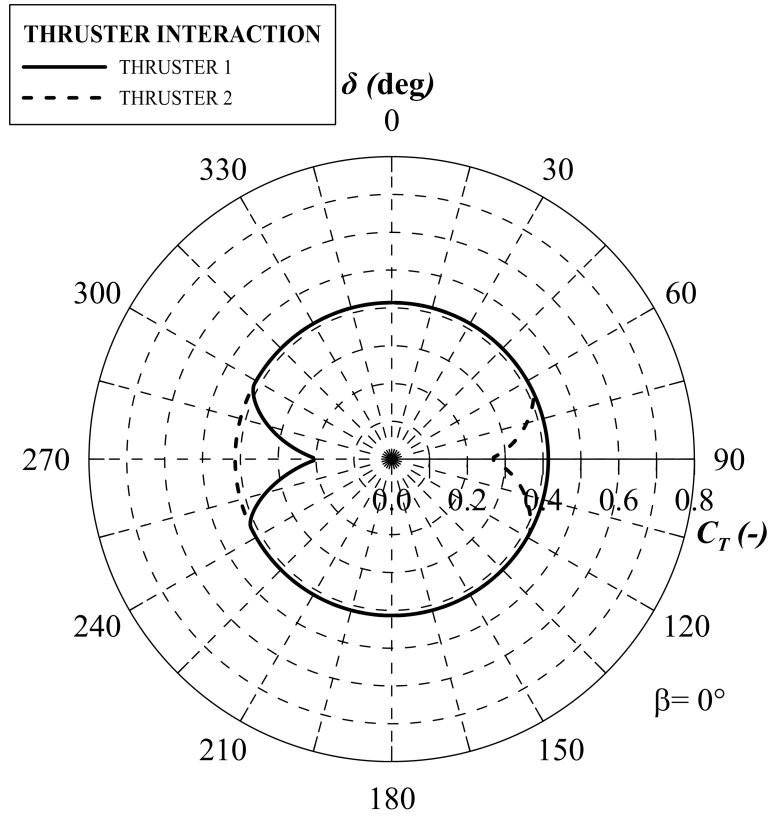
Figure 4.12: C_T for two thrusters considering interaction effects with $\beta = 0°$
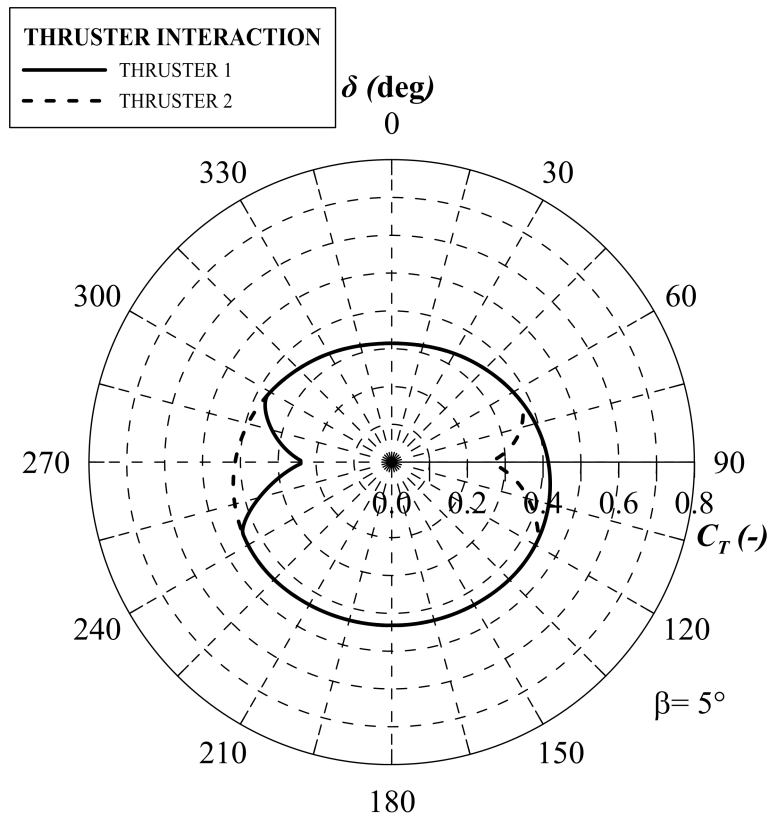
Figure 4.13: C_T for two thrusters considering interaction effects with $\beta = 5°$
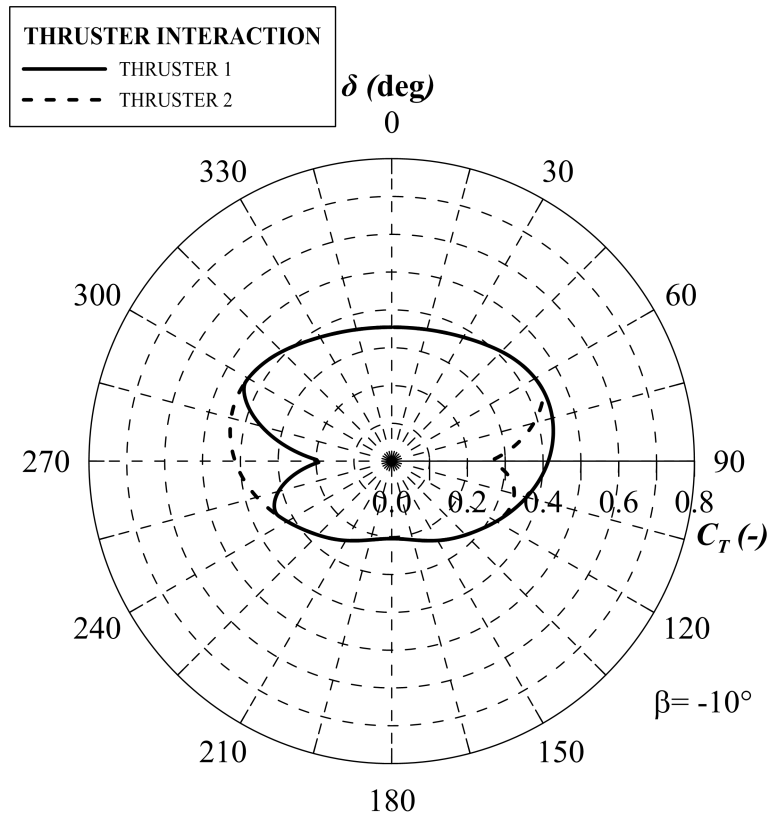
Figure 4.14: C_T for two thrusters considering interaction effects with $\beta = -10°$
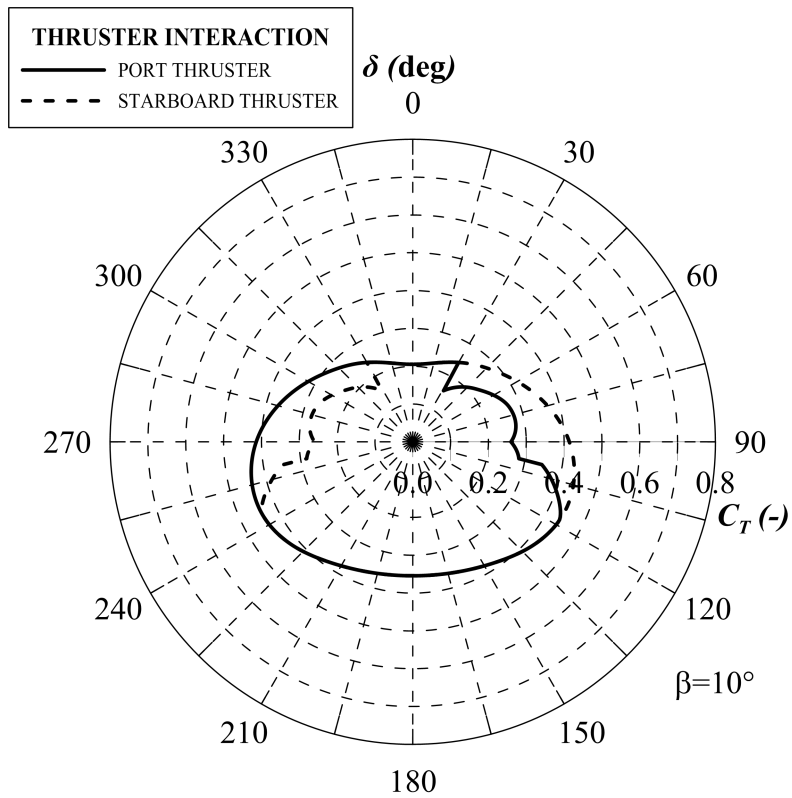
Figure 4.15: C_T for two thrusters with the presence of a skeg, for $\beta = 10°$
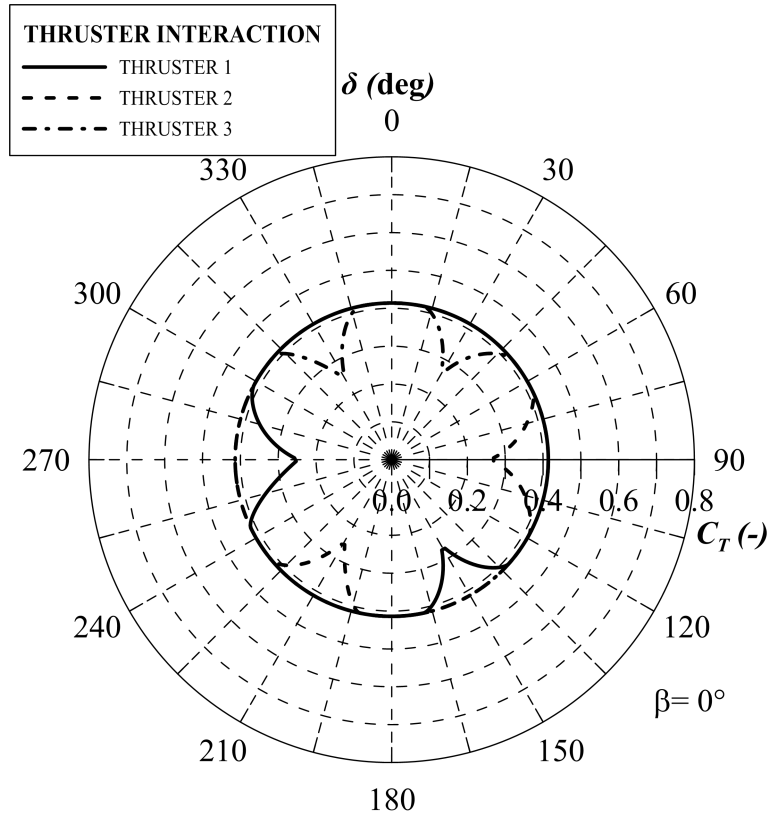
Figure 4.16: C_T for three thrusters considering interaction effects with $\beta = 0°$
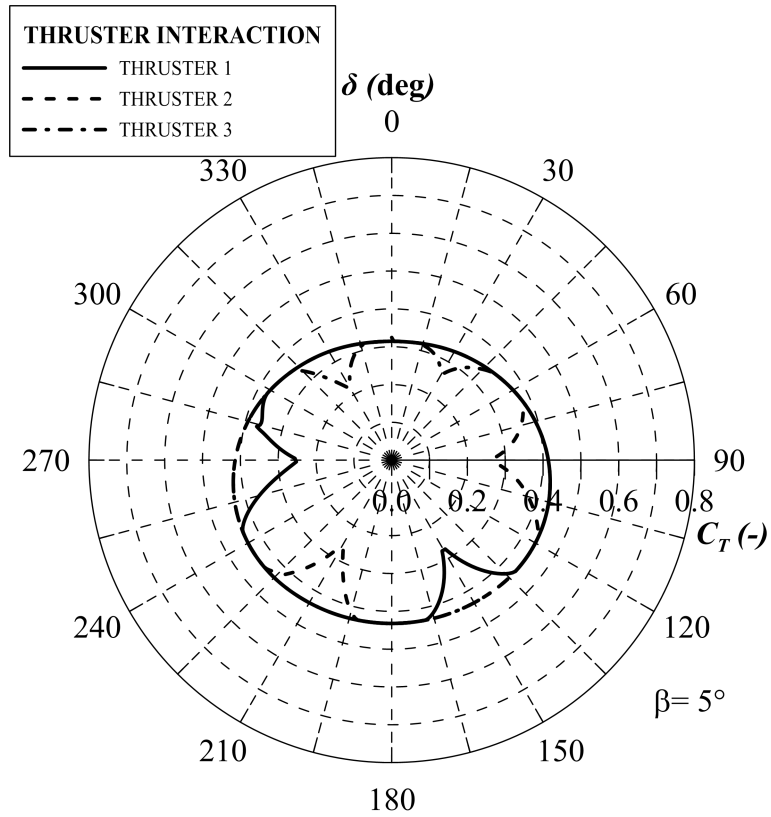
Figure 4.17: C_T for three thrusters considering interaction effects with $\beta = 5°$

being C_N an integration constant equal to 1.2 and ζ_0 the outflow direction from the first thruster with respect to propeller disc.

Finally, the interaction grade can be determined using the following formulation:

$$\xi = \frac{1}{2\pi} \left((\lambda_D - \sin \lambda_D) + \left(\frac{D_R}{D_D} \right)^2 (\lambda_R - \sin \lambda_R) \right) \tag{4.49}$$

where:

$$\cos \frac{\lambda_D}{2} = \frac{4e^2 + D_D^2 - D_R^2}{4eD_D} \tag{4.50}$$

$$\cos \frac{\lambda_R}{2} = \frac{4e^2 + D_R^2 - D_D^2}{4eD_R} \tag{4.51}$$

D_R and D_D are the open water and disturbed thruster diameter respectively. From the interaction grade ξ it is then possible to evaluate the effective forces delivered by the thruster in disturbed flow:

$$X = \xi (X_R - X_D) + X_D \tag{4.52}$$

$$Y = \xi (Y_R - Y_D) + Y_D \tag{4.53}$$

According to this modelling it is possible to evaluate the behaviour of the thrusters in interaction. In Fig. 4.12 the condition having β equal to zero is presented for the two thrusters, in Fig. 4.13 the same is presented for β of 5° and in Fig. 4.14 for β of -10°. It can be observed that the behaviour of the thrust is the same as described for the propeller in cross-flow, despite for the interaction areas, which are captured in accordance with experiments [25]. In Fig. 4.15 the particular case of the presence of a skeg is presented. The model has been extended also to simulate the behaviour of three or more thrusters, evaluating all the interaction areas. An example is given for three thrusters for β equal to zero in Fig. 4.16 and in Fig. 4.17 the same is given for β of 5°.

4.2 Thrust allocation

To solve accurately the thrust allocation problem is of primary importance, i.e.,to determine the orientation of each thruster and the amount of thrust that each device must deliver. Due to the large number of the steerable devices, this problem is over-controllable. Each thruster can operate with different orientations and delivered thrust remaining inside the feasible region, leading to

an ambiguity in thrust allocation, or, in other terms, the system of equilibrium equations is over-determined. The possible solutions for this over-controllable problem can be determined by the use of optimisation algorithms, with different kind of cost functions, like minimal thrust usage or minimal fuel consumption and subjected to several constraints like thrust saturation and eventually the existence of forbidden zones.

In this work different allocation strategies with different levels of sophistication have been considered and developed with the scope to identify the most suitable one to increase the capability of the DP system in extreme sea states when all the thrusters are working close to saturation and a *booster allocation* is desirable.

Five different allocation strategies are here presented:

- groups logic approach;

- pseudo-inverse matrix approach;

- Lagrange multipliers optimisation;

- Fully non-linear optimisation;

- Booster allocation with genetic algorithms.

The first one is a simple way to solve the allocation problem by grouping the nearby thrusters to reduce the number of unknowns without optimising strategy. The second method is the most simple optimisation procedure used in DP but is not directly using an objective function. The third one is the most commonly adopted algorithm (together with quadratic programming) for DP calculations. The fourth one is a fairly complex method that allows to select the shape of the objective function and constraints, without limitations to the function formulation. The last one shows an alternative and powerful way to approach and solve the full non-linear optimisation problem.

4.2.1   Groups logic

The present method is a deterministic approach used to solve the thrust allocation problem. It is not using the optimisation techniques. The procedure is based on the appropriate grouping of several thrusters in order to reduce the number of unknown variables in the equilibrium equations.

The system that should be solved for the static equilibrium of a vessel with N_{ACT} thruster devices during station keeping is described by system (2.3). It is convenient to rewrite the system according to the thruster forces components in x and y directions, resulting in:

$$\begin{cases} \sum_{i=1}^{N_{ACT}} F_{x_i} = F_{x_{ENV}} + F_{x_{EXT}} \\ \sum_{i=1}^{N_{ACT}} F_{y_i} = F_{y_{ENV}} + F_{y_{EXT}} \\ \sum_{i=1}^{N_{ACT}} \left(-F_{x_i} y_{T_i} + F_{y_i} x_{T_i} \right) = M_{z_{ENV}} + M_{z_{EXT}} \end{cases} \quad (4.54)$$

In system (4.54) the unknowns are represented by the $2N_{ACT}$ forces components F_{x_i} and F_{y_i}. Whether three thruster groups are accurately chosen, system (4.54) becomes:

$$\begin{cases} \sum_{i=1}^{3} F_{x_{G_i}} = F_{x_{ENV}} + F_{x_{EXT}} \\ \sum_{i=1}^{3} F_{y_{G_i}} = F_{y_{ENV}} + F_{y_{EXT}} \\ \sum_{i=1}^{3} \left(-F_{x_{G_i}} y_{T_{G_i}} + F_{y_{G_i}} x_{T_{G_i}} \right) = M_{z_{ENV}} + M_{z_{EXT}} \end{cases} \quad (4.55)$$

where:

$$F_{x_{G_i}} = \sum_{j=1}^{N_{G_i}} F_{x_j} \quad (4.56)$$

$$F_{y_{G_i}} = \sum_{j=1}^{N_{G_i}} F_{y_j} \quad (4.57)$$

$$x_{T_{G_i}} = \frac{\sum_{j=1}^{N_{G_i}} x_{T_j}}{N_{G_i}} \quad (4.58)$$

$$y_{T_{G_i}} = \frac{\sum_{j=1}^{N_{G_i}} y_{T_j}}{N_{G_i}} \quad (4.59)$$

N_{G_i} the number of thruster devices in each group, provided that $\sum_{i=1}^{3} N_{G_i} = N_{ACT}$. Also the simplified system (4.55) is over-determined, because there are now six unknowns: the three $F_{x_{G_i}}$ and the three $F_{y_{G_i}}$. Under the assumption that all the forces in x direction are equally distributed between the groups [150], the equilibrium can be easily found.

Once the forces are determined, the thrust of each single device can be computed knowing the contribution of every thruster inside the group. One of the limitations of this approach is that all

the thrusters inside the same group will have the same orientation. Moreover, it is not ensured that all the thrusters will be saturated at the maximum available thrust, since the allocation stops once one of the groups is delivering more thrust than possible, when, probably the other groups are far from the saturation. This could lead to a underestimation of the final capability of the vessel.

4.2.2   Pseudo-inverse matrix

By increasing the allocation strategy complexity, the pseudo-inverse matrix approach [154] can be used, which is a simple optimisation technique. To use this method, it is convenient to write system (4.54) in matrix form:

$$\begin{pmatrix} 1 & \cdots & 1 & 0 & \cdots & 0 \\ 0 & \cdots & 0 & 1 & \cdots & 1 \\ -y_{T_1} & \cdots & -y_{T_{N_{ACT}}} & x_{T_1} & \cdots & x_{T_{N_{ACT}}} \end{pmatrix} \begin{pmatrix} F_{x_1} \\ \vdots \\ F_{x_{N_{ACT}}} \\ F_{y_1} \\ \vdots \\ F_{y_{N_{ACT}}} \end{pmatrix} = \begin{pmatrix} F_{x_{ENV}} + F_{x_{EXT}} \\ F_{y_{ENV}} + F_{y_{EXT}} \\ M_{z_{ENV}} + M_{z_{EXT}} \end{pmatrix}$$

$$(4.60)$$

In this way the system (4.60) is of the classical form $\mathbf{Ax} = \mathbf{b}$, where $\mathbf{A}$ is a $(3 \times 2n)$ matrix. Since the rank of the matrix A is at most 3, the system (4.60) is under-determined, which means that it has infinite possible solutions. The solution with minimal norm can be determined using the Moore-Penrose pseudo-inverse matrix $\mathbf{A}^+$, obtained by the single value decomposition of matrix $\mathbf{A}$. By adopting this technique, the following solution can be found in the least square sense:

$$\bar{\mathbf{x}} = \mathbf{A}^+\mathbf{b} \tag{4.61}$$

The solution $\bar{\mathbf{x}}$ so obtained, is particular because is the one with the minimum norm $\|\mathbf{x}\|$ between the infinite possible solutions of the problem and, therefore, represents the optimum solution for the stated problem.

The optimisation procedure is really simple, but on the other hand shows some limitations. The solution does not ensure that the obtained thrust satisfies the maximum thrust constraints for each thruster. For this reason, an iterative method has been implemented, to ensure the satisfaction of

the initial constraints. If the solution x̄ allocate to a thruster a thrust higher than the maximum deliverable one, then system (4.60) is rewritten considering the overloaded thrusters fixed at their maximum deliverable force value. Thus, the new solution according to (4.61) allocate additional thrust only to the underloaded thrusters. This iterative procedure stops when all the thrusters are not overloaded or when all the thrusters results overloaded.

Adopting this allocation methodology, each thruster is analysed individually. Consequently all the orientations are in principle different in magnitude for each thruster.

As for the described deterministic method, the pseudo-inverse procedure cannot assure that all the thruster are saturated. In fact also in this case the procedure is stopped one thruster has reached the saturation, however with an iterative process it is possible to partially overcome this issue.

4.2.3 Lagrange multipliers

Method based on Lagrange multipliers solves the optimisation problem whose goal is to minimise an objective function subject to some equality constraints. In particular, the allocation is based on a minimisation of the total squared thrust such that the total thruster force equal the force required by the external environment. Also in this case, it is convenient to treat the problem selecting as variables the single thrust components instead of the thrust magnitude and angle. In any case, with such a kind of modelling, the application of a Lagrange multiplier method leads to the resolution of a non-linear system that, in the proposed case, is solved in an iterative way with Newton's method.

The objective function to minimise is written in the following form:

$$f\left(\mathbf{x}\right) = \sum_{i=1}^{N_{ACT}} \frac{F_{x_i}^2 + F_{y_i}^2}{T_{MAX_i}^2} + \sum_{i=1}^{N_{ACT}} w_i \left(\left(\frac{F_{x_i}^2 + F_{y_i}^2}{T_{MAX_i}^2} \right)^2 - 1 \right)^2 \tag{4.62}$$

The second sum of $f\left(\mathbf{F_x}, \mathbf{F_y}\right)$ is a penalty function that adds to the objective function an additional cost when the maximum available thrust for a thruster is exceeded. On this purpose w_i is a non negative weight factor defined as follows:

$$w_i = \begin{cases} k_i & \text{if } T_i > T_{MAX} \\ 0 & \text{else} \end{cases} \tag{4.63}$$

k_i is a positive constant value, this makes sure the penalty function is active only once the maximum thrust is exceeded and that the algorithm allocates the thrust from other thrusters

instead of the saturated one.

The objective function should be subjected to several constraints, which determine the set of feasible solutions. In this particular case the n constraints $c_i(\mathbf{x})$ are given by the equations of the equilibrium system (4.54). According to the Lagrange theorem, the solution of the problem is given by system:

$$
\begin{cases}
c_1(\mathbf{x}) = 0 \\
\vdots \\
c_n(\mathbf{x}) = 0 \\
\frac{\partial f(\mathbf{x})}{\partial F_{x_1}} + \lambda_1 \frac{\partial c_1(\mathbf{x})}{\partial F_{x_1}} + \cdots + \lambda_n \frac{\partial c_n(\mathbf{x})}{\partial F_{x_1}} = 0 \\
\vdots \\
\frac{\partial f(\mathbf{x})}{\partial F_{x_{N_{ACT}}}} + \lambda_1 \frac{\partial c_1(\mathbf{x})}{\partial F_{x_{N_{ACT}}}} + \cdots + \lambda_n \frac{\partial c_n(\mathbf{x})}{\partial F_{x_{N_{ACT}}}} = 0 \\
\frac{\partial f(\mathbf{x})}{\partial F_{y_1}} + \lambda_1 \frac{\partial c_1(\mathbf{x})}{\partial F_{y_1}} + \cdots + \lambda_n \frac{\partial c_n(\mathbf{x})}{\partial F_{y_1}} = 0 \\
\vdots \\
\frac{\partial f(\mathbf{x})}{\partial F_{y_{N_{ACT}}}} + \lambda_1 \frac{\partial c_1(\mathbf{x})}{\partial F_{y_{N_{ACT}}}} + \cdots + \lambda_n \frac{\partial c_n(\mathbf{x})}{\partial F_{y_{N_{ACT}}}} = 0
\end{cases}
\tag{4.64}
$$

which is a system with $n + 2N_{ACT}$ equations and $n + 2N_{ACT}$ unknowns. However, once penalty functions are active, the system is non-linear, therefore an iterative way should be applied to solve it, as the Newton method.

4.2.4   Non-linear optimisation

To solve the thrust allocation problem adopting optimisation techniques, other approaches, more complicated and more efficient can be used. It is a common practice to use methods which are adopting quadratic programming. However this technique allows to use an objective function in quadratic form and, even more important, leads to use linear constraints only. In the particular case of the DP problem, the maximum thrust constraint of a steerable thruster is given by a circle. Once the constraint should be linearised, to obtain a reasonable approximation, a high number of sub-constraints must be used, leading to the application of a large number of constraints for the global optimisation.

To overcome this issue in solving the DP thrust allocation problem, a non linear programming

technique has been implemented in the following general form:

$$\min f(\mathbf{x}) \tag{4.65a}$$

$$\mathbf{l} \leq \begin{pmatrix} \mathbf{x} \\ \mathbf{c(x)} \end{pmatrix} \leq \mathbf{u} \tag{4.65b}$$

where $f(\mathbf{x})$ is the selected objective function of n variables $\mathbf{x}$, $\mathbf{c(x)}$ is a vector of m constraint functions and $\mathbf{l}$ and $\mathbf{u}$ are vectors representative of lower and upper boundaries values for the variables and constraints. The only requirements for the objective function and constraints are that these functions should be continuously differentiable at points that satisfy the bounds for the given $\mathbf{x}$ and that it is possible to evaluate the gradient vector $\mathbf{g(x)} = \nabla f(\mathbf{x})$ and the Jacobian matrix $\mathbf{C} = \nabla \mathbf{c(x)}$.

By adopting this kind of procedure for the allocation problem, the constraints are no more forced to be linear, reducing the total number of constraints of the problem compared to a quadratic programming approach. Also the objective function can be selected with more freedom, without being limited to a quadratic form.

This allocation procedure allows to use and compare different kinds of objective functions, from a simple sum of thrusts to more complicated forms related to fuel consumption. To investigate the differences between several different objective functions is not the aim of this thesis.

In the particular case of DP allocation a non-quadratic objective function can be considered with in the following form:

$$f(\mathbf{x}) = \sum_{i=1}^{N_{ACT}} \left(\sqrt{F_{x_i}^2 + F_{y_i}^2} \right)^{3/2} \tag{4.66}$$

while the constraints $\mathbf{c(x)}$ are divided into two groups. The first set of 3 equality constraints is based on the equations of system (4.54). The second set of N_{ACT} constraints is representative of the maximum thrust that each device can deliver:

$$\sqrt{F_{x_i}^2 + F_{y_i}^2} \leq T_{MAX_i} \tag{4.67}$$

Here the solution method is an extended version of Robinson method [7], based on filtering and using a trust region obtained by adopting Ritz values.

It should be underlined that this allocation strategy allows to use a lower number of constraints compared to other optimisation approaches. Obviously in this kind of approach the thrusters are considered individually.

4.2.5   Booster allocation strategy

A promising technique in DP allocation strategies is based on using the genetic algorithms [92]. Genetic algorithms are adaptive heuristic search algorithms designed to simulate processes in natural systems necessary for evolution. This means that they represent an intelligent exploitation of a random search within a defined design space to solve a specific problem. Many real problems which involve finding of optimal parameters might be to difficult to solve with traditional methods, and in such cases the genetic algorithms are ideal. Thrust allocation problems can be solved by this kind of method, especially when the maximum capability of the DP system is investigated. The problem that has to be solved is an optimisation problem as the already described ones and considers the same unknowns, i.e. the thruster forces components. Also in this case the objective function is subjected to the equality constraints given by system (4.54). To handle the constraints inside the GA optimisation it is handy to adopt penalty functions [60, 56], so that the final objective function of the optimisation can be expressed as:

$$f^* \left(\mathbf{x} \right) = f \left(\mathbf{x} \right) + \sum_{i=1}^{3} \mathbf{kc} \left(\mathbf{x} \right) \tag{4.68}$$

where $f(\mathbf{x})$ is the objective function written as in equation (4.66), the constraints $\mathbf{c}(\mathbf{x})$ are expressed as in system (4.54) and $\boldsymbol{k}$ is a vector of penalty factors. $\boldsymbol{k}$ elements are considered if one of the following conditions is not satisfied:

$$\left| c_i \left(\mathbf{x} \right) - \epsilon_{c_i} \right| \leq 0 \tag{4.69}$$

The $\epsilon_{\mathbf{c}}$ is the tolerances vector, giving the maximum acceptable error on each constraint. For the thrust allocation problem, a value of 0.01 kN is selected for the equilibrium equations in x and y direction and 0.1 kNm for the momentum equation.

It is not necessary to set additional constraints to the $\mathbf{c}(\mathbf{x})$ with regards to the maximum deliverable thrust, since these limitations are intrinsically considered inside the generation of the populations. In fact, the initial issue to start a genetic optimisation procedure is to create a sample population of N_{POP} elements, inside the population each element can be characterised by M_P parameters. The initial size of the population can be set arbitrary, however it is suggested to set it as a function of M_P. Generally it is a good practice to assume $N_{POP} \geq 8M_P$. In case of the thrust allocation problem, the M_P parameters are representative of the $2N_{ACT}$ thruster forces components.

It is common to generate randomly the starting population, covering the entire feasibility range

(the search space). Once a more likely subspace for optimal solution can be predicted, the solutions may be *seeded* in a certain area, setting opportune constraints to the initial M_P parameters. Here, to ensure that the thrusters will be not overloaded, at first the y direction forces components F_{y_i} are generated between the feasible limits:

$$T_{MIN_i} \leq F_{y_i} \leq T_{MAX_i} \tag{4.70}$$

then the F_{x_i} are generated as a function of the determined F_{y_i}:

$$T_{MIN_i} \leq F_{x_i} \leq \sqrt{T_{MAX_i}^2 - F_{y_i}^2} \tag{4.71}$$

This process has to be performed for all the N_{POP} individuals of the initial population, resulting in a matrix of variables defined as:

$$\mathbf{X} = \begin{pmatrix} F_{x_{11}}^* & \cdots & F_{x_{1N_{ACT}}}^* & F_{y_{11}} & \cdots & F_{y_{1N_{ACT}}}^* \\ \vdots & \ddots & \vdots & \vdots & \ddots & \vdots \\ F_{x_{N_{POP}1}}^* & \cdots & F_{x_{N_{POP}N_{ACT}}}^* & F_{y_{11}}^* & \cdots & F_{y_{N_{POP}N_{ACT}}}^* \end{pmatrix} \tag{4.72}$$

where the $F_{x_{ji}}^*$ and the $F_{y_{ji}}^*$ are the F_{x_i} and F_{y_i} components generated for each of the j individuals of the population.

After setting the initial population, the objective function must be evaluated for each member of the population itself. There are no constraints regarding the shape of the objective function, even continuous differentiability through the calculation domain is not strictly required.

After the objective function has been evaluated for each member of the population, a portion of the population must be selected to generate the next generation of individuals. There are several methods to select the suitable individuals to proceed with the new generation step. In this case the best individual is searched during each generation step, the other members of this particular sub-population are randomly and distinctly selected between the rest of the population. It is not advisable to select only the best members for the new generation step, since in some cases the solution could remain around a local optimal point of the objective function.

The most important thing in the selection process is to ensure that the sub-population individuals are distinct. After this selection the new population can be generated. In order to create the new individuals a crossover procedure is performed. Basically, the crossover procedure is combining some of the properties of the different selected individuals according to appropriate schemes of decomposition.

For example, considering a simple system with only four selected individuals for the crossover,
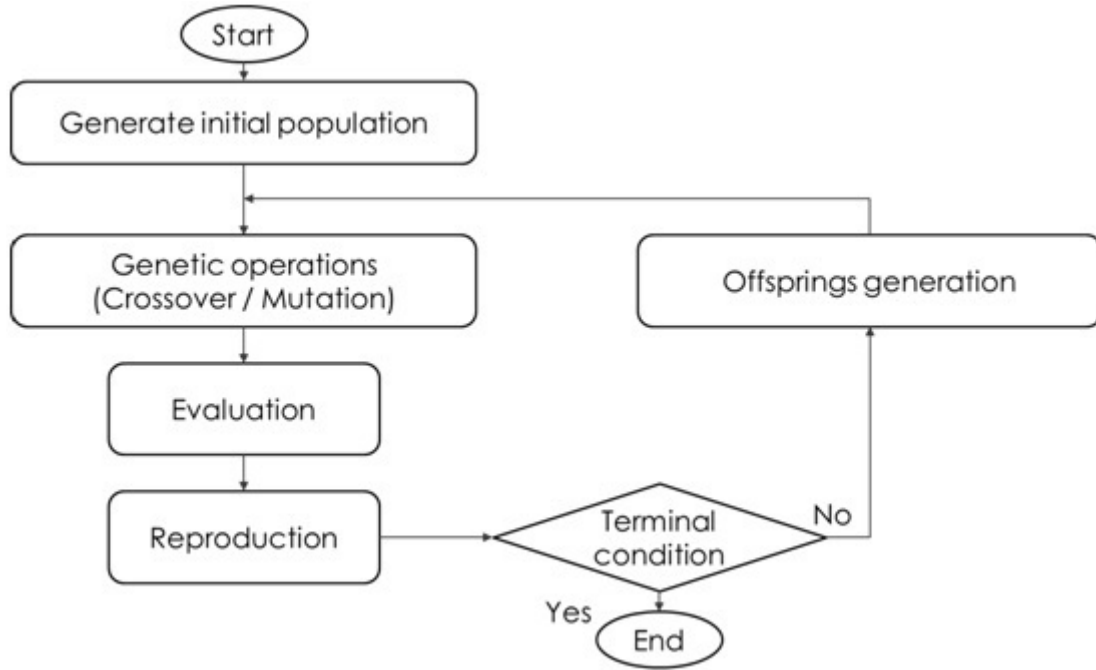
Figure 4.18: Evolution scheme of GA for optimum solution search

a simple and easy way to proceed with the new populations could be as follows:

$$
\begin{aligned}
X_{new}\left(j,i\right) = & X\left(1,i\right) + k_1\left[X\left(2,i\right) - X\left(3,i\right)\right] + \\
& + k_2\left[X\left(3,i\right) - \frac{1}{2}X\left(4,i\right) - \frac{1}{2}X\left(1,i\right)\right]
\end{aligned}
\tag{4.73}
$$

where k_1 and k_2 are the crossover probability factors. Here the result is more similar to a probabilistic replacement rather than a proper crossover procedure. In the algorithm implemented for the DP evaluation a more complicated and exhaustive crossover procedure has been used, as for example the replacement of equation (4.73) with an exponential scheme.

The crossover procedure is generating the so-called offsprings, every offspring is then used in the calculation of the objective function and is thereafter compared with his parent. If the child objective function value is higher than the parent (in case of maximum research, when a minimum is searched the value must be lower), the child is taken in the new population. By using this strategy, the new population is composed by a mixture of best parents and best children. The procedure continues up to the moment where the objective function reaches the maximum or minimum of the problem. The evolution procedure can be summarised in the scheme presented in Fig. 4.18, where the main processes provided at each generation step are schematically shown.

Table 4.2: Main dimension of the HLCV

	Symbol	Units	Value
Overall length	L_{OA}	m	162.00
Length between perpendiculars	L_{PP}	m	152.62
Design breadth	B	m	38.00
Design draught	T_{DES}	m	5.00
Displaced volume	∇	m^3	22626.34

Table 4.3: Thruster configuration HLCV

No.	Thruster	x_T(m)	y_T(m)
1	Tunnel Fwd	82.00	0.00
2	Azimuth Fwd	57.00	4.20
3	Azimuth Fwd	52.30	-4.20
4	Azimuth Mid	27.50	-15.00
5	Azimuth Mid	-22.50	15.00
6	Azimuth Aft	-60.00	15.00
7	Azimuth Aft	-60.00	-15.00
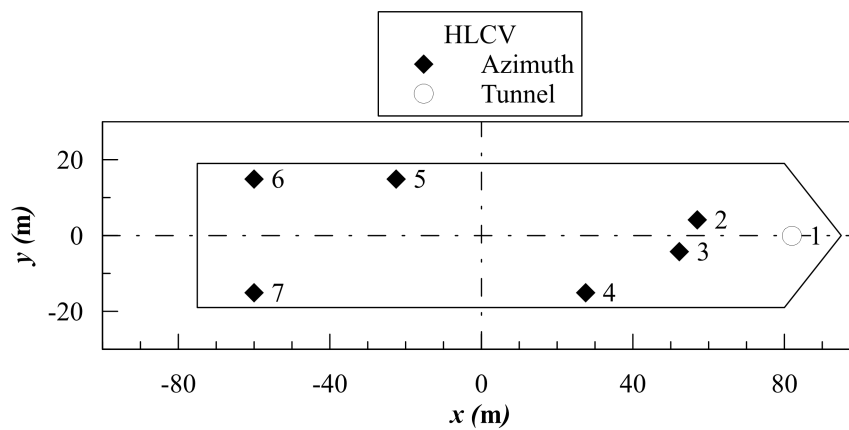
Figure 4.19: Thruster configuration HLCV

Table 4.4: Main dimension of the PLCV

	Symbol	Units	Value
Overall length	L_{OA}	m	205.00
Length between perpendiculars	L_{PP}	m	197.60
Design breadth	B	m	48.00
Design draught	T_{DES}	m	7.50
Displaced volume	∇	m^3	53658.54

Table 4.5: Thruster configuration PLCV

No.	Thruster	x_T(m)	y_T(m)
1	Tunnel Fwd	92.80	0.00
2	Azimuth Fwd	84.40	-6.00
3	Azimuth Fwd	65.20	-14.00
4	Azimuth Fwd	65.20	14.00
5	Tunnel Aft	-85.60	0.00
6	Azimuth Aft	-89.20	-14.00
7	Azimuth Aft	-89.20	14.00
8	Azimuth Aft	-98.80	0.00
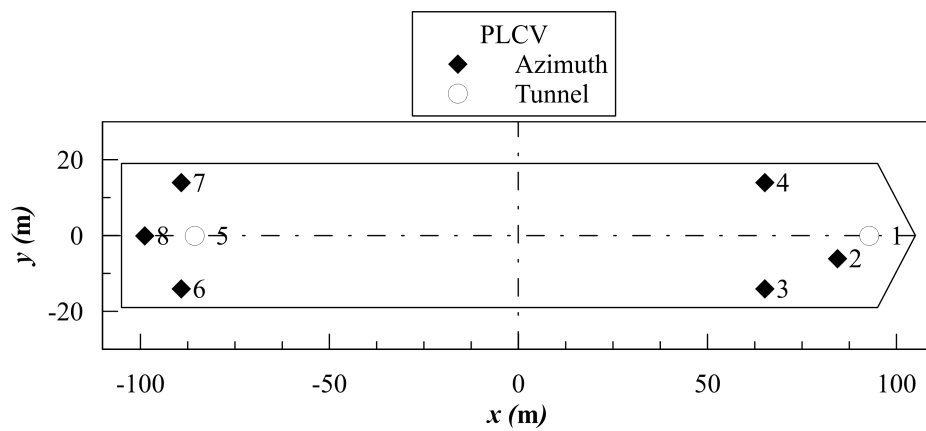
Figure 4.20: Thruster configuration PLCV

4.2.6 Procedures comparison

The effect of the previously described allocation strategies on the DP capability of am offshore vessel is here analysed, with the aim to find the best procedure to describe the thruster behaviour close to saturation. That means to study the possibility to allocate all the allowable thrust to overcome the external loads. For this purpose the previous allocation algorithms were tested on two different offshore vessels.The first test case is a specific Heavy Lift Crane Vessel (HLCV) and the second a Pipe Lay Crane Vessel (PLCV). The HLCV vessel has been selected for the particular thruster arrangement (completely unsymmetrical), on the other hand the PLCV presents a more traditional thrusters disposition. The main dimensions of the HLCV vessel are reported in Table 4.2, the ship is equipped with seven thrusters, six azimuthal devices and a tunnel thruster in the bow as reported in Table 4.3 and shown in Fig. 4.19. The PLCV main dimensions are reported in Table 4.4 and its thruster equipment composed by eight thrusters, a fixed one in the bow, another fixed in the stern and six azimuthal devices is reported in Table 4.5 and shown in Fig. 4.20. An additional external force can be applied to simulate the pipe lay operation. Once the thruster positions are defined, the DP capability plots of the two vessels were calculated according to four of the presented allocation procedures. The results of the Lagrange multiplier techniques are in-between pseudo-inverse matrix and non-linear modelling results, therefore, not to complicate to much the representation, they were neglected as less significant than the others.

The DP capability calculations were executed for two vessels with four different allocation strategies. In Figs. 4.21 and 4.22 the obtained capability plots are highlighted in terms of the so-called *rosettes*.

It is important to emphasise the differences between two selected test cases. The first vessel (HLCV) has a totally unsymmetrical thruster disposition and also the thrusters sizes are different, representing a really complex system to analyse. In particular to select the grouping of the thrusters to proceed with the deterministic approach, the configuration allows to choose different equivalent solutions, in this case three groups were chosen for the azimuth thrusters, while the fixed thruster was considered apart. On the other hand the second vessel (PLCV) presents a less significant asymmetry with respect to HLCV, however it is still representative of a more usual thruster disposition, where thrusters sizes are homogeneous. In this case the group identification is really simple, leading to select a single group for the fixed tunnel thrusters and grouping the azimuth thrusters in the bow group and the stern one.
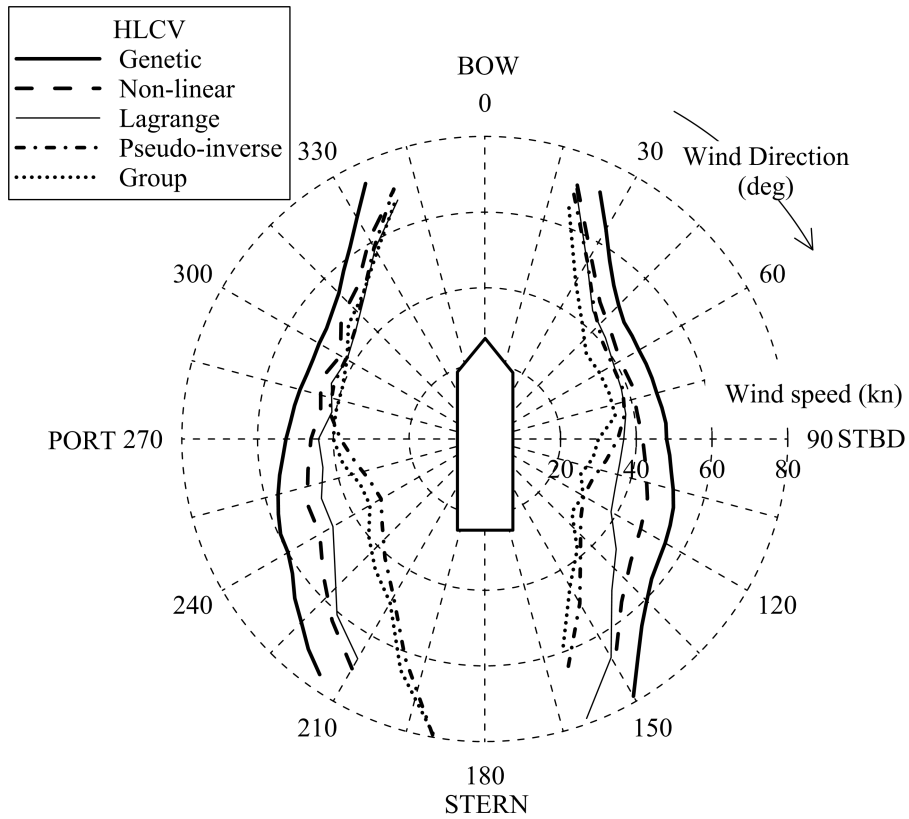
Figure 4.21: HLCV capability plots according to IMCA standards
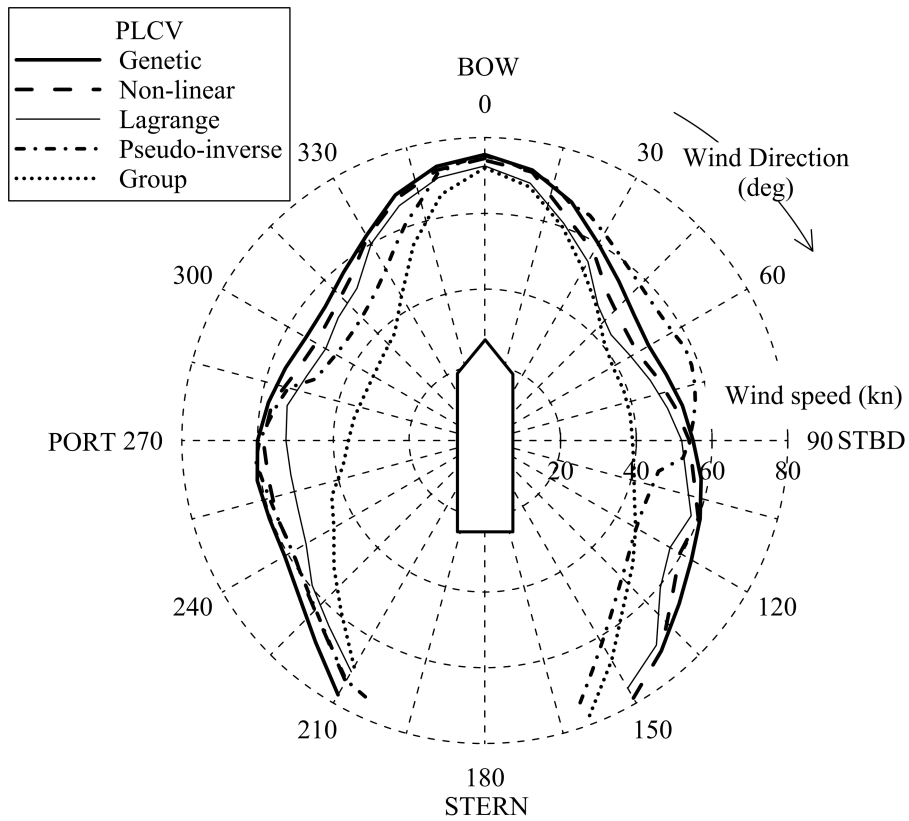
Figure 4.22: PLCV capability plots according to IMCA standards

In both analysed cases, the genetic algorithm approach predicts the higher capability area compared to other procedures. Also non-linear optimisation procedure gives satisfactory predictions, however this procedure is giving more instability in the solution when the thrusters work closely to saturation. In this kind of situation the optimisation algorithm is not always able to allocate the available thrust, especially in the case of HLCV vessel where the particular thruster disposition complicates the search of optimal solution. For the PLCV case, with a conventional thruster disposition, genetic and non-linear optimisation approaches give comparable results.

The pseudo-inverse matrix approach suffers more than the non-linear optimisation procedure the asymmetric disposition of the thrusters for the HLCV case, while the PLCV case is quite well described compared to the other approaches. Also for this case the main problem was to saturate all the thrusters to evaluate the extreme capability of the vessel.

The deterministic approach is giving the smallest envelope in both the analysed cases, this is provoked by the group saturation. In fact during the allocation procedure, once a group results were overloaded, the procedure was not able to load the other groups to find a new equilibrium. Since the final target of this thesis is oriented to the evaluation of DP capability in extreme operating conditions, to implement thruster-thruster interaction effects, the procedure which gives the best and more stable results was selected. Therefore the genetic algorithm approach was selected to study the impact of the thruster-thruster interaction effect on DP capability plots.

4.3 Propeller modelling in thrust allocation

In the above described methods to allocate thrust between the different actuators, the propeller is modelled as a pure thrust generator, without considering all the theories described in the first part of the chapter.

In this section three possible applications of the described propeller modelling will be described, highlighting the enhancement that the propeller modelling gives to the standard allocation procedures. In the first case, the application of bollard pull modelling will be applied to non-linear optimisation technique for thrust allocation. In the second case, the complete thruster-thruster interaction modelling considering the propeller in cross-flow is applied as post-processor to a standard allocation output with a fixed environment. Here the thrust losses will be compared with available experimental results. Finally the thruster-thruster interaction procedure will be incorporated in the *booster allocation* strategy.

Table 4.6: General particulars of the reference OSV.

Length between perpendiculars	L_{PP}	71.300	m
Length at design waterline	L_{WL}	75.420	m
Length overall submerged	L_{OS}	77.524	m
Breadth	B	16.000	m
Design draught	T_{DES}	5.000	m
Volume	∇	3773.2	m^3
Wetted surface	S	1569.6	m^3
Bare hull wetted surface	S_0	1517.6	m^2
Appendages wetted surface	S_{APP}	52.0	m^2
Longitudinal centre of buoyancy	LCB	-1.4	$\%L_{PP}$
Block coefficient	C_B	0.630	-
Midship coefficient	C_M	0.940	-
Prismatic coefficient	C_P	0.660	-

4.3.1   Modelling in non-linear objective function

As previously mentioned, the non-linear optimisation algorithm, allows to adopt as objective function a fully non-linear equation. To test the variation of the propeller modelling on the final capability of the vessel, another reference vessel has been selected. The cases referring to the comparison of the allocation algorithm were ships fitted only with steerable thrusters. The method will be applied on an Offshore Supply Vessel (OSV) having the characteristics reported in Table 4.6. The OSV is equipped with two propulsive steerable thrusters, mounting controllable pitch propellers with a diameter of 2.4 m. Each thruster has a nominal power of 2050 kW at a propeller rotation rate of 250 rpm, being able to deliver a nominal thrust of about 677 kN. Each bow thruster has a nominal power of 1000 kW at a rotation rate of 260 rpm, having a diameter of 1.75 m, being able to develop a nominal thrust of about 147 kN. Also the propellers of bow thruster tunnel are of controllable pitch type. This test is interesting, since it allows to test a CP propeller and two different kind of actuators.

By adopting this kind of modelling for the steerable thruster and a comparable one for the bow thruster, but starting from propeller 4468 with nozzle 37, it is possible to establish the *thrust/power* relationships for the devices installed on board. It can be stated that a thruster

during DP operation works really close to bollard pull condition, so the determination of the desired relationship can be restricted to the specific bollard pull case. To define the curve relating the thruster absorbed power P_T and the delivered thrust T, the empirical relationships available in literature [96] as:

$$P_T = \frac{1}{D} \left(\frac{T}{1.2} \right)^{1.5} \tag{4.74}$$

$$P_T = \frac{1}{D} \left(\frac{T}{1.082} \right)^{1.5} \tag{4.75}$$

The equations (4.74) and (4.75) are representative of a steerable thruster and of a bow thruster tunnel respectively. Analysing this two equations it can be observed that the equation form reflects the objective function given in equation (4.66), which represents the standard way to treat power in non-liner optimisation solvers for DP thrust allocation, providing that:

$$T = \frac{\sqrt{F_x^2 + F_y^2}}{\eta} \tag{4.76}$$

where η is a thrust loss factor that takes into account the in-line losses, the cross flow losses, fouling and ventilation effects. In DP calculations for early design stage, it is suggested to consider a value of 0.80 [62].

Considering a more detailed modelling of the CPP, the relationships between power and thrust will change. According to the above mentioned cases of the OSV vessel, the following relationships can be found for bollard pull operations, fitting the bollard pull curves:

$$P_T = 0.4424T^{1.42} \tag{4.77}$$

$$P_T = 0.6359T^{1.43} \tag{4.78}$$

$$P_T = 1.5543T^{1.29} \tag{4.79}$$

The above equations are representative of the steerable thruster and of the bow tunnel thruster in ahead and astern conditions respectively. All the equations are considering the power expressed in kW and the thrust in kN. As already mentioned, the tunnel thruster has different behaviours in astern and ahead conditions, which means the maximum thrust delivered will not be the same in the two pull directions.

Considering equations (4.77), (4.78) and (4.79) it is possible to modify the objective function (4.66), in such a way to consider the proper propeller modelling directly inside the allocation algorithm. In this way, standard DP calculations can be performed and compared with the ones coming from the new propeller modelling. It is necessary to perform a comparison for the total
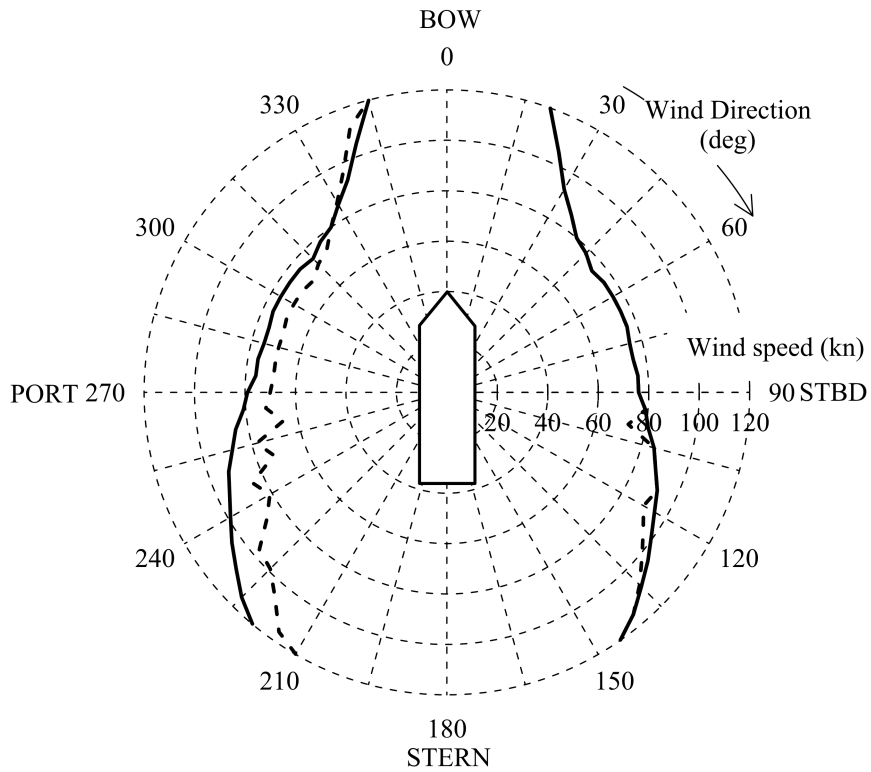
Figure 4.23: DP capability plot for the OSV considering a traditional (*continuous*) or an enhanced (*dashed*) propeller modelling
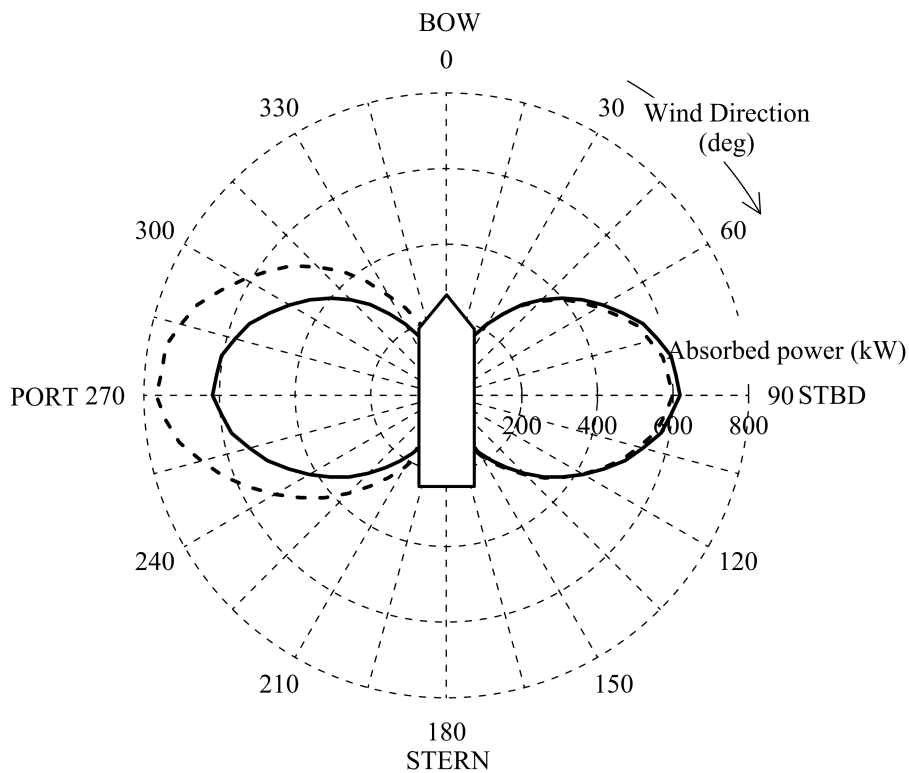
Figure 4.24: Total absorbed power for the OSV considering a traditional (*continuous*) or an enhanced (*dashed*) propeller modelling considering a wind speed of 20 knots

capability of the system but also for some specific environmental cases. A first DP analysis has been performed to determine the capability plot for the OSV. The calculations have been carried out testing both the power models given by equations (4.74) and (4.75) and the one given by equations (4.77), (4.78) and (4.79). For the specific case a wind/wave correlation according to IMCA has been adopted. Thereafter, a condition representative of one wind speed, i.e. 20 knots, is selected from the DP capability calculations, to better understand the differences in the absorbed power. The current has not been intentionally considered in such a way to justify the bollard pull assumption.

The obtained results for the capability plot are shown in Fig. 4.23, where it is possible to observe the differences due to different modelling of ahead and astern conditions of the tunnel thruster, resulting in an asymmetrical capability plot. In Fig. 4.24 the particular environmental condition of a wind speed of 20 knots is considered. Here it is possible to visualise the total power absorbed at each encounter angle; by applying the enhanced method a difference of about 5% is noted when bow thrusters are acting ahead (between 0° and 180°) while the differences are around 25% when the same thrusters are acting in astern condition (180° to 360°).

4.3.2 Interaction analysis on simple allocation strategy

A first step for the integration between a thrust allocation strategy and the thruster-thruster interaction model described in the previous section is given by the possibility to perform a post processing of an obtained equilibrium.

Once a simple allocation procedure is adopted, the final outcome for a single environmental condition is given by a set of thrust and thrusters orientation at each encounter angle. With these data at disposal, it is then possible to evaluate whether thruster are or not in an interaction condition, then evaluate the thrust interaction grade according to equation (4.49) and finally evaluate the effective thrust magnitude and orientation.

This kind of approach has been applied to the generic PLCV case previously described, having 6 thrusters located in two different groups as reported in Table 4.5. For this particular case, also model test (see Fig. 4.25) were executed by MARIN, with the aim to evaluate the total thrust losses with respect to propeller nominal thrust. In particular, two conditions named JL2T91 and JL2T94 will be considered, with all thruster running and with thruster 2 and 7 switched off respectively. An overview of the two configurations is given in Table 4.7.

The two evaluated conditions represent the same environmental condition, corresponding to a

Table 4.7: Configurations analysed for the PLCV

	Configurations	
	JL2T91	JL2T94
Thruster T1	ON	ON
Thruster T2	ON	OFF
Thruster T3	ON	ON
Thruster T4	ON	ON
Thruster T5	ON	ON
Thruster T6	ON	ON
Thruster T7	ON	OFF
Thruster T8	ON	ON
V_w	25.0 kn	25.0 kn
$H_{1/3}$	3.25 m	3.25 m
T_P	8.43 s	8.43 s
V_c	1.5 kn	1.5 kn

Table 4.8: Thrust losses during model test and calculations.

thruster No.	T losses model	T losses calc
2	16.0	15.1
3	17.0	15.1
4	14.0	15.9
6	5.0	6.2
7	7.0	7.7
8	9.0	7.8
total	22.0	24.9

Figure 4.25: PLCV model during current loads test at MARIN

constant wind speed of 25 knots, a corresponding wave height of 5.9 meters, and a current with speed 1.5 knots collinear with wind and waves. In Fig. 4.26 the condition referring to JLT91 is reported, considering the interaction effects and the propeller behaviour in the four quadrants. As it can be seen, for the reported condition, the thruster are not acting in interaction, and, since the adopted allocation considers all the thrusters acting in the same direction, also their behaviour is constant between the groups. However, with respect to a simple allocation, the final amount of thrust is reduced or increased by most the 10% while working in cross-flow.

The case reported in Fig. 4.27 is different, being representative of condition JLT94, with two inactive thrusters. In such a case the thrusters act in interaction conditions, and, each single thruster is not able to deliver the total required thrust, but loses a certain amount of it. While interaction phenomena occurs, the thruster acting in disturbed flow is losing up to 30% of its nominal thrust.

To estimate the reliability of the obtained results, they were compared with a special model test performed properly to evaluate interactions. In this test the thrusters were forced to be oriented against the current coming from the bow (heading 0°) with a speed of 0.79 m/s. In Table 4.8 the final outcome can be seen, highlighting a good agreement between the measured data and the calculations done with the propeller modelling.

However, despite the procedure gives a good estimation of the thrust losses, it does not provide a solution on how to modify the thruster orientation to avoid interaction, which means that a new approach should be studied to include this calculation process directly inside allocation.
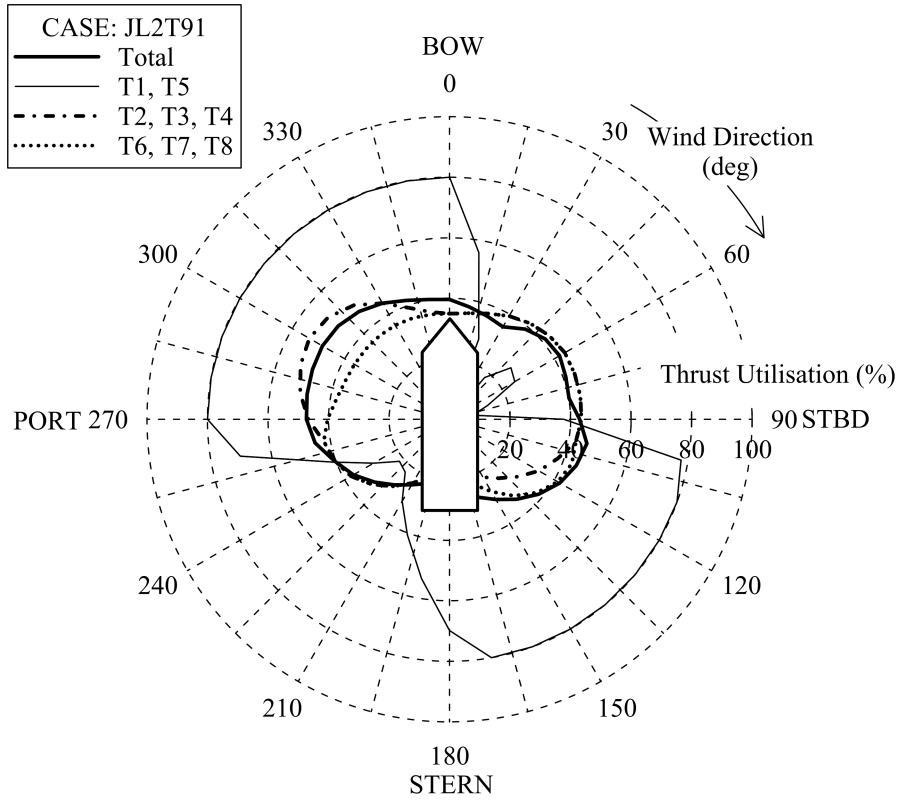
Figure 4.26: Thrust utilisation for condition JL2T91 considering interactions
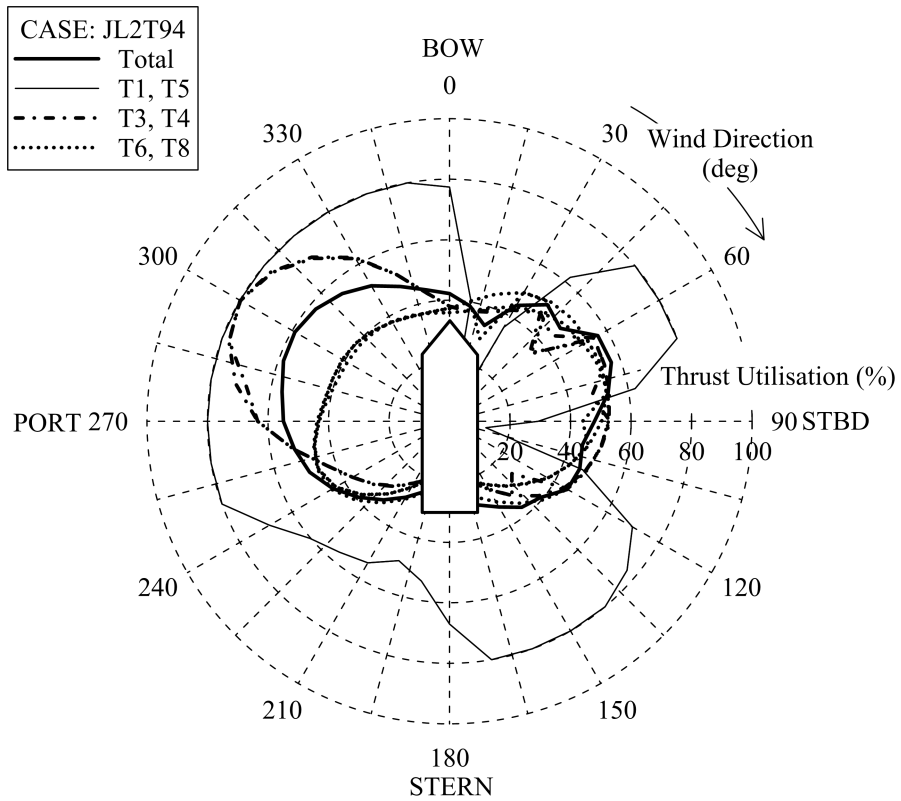
Figure 4.27: Thrust utilisation for condition JL2T94 considering interactions

4.3.3 Interaction in booster allocation strategy

The thruster-thruster interaction effect described in the previous paragraphs has been integrated here into the booster allocation strategy based on genetic algorithms.

To properly describe the behaviour of the interaction process, it is necessary to analyse a way to reproduce the interactions of a rotating thruster in the allocation strategy. By considering the coefficients obtained from the description, per each angle of orientation and mutual condition between the thruster, then the C_T can be determined. By using the proposed model, an interaction factor can be determined for each relative angle of rotation of the analysed thrusters. In such a way a new maximum available thrust vector is evaluated as function of the relative rotation angle. This kind of information is easy to implement in a genetic algorithm procedure, by just changing the limits of the variable generation as in equation (4.70).

By considering this interaction model combined with the genetic algorithm allocation strategy, it is possible to saturate all the thrusters at their relative maximum deliverable thrust for any particular case, modelling a sort of 'booster' effect [91], without some peculiar penalties given by the objective function of a standard optimisation procedure. For this reason the proposed thrust allocation procedure based on the genetic algorithm can be defined as 'smart'. With the newly implemented procedure, the two test cases previously described were analysed with the explicit target to consider thruster-thruster interaction impact on the capability plots.

The results of the simulations are presented in Fig. 4.28 for the HLCV and in Fig. 4.29 for the PLCV showing the differences between standard and interaction model. Giving a first look to the capability plots, no appreciable differences can be noted. The maximum deviations in both cases have the magnitude of about half knot of wind speed around the headings 130° and 230° for the HLCV and around 100° and 240° for the PLCV. Considering only the capability plots, it can be concluded that thruster-thruster interaction does not influence the final results and that the implemented procedure does not apparently work, because previous studies on thruster interaction shows that the thrust reduction can be of the magnitude of about 60% of the nominal thrust value. So it is hard to simply understand why the capability plots remain almost equal between the two different procedures.

To have an appropriate understanding of the working principle of this procedure, the thrusters behaviour should be analysed more in detail. Particular attention must be given to the single thruster orientation; for the HLCV case, particularly important is the interactions between thrusters T2 and T3 (as they are named in the test case description). These two thrusters are
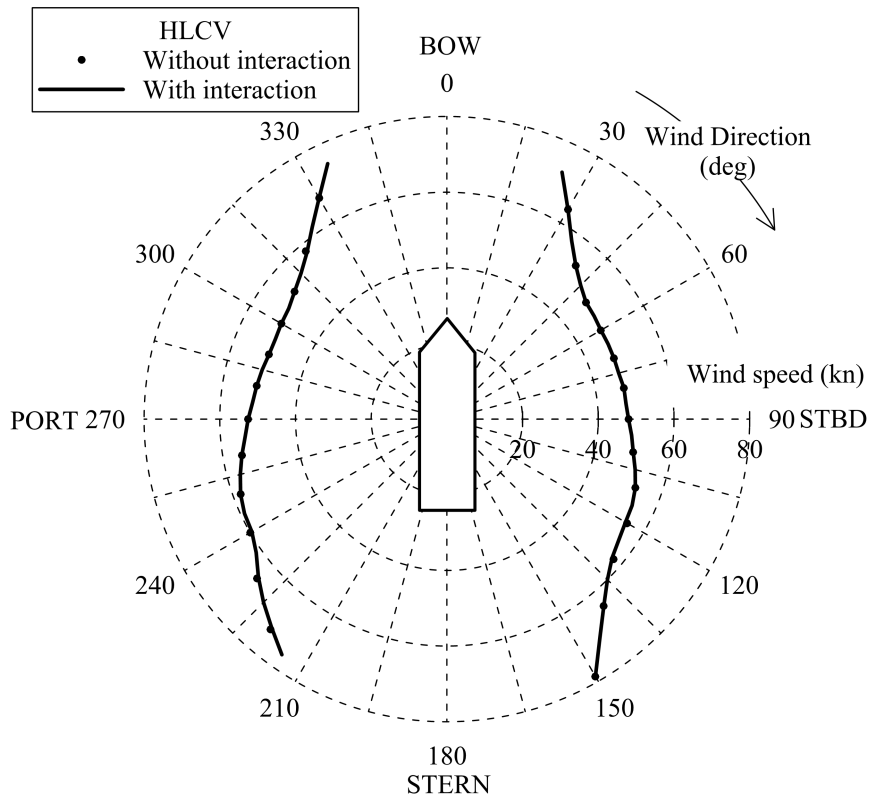
Figure 4.28: HLCV capability plots with interactions according to IMCA standards
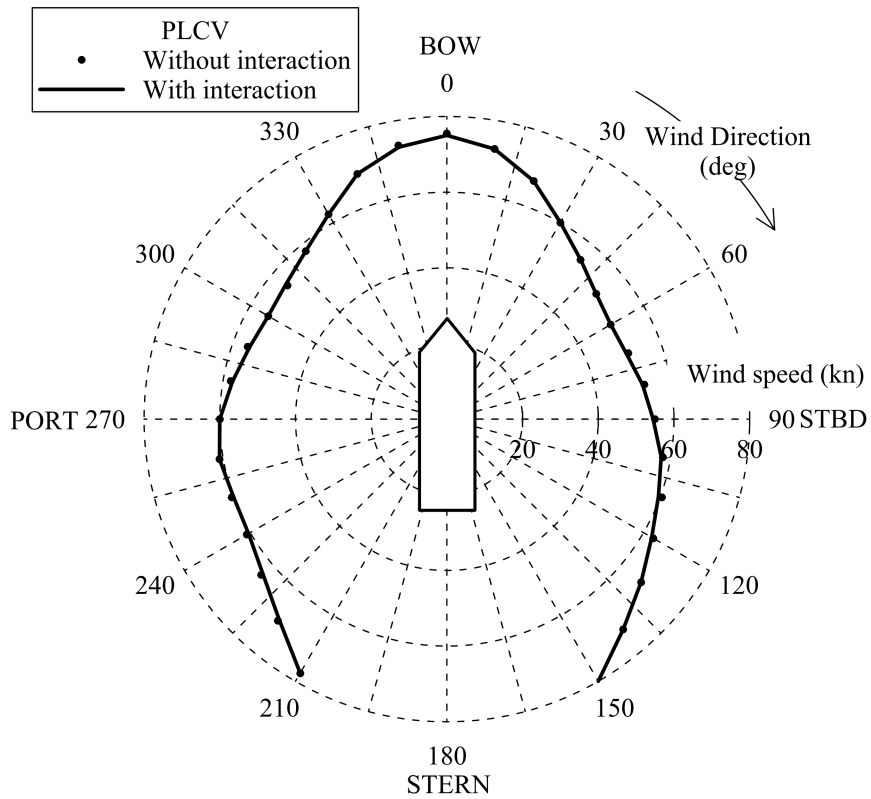
Figure 4.29: PLCV (*right*) capability plots with interactions according to IMCA standards

closely spaced and so interaction effect can be really high. Figs. 4.30-4.33 show the interacting areas between the two thrusters, considering the orientation of the thruster for each ship heading (in this case it corresponds to the incident angle of the external load) in normal allocation procedure and in the interaction one. It can be noted that in the standard allocation case, the thrusters are oriented in relative positions where interaction will occur. By observing the case with interaction, the downstream thruster is never oriented in the interaction area. It means that the genetic allocation strategy automatically orients the thrusters in such a way that they never work in interaction condition, or at most in area where the interaction penalty is not significant. It must be noted that even though the thrusters orientation changes, the thrust magnitude in extreme conditions remains almost constant, because the genetic algorithm will always try to saturate each thruster.

Same considerations can be made on PLCV test case. The entire group is taken into consideration, considering the interaction of the three thrusters of the fore or aft group. In such a way six different interaction areas can be determined and once again (see Fig. 4.32) the genetic allocation algorithm automatically avoids the interaction areas.

It can be stated that the implemented genetic procedure is generates some kind of *fuzzy forbidden zones*, to make the thrusters able to deliver in any condition the maximum allowable thrust to grant the equilibrium in extreme conditions, which means that thrusters are always working close to saturation.

On the other hand this procedure is generating a discontinuity in the thruster orientations, but this is not a problem for a capability study, because in real operations the control system will never evaluate this kind of load variations during operations at sea. It must also be noted that once a single environmental condition is analysed, the genetic algorithm is allocating thrusters in interaction condition. The fuzziness of the interaction area plays a significant role only when extreme conditions are investigated.

The implementation of thruster-thruster interaction inside the genetic allocation is not giving significant changes in the operational rosettes. It means that by using a genetic allocation procedure the thruster-thruster interaction has no impact on the DP capability of a vessel. However interaction got a substantial effect in the orientation of the thrusters with the appearance of the so called fuzzy forbidden zones, where the thruster cannot deliver the maximum nominal thrust. The presented genetic procedure is also flexible for the implementation of thrust loss effects. Further work has to be done to analyse other possible causes of thrust losses, like for example
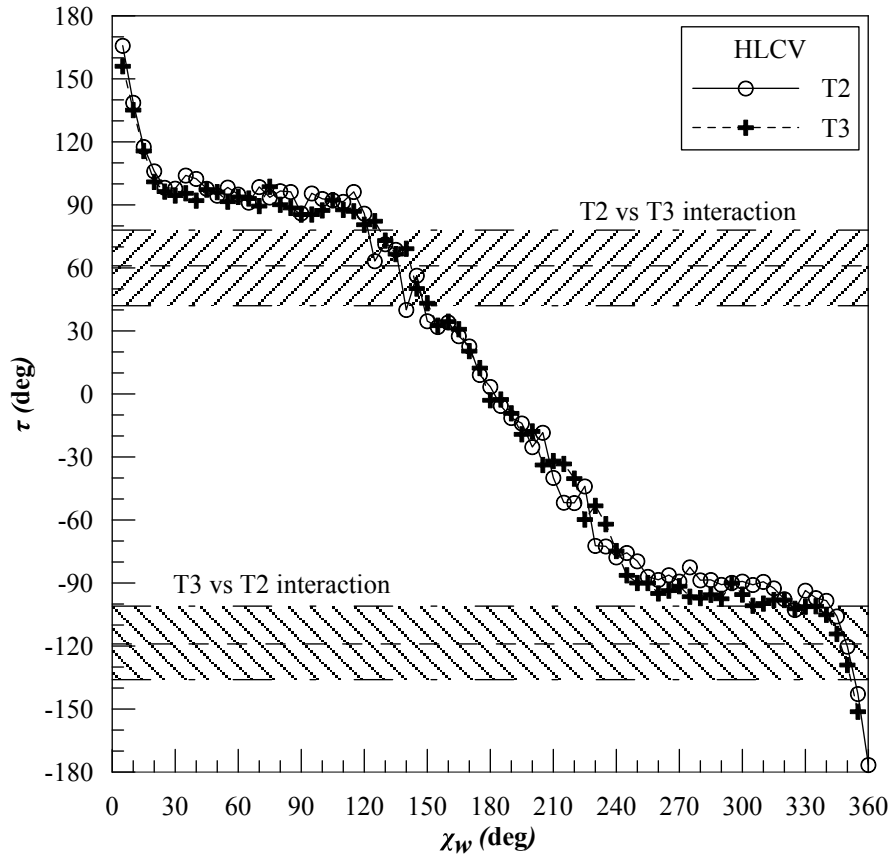
Figure 4.30: HLCV, T2 and T3 orientation without interaction
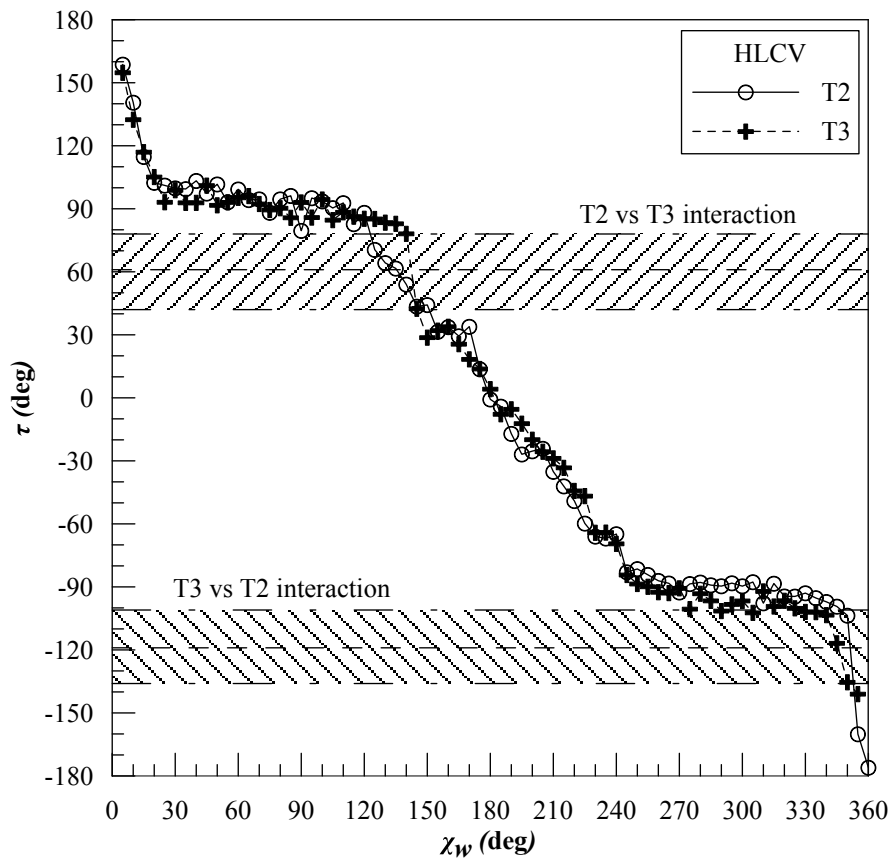
Figure 4.31: HLCV, T2 and T3 orientation with interaction
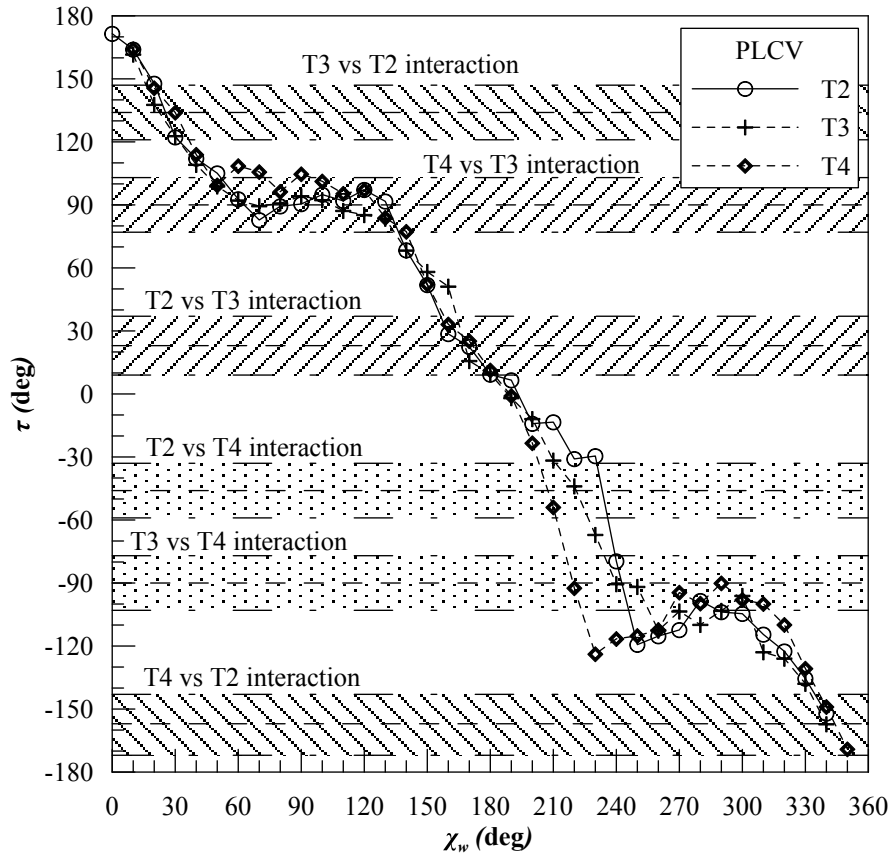
Figure 4.32: PLCV, T2, T3 and T4 orientation without interaction
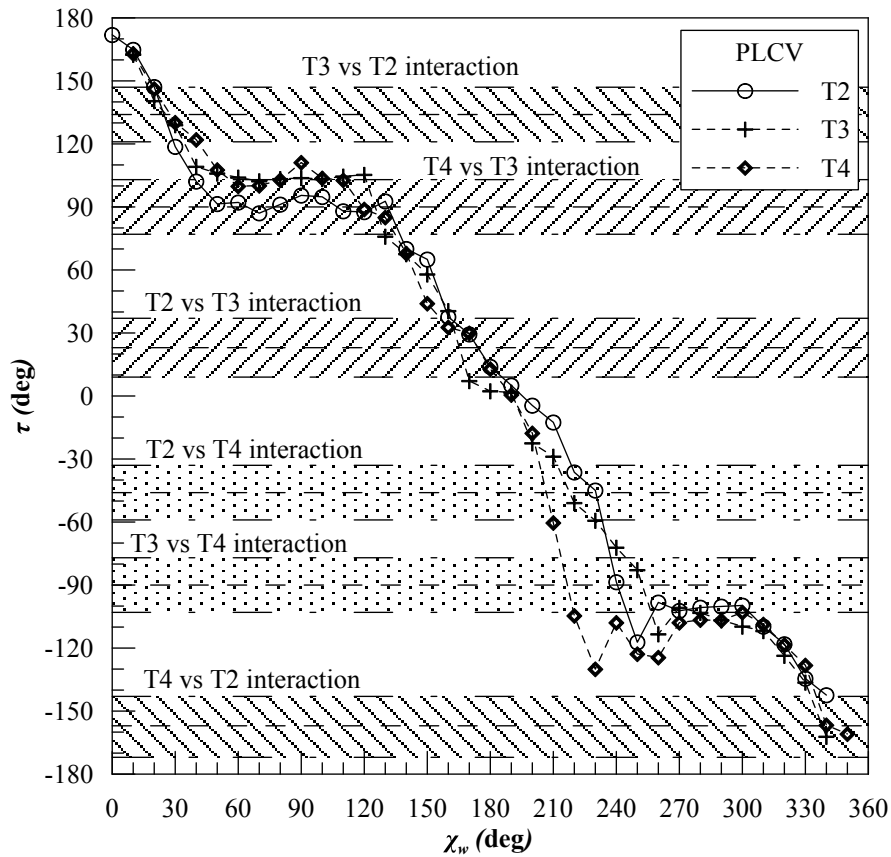
Figure 4.33: PLCV, T2, T3 and T4 orientation with interaction

the behaviour of the propellers in presence of an incoming current. In fact, the behaviour of the thruster in inclined or accelerated flow can lead not only to simple thrust losses but also to noise, vibration and cavitation of the propeller that could increase the total power absorbed and the total fuel consumption.

Chapter 5

Optimal thruster location

During the design process of an offshore vessel, the DP system does not represent one of the primary constraints for the general arrangement of the vessel. Usually the location of the thruster devices is driven by the internal spaces available, i.e. the thrusters position is not optimised to reach the maximum capability. This is also true for a conversion of an existing vessel. Nowadays almost all offshore vessels require the installation of a DP system on board, means that it could be worthy to study more in detail the arrangement of the thrusters to maximise the capability of the vessel to keep position with a determined amount of power installed on board.

The thruster's locations of a DP system are usually related to particular issues due to the internal subdivision of the offshore vessel where the device should be installed. In fact the general arrangement is studied to optimise the internal spaces needed for primary operations of the vessel [152], like the drilling area for a drill-ship or the pipe launching line for a Pipe-Lay Vessel (PLV). For converted ships the problem of thruster's disposal is of secondary importance. Once a conversion of an existing vessel is investigated, the thruster location is determined by the free spaces remaining after the installation of the new equipments, often leading to asymmetric configurations [99]. Another issue is related to the size of the steerable devices [150]. Due to regulations given by classification society, the necessity to grant a particular class notation as DP2 or DP3 [37] requires the installation of more power than it is necessary for vessel operations.

In a preliminary design stage of a new built offshore vessel, once the final configuration of the thrusters is approximately known, it is convenient to perform dedicated DP calculations to roughly evaluate the current system capability. In particular, it is possible to assess the real limiting environment for operations including also the DP capability [90], highlighting that the

power installed on board is lower/higher than necessary. Because the number of devices installed on board cannot be reduced due to redundancy requirements, a dedicated study can be carried out to improve the total efficiency of the DP system. For this purpose a complete time domain simulation is not recommended due to its intrinsic complexity, while a quasi-static approach can give a sufficiently accurate capability estimation for preliminary design stage with a relatively short calculation time.

At present it is really difficult or even impossible to find an analytical formulation for the DP capability as function of the thruster's position and rated power. Therefore, the area of the capability plot has been used to compare different design solutions, the best ones having the larger areas. Alternatively, other targets can be used by the designer according to his experience. In order to maximise the capability plot area [62], an optimisation procedure based on genetic algorithms (GA) has been used and, for each generated thrusters configuration, a complete DP calculation has been carried out to determine the final area of the capability plot and thus rate the overall DP capability of the vessel.

As well known, the capability plot shape and area are strongly influenced by the thrust allocation algorithm used for the calculations [91], while the calculation complexity of the most powerful procedures [92], is not adaptable with the optimisation procedure selected. So less complicated thrust allocation approaches have to be used, at the preliminary design stage, to avoid too much computational effort, as for example a procedure based on pseudo-inverse matrix. As a first step, the location of any single device can be optimised to improve the total capability of the vessel without changing the thruster sizing. Another step can be to change the thrusters size without changing their position or manage a combination of the previous two possibilities.

To better understand the impact of this procedure on the final design, the pseudo-inverse matrix procedure has been applied on a PLV vessel under conversion, highlighting the differences in terms of thruster configurations that can be obtained when adopting different strategies.

5.1   Optimisation strategy

The purpose of the strategy is to obtain an optimal thruster location in order to increase the total DP capability of the vessel. To do that an optimisation procedure has been implemented to maximize the goal. The allocation procedure used to solve the station-keeping problem, as stated in Chapter 4, requires by itself a dedicated optimisation strategy. For such a reason

the complete problem to be solved refers to an optimisation process that should run multiple optimisations related to thrust allocation at each step.

The problem of optimal thruster location on the hull bottom in sense of maximum DP capability is not easy to model because multiple sub-problems can rise up once different constraints are given. Through this study only the simple problem of location is considered, selecting to keep the thruster size constant. Limitations in terms of feasible positions can be set for each thruster or only for some of them, letting the other positions free to change. Questions can rise up for the optimal selection of thruster sizing and so on. Based on this kind of considerations more details can be added to the function that should be optimised as objective of the stated problem.

5.1.1 Objective function

Once the problem to solve has been defined, means the optimum location of thrusters with a fixed rated power, it is necessary to define what is the objective function to optimise. Since the capability of the DP system is considered as a function of the maximum wind speed that the thrusters can face at each encounter angle, here the assumed function to optimise is the inner area of the capability plot, which is certainly representative of the overall capability of the DP system.

Because the unknowns of the problem are x_{T_i} and y_{T_i} coordinates of the thruster axis, by adopting standard optimisation methods, like Lagrange multipliers, quadratic programming or non-linear optimisation processes [7], the objective function and the constraints should include the unknowns. It is really hard to find an objective function including the thrusters locations coordinates, however, as already mentioned, the inner area of the capability plot, which is a function of the maximum sustainable wind speed the system is able to face at each incoming angle, could serve as a good measure for the capability of the DP system. Thus, the inner capability plot area A_{cp} has been here assumed as the objective function of the problem:

$$A_{cp} = \frac{1}{2} \int_0^{2\pi} \left[V_{w_{MAX}} \left(\chi_w \right) \right]^2 \mathrm{d}\chi_w \tag{5.1}$$

where χ_w is the angle representing the wind direction with respect to the vessel bow and $V_{w_{MAX}}$ is the maximum sustainable wind speed of the DP system calculated at each angle χ_w.

Equation (5.1) is not explicitly including the variables of the optimisation problem, i.e. the thruster position, but is the value that will be used to rank the different solution. On this purpose, an optimisation technique have to be used, capable to deal with objective functions that

are not explicitly including the variables.

5.1.2   Genetic algorithm

A promising approach to solve the stated optimisation problem is based on genetic algorithms [58]. In fact, it deals with a problem where the objective function (5.1) of the optimisation process comes from a simulation in which the unknown positions modify the output but are not explicitly a part of the objective function. In fact the thruster locations x_{Ti} and y_{Ti} are not part of function (5.1) explicitly, however they appear implicitly through the pseudo inverse matrix $\mathbf{A}^+$. By using alternative optimisation techniques the problem would be the same, because locations are present only in the constraints definitions of the optimisation problem. For such a reason it is necessary to explore the possible changes of equation (5.1) inside the feasible location space for the thrusters along the vessel.

GA can be suitably used to find the solution inside the design space, trying to search an optimal value for the selected objective. Being heuristic adaptive search algorithms, the GA are based on the evolutionary ideas of selection and genetics. So they represent a suitable exploitation of a random search aimed to solve constrained or unconstrained optimisation problems. Even though the process is based on a randomised generation procedure, the algorithm itself is not random at all, using the history of consecutive generations to direct the search into the optimal values region inside the search space. Once the space search is consistently wide or the search involves multi-modal state space or n-dimensional surfaces, a genetic algorithm can provide more benefits than conventional optimisation techniques [93].

The procedure starts with the generation of a feasible population, to do that firstly the longitudinal thruster coordinates x_{Ti} are generated in such a way that:

$$(X_{min})_i \leq x_{Ti} \leq (X_{max})_i \tag{5.2}$$

where $(X_{min})_i$ and $(X_{max})_i$ are the maximum and minimum longitudinal coordinate for each thruster. Once the x_{Ti} coordinates are generated, the transverse thruster coordinates y_{Ti} should be determined. In this case the generation procedure is slightly more complicated, because the steerable thrusters are preferably installed on the flat of bottom (in case of retractile thrusters it is mandatory). For this reason the boundaries for transverse direction should be defined according to the flat of bottom geometry. This means that y_{Ti} boundaries are function of the x_{Ti} previously

generated:

$$(Y_{min})_i \mid_{x_{T_i}} \leq y_{T_i} \leq (Y_{max})_i \mid_{x_{T_i}} \tag{5.3}$$

In addition to the above mentioned procedure, supplementary location constraints can be added, discarding all the individuals that are not satisfying them. In the case of a limiting distance between the rotation centres of two thrusters, the constraint can be expressed in the following form:

$$\left(x_{T_i}^2 - x_{T_j}^2\right)^2 + \left(y_{T_i}^2 - y_{T_j}^2\right)^2 \geq 16 D_{M_{ij}}^2 \tag{5.4}$$

where $D_{M_{ij}}$ represents the maximum between i-th and j-th thruster diameter.

After the determination of the initial population, all the individuals are evaluated according to the objective function given by equation (5.1) and the reproduction procedure can start. During the first iteration, the offsprings are generated in order to maintain the best individuals. From the second iteration and next, the generation step is substituted by the crossover an mutation procedure. In particular the crossover procedure has been implemented according to an exponential scheme, considering two crossover probability factors that are used to combine the chromosomes of four different distinct individuals. The children resulting from crossover and mutation are then compared according to objective function (5.1). In case that function value is higher than the one of respective parents, then the individuals will replace the parents in the next generation. This kind of process is repeated until a suitable final value for the objective function is reached.

5.2 Test case

The simulation study has been carried out on the generic HLCV shown in Fig. 5.5 already used for thrust allocation studies. This vessel has been selected because it presents a particular non-symmetrical thruster disposition and has been designed with thrusters of different size. As already mentioned in chapter 4, the vessel is equipped with a total of 7 thruster devices, 6 azimuthal thrusters and a fixed bow tunnel thruster. As provided by operators, only 6 steerable devices are used during DP operation while the tunnel thruster is not considered in the calculations. For the present vessel, environmental loads are available for wind, waves and current, so they will be used to perform the DP calculations. All the DP calculations performed in this Chapter are referring to the same environment modelling. All the environmental loads,

Table 5.1: Thruster and pipe location and main characteristics for case TS-00

No.	Thruster ID	D	$P_{T_{MAX}}$	T_{MAX}	x_T	y_T
		(m)	(kW)	(kN)	(m)	(m)
2	RF Thruster	2.40	2050	338	57.0	4.2
3	LF Thruster	2.40	2050	338	52.3	-4.2
4	LM Thruster	2.00	1400	230	27.5	-15.0
5	RM Thruster	2.00	1400	230	-22.5	15.0
6	RA Thruster	2.40	2050	338	-60.0	15.0
7	LA Thruster	2.40	2050	338	-60.0	-15.0
NUM	Line ID	x_L	y_L		Fx	Fy
		(m)	(m)		(kN)	(kN)
1	Pipe line	-77.31	4.00		-490.50	0.00

i.e. wind, wave and current, have been considered collinear. Wind and waves are correlated according to the IMCA wind-wave correlation and the current speed V_c has been fixed to 2.0 knots.

5.2.1   Reference ship (case TS-00)

Due to general arrangement constraints, the thrusters are located in an unusual way, partly non-symmetric (see Table 5.1 and case TS-00 in Fig. 5.6). Thrusters 2-5 are on the flat of bottom, while 6 and 7 are at the stern on the inclined buttocks and are used also for the propulsion during transfer. The fore group of steerable devices consists of two closely spaced thrusters at different longitudinal positions. Instead of a standard division in stern and fore thrusters, two thrusters are located more close to midship at different longitudinal positions and on the opposite sides of the ship (thruster 5 on starboard side and thruster 4 on port side). In such a way the thruster location is non-symmetric with respect to longitudinal axis. The only symmetric thrusters with respect to the longitudinal direction are the two stern thrusters, mainly because they are used also for standard propulsive duties of the vessel and not for DP purposes only.

It must be noted that also the size of the thrusters is different, not in terms of dimensions (propeller diameter is fixed) but in terms of power. In fact the thrusters located close to midship have a lower available power with respect to the others.

The vessel has been designed for S-lay operations with a stinger mounted in non-symmetric position. To properly take into account the pipe-lay operation in DP calculations, a fixed external load due to pipe tension has been considered, acting on the vessel with coordinates and magnitude given in Table 5.1. Data are available for the environmental loads from dedicated experiments on model scale for the selected S-lay operational mode, granting a sufficiently accurate estimate of vessel's DP capability.

5.2.2 Optimal location

The search of optimal location ensuring the maximum capability for the vessel has been divided in two different cases in agreement with the fact that the two back thrusters 6 and 7 are not dedicated exclusively to the dynamic positioning, but are also used for the propulsive duties during transit. Therefore, see Fig. 5.5, two stern thrusters are not located on the flat of bottom of the vessel, but are integrated with the stern buttocks like in any propulsive configuration.

For such a reason, considering the retractile thrusters installed on the flat of bottom, according to the designers request it has been decided to keep fixed the position of propulsive thrusters in both the tested hypotheses. In the first case (TS-01), the remaining four thrusters are moved during the optimisation process while in the second case (TS-02), a completely independent DP system is supposed to be mounted on the vessel by considering the propulsion system independent from the DP.

First case (Case TS-01)

In the first case TS-01 a vessel with the same thruster configuration of the original vessel, considering two propulsive thrusters (6,7) of the same size is examined. The other 4 thrusters are also the same, but the *i-th* positions can vary along the flat of bottom of the vessel to optimize DP capability.

With these preliminary considerations, the total amount of unknowns is 8, being representative of two spatial coordinates of four thrusters on the flat of bottom. To ensure that the thrusters will be located on the flat of bottom, each time that a thruster is located in a determined longitudinal position, the transverse bounds are automatically updated according to the available outreach.

Having 8 unknowns, each population is composed by 64 individuals. Due to the complexity of the objective function, it is not granted that the function values of the best individual will change at each iteration, for such a reason, the exit point of the algorithm is set to a predetermined
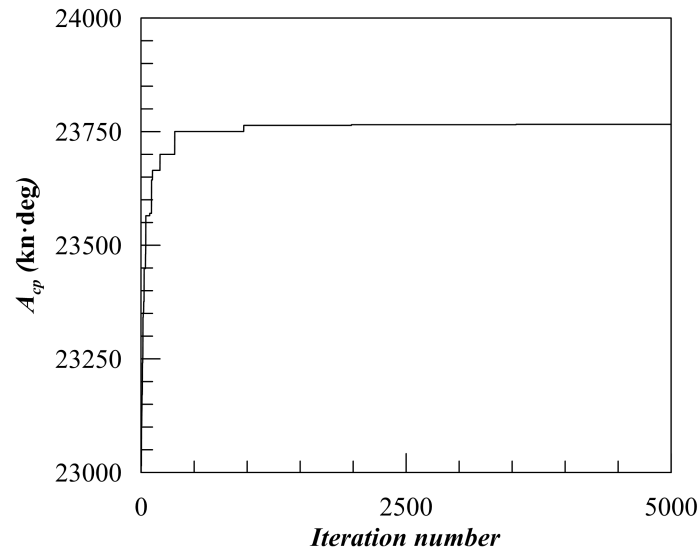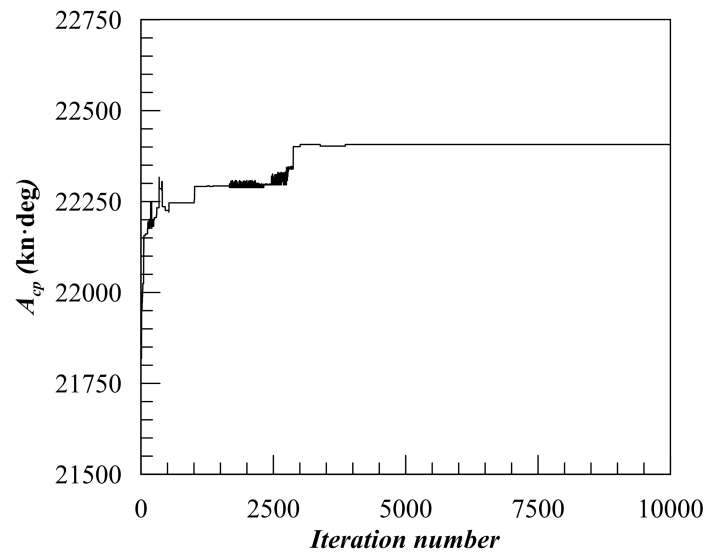
Figure 5.1: Genetic algorithm convergence diagram for case TS-01
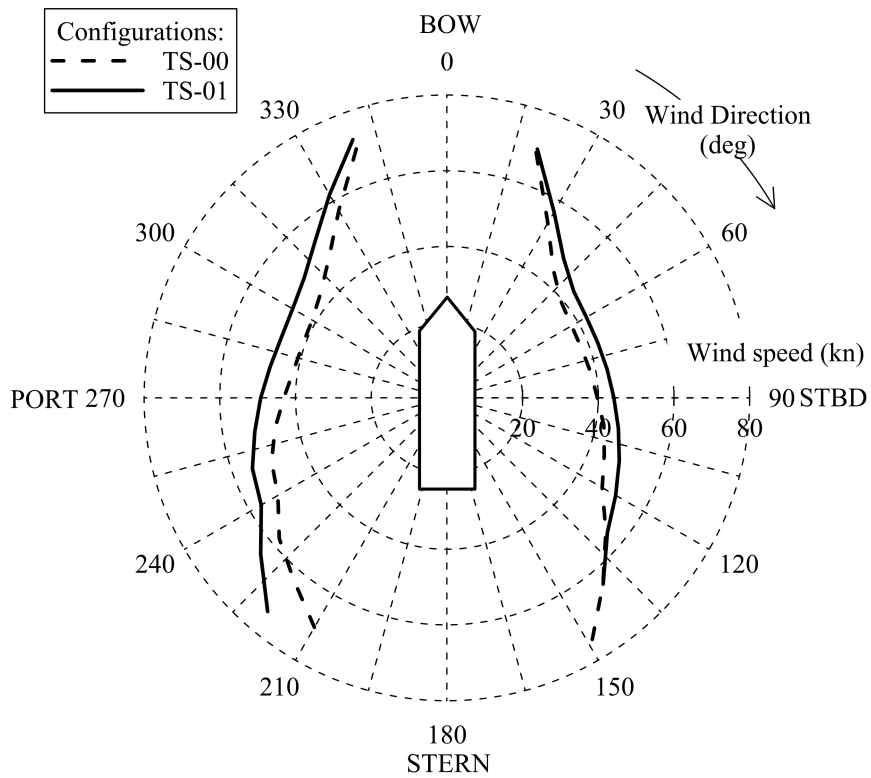
Figure 5.2: DP capability plot comparison between cases TS-00 and TS-01, resulting from optimisation procedure

number of iteration runs, keeping as optimum the final value of the objective function. After several tests it has been found that 5000 consecutive iterations are ensures convergence for the algorithm. The algorithm convergence diagram for the specific case is shown in Fig. 5.1, highlighting that a total increase of objective function of about 9% has been found during the optimisation process (see Fig. 5.2). The final obtained thruster configuration is presented in Fig. 5.6 and in Table 5.2 in graphical and tabular form. In this case, the fore thrusters 2 and 3 maintain a relative spacing above the four diameters, without the need to consider the additional constraints given by equation (5.4).

Second case (Case TS-02)

The second analysed case TS-02 refers to a new idealised configuration, where a dedicated DP system is assumed for the vessel, considering the installation of a set of 6 retractile thrusters on the flat of bottom (2-5, 8 and 9). The total installed power is then comparable with the previous configuration, because the thrusters 6 and 7 are used for propulsion only, so they are switched-off during DP operations. The constraints on the transverse position of each thruster are automatically implemented as function of longitudinal position, according to the flat of bottom geometry.

For this case, the total number of unknowns is 12, so each population is composed by 96 individuals. As for the previous tested case a set of trial rounds has been carried out to find the necessary iteration number to reach convergence. Having increased the unknowns, for the specific case a total number of 10000 iterations has been considered for the genetic algorithm procedure. The specific convergence diagram for this case is reported in Fig. 5.3, the optimising process led to a capability increase of about 6% in objective function (see Fig. 5.4) by adopting a configuration as reported in Fig. 5.6. However, as it can be observed in Fig. 5.6, the thrusters are located in two distinct groups, one in the fore-ship and one in the aft., being too close to each other. This is due to the simplifications used in the allocation algorithm, that is not considering the presence of thruster-thruster interaction effects and forbidden zones. For such a reason, it has been selected to study another case, imposing position constraints between the thrusters according to equation (5.4).
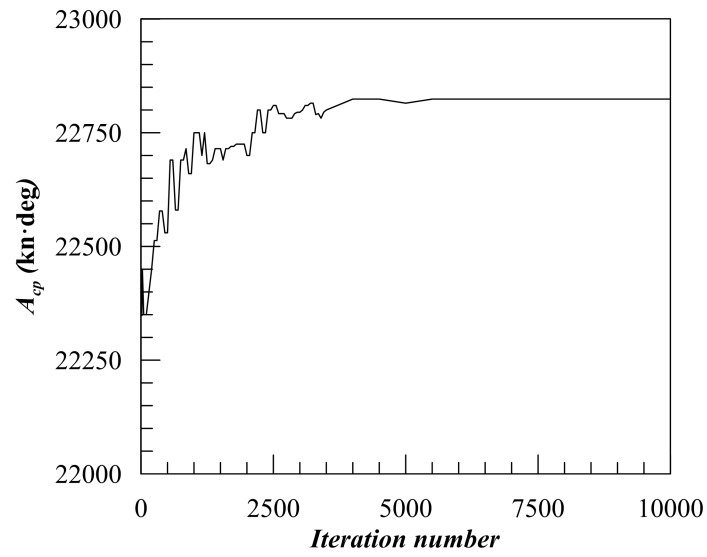
Figure 5.3: Genetic algorithm convergence diagram for case TS-02
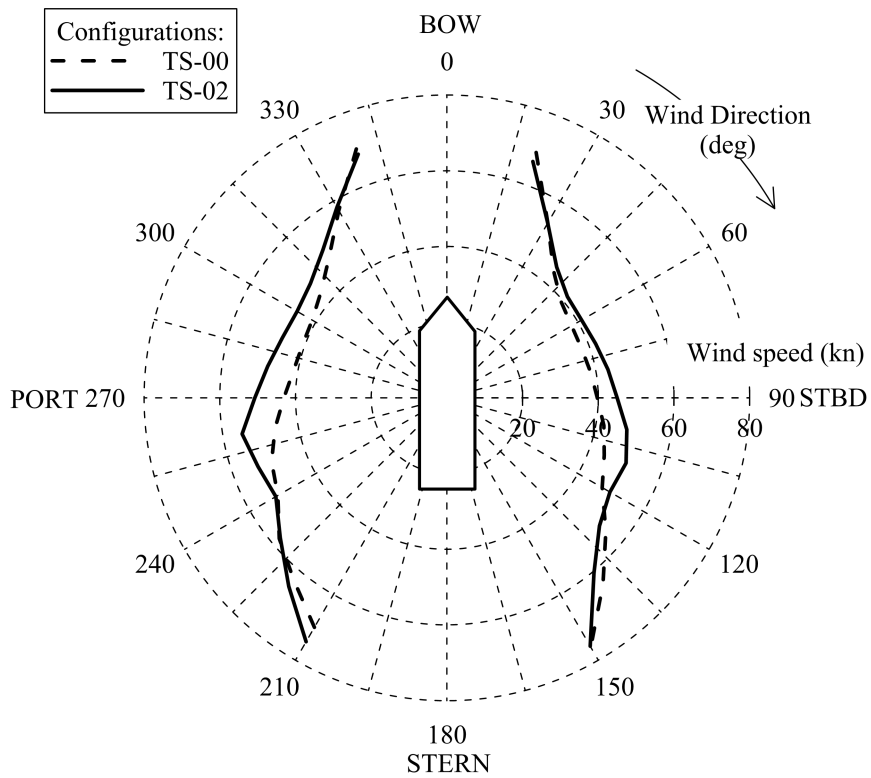
Figure 5.4: DP capability plot comparison between cases TS-00 and TS-02, resulting from

optimisation procedure
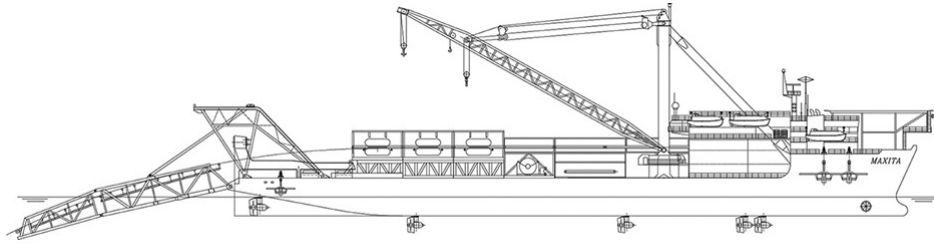
Figure 5.5: Profile view of the HLCV vessel under analysis
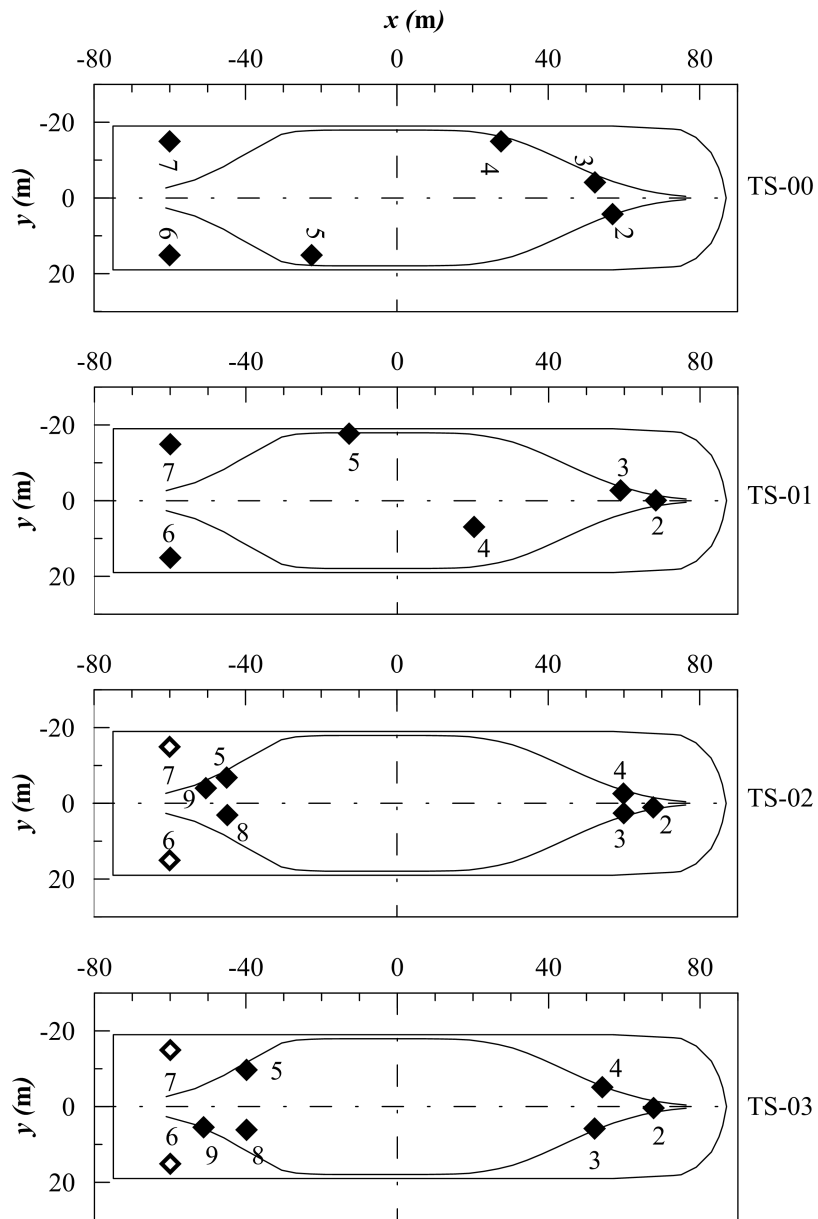
Figure 5.6: Thruster positions for cases TS-00, and optimal thruster positions TS-01, TS-02

and TS-03

Table 5.2: Power and optimal thruster positions TS-01, TS-02 and TS-03

No.	Thruster ID	TS-01			TS-02			TS-03		
		$P_{T_{MAX}}$	x_T	y_T	$P_{T_{MAX}}$	x_T	y_T	$P_{T_{MAX}}$	x_T	y_T
		(kW)	(m)	(m)	(kW)	(m)	(m)	(kW)	(m)	(m)
2	RF Thruster	2050	68.4	0.2	1800	67.8	1.0	1800	67.8	0.3
3	LF Thruster	2050	59.0	-1.0	1800	59.9	-2.6	1800	54.2	-5.2
4	LM Thruster	1400	20.3	2.9	1800	60.0	2.5	1800	52.2	5.7
5	RM Thruster	1400	-12.7	-10.0	1800	-45.0	-6.9	1800	-39.9	-9.7
6	RA Thruster	2050	-60.0	15.0	-	-60.0	15.0	-	-60.0	15.0
7	LA Thruster	2050	-60.0	-15.0	-	-60.0	-15.0	-	-60.0	-15.0
8	RA1 Thruster	-	-	-	1800	-44.8	3.0	1800	-39.8	6.1
9	LA1 Thruster	-	-	-	1800	-50.5	-4.1	1800	-51.2	5.4

Third case (TS-03)

Case TS-03 refers to the same configuration as TS-02, considering the installation set of 6 retractile thrusters on the flat of bottom (2-5, 8 and 9), having the same size as the previous case. In addition to the transverse position constraints according to the bottom geometry, additional constraints have been imposed per each thruster, forcing that the thruster centre of rotation should be distant more than 4 propeller diameters to all the other thrusters. This kind of constraints has been selected to overcome to the thruster allocation algorithm simplifications, neglecting thruster-thruster interaction and forbidden zones.

Also in this case, having 12 unknowns and populations composed by 96 individuals, 10000 iterations have been considered for the GA procedure. The convergence diagram is reported in Fig. 5.7. Case TS-03 has a lower capability with respect to case TS-02 (see Fig. 5.8), but still increases the objective function value of about 3.5% compared to the original configuration. The resulting thruster positions are also reported in Fig.5.6 and in Table 5.2, showing that the fore and aft groups of thrusters are spaced according to the selected constraints. Since it is generally recognized and assumed that the interaction effect between two thrusters can be neglected once the distance between them is higher than four diameters, it is reasonable to assume that the allocation algorithm adopted is giving a reliable solution.

Figure 5.7: Genetic algorithm convergence diagram for case TS-02
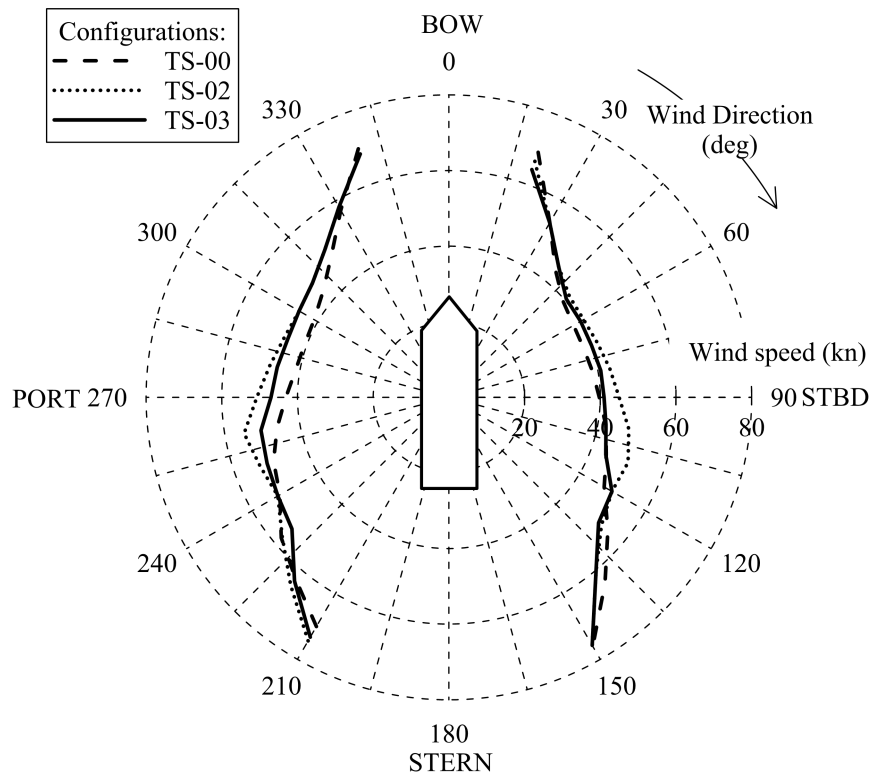
Figure 5.8: DP capability plot comparison between cases TS-00, TS-02 and TS-03, resulting

from optimisation procedure
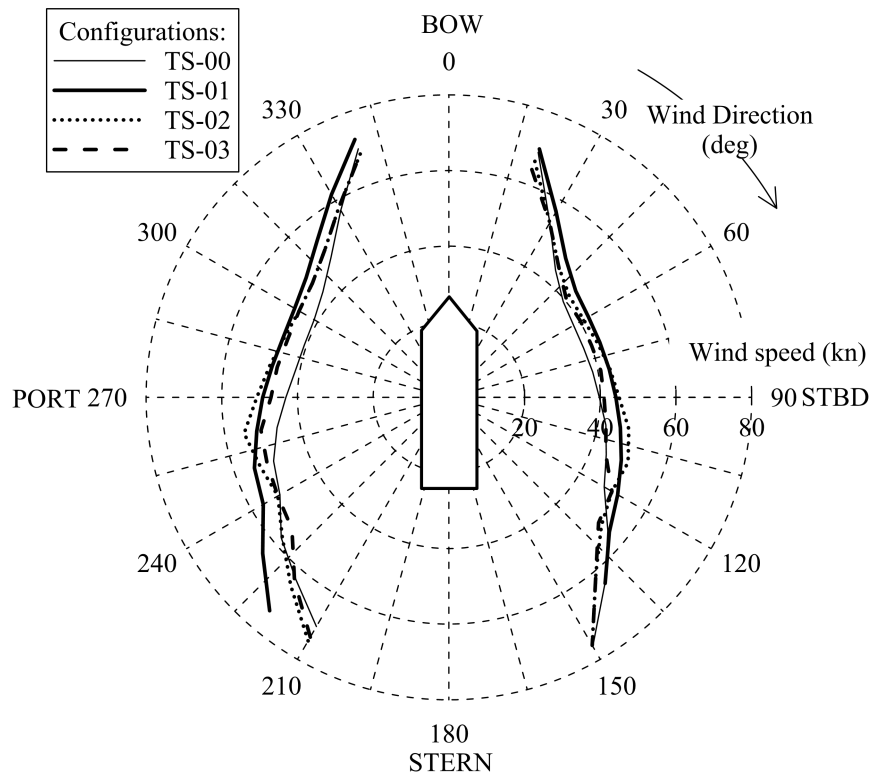
Figure 5.9: DP capability plot comparison between cases TS-00, TS-01, TS-02 and TS-03, resulting from optimisation procedure

Results

By comparing the solutions obtained from the examined cases (Fig. 5.9), several considerations can be drawn out. As first, the first solution TS-01 is giving a higher DP capability compared to the original thruster configuration. That means the original thruster configuration was not the best possible choice for the selected vessel. Also the second option, represented by case TS-02 is giving a higher capability area compared to the original one, however the solution was not feasible, being the thrusters too close to each other. Considering the additional constraint to avoid interaction on the thruster mutual location (case TS-03) the capability is still higher than the original one.

Comparing the two optimised solutions TS-01 and TS-02, it can be highlighted that condition TS-02, the one with equal thrusters, increases the capability of the vessel for beam seas conditions, without losing a lot of area for head seas while condition TS-01, the one obtained by changing only 4 thrusters, is gains area for stern and stern quartering directions. However, while considering the feasible solution TS-03, the capability increase in the side area is lower (Fig. 5.8) as expected due to interactions; this is mainly due to the fact that the thrusters are no more

closely grouped in the fore and aft part of the flat bottom of the vessel.

Finally, comparing the solutions TS-01 an TS-03, it can be stated that, for the analysed vessel,the configuration with the two main propulsive thrusters adopted for DP is more favourable than the one with 6 thrusters mounted on the flat bottom.

5.2.3 Additional remarks

The presented procedure for the optimal thruster location on an offshore vessel gives the possibility to find thruster configurations that can improve the total DP capability of the vessel. An improvement with respect to the original thruster disposal has been found for both tested configurations TS-01 and TS-02, with a capability increase of about 9% in the first case and 6% in the second one in term of DP plot area. Since case TS-02 was not feasible, due to the close proximity of the thrusters, additional constraints have been added, determining a feasible solution that is still 3.5% better than the original configuration.

Due to the huge amount of calculations needed to determine the objective function a simple thrust allocation algorithm has been used to obtain the capability of each generated individual. In the current study no specific design constraints due to vessel general arrangement were applied, because they are unknown, even if the proposed procedure is able to investigate cases with more restrictive constraints as demonstrated with the third analysed case. To decrease the calculation time the objective function can be changed, limiting it to the single environmental condition, which is the most representative for the particular DP operation of the vessel, and investigate, for example, the configuration with minimal fuel consumption, by adopting more complicated thrust allocation procedures.

Chapter 6

Combined predictions and operability index

With the continuous moving of offshore activities towards deeper waters, DP system is the most suitable method to keep position [2] and, for auxiliary and support vessels, DP is probably the most flexible choice also for less deep waters. Therefore, for new build and existing vessels, good station keeping performances are mandatory. Besides station-keeping requirements, the operation capability of a vessel is also determined by level of motions during standard operations, both in stationing and in seagoing operations [103]. This means that both the aspects should be jointly evaluated [98], since the preliminary design state, even if nowadays this two characteristics are predicted separately. In fact, standalone DP calculations are performed, without taking in consideration eventual restrictions due to ship motions during the field operations. On the other hand, seakeeping calculation for ship motions are not used to establish proper constraints to DP calculations. As mentioned in Chapters 2 and 3 the regulations for DP assessment refer to a constant wind speed, not depending from the vessel heading, that the DP system should be able to balance considering a constant current and a wave associated to the wind speed with a dedicated correlation.

Despite no specific regulations or guidelines are given in literature, the general opinion is that by performing seakeeping calculations during the station keeping analysis will give additional information to the naval designers, in order to identify the effective DP capability of the vessel during different kinds of operations or under different environmental conditions. When designers or operators could provide motion criteria for operation or rough sea state condition, it is possible to convert these criteria into wind speed that can be used in DP capability plots to establish

an effective environmental limit for DP calculations, through a quasi-steady approach [90] or a time-domain simulation [126]. However an alternative option can be considered. Instead to perform DP calculations according a specific wind-wave correlation, dedicated calculations can be carried out considering the wave scatter diagram of specific sea areas [57]. In such a case the dynamic positioning predictions are made for the specific conditions of seakeeping ones, and not only for assumed combination of sea states determined by the wind-wave correlations.

Since it is the intention to develop a methodology suitable for early design stage, quasi-steady DP calculations will be performed to assess vessel station-keeping capability. This simplification is necessary to speed up the calculation process in the early design stage, where multiple design variations can be analysed and compared. A quasi-steady approach intrinsically neglects the dynamics involved in a DP operation, as, e.g., thruster/rudder dynamics [114], dynamic thrust loss effects, external loads variations and transient effects [130]. The calculation is, then limited to a static balance between environmental and thruster forces. It is well known that the quasi-steady DP calculations overestimate the vessel capability with respect to time-domain simulations [130, 89], which are more time consuming but easier to validate with full scale data, as already stated in Chapter 2. Quasi-steady calculations can be enhanced by including correction factors with respect to time-domain simulations [130] or by modelling additional features, like offset determination [8] or thrust losses [13], to overcome the absence of vessel dynamics. Also with these enhancements coming from time domain-calculations, an error level in the final prediction cannot be provided [126]. That means an universal confidence cannot be stated, but quasi-steady codes can be compared with each other to determine their reliability and compliance [148]. Despite these limitations quasi-steady programs are acceptable for early-design stage and their use is allowed by classification societies.

In the present thesis a newly developed methodology is proposed to perform preliminary seakeeping and DP calculations on a wave scatter diagram in order to establish an enhanced DP operability index for early design stage. The present method, as assumption, still considers seakeeping and station-keeping dissociate, but ensures that both calculations will refer to the same environmental modelling. An example will be given on a reference vessel, comparing the obtained results with basic DP analysis for early design. As reference, the HLCV case introduced in Chapter 4 will be used. Here the vessel will be named PLV, since the adopted criteria will refer to pipe-laying operations, so considering this particular operative profile for the vessel.

6.1 Basic seakeeping analysis

Another important aspect for the design of an offshore vessel is the determination, since the early design stages, of the seakeeping responses during field operations. For this purpose dedicated calculations can be carried out using bi-dimensional or three-dimensional analytical methods, where a large amount of seakeeping codes are available. The selection of the method to adopt should not be justified by semantics, but by the accuracy level that should be reached in the specific design stage and by the reliability of the procedure.

When the seakeeping performances of an offshore vessel should be assessed, generally the following four items have to be analysed:

- Wave response characteristics of the vessel, depending on form, dimensions and weight distribution of the vessel.

- Sea wave/extreme conditions.

- Ship speed and heading, determining the encounter of the vessel with incoming waves.

- Quantitative and qualitative criteria for passenger/crew safety and equipment for vessel operations.

The implementation of the seakeeping hydrodynamic model necessary to execute the calculations is not an easy task and cannot be underestimated since early design stages. The particular problematic situation could arise when it is necessary to determine characteristics related to roll motion, where it has been always recognised that the prediction of damping close to natural frequency is not easy to evaluate accurately. Viscous phenomena acting in the roll motion damping require the use of viscous codes, requiring a lot of computational time, to be modelled. For such a reason empirical or semi-empirical methods still play an important role in roll motion prediction. In particular for offshore vessels, where geometry is not comparable with conventional ships due to the presence of huge skegs, sharp edges or moonpools, the lack of extended databases make the problem even harder. In fact, without sufficient data necessary to tune empirical methods, the reliability of the hydrodynamic model cannot be always ensured.

For the reference ship, dedicated seakeeping calculations have been carried out, using a code based on 2D strip theory [128], being able to determine the RAOs for the 6DOF motions of the vessel [94, 51]. From the obtained RAOs it is then easy to evaluate root mean square (RMS) or single value amplitudes of vessel motions, considering an appropriate wave spectrum. It must

Table 6.1: Limiting criteria for a PLV

	Maximum single amplitude	
Operational modes	Pitch (deg)	Roll (deg)
Pipe-lay operations	1.0	5.5
Standby	1.5	8.0
Transit	10.0	20.0

be noted that the seakeeping calculations have been carried out considering the vessel symmetry along *x* direction. This assumption has been made because stinger was not implemented in the hydrodynamic model. Due to the stinger asymmetrical position it can be reasonable to presume that also motion responses will be asymmetrical, giving also different values for added mass and damping coefficients for the 6DOF motions. However, for a preliminary prediction, this kind of details can be neglected and reconsidered during an advanced design stage.

Besides problems related to hydrodynamic modelling, the main difficulty to establish seakeeping performances of a vessel is the specification of limiting values for the vessel responses or motion related criteria which will cause performance degradation. Those criteria are the ones that should be set to determine ship operability. In case of the reference PLV vessel, the typical limits for S-lay operations, as given by operators, are primary due to roll and pitch motions. An overview of the limits given by the ship operator, expressed in term of maximum single amplitude, is given in Table 6.1. Here the limits are reported for three different conditions: *Pipe laying*, *Standby* and *Transit*. The first limit refers to the maximal motions that are sustainable for pipe lay operation. The second one is representative of the maximal motions that are sustainable to keep the pipe connected to the vessel, while the third limit refers to transit condition, which are not directly related to DP issues. Through this thesis the pipe-lay condition only has been considered, in such a way to be coherent between seakeeping and DP calculations.

To visualise seakeeping calculations results it is common practice to use diagrams and graphs. In particular, when the operability is investigated, several kinds of graphs can be used. In any case, the most of the options always highlight a critical curve, indicating that a certain parameter has been exceeded. Critical curves can be visualised directly on wave scatter diagrams, by plotting it as function of *Zero-Crossing period T_z* and *significant wave height $H_{1/3}$*. In such a way, a critical border can be drawn for each encounter condition and for each motion/operation criteria. This will result in a set of curves superposed to the scatter diagram itself.
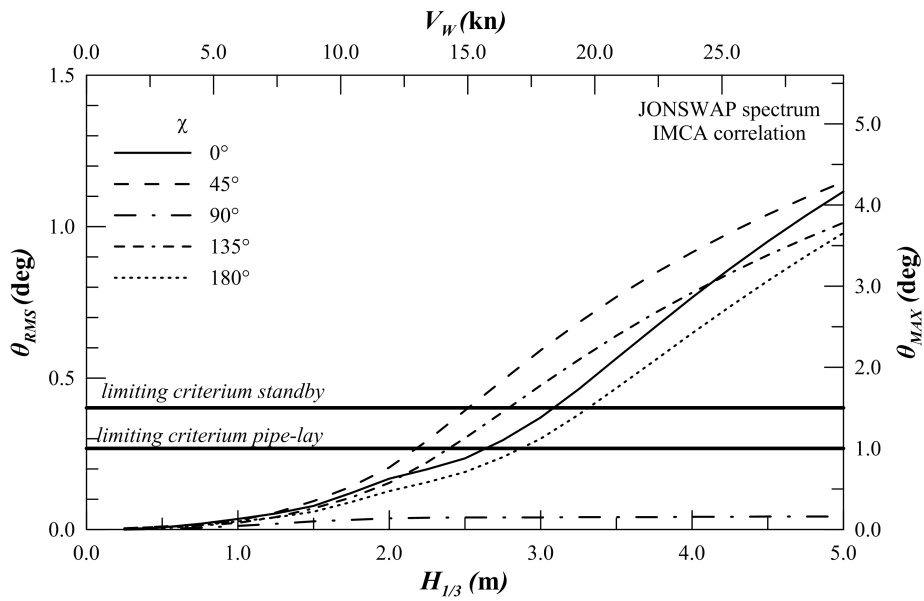
Figure 6.1: Limiting criterion for pitch motion in pipe-lay operation and standby on the reference PLV, for different headings at zero speed
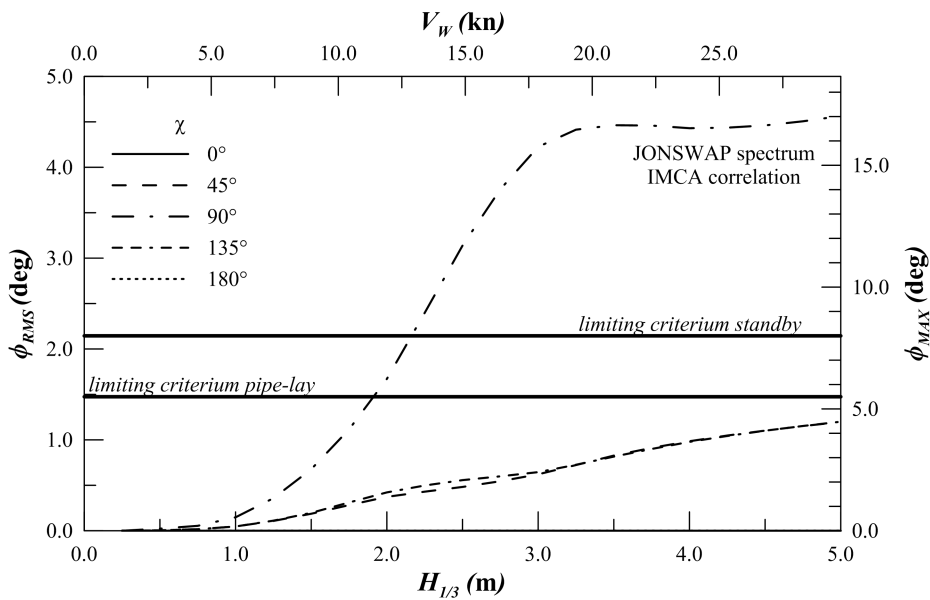
Figure 6.2: Limiting criterion for roll motion in pipe-lay operation and standby on the reference PLV, for different headings at zero speed

Another way to visualise the results is to directly plot RMS or maximum single amplitude values as function of the $H_{1/3}$ adopted for the calculations. This should be done in accordance with a specific wave spectrum which is determined by a wind-wave correlation. Then the motion criteria can be automatically visualised on the graph. For the tested ship the second approach has been used with IMCA wind-wave correlation. For pipe-lay condition, the results are reported in Fig. 6.1 for pitch motion and in Fig. 6.2 for the roll motion, considering the limitations as per Table 6.1.

6.2   Integrated station/seakeeping predictions

The previous two sections currently represent the basic way to analyse station-keeping and seakeeping of a vessel in an early design stage. Here, separate predictions and different environmental conditions are adopted to determine a final index for operability.

However it is obvious that the two thematics are not distinct, but strictly related especially for the limiting environment determination. As it can be seen in Figs. 6.1 and 6.2, the seakeeping limiting environment is highly dependent on the ship heading, being the vessel responses significantly different with heading. On the other hand, as example, for ERN determination the limiting environment is represented by a constant wind speed limit which is invariant to vessel heading. However, the environmental loads evaluated for dynamic positioning predictions are heading dependent. Therefore it is reasonable to expect that the limiting environment can be established combining both DP and seakeeping.

A possible way to combine the predictions is to use the critical curves obtained during seakeeping analysis to compute a new limiting environment in the capability plots due to ship motions [90]. In such a way it is possible to combine the operating conditions, usually determined by limitations of motion or acceleration for certain equipments (like derrick, cranes, stingers, etc.), together with station-keeping capability determined with quasi-steady calculations and reported on capability plots.

The critical curves used to determine seakeeping criteria are expressed as function of heading χ, $H_{1/3}$ and T_z, covering all the possible combinations between wave heights and wave periods that can be found for a certain sea area. However standard station-keeping calculations are not covering all the scatter diagram combinations, but they are made following a specific wind-wave correlation. The correlation curve to adopt can be selected according to the calculation
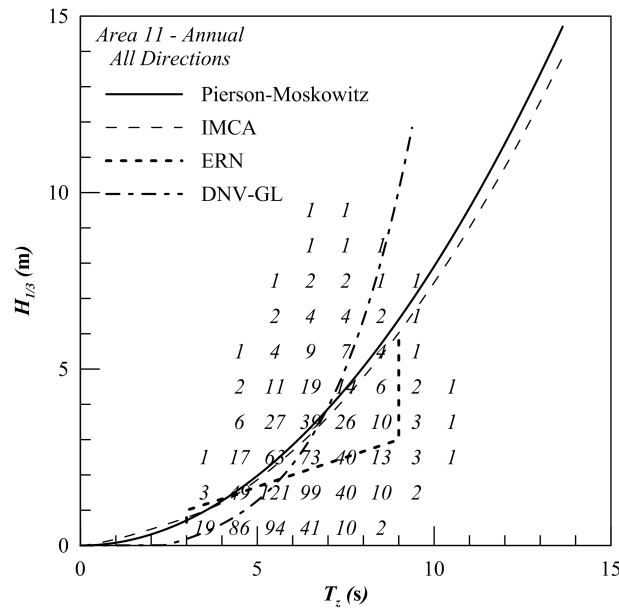
Figure 6.3: DNV, ERN, IMCA and Pierson-Moskovitz wind wave correlation on North Sea scatter diagram

that should be made, generic correlation can be used such as ERN suggested one or Pierson-Moskowitz spectrum derived formulations. Other possibilities are given by the adoption of more specific correlation, like IMCA which is used for the North Sea.

In particular IMCA correlation is widely used for DP calculation, also outside specific ambient of North Sea area, where reference is made to a JONSWAP spectrum. The wind-wave correlations can be drawn on a scatter diagram and compared with each others. In fact standard wind-wave correlations are usually given in tabular form, but have all the information needed to be plotted together with the general Pierson-Moskovitz correlation on a scatter diagram.

As it can be seen in Fig. 6.3, the different wind-wave correlations are quite similar and are going through the same cells of the wave scatter diagram. Apart from the ERN correlation, which is following a completely different law. This one is representing sea states that are less restrictive than the other two correlations. It can be also observed that for the North Sea area the IMCA correlation is representative of a sort of border between the most and the less probable waves for North Sea.

The small differences between different correlation curves, highlights that no huge difference will be made by using IMCA curve instead of Pierson-Moskovitz correlation. To be coherent between the seakeeping and DP calculation it is reasonable to use relations coming from comparable sea spectra.
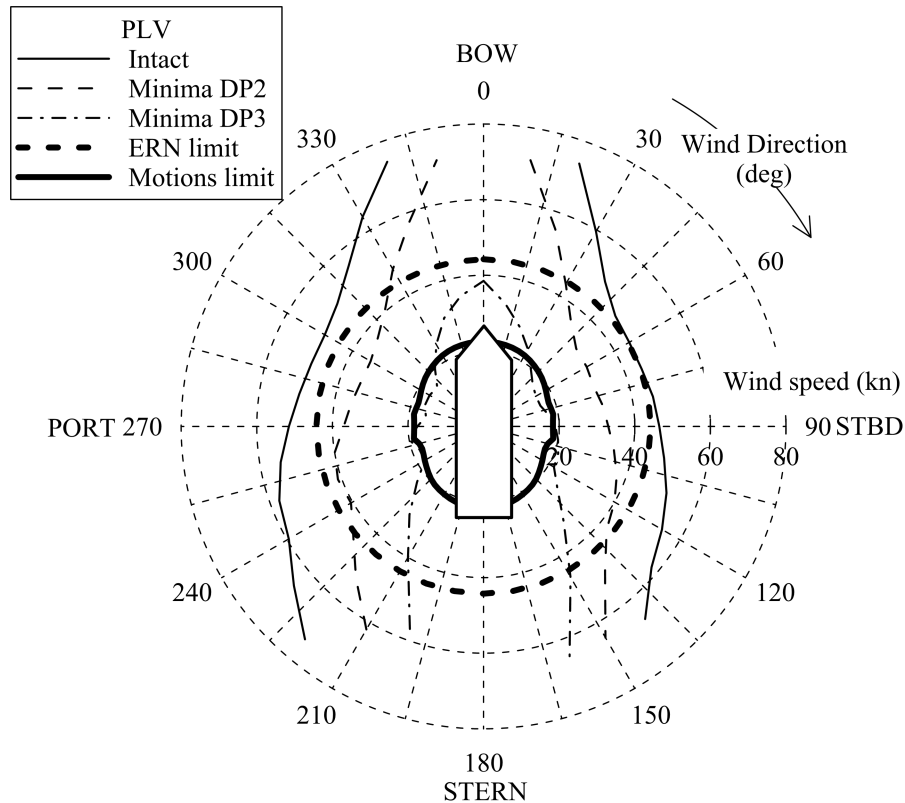
Figure 6.4: Comparison between motion limiting curve and environmental limiting curve given by ERN regulation for the reference ship

Considering the reference vessel, seakeeping calculations have been already made according to IMCA correlation. So the intersections of the limiting curves with maximum values curves presented in Figs. 6.1 and 6.2 are directly representative of the motion limiting environment as function of maximum sustainable wind/wave per each heading. In fact, the *limiting criterion* curves intersect the RMS ones in a single point. This corresponds to a specific sea state condition given by IMCA correlation. In such a way the determination of the maximum sustainable wind speed/wave height is straight forward.

The resulting motion limiting environment for the PLV vessel is reported in Fig. 6.4 together with the standard ERN one. In this specific case the pitch is restrictive, leading to a really low maximum sustainable wind/wave at each heading. From a rough analysis of the obtained motion limiting environment, it can be expected that the operative condition of pipe-laying can be exploited also in case of DP3 failure. Since the present plot does not consider dynamic allowances, it is reasonable to presume that the vessel will be able to operate only with a single failure.

However, the previous approach is not able to represent all the possible environmental conditions

that the vessel can encounter during field operations, which can be represented in terms of wave height - wave peak period combinations. That means it is not able to give a well determined indication regarding the effective DP system operability.

6.3 DP operability index

Standard regulations and the above described combined predictions are not able to clearly define the capability characteristics of the system, since all feasible wave height - wave peak combinations cannot be examined in terms of specific working area. For this purpose a different strategy can be adopted. Instead to perform standard DP calculations to determine a capability plot, it is proposed to execute a dedicated calculation for each possible combination of $H_{1/3}$ and T_z for the selected operational area, adopting a *cell based approach*. Calculations can be carried out for each heading, evaluating whether the DP system is able or not to keep the vessel in position with the selected sea environment.

In a scatter diagram, each cell is defining only the wave conditions representative of a selected area, no indication is given regarding the other environmental loads associated to a DP calculation. In particular it is necessary to define the related conditions for wind and current.

Standard correlations are used to determine a single combination of $H_{1/3}$, T_z and V_w, which is covering only certain cells in the wave scatter diagram. Evaluate the wind speed generating the other parameter combinations is not an easy task and is a problem that needs to be properly analysed. In an early design stage some assumptions can be made to simplify the issue.

Starting from the assumption to model the sea state by means of a Pierson-Moskovitz spectrum [118], the following relations can be used to correlate wave parameters with wind speed:

$$T_z = \frac{2\pi}{g \sqrt[4]{\pi\beta}} V_w \tag{6.1}$$

$$H_{1/3} = \frac{2}{g} \sqrt{\frac{\alpha}{\beta}} V_w^2 \tag{6.2}$$

where α and β are two constants set to 0.0081 and 0.74 respectively.

Modelling the environment according to the above formulations, leads to an ambiguity, since the two equations are giving a single solution only for values described by the wind-wave correlation derived from Pierson-Moskowitz spectrum. For the rest of the remaining scatter diagram area a solution should be found in order to roughly evaluate a reasonable wind speed. According to the above mentioned relations there are two different equations by using $H_{1/3}$ or T_z, giving totally

different kind of possible wind speeds.

From data analysis done in the oceanic engineering, a strong correlation has been always found between wave height and wind speeds. Correlations involving also the T_z are not easy to derive and maybe possible correlations are changing zone by zone. Starting from this consideration it is reasonable to use the correlation given by equation (6.2) as single relationship to establish the wind speed. In such a way there will be no dependency on T_z. Taking in consideration equation (6.1), then, for combination below the Pierson-Moskowitz correlation curve, the resulting V_w will be higher than the wind speed resulting from equation (6.2). Above the correlation, equation (6.2) becomes higher.

Another possibility is to take into account the T_z dependency and consider equation (6.1) below correlation curve and equation (6.2) above it. By doing this, the maximum possible V_w is selected for each $H_{1/3}$, T_z combination. This kind of approach can be considered on the safety side, once probably will overestimate the possible loads due to wind. In a preliminary design stage can be considered acceptable.

Another issue is the current load. In this case the same settings of IMCA standards have been adopted, considering a constant current speed collinear with wind and waves.

Having determined the environmental condition settings it is then possible to perform DP calculations for each cell of the scatter diagram. In such a way it can be determined weather the vessel is able to keep position or not. The process should be repeated for all the possible vessel headings. Then, considering the wave occurrences it is possible to evaluate the DP operability in the selected area according to the following formulation:

$$OP_{DP} = \sum_{i=1}^{N_h} p_{h_i} \sum_{i=1}^{N_w} p_{g_i} I_{DP} \tag{6.3}$$

where p_h is the probability associated to each N_h vessel heading, p_g is the probability associated to each N_w specific wave condition. p_g is associated to the wave occurrence in a scatter diagram, while p_h should be given by the operator in case the vessel will keep position according to preferential headings. In case no information is available, p_h can be considered uniform along all the heading range.

Function I_{DP} is defined as:

$$I_{DP} = \begin{cases} 1 & \text{when DP system holds position} \\ 0 & \text{when DP system loses position} \end{cases} \tag{6.4}$$
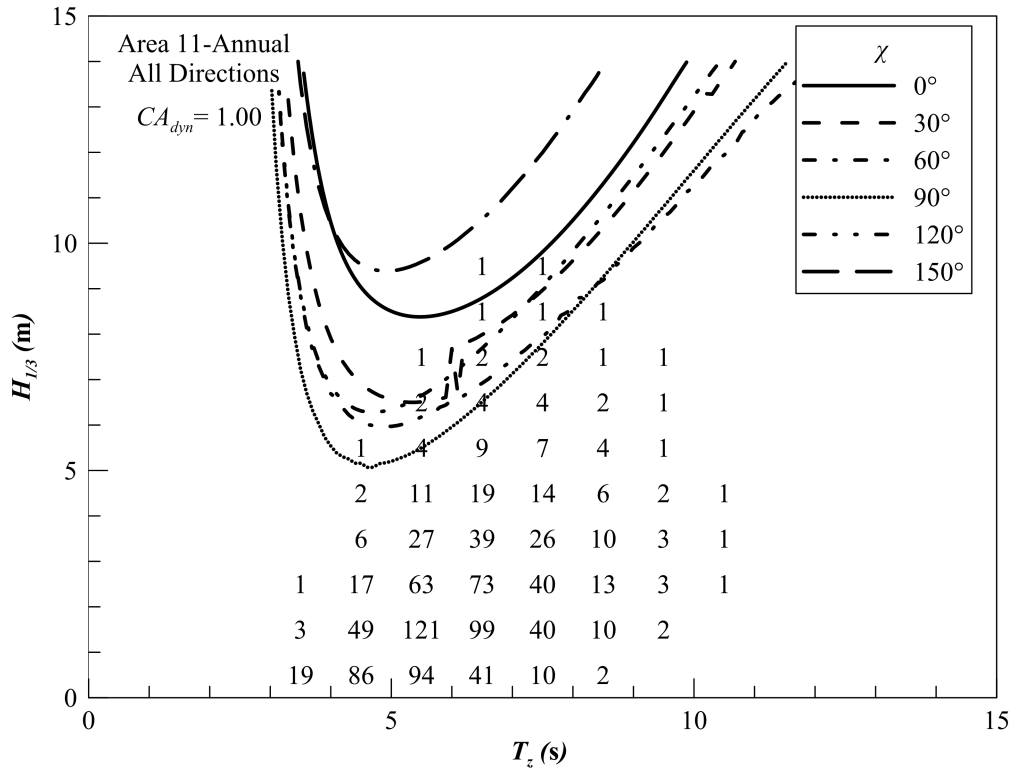
Figure 6.5: DP critical curves for the generic PLV vessel considering all thruster running (intact)
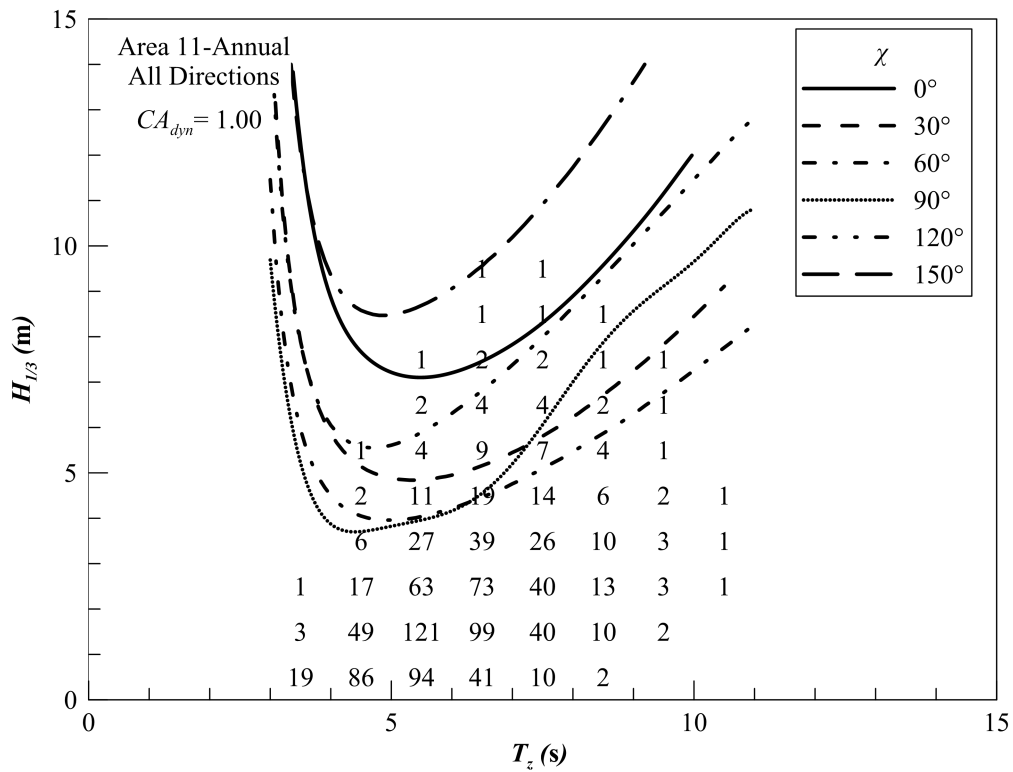
Figure 6.6: DP critical curves for the generic PLV vessel considering a single failure case (DP2)
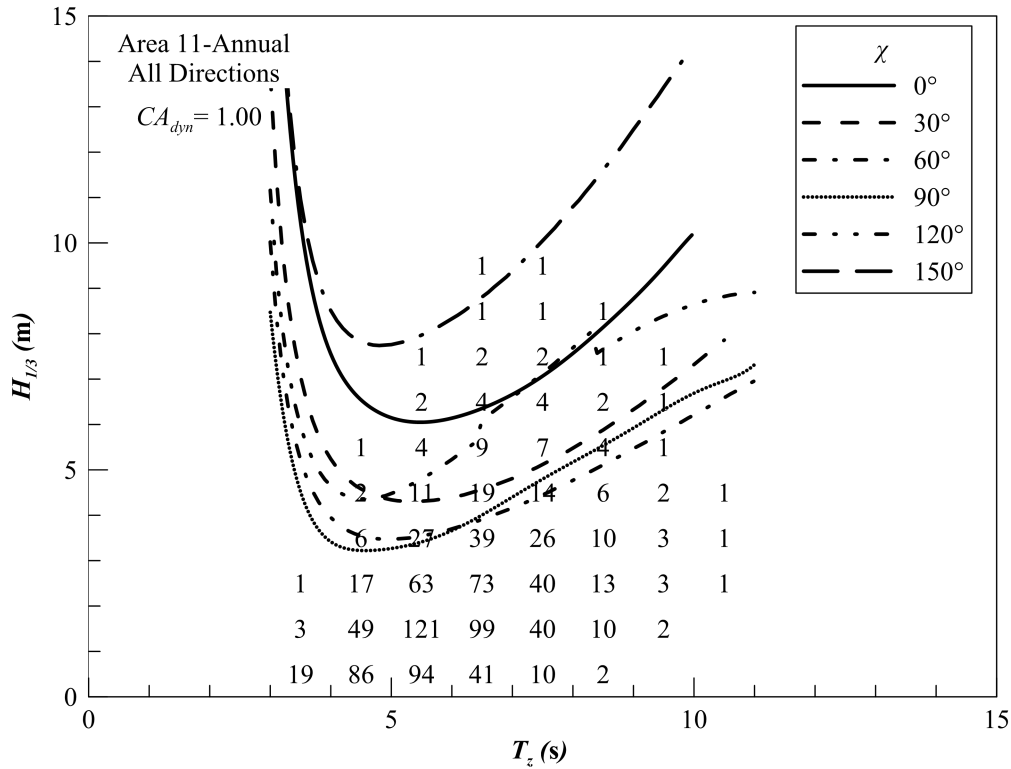
Figure 6.7: DP critical curves for the generic PLV vessel considering two failures (DP3).

With this assumption it is possible not only to establish operability index OP_{DP} but also to draw critical curves related to DP system. This kind of calculation can be also carried out for all the failure conditions so giving the overall operability evaluation.

From the previous combined prediction, the motion limitation to DP operations have been highlighted. However, because DP calculation are carried out only for a specific wind-wave correlation curve, it is not possible to directly establish whether the DP system is suitable to keep the vessel in position for all the other possible $H_{1/3}$, T_z combinations.

For this purpose specific calculation have been carried out changing systematically the wave conditions (and consequently wind speed) as described in the previous sections, with the aim to establish DP critical curves. As it can be seen in Figs. 6.5, 6.6 and 6.7, the critical curves can be obtained for each considered heading angle, taking into account also different failure conditions. In Fig. 6.5 the intact condition has been considered, so the critical curves refers to a condition with no failure. In Fig. 6.6, a condition representative of a DP2 case is considered, here thruster No. 2 (with reference to Table 5.1) is not working and as it can be seen the critical curves are lower than the intact condition case presented in Fig. 6.5. In Fig. 6.7 two thrusters are considered as not operative (thruster No. 2 and No. 5), one in the front and one in the back of the vessel, being representative of a DP3 case. In this case the critical curves are the lowest
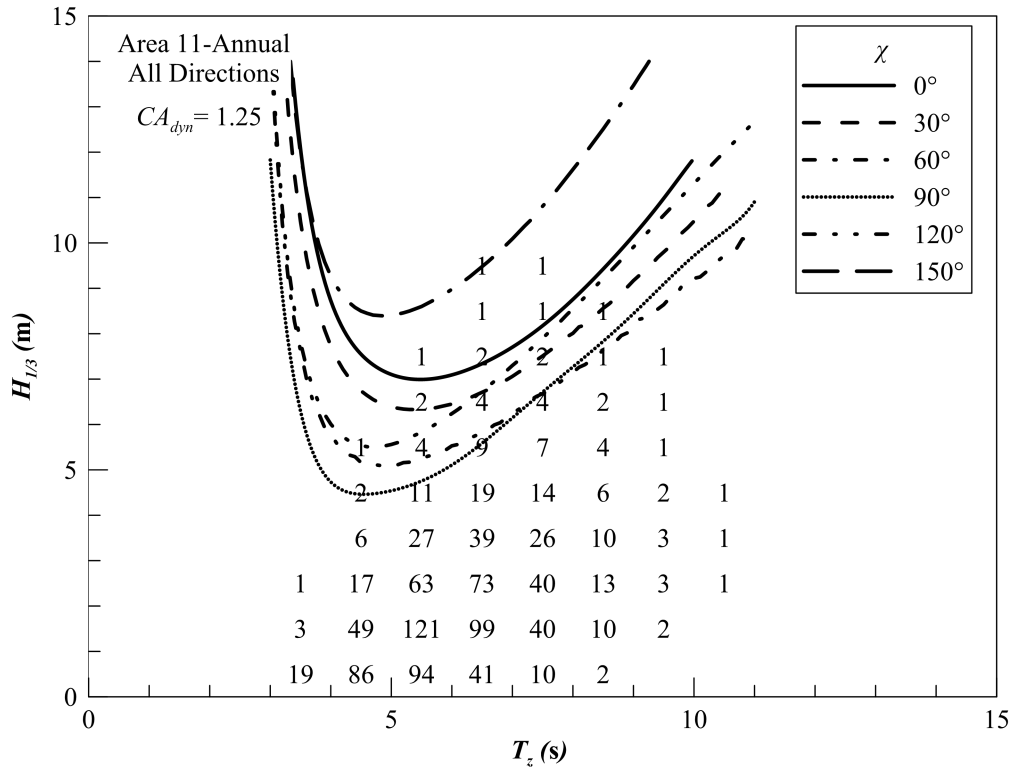
Figure 6.8: DP critical curves for the generic PLV vessel considering no failures (intact) and a CA_{dyn} of 1.25.
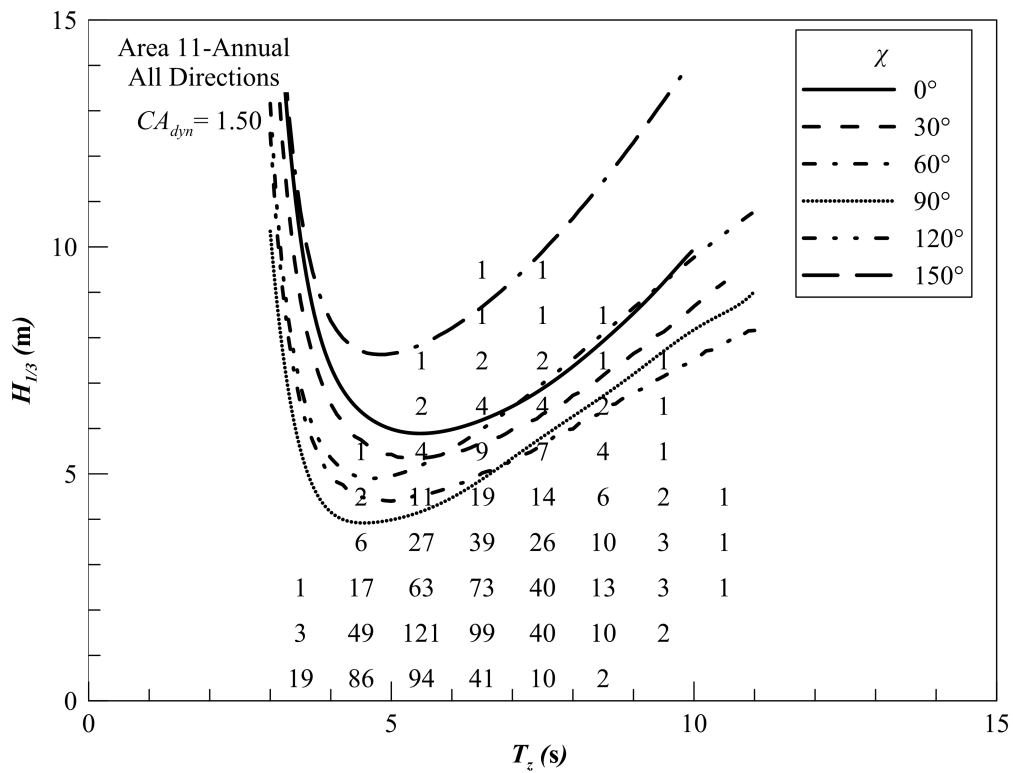
Figure 6.9: DP critical curves for the generic PLV vessel considering no failures (intact) and a CA_{dyn} of 1.50.
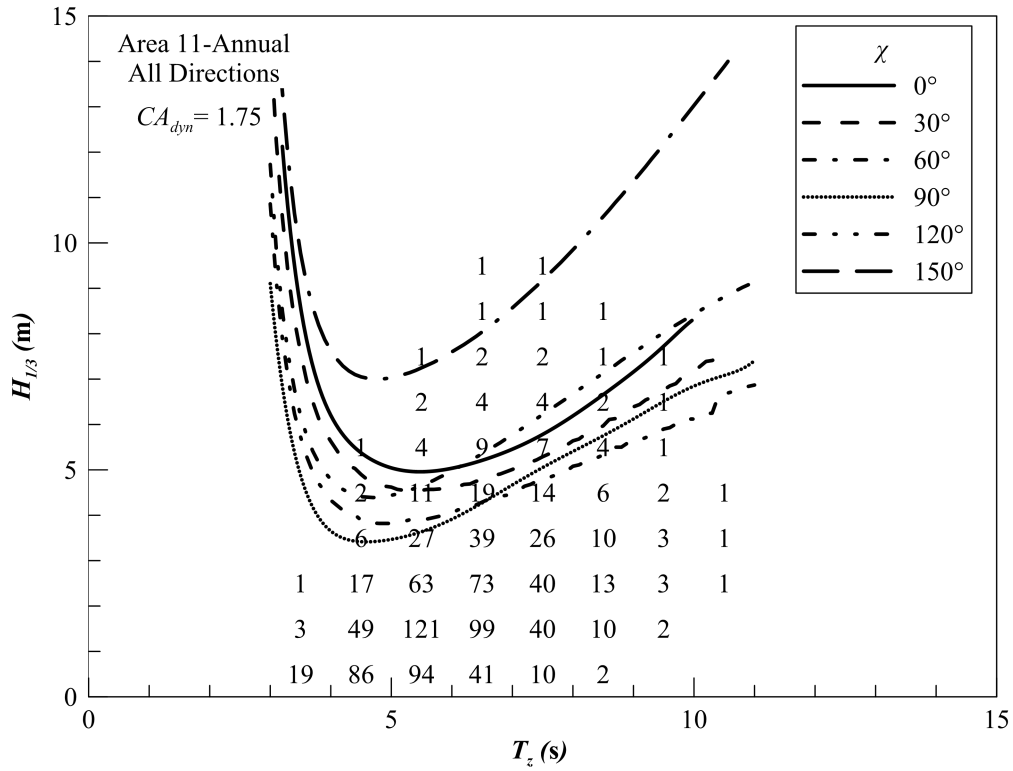
Figure 6.10: DP critical curves for the generic PLV vessel considering no failures (intact) and a CA_{dyn} of 1.75.
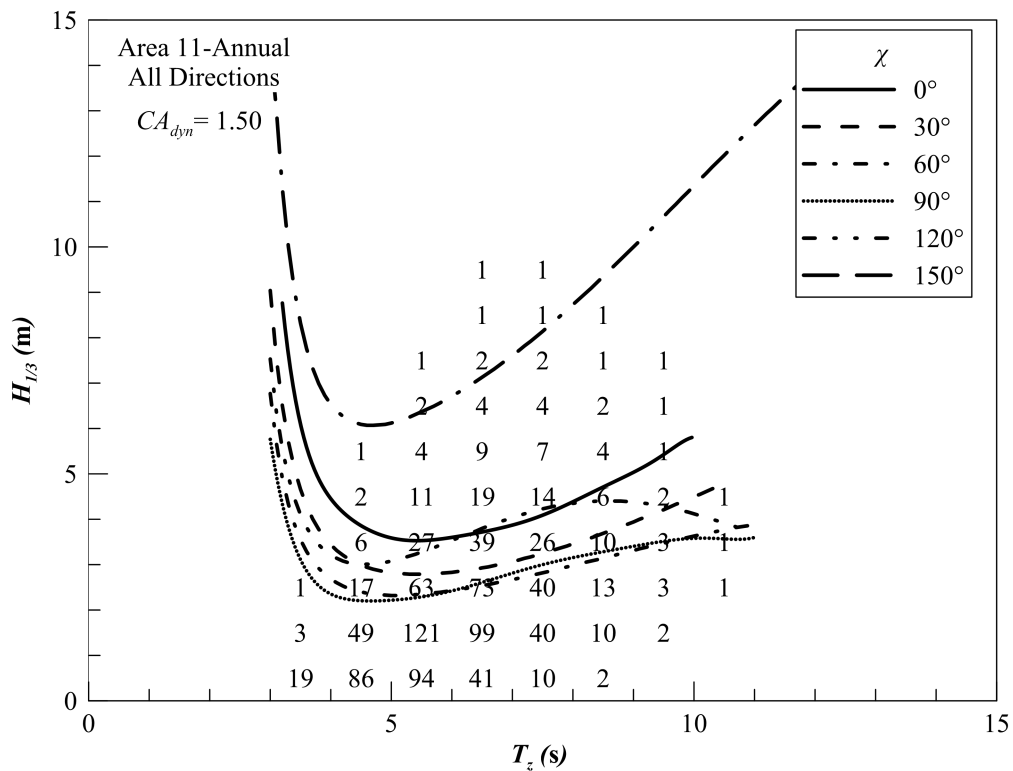
Figure 6.11: DP critical curves for the generic PLV vessel considering two failures (DP3) and a CA_{dyn} of 1.50.
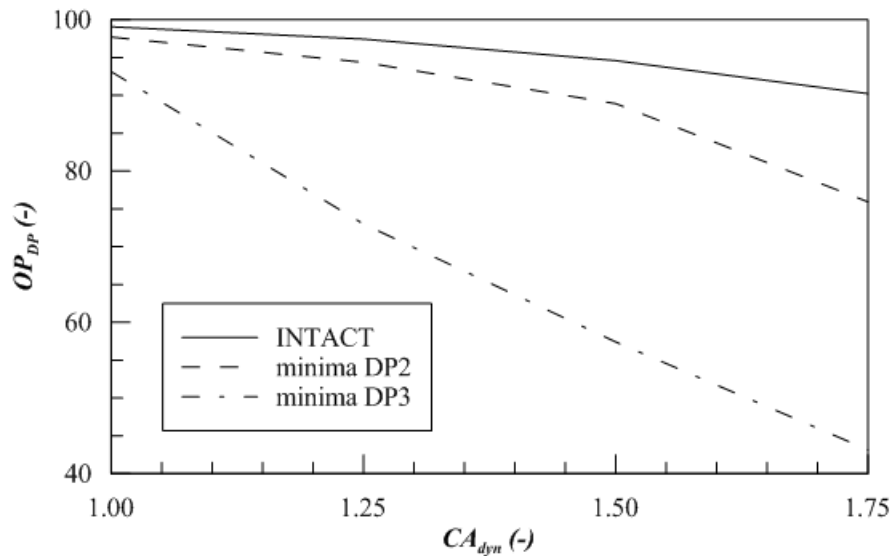
Figure 6.12: Effect of dynamic allowances on the OP_{DP} index

between all the reported cases as it was reasonable to presume.

On the basis of these calculations, the operability of the DP system can be evaluated in each cell for every heading and every failure condition, by computing for each failure case an operability index using equation (6.3).

As already mentioned, quasi-steady calculations overestimate the final capability of the vessel compared to time-domain simulations. In basic DP analysis, dynamic allowances are considered to take care of all the dynamic effects that are neglected by a quasi-steady approach. For such a reason, the variability of the critical curves and consequently of the OP_{DP} has been studied against CA_{dyn} coefficient, on a range between 1.00 and 1.75. It can be observed in Figs. 6.8-6.10 for the intact condition that the dynamic allowance has a strong impact on the critical curves. Considering the failure cases, the impact is even higher as it can be seen in Fig. 6.11 for a DP3 case with a CA_{dyn} of 1.50. The effect on the critical curves reflects also in the OP_{DP} index determination, resume of the variability is given in Fig.6.12, where the OP_{DP} index is plotted against the CA_{dyn} value for intact and worst DP2 and DP3 cases. As it can be seen for intact condition the operability level remains high; however, for failure conditions, the index reduction is significant, especially for DP3 cases which registers an operability reduction of around 50%. For such a reason, once it is possible to estimate the dynamic allowance accurately, it is suggested to use a suitable CA_{dyn} value, or, at least, being in an early design stage, to use a value of 1.25 as suggested by DNV-GL [40].

In the specific case reported in Table 6.2, a condition where all the headings have the same

Table 6.2: DP operability index for the generic PLV without ($CA_{dyn} = 1.00$) and with ($CA_{dyn} = 1.25$) dynamic allowances

Case	failure	$OP_{DP}(\%)$ 1.00	1.25	Case	failure	$OP_{DP}(\%)$ 1.00	1.25
1	Intact	99.08	97.45	12	T1T6 DP3	93.21	74.10
2	T1 DP2	97.77	90.78	13	T2T3 DP3	94.05	75.70
3	T2 DP2	97.78	90.94	14	T2T4 DP3	93.47	74.41
4	T3 DP2	98.21	95.77	15	T2T5 DP3	93.23	74.11
5	T4 DP2	98.21	95.81	16	T2T6 DP3	93.23	77.21
6	T5 DP2	97.71	94.38	17	T3T4 DP3	96.65	76.32
7	T6 DP2	97.71	94.38	18	T3T5 DP3	95.19	76.23
8	T1T2 DP3	95.99	75.88	19	T3T6 DP3	95.19	76.15
9	T1T3 DP3	94.06	74.12	20	T4T5 DP3	95.19	76.17
10	T1T4 DP3	93.17	73.00	21	T4T6 DP3	95.19	76.13
11	T1T5 DP3	93.21	74.10				

probability of occurrence has been applied. As it can be seen the operability index is high for this vessel considering the intact condition, because the scatter areas where the system is not able to keep the position are the one with a low probability. In the specific case, the operational limits for S-lay operation are really low, so pitch criterium is restrictive for all the cases. However, as for example by studying survival conditions, when the motion limitation are less restrictive (see Table 6.1) then the DP critical curves can be more restrictive than motion ones for certain wave conditions.

As mentioned, the commonly adopted preliminary DP calculations are executed according to a specific wind-wave correlation. This is representative of a single curve on a scatter diagram as it can be seen in Figure 6.3. As consequence, the environmental limits represented in a capability plot are referring to $H_s - T_z$ couples that can not be present in the considered sea area. For the analysed vessel, the resulting OP_{DP} index is high, being over 90% also in case of single failures, considering a CA_{dyn} of 1.25. However, according to standard DP calculations (see chapter 4), it was reasonable to expect a strong reduction of the operability index, while this is true only applying high dynamic allowances. In fact, the evaluated capability area is almost halved compared to intact condition and also ERN number is slightly lower. That happens because

standard calculations do not refer to the real environment the vessel will face. The decrease of the operability index is more significant once dynamic allowances are considered, especially for multiple failure cases.

As described before, the motions criteria for operation are low, leading to a maximum sustainable wave height under 3 metres. According to DP calculations, also with a single failure the DP system is able to keep position with a wave height of 5 metres. It can be than stated that a vessel having a OP_{DP} index with such a high value, also for failure conditions, can be considered overpowered for the selected environmental scenario. On the base of these considerations, it will be then a choice of the designer, together with the operator, to select, according to their own experience and/or necessities, whether it can be convenient or not to derate the DP system.

In any case, due to the assumptions, limitations and simplifications of the proposed methodology, the obtained DP operability index cannot be considered as an absolute evaluation number, but can be used to compare different possible design solutions in early design stage. Moreover, the method is suitable to give to the designers more informations regarding vessel in-site DP operations with respect to a basic DP calculation.

The proposed method is based on the principle to perform DP calculations for all the wave combinations that can be found in a certain sea area, having a correspondence with the standard seakeeping operability.

The application of the methods on a PLV vessel highlights that critical curves for Dynamic Positioning can be found for intact condition, but also for different failure cases, being able to directly compare the DP criticality with motion ones for all the possible wave combinations in a selected sea area.

In the specific analysed case, the DP does not present a limitation for the total operability of the vessel, because of the use of the really low limits in pitch motions. In any case this kind of analysis also highlights that for such a kind of S-lay operation the DP system is largely over dimensioned. To fully understand whether the installed DP system is really over dimensioned, it is essential to go further with this kind of analysis since early stage design. Essential is also a good understanding of operational criteria, something that can be obtained only with the help of the operators and equipment producers.

The proposed calculation method is based on certain assumptions that still need to be firmly confirmed. In fact, further investigations, complying the analysis of a lot of environmental records, have to be done regarding the effective correlation between average wind speed and

generated wave in a scatter diagram.

However, the proposed methodology will be a good starting point to further study a combined operability index, considering the effective combination of DP and motion criteria.

6.4   Global operability index

In the previous section, a novel method has been presented to define the operability of the DP system in a scatter diagram.

In standard seakeeping calculations [90], it is common practice to adopt the wave scatter diagrams to plot the critical values of motion criteria. Having then a set of critical curves of DP and a set of critical curves coming from seakeeping calculations, it is then possible to combine the two solutions since they refer to the same environmental conditions.

In fact, according to the same calculation assumptions proposed for the OP_{DP} index, while the same spectrum is used also for seakeeping responses, then the calculations are compliant. For such a reason, by plotting the DP critical curves and the motion ones directly on the wave scatter diagram it will be possible to immediately visualise the effective operability area of the vessel under analysis.

In such a way it is straight forward to evaluate a global operability index for the vessel adopting the following formulation:

$$OP_{TOT} = \sum_{i=1}^{N_h} p_{h_i} \sum_{i=1}^{N_w} p_{g_i} I_{TOT} \tag{6.5}$$

where p_h is the probability associated to each N_h vessel headings and p_g is the probability associated to each N_g specific wave conditions as for the DP_{OP} definition. Different is the definition of the I_{TOT} function, which is defined as:

$$I_{TOT} = \begin{cases} 1 & \text{if } I_{DP} = 1 \vee I_C = 1 \\ 0 & \text{elswhere} \end{cases} \tag{6.6}$$

in the present formulation I_C is a function which is 1 once all the motion criteria are satisfied, and becomes 0 once one of the motion criteria is not satisfied. In Fig. 6.13 an example is given for the vessel adopted also for OP_{DP} calculations. According to the limitation expressed in Table 6.1 for the pipe-laying condition, the most restrictive criteria is given by a combination of the three criteria reported in the graph. Considering the 0° condition, the minimum critical
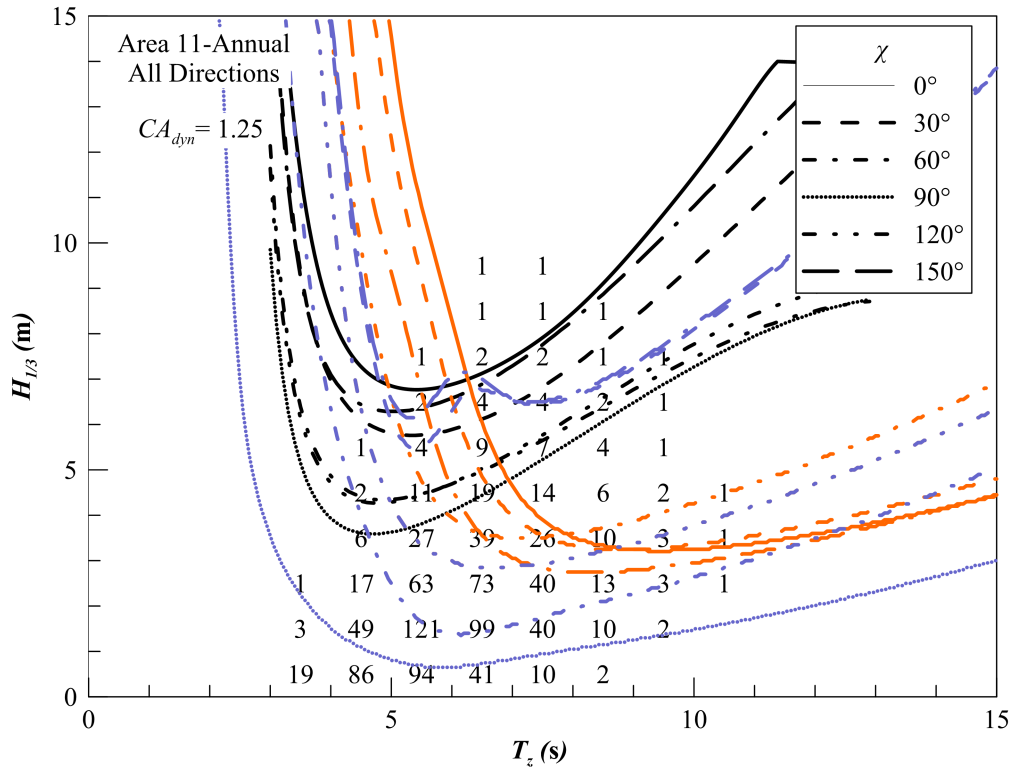
Figure 6.13: Critical curves according to different criteria: DP (*black*), pitch (*orange*) and roll (*purple*) on a generic PLV vessel.

curve is composed by a combination between DP and pitch critical curves. Then from 120° and 60° the limiting criterion is a combination between roll and DP while for 90° the roll has the most limiting condition.

That means it is essential to evaluate also the DP contribution to the total operability of the vessel and determine then the OP_{TOT} index. For the evaluated case, the final operability index OP_{TOT} has been evaluated assuming that all the vessels headings have the same weight, means the same value of p_h. In case the vessel operation requires a preferential heading, then the p_h values should be given by the operator. Under these assumptions, the obtained index is equal to 64.81%.

6.4.1 Operability index for vessels comparison

To consider whether the index is suitable to evaluate differences between different ships, the same process has been applied on two variations of the generic PLV vessel, having a different hull shapes but same hull main dimensions and displacement. Also the thruster sizing has been considered equal between the ships, but the layout has been changed. The original PLV vessel is
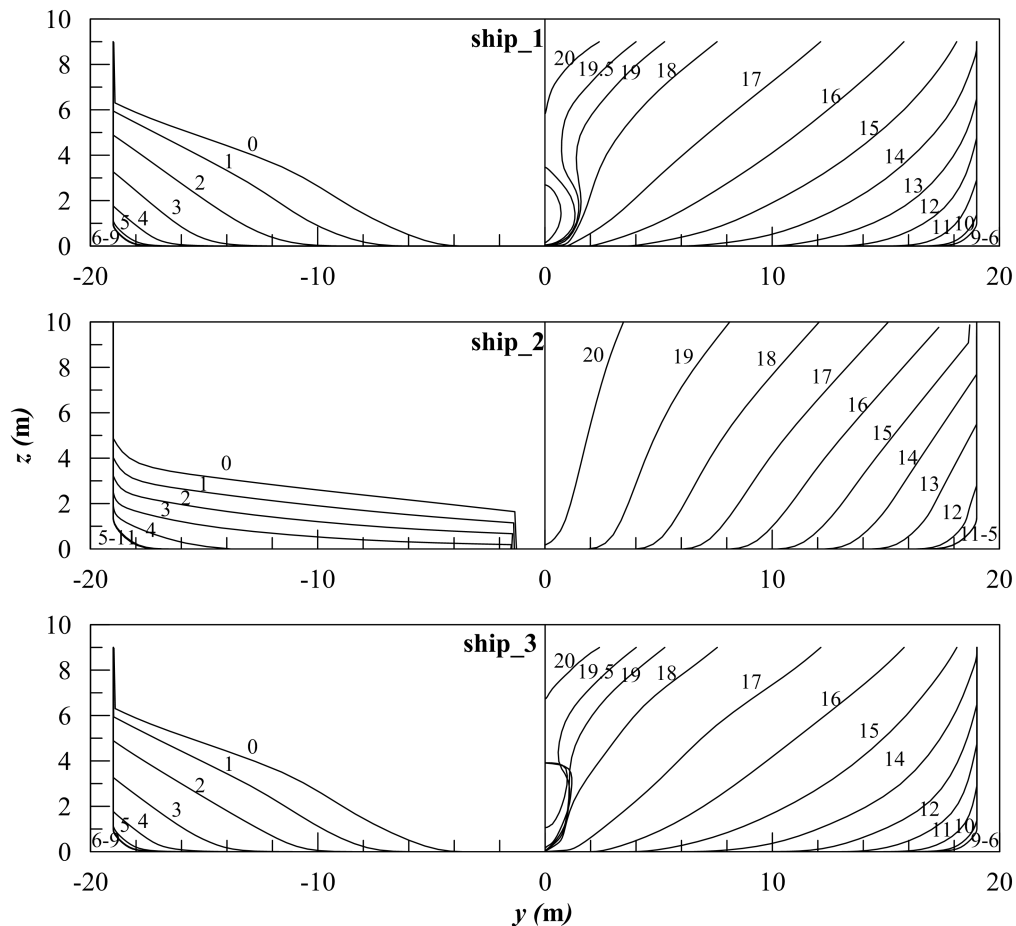
Figure 6.14: Transversal sections of the three considered vessels

referring to the TS-00 layout reported in Chapter 5, while the two variations are equipped with thruster as per TS-01 layout. For such a reason, the differences between the final indexes will be related both by motion critical curves and DP ones. An overview of the three hulls is given in Figure 6.14, where *ship_1* is the original PLV hull form, while *ship_2* and *ship_3* are two new hull form variations.

It can be observed that *ship_3* is a variation of the original hull, aimed to improve the vessel propulsive performances during transfer. In fact, the variations are related to the bulb shape and to the fore shoulder of the hull, keeping the original physiognomy of the original hull. *Ship_2*, on the contrary, is representative of a totally different hull form concept. As already mentioned, the main dimensions and the final displacement is kept constant, however the shape is totally different. The hull is provided with a vertical bow, discarding the bulb, the parallel middle-body has been lengthen and the aft-body has been changed into a pram shape with a longitudinal skeg. Despite the completely different shapes of the three hulls, the differences between the vessel's performances are not expected to drastically change, since main dimensions and mass are not
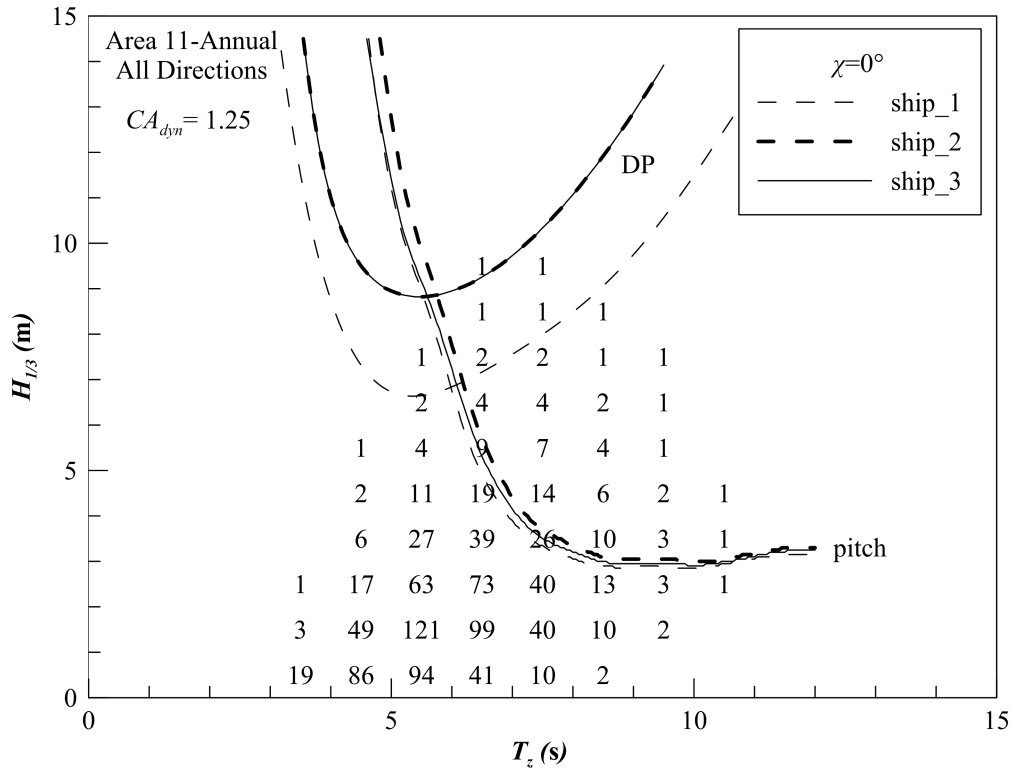
Figure 6.15: Motion and DP critical curves at zero speed and vessel's heading 0°
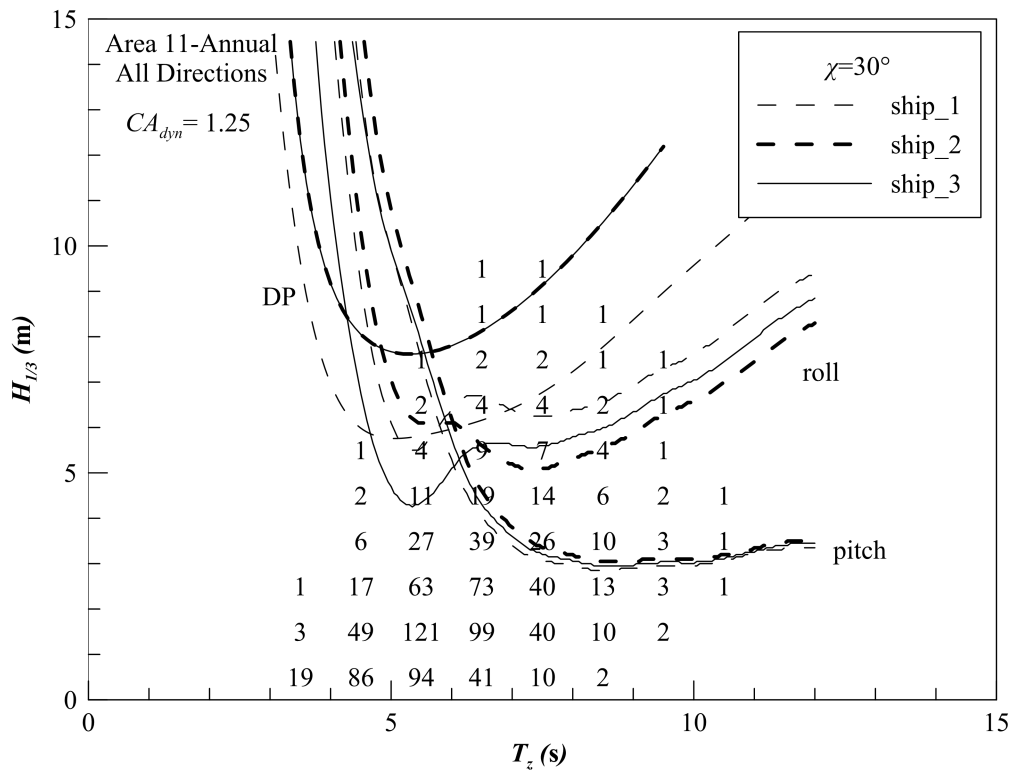
Figure 6.16: Motion and DP critical curves at zero speed and vessel's heading 30°
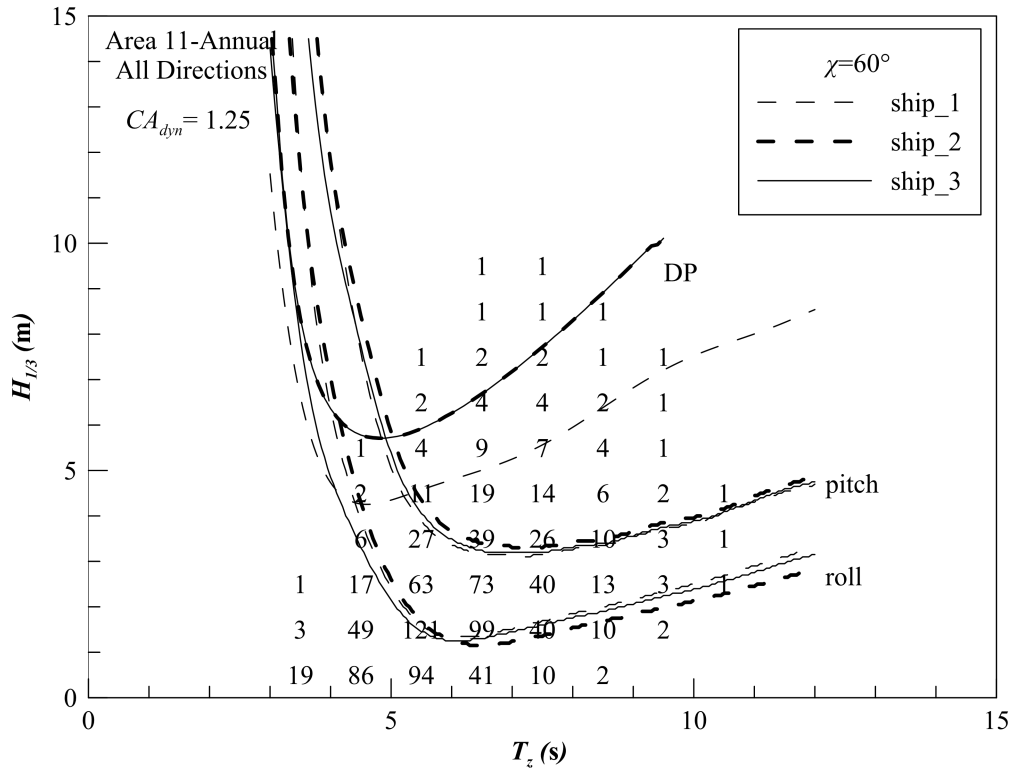
Figure 6.17: Motion and DP critical curves at zero speed and vessel's heading 60°
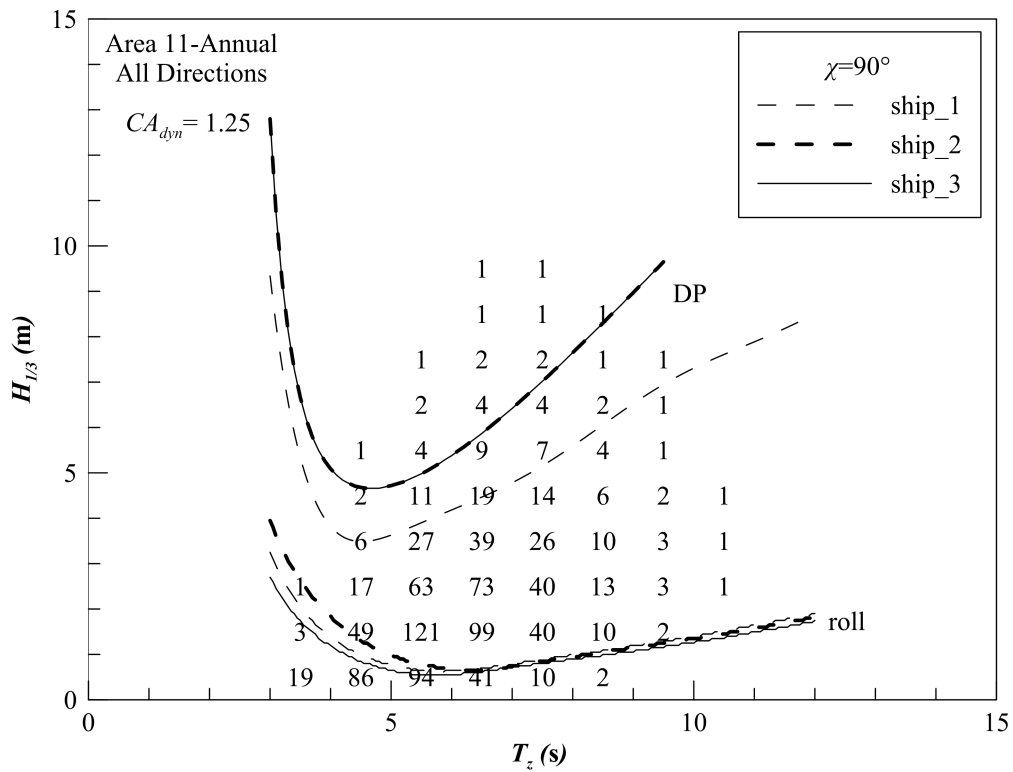
Figure 6.18: Motion and DP critical curves at zero speed and vessel's heading 90°
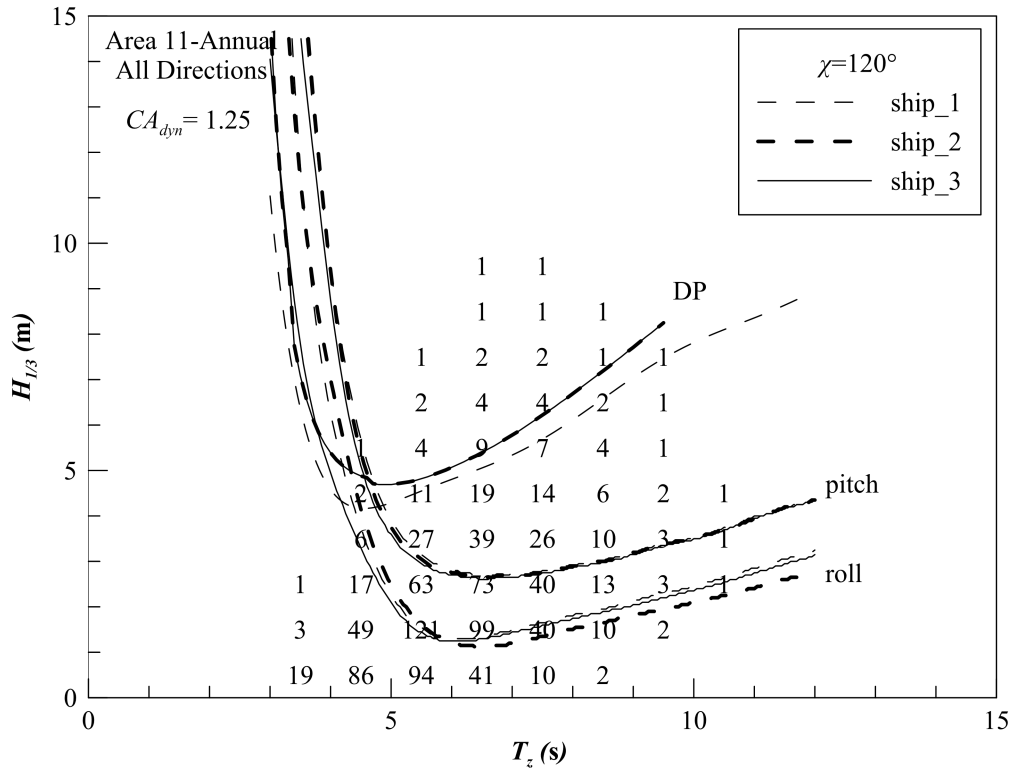
Figure 6.19: Motion and DP critical curves at zero speed and vessel's heading 120°
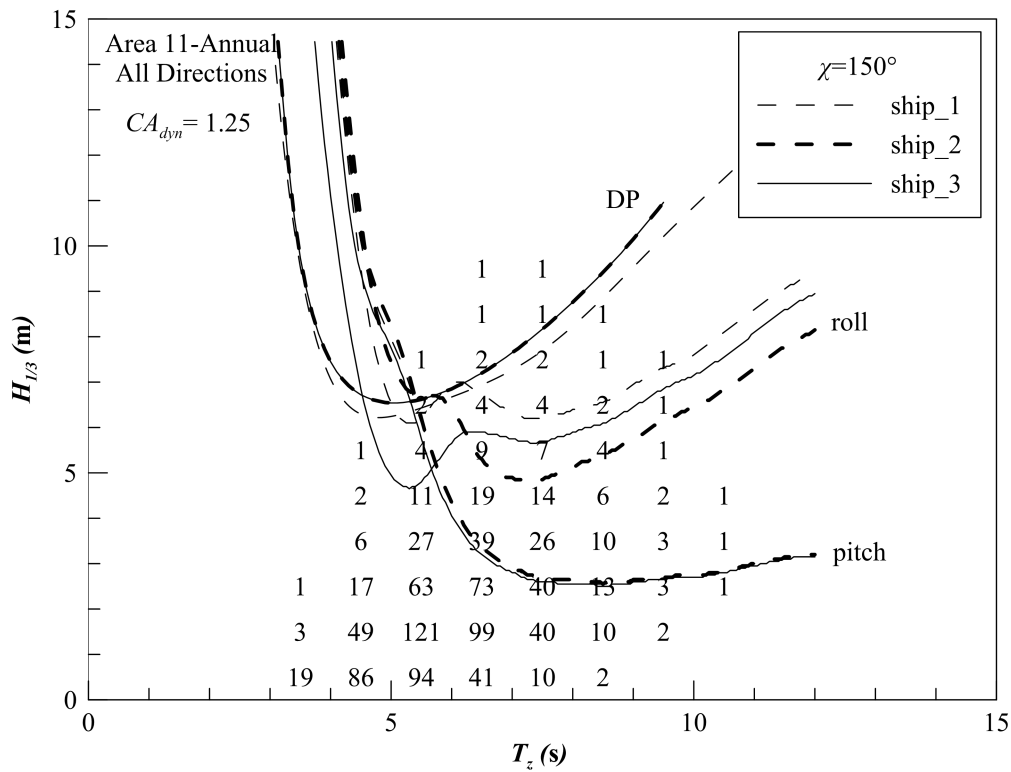
Figure 6.20: Motion and DP critical curves at zero speed and vessel's heading 150°
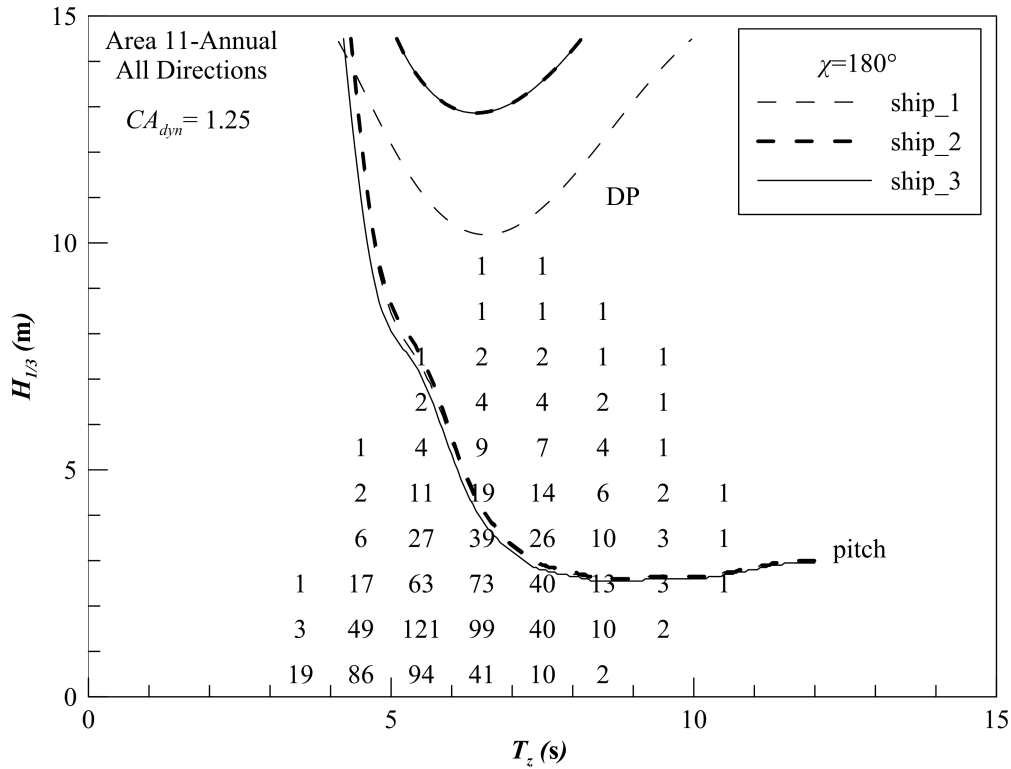
Figure 6.21: Motion and DP critical curves at zero speed and vessel's heading 180°

changed. However the form effect can be captured by the adopted calculation methods and then different operability can be evaluated ship per ship.

In the present example, the critical curves refer to the already presented motion limitations for pipe-laying conditions given in Table 6.1. Dedicated seakeeping calculations have been performed for *ship_2* and *ship_3* at zero speed for multiple heading angle conditions. Regarding DP calculations, the limiting curves have been also determined for the pipe-laying conditions according to the previously mentioned cell based approach. Regarding environmental loads, since model test data where available for *ship_1* for the same condition, including the presence of the stinger and since those data where already used trough the whole study, the loads coefficients have been supposed equal between three ships. That means, differences in DP critical curves are related to thruster position only. The same dynamic allowance CA_{dyn} equal to 1.25 has been used through all the calculations.

The obtained results are presented in graphical form in Figs. 6.15-6.21, where the critical curves of the vessels are compared for headings from 0° to 180° with step of 30°. In such a way, at each angle it is possible to visualize which is the more restrictive limiting criterion between three selected (pitch, roll and DP) at different environmental conditions and evaluate which vessel has a higher global operability. At a heading of 0° (Fig. 6.15) it can be seen that the limiting criteria

is given by DP and pitch motion only, showing that *ship_3* has a higher operability compared with the other two vessels, both in terms of DP and pitch motion. At 30° (Fig. 6.16) also roll criteria appears, being a globally limiting criteria for T_z of 4-6 seconds with corresponding H_s between 4-8 m. At 60° (Fig. 6.17) and 90° (Fig. 6.18) the roll is always the most limiting criterion. The same considerations can be made for the stern seas conditions presented in the last three figures.

By applying equation (6.5) for Area 11, considering the headings with equal weight p_w, then *ship_1* got an operability index OP_{TOT} of 64.81%, *ship_2* of 69.92% and *ship_3* of 67.06%. The main differences between *ship_1* and the other vessels is mainly due to DP, because *ship_2* and *ship_3* have a better thruster location along the hull. In fact, *ship_3* is presenting the worst behaviour regarding the ship motion, but is gains operability in the areas where DP is the stringent criterion. *ship_2* and *ship_3* have operability indexes with a difference of about 3%. Since these two vessels have the same thruster layout and the DP critical curves results similar between them, then the difference is mainly due to the motion criteria.

This short example highlights that, having a tool capable to determine the effective operability of the vessel in an early design stage, different design solutions can be compared during an early design stage both in terms of motions and DP.

Chapter 7

Conclusions

In this thesis a dedicated study has been carried out regarding the execution of DP calculations and the use of their outputs during an early design stage.

Starting from the methodology that can be used to perform calculations, the two possibilities given by quasi-steady and time-domain calculations have been analysed and compared. As results the quasi-steady calculations have been selected since they are faster and more easier to use inside more complex optimisations and investigations that may occur during preliminary design phase. In any case the time domain simulation will always remain a powerful tool that can be used in a more advanced phase or can be also adopted to tune the parameters for the quasi-steady calculations, e.g. CA_{dyn} coefficient determination.

The reliability of a successful DP computation is also given by the accuracy of the environmental loads determination. The focus has been given to the enhancement of existing regression methods to perform a better estimation of the wind loads coming from databases of wind model tests. In the specific, the Blendermann database has been adopted as data source for the regression, highlighting that the proposed enhanced formulation is particularly suitable to reproduce the behaviour of the loads, especially for the yawing moment. For the current a method to perform regression analysis on a database of CFD calculations has been studied. Based on validated calculation grids, simulations have been performed on a drill-ship family on a fictitious model scale, where geometric characteristics of the hull were systematically varied. A method has been proposed to extrapolate the obtained model scale coefficients to full scale according to Reynolds number scaling. For waves the smart adoption of coefficients coming from diffraction theory has been presented in such a way to give more flexibility to the environmental condition modelling, allowing the adoption of specific wave spectra of a determined sea area. All these enhancements

led to the determination of environmental loads in line with the loads determined by means of experiments. The proposed methods to evaluate environmental loads does not increase the total calculation time with respect to classification societies methods for early design stage but increase the quality of the final results. Moreover the model can be further improved or extended, as for CFD computations, the proposed methods can be used on different hull types. For the wave loads, the same strategy adopted for current loads could also be investigated.

Another important aspect was given by the enhancement of the thrust allocation procedures that can be used during preliminary calculations. An accurate modelling of the propeller acting inside a thruster nozzle is essential to effectively evaluate the real capability of the vessel. However the behaviour of the propeller cannot be easily introduced inside the allocation algorithms. For this purpose more complex allocation strategies have been developed and implemented to enhance the evaluation of the vessel final capability considering the propeller behaviour and the interactions between them. Once thruster-thruster interaction have to be considered in simple allocation procedures, then a dedicate method has been proposed to perform the interaction analysis as post-processing of a standard calculation. In case of the modelling of the interaction procedure inside an allocation algorithm, a novel allocation approach named *booster strategy* is used, suitable to evaluate vessel capability in the extreme conditions, automatically recognizing interaction areas and avoiding it once the total amount of power is required by DP system. Additionally, the implementation of both FP and CP propellers has been investigated, and in case of fixed tunnel thrusters also the behaviour in ahead and astern conditions. In such a case, it is essential to adopt a fully non-linear allocation strategy, which is capable to describe the behaviour of such kind of propellers. In conclusion it can be stated that different kind of predictions can be adopted, with different accuracy levels, according to the specific problem that should be faced.

The enhancements reached in terms of environmental and thruster modelling and the study of multiple allocation strategies, led to the possibility to investigate new applications of DP calculations during the vessel design process.

Traditionally DP calculation have been never used as a design tool, but only as an analysis tool. Here it has been changed this kind of purpose and a design tool based on DP calculation has been developed. In fact, the study on the optimal position is one of the first examples of design tool based on DP calculations. Of course, due to the complexity of the genetic optimisation, the most powerful allocation algorithm cannot be adopted at this moment due to the required calculation

time. In any case the obtained results show the possibility to deeper investigations, developing more complex and reliable allocations strategy also for that specific purpose. The chance to have a powerful tool since early design stage, capable to optimise thruster positions along the hull considering also certain constraints, will give for sure an additional help to designers in order to improve offshore vessels design efficiency.

Finally the issues related to the possible coupling between seakeeping and station-keeping during a preliminary design stage has been covered. In the first step the methodology to define the motion criteria on a DP capability plot has been investigated. This has been achieved by analysing the specific conditions where DP calculations are performed. Being stationkeeping environment defined according to a predetermined wind-wave correlation, then also seakeeping data should refer to the same environmental condition. In such a way limiting wind speed and wave height can be determined for the motions at each heading and reported on a capability plot. However, this kind of approach is not suitable to reproduce all the possible combinations of wave heights and periods. For this purpose a new methodology based on cell approach has been developed, arriving to the definition of a DP operability index OP_{DP} suitable to evaluate critical curves for dynamic positioning directly on a scatter diagram. The developed method is suitable to have a ranking of the DP operability of the vessel which is not absolute, but related to the specific sea area where a vessel is supposed to operate. Moreover the calculation conditions related to environmental loads are the same as per standard seakeeping motions calculations, leading to fully comparable critical curves.

In this sense, a completely new method has been studied and developed, to combine DP critical curves with the ones coming from traditional seakeeping calculation for ship motions. The proposed cell based approach allows to directly evaluate the criticality given by each limiting criteria (e.g. motions or DP) at different encounter angle conditions. Moreover, extracting a envelop limiting curve from all the selected criteria, a global operability index OP_{TOT} can be determined, combining all the criteria related to vessel operations and considering at the same time the specific vessel operating profile.

It has been shown that this kind of index is suitable to compare different vessels having the same limiting criteria and operating profile. Moreover, the method is also suitable to rank different project solutions since early design stage, giving to the designer an idea on the influence of motion an DP on the operability of different designs.

The thesis analyses for the first time DP predictions in the early design stage in combination

with seakeeping ones. On this purpose, a completely original approach to DP calculation has been developed to visualise DP and seakeeping limiting curves on the same chart, leading to the determination of a global operability index. Furthermore, the DP calculations include notable enhancements for the environmental loads determination, propeller modelling and thrust allocation algorithms. Besides, the original method developed for the optimal thruster location along the hull will help ship designers to study different configurations aimed to improve the DP capability of a vessel. In this sense, the research fully achieves the expected scientific contribution.

Future studies and developments

The present study has presented a global enhancement in both the method and usage of DP preliminary predictions for early design stage. In particular, having proposed a new method to visualise the DP calculation outputs on a cell-based technique instead of a capability plot, new possibilities for a further integration between stationkeeping and seakeeping will arise.

To effectively promote the use of global operability index OP_{TOT}, further studies are needed to properly define the effective reliability of the proposed method. In fact, at this time, a sensitivity study has been carried out only for the CA_{dyn} coefficient with respect to the OP_{DP} index, while, in the future, the study should be extended also to different thrust allocation algorithms and also to the methods that can be used to determine vessel motions. For further developments it should be essential to define the sensibility of both the aspects related to motions and DP, identifying different combinations between methods having different reliability levels. In fact, the use of different allocation algorithms will lead to a certain sensibility on the global index, e.g. it has an effect on the OP_{DP} only. However, also different motion evaluation methods could influence, maybe in a totally different manner, the final OP_{TOT} by adopting the same DP calculation scheme.

Another possible investigation field is also related to the further enhancement of the design tool for optimal thruster location along the hull. As exposed, in the present study the application of only one thrust allocation technique has been applied for the DP calculations on each population individual. The allocation algorithm that has been up to now used, is not one of the most complex and complete presented in this thesis. In fact, the complexity to implement multiple optimisation processes (for DP capability) inside a global optimisation process (for position determination), led to the selection of a simple optimisation strategy for thrust allocation as starting point for

the investigation. However, to enhance the algorithm performances, the inclusion of effects like thruster-thruster interaction or propeller ventilation will give an higher reliability to the design tool. The fact that a DP operability index has been defined, may suggest to adopt OP_{DP} as objective function for the global optimisation, instead of capability plot area. In fact, the proposed cell based approach for OP_{DP} index, is decreasing the total number of calculations needed to perform a DP prediction as per the standard capability plot. In such a way, the adoption of more complex and efficient thrust allocation procedures can be furthermore facilitated.

Another possible integration of the enhancements proposed in this thesis could be the study of the absorbed power during DP operations. This can be done both in case of a standard DP calculation and in case of a cell based approach. This will give a more detailed idea on the optimal management of the power system installed on-board, giving the possibility to study possible alternative solutions to reduce fuel consumption and environmental impact of offshore vessels during operations. Especially the environmental protection should be treated with accuracy, since a lot of areas of interest for DP operations (e.g. North Sea and Gulf of Mexico) are classified as Emission Control Areas (ECA). Once a vessel is operating in an ECA area is subjected to environmental constraints on exhaust emission, means green solution should be applied to reduce it. In such a case an estimate of the power demand during the whole operations since early design stage will be for sure useful for designers.

As final consequence, when all the proposed tools capable to assess DP and global operability of an offshore vessel since early design stage will achieve an adequate reliability, a shift of these analyses to concept design could be made. The flexibility shown by the proposed indexes will allow to easily integrate the procedures inside a concept design multi-attribute selection process. By including directly DP calculations into concept design phase, then DP will be effectively considered as primary design attribute for an offshore vessel, influencing the choices related to vessel geometrical parameters and main dimensions at the same level of other hydrodynamics attributes as resistance/powering or ship motions.

Bibliography

[1] A.B. Aalbers, R.J.P.E. Kuipers, F. van Walree, and R.B.H.J. Jansen. Developements in dynamic positioning systems for offshore stationkeeping and offloading. In *Proceedings of ISOPE Conference*, The Hague, 1995.

[2] A.B. Aalberts, R.J.P.E. Kuipers, F. van Walree, and R.B.H.J. Jansen. Developements in dynamic positioning systems for offshore stationkeeping and offloading. In *ISOPE Conference*, The Hague, 1995.

[3] A.B. Aalberts and U. Nienhuis. Wave direction feed forward on basis of relative motion measurements to improve dynamic positioning. In *Procceddings of Offshore Technology Conference OTC1987*, 1987.

[4] A.B. Aalberts, O.J. Waals, R.F. Tap, and N.J. Davison. Wave feed forward dp and analysis of the effect on shuttle tanker operation. In *Proceedings of MTS DP Conference*, Houston, USA, 2004.

[5] G.N. Abramovich. *The Theory of Turbulent Jets (English Edition)*. MIT Press, 1960.

[6] ABS. Guide for dynamic positioning systems. Technical report, American Bureau of Shipping, 2014.

[7] P. A. Absil, R. Mahony, and R. Sepulchre. *Optimization Algorithms on Matrix Manifolds*. Princeton university Press, 2008.

[8] W. Antheunisse, D. Chalkias, and R. Huijsmans. Offsets requirements in quasi-static dp capability calculations. In *Proceedings of the twenty-sixth International Ocean and Polar Engineering Conference ISOPE*, 2016.

[9] API. Api 2p-rp 1984. Technical report, American Petroleum Institute, 1984.

[10] API. Api 2p-rp 1987. Technical report, American Petroleum Institute, 1987.

[11] API. Api bulletin 2int-met: Interim guidance on hurricane conditions in the gulf of mexico. Technical report, American Petroleum Institute, 2007.

[12] F. Arditti, H. Cozijn, and E.F.G. van Daalen. An advanced thrust allocation algorithm for dp applications, taking into account interaction effects and physical limitations. In *Proceedings of OMAE 2014 Conference*, San Francisco, USA, 2014.

[13] F. Arditti, F. Souza, T. Martins, and E. Tannuri. Thrust allocation algorithm with efficiency function dependent on azimuth angle of the actuators. *Ocean Engineering*, 105:206–216, 2015.

[14] F. Arditti and E.A. Tannuri. Experimental analysis of a thrust allocation algorithm for dp systems considering the interference between thrusters and thruster-hull. In *Proceedings of 9th IFAC Conference on Manoeuvring and Control of Marine Craft*, Genoa, Italy, 2012.

[15] ASME. Standard for verification and validation in computational fluid dynamics and heat transfer. Technical report, American Society of Mechanical Engineers ASME, V&V Committee, 2009.

[16] W. Bascom. *A Hole in the Bottom of the Sea: The Story of the Mohole Project*. 1961.

[17] W. Blendermann. Shiffsform und windlast-korrelations und regressionanalyse von wind-kanalmessungen an modell. Technical Report 533, Institut fur Schiffbau der Universität Hamburg, 1993.

[18] W. Blendermann. Parameter identification of wind loads on ships. *Journal of Wind Engineering and Industrial Aerodynamics*, 51:339–351, 1994.

[19] W. Blendermann. Estimation of wind loads on ships in wind with a strong gradient. In *Proceedings of the 14th International Conference on Offshore Mechanics and Artic Engineering OMAE*, New York, 1995.

[20] W. Blendermann. Floating docks: prediction of wind loads in extreme winds. *Schiff und Hafen*, 48(4):67–70, 1996.

[21] W. Blendermann. Wind loading of ships - collected data from wind tunnel tests in uniform flow. Technical Report 574, Institut für Shiffbau der Universität Hamburg, December 1996.

[22] G. Box and D. Behnken. Some new three levels designs for the study of quantitative variables. *Technometrics*, 2:455–475, 1960.

[23] G.E.P. Box and D.W. Behnken. *Technometrics*. 1960.

[24] G.E.P Box, W.G. Hunter, and J.S. Hunter. *Statistix for experiments*. Wiley, New York, 1978.

[25] P. Brandner and M. Renilson. Interaction between two closely spaced azimuthing thrusters. *Journal of Ship Research*, 42(1):15–32, March 1998.

[26] N Bulten and P. Stoltenkamp. Full scale thruster-hull interaction improvement revealed with cfd analysis. In *Proceedings of OMAE 2013 Conference*, Nantes, France, 2013.

[27] H.W. Chang. A data mining approach to dynamic multiple responses in taguchi experimental design. *Expert Systems with Applications*, 35(3):1095–1103, 2008.

[28] J.L. Cortijo, A. Duggal, R. van Dijk, and S. Matos. A new solution for floating production in ultra deep waters. In *Proceedings of Offshore West Africa Conference*, 2003.

[29] H. Cozijn and E. Frickel. Past, present and future of hydrodynamic reserch for dp applications. In *Proceedings of Dynamic Positioning Conference*, 2015.

[30] H. Cozijn and R. Hallmann. The wake flow behind azimuthing thrusters - measurements in open water, under a plate and under a barge. In *Proceedings of OMAE 2012 Conference*, Rio de Janeiro, Brazil, 2012.

[31] H. Cozijn and R. Hallmann. Thruster-interaction effects on a dp semi-submersible and a drill ship - measurement and analysis of the thruster wake flow. In *Proceeding of OMAE 2013 Conference*, Nantes, France, 2013.

[32] H. Cozijn and R. Hallmann. Piv measurements in thruster-interaction research. In *Proceedings of MTS DP Conference*, Houston, USA, 2014.

[33] H. Cozijn and R. Hallmann. Thruster-interaction effects on a dp shuttle tanker -wake flow measurements of the main propellers and bow tunnel thrusters. In *Proceedings of OMAE 2014 Conference*, San Francisco, USA, 2014.

[34] W.E. Cummins. The impulse response function of ship motions. In *Proceedings of 8th International Symposium on Ship Theory*, Hamburg, 1962.

[35] E.F.G van Daalen, H. Cozijn, C. Loussouran, and P.W. Hemker. A generic optimization algorithm for the allocation of dp actuators. In *Proceedings of OMAE 2011 Conference*, Rotterdam, The Netherlands, 2011.

[36] A.G. Davenport. The spectrum of horizontal gustiness near the ground of high winds. *Quarterly Journal of Royal Meteorological Society*, 87, 1961.

[37] Det Norske Veritas DNV. *Rules for classification of ships*, July 2011.

[38] DNV. *Rules for the classification of ships, Part 6, Chapter 7*, 2013.

[39] DNV-GL. *Assessment of station keeping capability of dynamic positioning vessels*, 2016.

[40] DNV-GL. Dnvgl-st-0111: Assessment of station keeping capability of dynamic positioning vessels. Technical report, DNV-GL, 2018.

[41] L. E ca, G.N.V.B. Vaz, and M. Hoekstra. Code verification, solution verification and validation in rans solver. In *Proceedings of 29th International Conference on Ocean, Offshore and Artic Engineering OMAE*, Shanghai, 2010.

[42] S. Erikstad and K. Levander. System based design of offshore support vessels. In *Proceedings of the 11th International Marine Design Conference IMDC 2012*, 01 2012.

[43] O.M. Faltinsen. *Handbook of Sea Loads on Ships and Offshore Structures*. Cambridge University Press, 1990.

[44] J.H. Ferziger and M. Perić. *Computational Methods for Fluid Dynamics, 3rd rev.* Springer-Verlag, Berlin, 2002.

[45] T.I. Fossen and T. Perez. Kalman filtering for positioning and heading control of ships and offshore rigs. *IEEE Control System Magazine*, pages 33–46, 2009.

[46] T. Fujiwara and Nimura T. New estimation method of wind forces acting on ships on the basis of mathematical model. In *Proceedings of the 15th International Offshore and Polar Engineering Conference*, Seoul, Korea, 2005.

[47] T. Fujiwara, Y. Tsukada, F. Kitamura, H. Sawanda, and S. Ohmatsu. Experimental investigation and estimation on wind forces for a container ship. In *Proceedings of the 19th International Offshore and Polar Engineering Conference*, Osaka, Japan, 2009.

[48] F. Gaudiano. Development of a time domain dynamic positioning simulation program. Master's thesis, University of Trieste, 2018.

[49] M. Gertler. Resistance experiments on a systematic series of streamlined bodies of revolution for application to the design of high speed submarines. Technical report, David Taylor Model Basin, 1950.

[50] R.W.F. Gould. The estimation of wind loads on ship superstructures. In *The Royal Institution of Naval Architects*, number 8, page 34. 1982.

[51] R. Graham, A.E. Baitis, and W.G. Meyers. On the development of seakeeping criteria. *Naval Engineers Journal*, 104(4):259–275, 1992.

[52] N.C. Groves, T.T. Huang, and M.S. Chang. Geometric charachteristics of darpa suboff models (dtrc model nos. 5470 and 5471). Technical Report 1298-1, DTRC, 1998.

[53] M. Gutsch, F. Sprenger, and S. Steen. Design parameters for increased operability of offshore crane vessels. In *Proceedings ASME 2017 of 36th International Conference on Ocean, Offshore and Arctic Engineering*, volume 9, Trondheim, Norway, 2017.

[54] M.R. Haddara and C. Guedes Soares. Wind loads on marine structures. *Marine Structures*, 12(3):199–209, April 1999.

[55] R.I. Harris. On the spectrum and auto-correlation function of gustiness in high winds. *E.R.A. Report*, 5273, 1968.

[56] F. Hoffmeister and J. Sprave. Problem-independent handling of constraints by use of metric penalty functions. In *Proceedings of the Fifth Annual Conference on Evolutionary Programming*, pages 289–294, 1996.

[57] N. Hogben, N.M.C. Dacunha, and G.F. Olliver. *Global Wave Statistics*. British Maritime Technology Limited, 1986.

[58] J.H. Holland. Adaptation in natural and artificial systems. *University of Michigan Press*, 1975.

[59] J. Holtrop. Extrapolation of propulsion tests for ships with appendages and complex propulsors. In *Proceedings of SNAME Canadian Atlantic section conference*, St. John's (Canada), 2000.

[60] A. Homaifar, C.X. Qi, and S.H. Lai. Constrained optimization via genetic algorithms. *Simulations*, 62:242–253, 1994.

[61] G. Hughes. Model experiments on the wind resistence of ships. *Transaction RINA*, LXXII, 1930.

[62] IMCA. Specification for dp capability plots imca m 140 rev. i. Technical report, The International Marine Cotractors Association IMCA, 2000.

[63] IMCA. M 178 fmea management guide. Technical report, IMCA, 2005.

[64] IMO. Guidelines for vessels with dynamic positioning system. Technical report, IMO, 1994.

[65] R.M. Isherwood. Wind resistance of merchant ships. *The Royal Institution of Naval Architects*, 115:327–338, 1972.

[66] ITTC. Recommended procedures and guidelines; practical guidelines for ship cfd applications. ittc 7.5-03-02-03. Technical report, International Towing Tank Conference, 2011.

[67] ITTC. Recommended procedures and guidelines; example for uncertainty analysis of resistance test in towing tank. ittc 7.5-02-02-01. Technical report, International Towing Tank Conference, 2014.

[68] N.A. Jenssen. Mitigating excessive pitch and roll motions on semi-submersibles. In *MTS DP Conference*, Houston, USA, 2010.

[69] X. Jin, L. Wang, S. Xu, and L. Yang. Positioning accuracy analysis for a dp platform with roll and pitch motion control. In *Proceedings of ISOPE Conference*, Busan, Korea, 2014.

[70] T.A. Johansen, T.I. Fossen, and S.P. Berge. Constrained nonlinear control allocation with singularity avoidance using sequential quadratic programming. *IEEE Transactions on Control System Technology*, 12:211–216, 2004.

[71] D. Jürgens, M. Palm, and A. Brandner. Comparative investiation on influence of the positioning time of azimuth thrusters on the accuracy of dp. In *MTS DP Conference*, Houston, USA, 2012.

[72] S. Kerkeni, M. Poirier, and F. Rongére. Standardization and the need of new tools for the dp industry. In *Proceedings of Dynamic Positioning Conference*, 2015.

[73] Kongsberg. Dp capability analysis adams arrow. Technical report, Kongsberg Maritime, 2008.

[74] A. Koop. Shallow water current loads on a lng carrier using cfd. In *Proceedings of OMAE ASME 34th International Conference on Ocean, Offshore and Arctic Engineering*, St. John's, Newfoundland, Canada, 2015.

[75] A Koop. Determining side-by-side current loads using cfd and model tests. In *Proceedings of OMAE ASME 35th International Conference on Ocean, Offshore and Arctic Engineering*, Busan, Korea, 2016.

[76] A. Koop, C. Klaij, and G. Vaz. Viscous-flow calculations for model and full-scale current loads on typical offshore structures. In *Proceedings of MARINE 2011, IV International Conference on Computational Methods in Marine Engineering (Selected Papers), Computational Methods in Applied Sciences*, 2013.

[77] G. Kuiper. *The Wageningen Propeller Series*. MARIN Pubblication, 1992.

[78] W.P.A. van Lammeren. Enige gezichtpunten bij het ontwerpen van scheepsschroeven. *Schip en Werf*, pages 88–151, 1940.

[79] W.P.A. van Lammeren, J.D.. van Manen, and M.W.C. Oosterveld. The wageningen b-screw series. *Trans. S.N.A.M.E.*, 77:269–317, 1969.

[80] C.H. Lee. Second-order wave forces on floating bodies. In *Proceedings of 4th International Worshop on Water Waves and Floating Bodies*, Oystese, Norway, 1989.

[81] H.W. Lerbs. Moderately loaded propellers with a finite number of blades and an arbitrary distribution of circulation. *Trans. of the Society of Naval Architects and Marine Engineers*, 60:73–117, 1952.

[82] H.L. Liu and T.T. Huang. Summary of darpa suboff experimental program data. Technical Report HD-1298-11, CRDKNSWC, 1998.

[83] A. Lübke, S. Krüger, and J. Christiansen. Calculation of the dynamic positioning capability in time domain in early design stages. In *Proceedings of IMDC 2015*, Tokyo, Japan, 2015.

[84] P. Maciel, A. Koop, and G. Vaz. Modelling thruster-hull interaction with cfd. In *Proceedings of OMAE 2013 Conference*, Nantes, France, 2013.

[85] J.D. van Manen. Open water test series with propellers in nozzles. *International Shipbuilding Progress*, 1, 1954.

[86] MARIN. *Ship Hydrodynamics*, 2012.

[87] F. Mauro, P. Cerni, and R. Nabergoj. Rans calculations of submerged bodies. In *Proceedings of the 23th International Conference Engineering Mechanics 2017*, Svratka, Czech Republic, 2017.

[88] F. Mauro and E. Duranti. Effect of propeller modelling on station-keeping thruster allocation strategy. In *Proceedings of NAV 2018 Conference*, Triest (Italy), 2018.

[89] F. Mauro and F. Gaudiano. Station-keeping calculations in early design stage: two possible approaches. In *Proceedings of of 19th International Conference on Ships and Shipping Research NAV 2018*, Triest (Italy), 2018.

[90] F. Mauro and R. Nabergoj. Integrated station-keeping and seakeeping predictions. In *Proceedings of 16th International Congress of the International Maritime Association of the Mediterranean IMAM*, Pula (Croatia), 2015.

[91] F. Mauro and R. Nabergoj. Advantages and disadvantages of thruster allocation procedures in preliminary dynamic positioning predictions. *Ocean Engineering*, 123:96–102, 2016.

[92] F. Mauro and R. Nabergoj. Smart thrust allocation procedure in early design stage dynamic positioning predictions. *18th International Conference on Ships and Shipping Research*, NAV, Lecco, 2015.

[93] J. McCall. Genetic algorithms for modelling and optimisation. *Journal of Computational and Applied Mathematics*, 184:pp. 205–222, 2005.

[94] W.G. Meyers and A.E. Baitis. Improvements to capability and prediction accuracy of the standard ship motion program. Technical Report SPD-0936-04, Carderock Division, Naval Surface Warfare Center, September 1985.

[95] J. Millan. Thrust allocation techniques for dynamically positioned vessels. Technical Report LM-2008-04, Institute for Ocean Technology (OE), St John's, Canada, 2008.

[96] D.O. Monlar. Ships thruster allocation logic with rudder interactions. In *IEEE and Marine Tecnology Society Conference*, 1978.

[97] P. Naaijen and Huijsmans. Real-time prediction of second order wave drift forces for wave force feed forward in dp. In *Proceedings of OMAE2010 Conference*, Shanghai, China, 2010.

[98] R. Nabergoj. Station-keeping and seakeeping in offshore vessel design. In *Proceedings of 1st INT-NAM*, Istanbul, 2011.

[99] R. Nabergoj, K. Ardavanis, L. Cok, and R. Faldini. Dp upgrade after vessel refitting. In Krylov shipbuilding Research Institute Ed., editor, *Proceedings of 10th International Conference on Hydrodynamics*, St. Petersburg, Russia, 2012.

[100] R. Nabergoj, J. Prpić-Oršić, and M. Valčić. Sensitivity of thrust efficiency loss in dynamic positioning predictions. In *Proceedings of 2nd International Symposium on Naval Architecture and Maritime, INT-NAM 2014*, Istanbul, 2014.

[101] D.T. Nguyen. Practical experiences on the use of dnv-gl dp capability standard st-0111 and web-tool. In *Dynamic Positioning Asia 2018*, Singapore, 2018.

[102] U. Nienhuis. *Analysis of Thruster Effectivity for Dynamic Positioning and Low Speed Manoeuvring*. PhD thesis, Delft University of Technology, 1992.

[103] Nordforsk. *Assessment of Ship Performance in a Seaway: The Nordic Co-operative Project: "Seakeeping Performance of Ships"*. Norforsk, 1987.

[104] NPD. Regelverksamling for petroleumvirksamheten. Technical report, Norvegian Petroleum Directorate, 1994.

[105] OCIMF. Prediction of wind loadsand current loads on vlccs. Technical report, OCIMF, 1994.

[106] T.F. Ogilvie. Recent progress towards the understanding and prediction of ship motion. In *Proceedings of 5th Symposium on Naval Hydrodynamics*, Bergen, 1964.

[107] M.W.C. Oosterveld. *Wake Adapted Ducted Propellers*. PhD thesis, Technical University Delft, 1970.

[108] M.W.C. Oosterveld. Ducted propeller characteristics. In *Proceedings of RINA Symposium on ducted propellers*, 1973.

[109] M.W.C. Oosterveld and P. van Oossanen. Representation of propeller charachteristics suitable for preliminary design studies. In *Proceedings of Int. Conference on Computer Applications in the Automation of Shipyard Operation and Ship Design*, Tokyo, 1973.

[110] M.W.C. Oosterveld and P. van Oossanen. Further computer-analysed data of wageningen b-screw series. *International Shipbuilding Progress*, 22, 1975.

[111] H. Ottens, R. van Dijk, and G. Meskers. Benchmark study on thruster-hull interactions on a semi-submersible crane vessel. In *Proceedings of OMAE 2011 Conference*, Rotterdam, The Netherlands, 2011.

[112] G. Pahl and W. Beitz. *Engineering Design*. Springer-Verlag, New York, 1984.

[113] G. Pahl and W. Beitz. *Engineering Design: A Systematic Approach*. Springer-Verlag, London, 2nd edition, 1999.

[114] M. Palm. Influence of thruster response time on dp capability by time-domain simulations. In *Proceedings of DP Asia Conference and Exhibition*, 2018.

[115] E.E. Papmel. *Practical Design of the screw propeller*. Leningrad, 1936. in russian.

[116] S.V. Patankar. *Numerical heat transfer and fluid flow*. McGraw-Hill, New York, 1980.

[117] J.F.N. Pessoa. Investigation of depth effects on the wave exciting low frequency driftforces by different approximation methods. *Applied Ocean Research*, 42:182–199, 2013.

[118] J.W. Pierson and L.A. Moskowitz. A proposed spectral form for fully developed wind seas based on similarity theory of s.a. kitagordskii. *Journal of Geophysical Reasearch*, 69:pp. 5181–5190, 1964.

[119] J.A. Pinkster. Wave feed forward as a means to improve dynamic positiioning. In *Proceeding of Offshore Technology Conference OTC1978*, 1978.

[120] F. Quadvlieg, R. Hallmann, G. Hughes, and R. Harris. Improved dynamic positioning using wave feed forward. In *Proceedings of OMAE2011 Conference*, Rotterdam, The Netherlands, 2011.

[121] G.F.M. Remery and G. van Oortmersen. The mean wave , wind and current forces on offshore structures and their role in the design of a mooring system. In *Proceedings of the Offshore Technology Conference*, Houston, USA, 1973.

[122] C.M. Rhie and W.L. Chow. A numerical study of the turbulent flow past an isolated airfoil with trailing edge separation. *AIAA Journal*, 21:1525–1532, 1983.

[123] P.J. Roache. *Verification and Validation in Computational Science and Engineering*. Hermosa Publisher, Albuquerque, 1998.

[124] R.F. Roddy. Investigation on the stability and control characteristics of several configurations of the darpa suboff model (dtrc model 5470) for captive-model experiments. Technical Report DTRC/SHD-1298-08, DTRC, 1990.

[125] J.J. Serraris. Time-domain analysis for dp simulations. In *Proceedings of OMAE Cconference*, Honolulu, 2009.

[126] J.J. Serraris and J.L. Cozijn. Dp stationkeeping accuracy: a calculation approach, integration in dp plots and results of a case study. In *Proceedings of Dynamic Positioning Conference*, 2017.

[127] G. Shieh. Improved shrinkage estimation of squared multiple correlation coefficient and squared cross-validity coefficient. *Organizational Research Methods*, 11(2):387–407, 2008.

[128] T.C. Smith and W.G. Meyers. Smp93-pc: Standard ship motion program for personal computer with small boat capability. Technical Report AD-A282 341, Carderock Division, Naval Surface Warfare Center, June 1994.

[129] O. Smogeli, D.T. Nguyen, and L. Pivano. Dyncap - full scale validation of a vessel's station-keeping capability analysis. In *Proceedings of Dynamic Positioning Conference*, 2015.

[130] O. Smogeli, N.D. Trong, B. Borhaug, and L. Pivano. The next level dp capability analysis. In *Dynamic Positioning Conference*, 2013.

[131] O.J. Sørdalen. Optimal thrust allocation for marine vessels. *Control Engineering Practice*, 5:1223–1231, 1997.

[132] E.A. Tannuri, C.P. Pesce, G.S. Alves, I. Masetti, P.P. Ribas Ferrera, and C.H. Umeda. Dynamic positioning of a pipeline launching barge. In *Proceedings of the 12th International Offshore and Polar engineering conference*, Kitakyushu, Japan, 2002.

[133] D.W. Taylor. *The Speed and Power of Ships. Second Revision*, volume 19. U.S. Government Printing Office, Washington, 1943.

[134] P. Temarel, W. Bai, A. Bruns, Q. Derbanne, D. Dessi, S. Dhavalikar, N. Fonseca, T. Fukasawa, X. Gu, A. Nestegård, A. Papanikolaou, J. Parunov, K.H. Song, and S. Wang. Prediction of wave-induced loads on ships: Progress and challenges. *Ocean Engineering*, 119:274–308, 2016.

[135] S.L. Toxopeus. Shwg collaborative cfd exercise - bare hull darpa suboff submarine at straight flight and drift angle. Technical Report 21668-1-CPM, MARIN, 2007.

[136] S.L. Toxopeus. Viscous-flow calculations for bare hull darpa suboff submarine at incidence. *International Shipbuilding Progress*, 55(3):227–251, 2008.

[137] S.L. Toxopeus. *Practical application of viscous-flow calculations for the simulation of maneouvring ships*. PhD thesis, TU Delft, 2011.

[138] S.L. Toxopeus and S.W. Lee. Comparison of manoeuvring simulation programs for siman test cases. In *SIMMAN Workshop on Verification and Validation of ship Maneuvring Simulation Methods*, Copenhagen, Denmark, 2008.

[139] L. Troost. Open water test series with modern propeller forms, part 3: Two and five bladed propellers. *Trans. Morth East Coast Inst. of Engineers and Shipbuilders*, 67, 1951.

[140] A. Turk and J. Prpić-Oršić. The estimation methods for wind loads on marine objects. In *Proceedings of Sorta Symposium*, Opatija (Croatia), 2006.

[141] A. Turk and J. Prpić-Oršić. Estimation of extreme wind loads on marine objects. *Brodogradnja*, 60(2):147–156, 2009.

[142] M. Ueno, F. Kitamura, N. Sogihnara, and T. Fujiwara. A simple method to estimate wind loads on ships. In *Advances in Civil, Environmental and Materials Research ACEM 12*, Seul, Korea, August 2012.

[143] M. Valčić and J. Prpić-Oršić. Wind load estimation method based on elliptic fourier descriptors. In *Proceedings of the 16th International Congress of the International Maritime Association of the Mediterranean IMAM 2015*, 2015.

[144] M. Valčić, J. Prpić-Oršić, and R. Nabergoj. Impact of thruster interaction effects on optimal thrust allocation in dynamic positioning systems. In *Proceedings of XXI Symposium Sorta*, Baška, Croatia, 2014.

[145] R. van't Veer and Gachet M. Dynamic positioning- early design, capability and offsets, a novel approach. In *Proceedings of ASME 2011 30th International Conference on Ocean, Offshore and Artic Engineering OMAE 2011*, Rotterdam, The Netherlands, June 2011.

[146] H.L. Vidal, H.M. Gaspar, L. Weihmann, and L.E.B. Minioli. A parametric model for operability of offshore support vessels via configuration-based design. *Marine systems and Ocean Technology*, 10(1):47–59, March 2015.

[147] K.M. Wallace and C. Hales. Detailed analysis of an engineering design project. In *Proceedings of International Conference on Engineering Design ICED'87*, volume 1, pages 94–101. The American Society of Mechanical Engineers, 1987.

[148] L. Wang, J. Yang, and S. Xu. Dynamic positioning capability analysis for marine vessels based on a dpcap polar plot program. *China Ocean Engineering*, 32(1):90–98, 2018.

[149] Wärtsilä. *Wärtsilä Solutions for Marine and Oil & Gas Markets*, 2016.

[150] J. Wichers, S. Buitema, and R. Matten. Hydrodynamic research and optimizing dynamic positioning system of a deep water drilling vessel. In *OTC Offshore Technology Conference*, Houston, 1998.

[151] J.E.W. Wichers and R. van Dijk. Benefits of using assisted dp for deepwater mooring systems. In *Proceedings of Offshore Technology Conference*, 1999.

[152] A. M. van Wijngaarden. Upgrades and conversions of floating offshore units. In Royal Institution of Naval Architects, editor, *International Conference on ICSOT: Developments in Fixed and Floating Offshore Structures*, 2012.

[153] D.C. Wilcox. *Turbulence modeling for CFD*. DCW Industries Inc., second edition edition, 1998.

[154] S.Z. Yang, L. Wang, and P. Sun. Optimal thrust allocation logic design of dynamic positioning with pseudo-inverse method. *Journal of Shanghai Jiaotong University*, 16(1):118–123, 2011.

[155] K. Yosifov, Z. Zlatev, and A. Staneva. Optimum characteristics equations for the k-j ducted propeller design charts. In *Proceedings of International Congress on Marine Technology*, Athens (Greece), 1984.

Appendices

Appendix A

Limiting environment determination

To evaluate the capability plot of the simplified quasi-steady calculations, a methodology suitable to capture the limiting environment that the vessel is capable to face during the operation in a certain condition should be used.

The reliability of the DP system is evaluated considering three different zones:

- the vessel is in the *green zone* if the distance from the required point is not greater than 5 m and yaw angle does not exceed ± 3°. In this case the vessel maintains its position and heading;

- if the aforementioned distance is between 5 and 10 m and yaw angle is greater than ± 3° but less than ± 6°, the vessel is said to be in the *yellow zone*; the keeping of position starts being compromised;

- the *red zone* is reached when the distance is between 10 and 15 m and yaw angle exceeds ± 6° but not ± 10°, so that the vessel loses its position and heading;

- a full loss of position occurs when the red zones limits are exceeded.

By plotting and analysing the results about ship's distance from the required point and yaw angle for every environmental condition, it can be seen that those two quantities do not seem to follow any statistical distribution because their peaks are not distributed in the same way at each simulation, i.e. varying the wind speed and consequently wave height and period. In fact, Figs. A.1 and A.2 show bar chart plots where the ratio between the number of observations per bin and the total number of observations is plotted against the bin for different wind speeds, but at the same encounter angle.

171
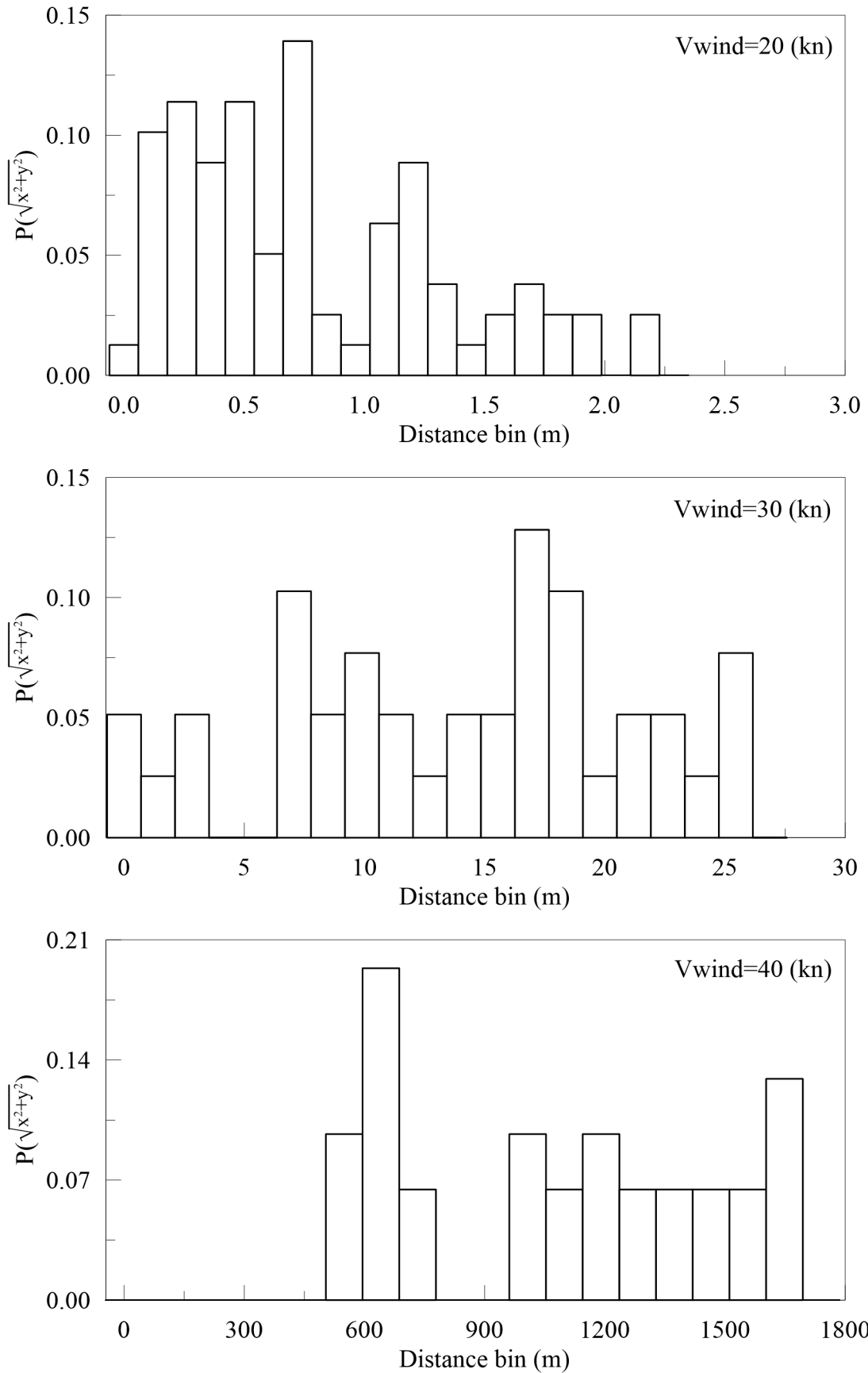
Figure A.1: Probability of distance function (χ_w=60°)[48]
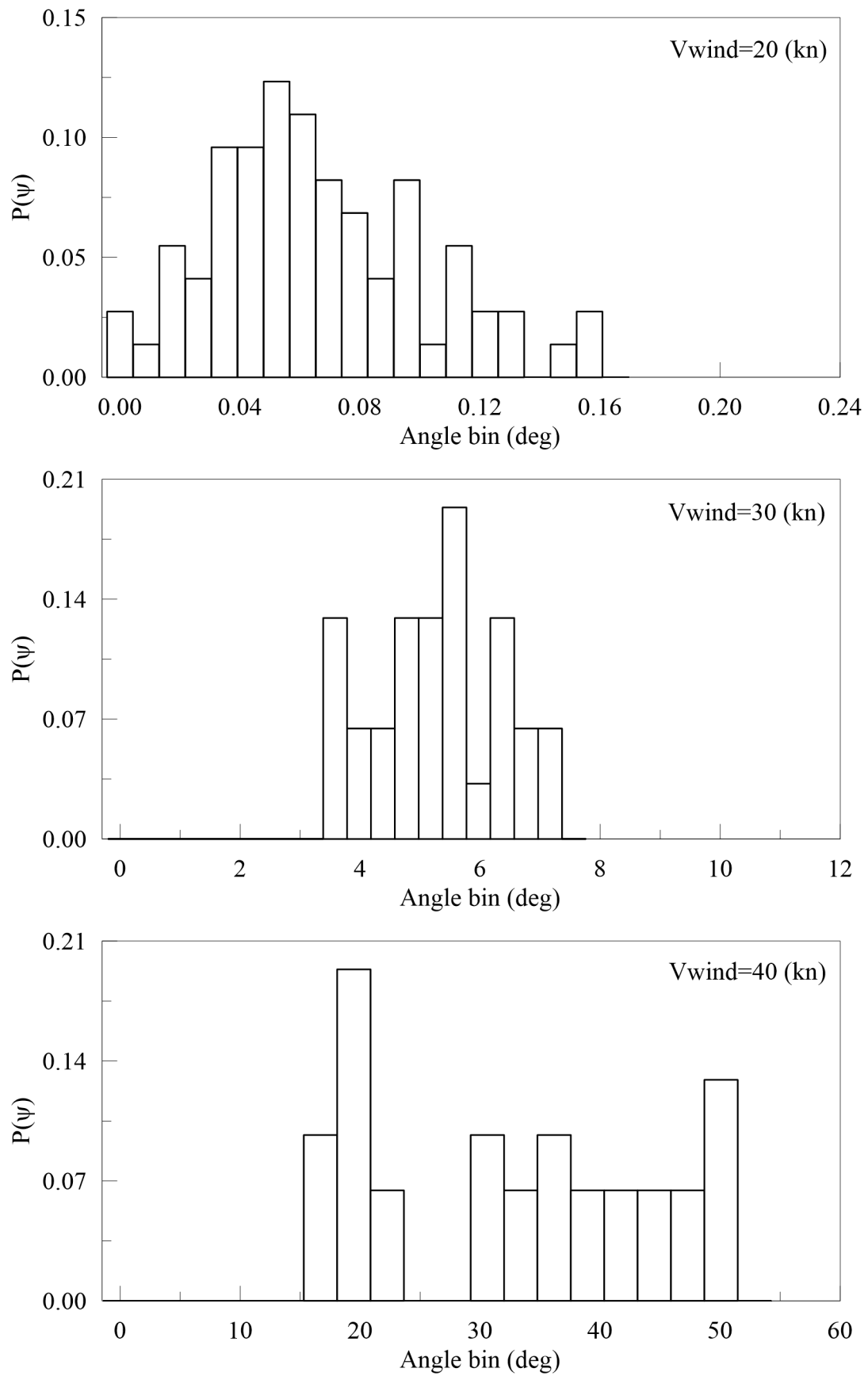
Figure A.2: Probability of yaw angle function (χ_w=60°)[48]

Therefore it is convenient to evaluate, during the 3 hours simulation, how much time the distance, or yaw angle, does not exceed each zone limit.

If the time the ship remains in the green zone is known, it can be plotted against wind speed for each encounter angle. Typically, the plot has a downward trend (Fig. A.3), so when the time in green zone reaches the 90% of the simulation time (i.e. 3 hours), the maximum sustainable wind speed can be determined for each encounter angle. This value is then representative of the maximum sustainable wind speed for the tested heading and can be represented as a point on the capability plot. With reference to the above mentioned case, the maximum wind speed that the vessel can sustain at each encounter angle is shown in Table A.1.
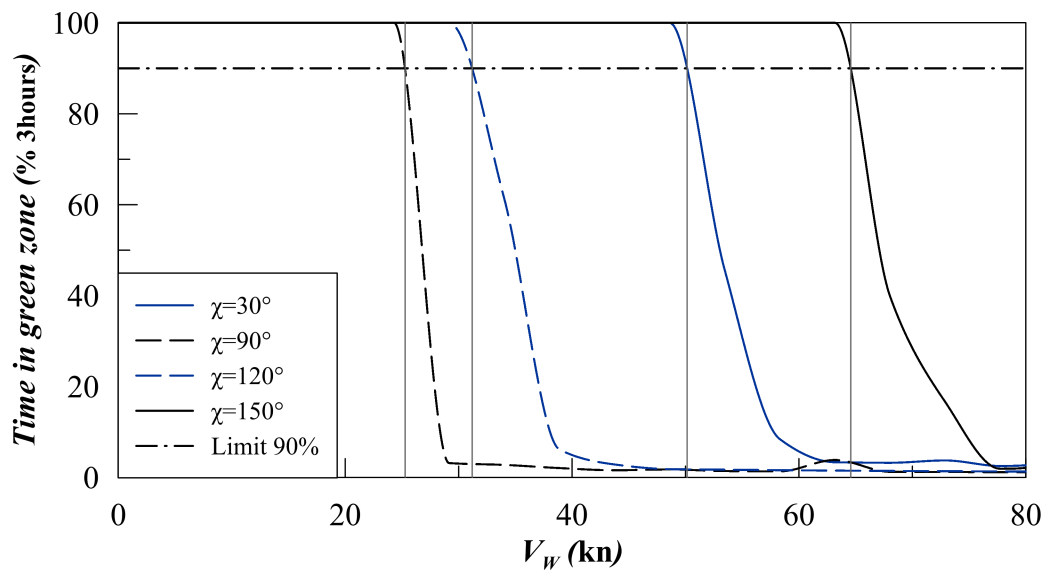
Figure A.3: Percentage of the time in green zone

Table A.1: Maximum sustainable wind speed for different encounter angles

χ_w	$V_{w_{MAX}}$
(deg)	(kn)
30	50.15
90	25.27
120	31.19
150	65.10

Appendix B

Drillship systematic series

Here the main characteristics of the systematic series of drillship developed for the current load study will be described. According to the main dimensions of the drillships composing the worldwide fleet, several indications were spotted regarding the constraints to adopt for the geometry generation.

The starting database included 40 drillships. However, since some of them are sister ships having the same main parameters, the database has been reduced to 22 ships. In Table B.1 the main characteristics of the ships are reported, together with the main parameters that can be evaluated from the main available data, means L/B, B/T and C_B.

These parameters are used to determine the variations needed to establish a suitable design space capable to cover the selected population. It must be also noted that some of the parameters in the database are somewhat suspicious, since it is not reasonable to presume that a vessel as a drillship got a C_B lower than 0.80 for operative conditions. On this purpose, those data were removed from the database, resulting in a reduced number of vessels. According to the shortened database, the following intervals have been chosen to perform the investigation:

$$5.00 \ \leq L/B \leq \ 6.80 \tag{B.1}$$

$$2.90 \ \leq B/T \leq \ 3.60 \tag{B.2}$$

$$0.83 \ \leq C_B \leq \ 0.90. \tag{B.3}$$

Based on this kind of intervals it is then necessary to properly define the parameter variations to cover the selected design space in a proper way.

Table B.1: Drillship main dimensions database

ID	L	B	T_{DES}	Δ	L/B	B/T	C_B
-	(m)	(m)	(m)	(ton)	-	-	-
1	238	42.0	11.9	104000	5.667	3.529	0.853
2	228	42.0	12.0	96273	5.429	3.500	0.817
3	228	42.0	12.0	96507	5.429	3.500	0.819
4	229	42.0	12.0	96000	5.452	3.500	0.811
5	229	42.0	12.0	96507	5.452	3.500	0.816
6	229	42.0	12.0	96000	5.452	3.500	0.811
7	230	38.0	11.0	78643	6.053	3.455	0.796
8	230	38.0	11.0	78463	6.053	3.455	0.796
9	230	38.0	11.0	77000	6.053	3.455	0.781
10	228	42.0	12.0	96000	5.429	3.500	0.815
11	230	36.0	11.0	70205	6.389	3.273	0.752
12	228	42.0	11.9	96000	5.429	3.529	0.822
13	218	42.0	12.2	90661	5.190	3.443	0.792
14	228	42.0	12.0	96000	5.429	3.500	0.815
15	228	42.0	12.2	90661	5.190	3.443	0.792
16	229	36.0	11.0	69900	6.361	3.273	0.752
17	228	42.0	12.0	97500	5.429	3.500	0.828
18	228	42.0	12.0	96142	5.429	3.500	0.816
19	238	42.0	12.0	103978	5.667	3.500	0.846
20	238	42.0	11.9	104184	5.667	3.529	0.854
21	228	42.0	11.9	87072	5.429	3.529	0.745
22	228	42.0	11.9	97978	5.429	3.529	0.839

B.1 Response surface methodology and Box-Behnken design

In recent years, Design of Experiments (DOE) has been frequently used to reduce the number of experiments that need to be executed, resulting in a lower effort for experimentation and calculation work [27]. Besides, Response Surface Methodology (RSM) also quantifies the

relationship between the controllable input parameters and the obtained response surfaces. The design procedure of RSM is as follows:

- Designing a series of experiments for adequate and reliable measurement of the analysed response.

- Developing a mathematical model of the response surface with the best fitting.

- Finding the optimal set of experimental parameters that produce the maximum or minimum value of a response.

- Representing the direct and interactive effects of process parameters through two or three dimensional plots.

When all the considered variables of the problem can be considered as measurable, the response surface can be expressed as follows:

$$y = f(x_1, x_2, x_3, \ldots, x_n) \tag{B.4}$$

where y is the output of the system and x_i are the n variables of action called factors.

It is assumed that the independent variables are continuous and controllable by experiments with negligible errors. It is required to find a suitable approximation for the true functional relationship between independent variables and the response surface. Once a second-order model is utilized using the response surface methodology, the regression model becomes:

$$y = \beta_{r_0} + \sum_{i=1}^{n} \beta_{r_i} x_i + \sum_{i=1}^{n} \beta_{r_{ii}} x_i^2 + \sum_{i=1}^{n-1} \sum_{j=2}^{n} \beta_{r_{ij}} x_i x_j + \epsilon_r \tag{B.5}$$

where β_{r_i}, $\beta_{r_{ij}}$ are unknown parameters and ϵ_r is the random error. The unknown parameters are usually determined by using the least square method. The equation (B.5) can be also written in matrix form as:

$$\mathbf{Y} = \mathbf{bX} + \epsilon_{\mathbf{r}} \tag{B.6}$$

where $\mathbf{Y}$ is defined to be the matrix of measured values, $\mathbf{X}$ to be the matrix of independent variables. The matrices $\mathbf{b}$ and $\epsilon_{\mathbf{r}}$ consist of coefficients and errors, respectively. Using the matrix formulation, the solution which defines the coefficients of the model, has the following form:

$$\mathbf{b} = (\mathbf{X}'\mathbf{X})^{-1} \mathbf{X}'\mathbf{Y} \tag{B.7}$$

where $\mathbf{X}'$ is the transpose of the matrix $\mathbf{X}$ and $(\mathbf{X}'\mathbf{X})^{-1}$ is the inverse of matrix $\mathbf{X}'\mathbf{X}$.

Between the possible available choices for applying DOE techniques, in this study Box-Behnken experimental design has been chosen for finding the relationship between the hull parameters and the current forces. Box-Behnken design [24, 23] is a rotatable second-order design based on three-level incomplete factorial designs. The special arrangement of the Box-Behnken design levels allows the number of design points to increase at the same rate as the number of polynomial coefficients. For three factors, as per the current study, the design can be constructed as three blocks of four experiments consisting of a full two-factor factorial designs with the level of the third factor set to zero.

Box-Behnken design requires a number of experiments that can be defined as per the following formula:

$$N = n^2 + n + c_p \tag{B.8}$$

where n is the number of factors and c_p is the replicate number of the central point. In general Box-Behnken is a spherical, revolving design. Viewed as a cube, it consists of a central point and the middle point of the edges. However, it can also be viewed as consisting of three interlocking 2^2 factorial design and a central point. An overview of these two possible visualizations of Box-Behnken design is given in Fig. B.1, where an example for three parameters is presented. Applying equation (B.8) for a three-level three-factorial Box-Behnken experimental design, a total of 15 experimental runs are needed. The RSM model then becomes:

$$y = \beta_{r_0} + \beta_{r_1} x_1 + \beta_{r_2} x_2 + \beta_{r_3} x_3 + \beta_{r_{11}} x_1^2 + \beta_{r_{22}} x_2^2 + \beta_{r_{33}} x_3^2 + \beta_{r_{12}} x_1 x_2 + \beta_{r_{13}} x_1 x_3 + \beta_{r_{23}} x_2 x_3$$

$$\tag{B.9}$$

In this case the β coefficients can be easily determined by applying the methodology expressed by equation (B.7).

B.2 Drillship design space

Applying the Box-Behnken design technique on the selected design variables for the drillship database, 15 different hull forms should be determined. The adopted is particularly indicated for the selected problem because it allows to reduce at minimum the number of numerical simulations that should be performed to determine the current loads on a family of vessels.
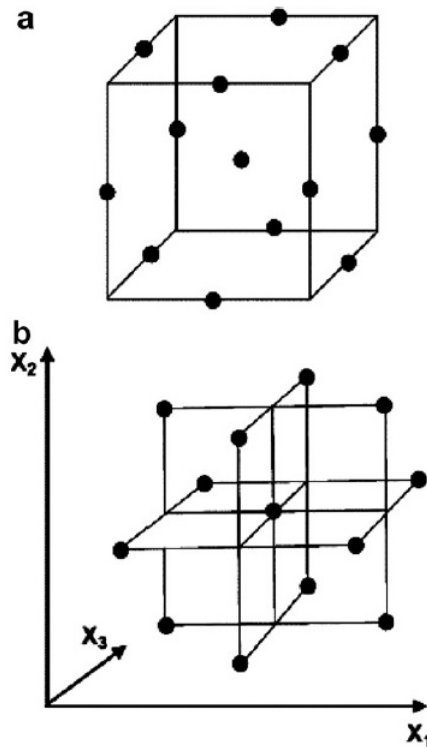
Figure B.1: Box-Behnken design viewed as a cube (a) or as representation of interlocking 2^2 factorial experiments (b) [24].

In fact, once more complicated and complete kind of DOE could be applied, then the number of experiments is always above 19. An overview of the characteristics of the 15 drillship is presented in Table B.2, where the parameters x_1, x_2 and x_3 are representatives of the relative location of the variables inside the design space. Here, the non dimensional and dimensional parameters for the drillship family are given. In the specific, the design space was chosen according to non dimensional coefficients variations. However, to determine the calculation geometry it is essential to define also the dimensional values of the reference hulls. For such a reason it is mandatory to fix at least one of the dimensional values and change all the others according to the non dimensional parameters variations.

On this purpose, the value with less variability has been chosen as fixed dimensional value, in this case the breadth B. In fact, as it can be seen in Table B.2, all the vessels have a fixed B of 42.0 metres. Then all the other main dimensions are varied accordingly.

To properly define the final geometries, other parameters should be defined, as, for example the midship coefficient C_M and the position of the longitudinal centre of buoyancy LCB. Here it has been chosen to keep those two values constant, in order to avoid effects due by the two

Table B.2: Drillship hull parameters according to Box-Behnken design

ID	x_1	x_2	x_3	L/B	B/T	C_B	L_{PP}	B	T_{DES}
-	-	-	-	-	-	-	(m)	(m)	(m)
1	-1	-1	-1	5.00	2.90	0.830	210.0	42.0	14.483
2	-1	-1	1	5.00	2.90	0.900	210.0	42.0	14.483
3	-1	1	-1	5.00	3.60	0.830	210.0	42.0	11.667
4	-1	1	1	5.00	3.60	0.900	210.0	42.0	11.667
5	1	-1	-1	6.80	2.90	0.830	285.6	42.0	14.483
6	1	-1	1	6.80	2.90	0.900	285.6	42.0	14.483
7	1	1	-1	6.80	3.60	0.830	285.6	42.0	11.667
8	1	1	1	6.80	3.60	0.900	285.6	42.0	11.667
9	-1	0	0	5.00	3.25	0.865	210.0	42.0	12.923
10	1	0	0	6.80	3.25	0.865	285.6	42.0	12.923
11	0	-1	0	5.90	2.90	0.865	247.8	42.0	14.483
12	0	1	0	5.90	3.60	0.865	247.8	42.0	11.667
13	0	0	-1	5.90	3.25	0.830	247.8	42.0	12.923
14	0	0	1	5.90	3.25	0.900	247.8	42.0	12.923
15	0	0	0	5.90	3.25	0.865	247.8	42.0	12.923

coefficients on the final forces. C_x has been selected equal to 0.98 and LCB has been set to -1.6% of L_{PP}. According to these indications, the final geometries suitable to perform CFD calculations have been developed.

Appendix C

Current loads determination with CFD computations

CFD calculations can be performed to determine forces along the hull, not only in an uniform flow oriented against vessel heading direction, but also in drift angle conditions. In such a case, the forces and moments generated on the hull by a current acting with a certain incidence angle and speed can be evaluated. There are plenty of methods available to solve the described problem; in this appendix the methods used to perform current calculations are described, together with the mesh validation study performed prior to determine current loads on the drill-ship family described in Appendix B.

C.1 Viscous flow calculations

The modelling of the viscous flow around the hull has here been performed by means of Reynolds Averaged Navier-Stokes (RANS) equations. The resolution of the governing equations of continuity and momentum in viscous flow has been carried out by means of *STAR-CCM+* solver. In this case the RANS equations have been solved with a segregated approach on algebraic multi grids [44], with the Rhie-Chow interpolation scheme for pressure-velocity coupling [122] while the control over the total solution is obtained applying the SIMPLE algorithm [116]. The reproductions of the turbulent fluctuations on the mean flow have been modelled by means of the approximation given by realizable $k - \omega$ turbulence model [153], adopting a two layer formulation solving only a single equation for k in the near wall region and determining ω algebraically as function of the wall distance.

Since the current speed is not so high to imply Froude depended phenomena, the double-body approximation has been selected, modelling only the immersed part of the hull shape. A second order scheme has been considered for the fluid convection term and for turbulence equation. In such a way the numerical diffusion inside the calculation domain is reduced, leading to more accurate estimation of the body forces.

Having selected a segregated flow approach, the implicit time step to adopt through the simulation has been selected according to specific indications given by the International Towing Tank Conference (ITTC) [66]. All the calculations have been carried out considering fresh water with density ρ_w=997.561 kg/m^3 and dynamic viscosity μ_w=$8.887 \cdot 10^{-4}$ Pa s.

C.1.1   Calculation domain

The calculations have been executed on a 3-dimensional rectangular domain representing the so-called virtual towing tank. For standard resistance calculations, the domain is considering symmetry on the vertical plane, means that only half side of vessel and tank are modelled. Once different inflow directions should be considered, this kind of simplification is no more valid and the whole vessel and tank should be modelled. This will increase the computational effort needed to perform the calculations, since the total cell number is doubled with respect to a standard resistance calculation.

A hexahedral non-structured grid has been adopted for all the simulations. Each hexahedron is generated by trimming the virtual towing tank, so the finite volume domain is generated by trimmed hexahedral cells, with proper refinements to better define the flow properties and features near the body. In the near-wall region, a prism layer mesh has been adopted in order to generate orthogonal prismatic cells in the boundary region close to the hull surface.

To make the domain discretisation easily scalable and usable for several geometries and speeds, all the geometrical mesh generation parameters have been parametrised as function of a reference length (L). Particular attention has been given to the prism layer thickness, obtained from geometrical progression of the first near-wall cell. The first-cell thickness has been determined in such a way to have a target y^+ value around 55 through all the Re tested in this study.

In each case a prism layer with a number of layers (Npl) equal to 8 and a stretching factor of 1.3 has been considered. Applying these settings it is then possible to automatically build the mesh for every considered Re. Velocity inlet boundary conditions have been adopted for the domain sides, except for the symmetry plane (in this case the Top boundary), where symmetry condition
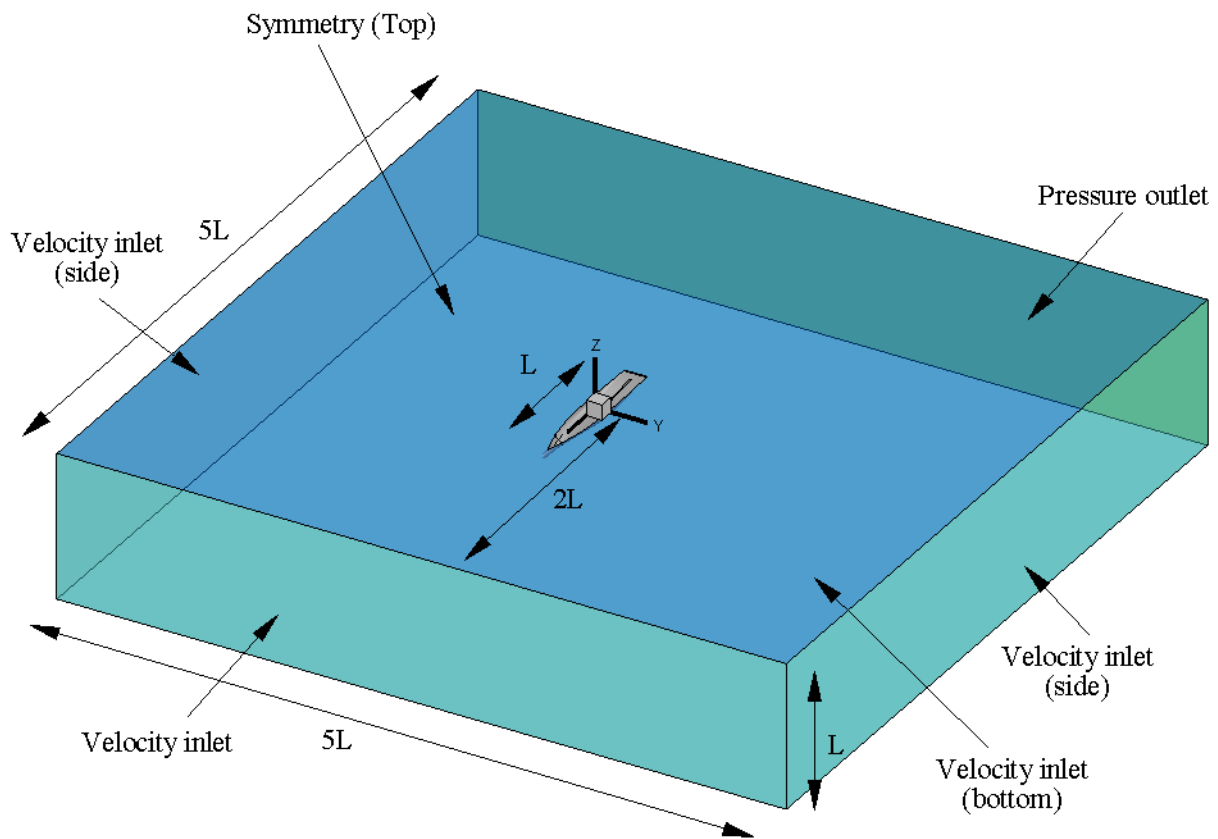
Figure C.1: Calculation domain adopted for the CFD simulations

is used, and the outlet boundary, where the pressure condition is considered. An overview of the calculation domain adopted through this study is presented in Fig. C.1, where the dimensions and the boundary conditions adopted are highlighted.

C.2 Verification and validation on standard cases

Prior to execute the calculation on the final geometries, a validation study has been carried out to study mesh independence and the total uncertainty of the forces evaluation procedure. To ensure that the calculations have a sufficient grade of accuracy, it is essential to perform this kind of study to establish the reliability of the adopted code and settings on similar geometries. Of primary importance is to determine errors and uncertainties of the total process in such a way to determine the reliability of the obtained results. Error is intended as the difference between the obtained result of the computation and the one coming from experiments. On the other hand, an uncertainty defines an interval containing the true value within a certain degree of

confidence. The numerical error (δ_{SN}) is the first focus of a validation study; this one can be divided into three different categories [123]: the round-off error, the iterative error (δ_I) and the discretisation one (δ_D). The first one is negligible with respect to the other because of the double precision nature of the calculations. Iterative error is related to equations resolution, so it can be minimized by reaching a convergence level close to machine accuracy. Reach such kind of convergence can be easy once steady flow condition are examined, however, for unsteady flow assumption this grade of convergence is hard to reach. In any case, once the convergence level between two consecutive iterations is lower than 10^{-3}, then iterative error can be considered of a lower level with respect to discretisation one, so the following assumption can be made:

$$\delta_{SN} = \delta_I + \delta_D \approx \delta_D \tag{C.1}$$

A possible way to determine δ_D is to perform a mesh independence study on similar meshes with different levels of resolution and evaluate by means of *Grid Convergence Index* (GCI) the asymptotic region of the solution with respect to the real value ϕ_0 determined by means of the Richardson extrapolation. In order to achieve the independence study it is essential to have a calculation domain parametrised, in order to capture the effect of cell dimensions on the final solution. For this reason, also all the refinement blocks have been parametrised as function of the mesh base size parameter B_S. So considering a constant refinement ratio h, starting from an initial base size value B_{S_0}, a set base sizes B_{S_i} is determined. Then it is possible to determine δ_D as follows:

$$\delta_D \approx \phi_i - \phi_0 = \epsilon_e \left(\frac{B_{S_i}}{B_{S_0}} \right)^{p_a} \tag{C.2}$$

where ϵ_e is a constant and p_a is the observed order of accuracy and:

$$B_{S_i} = \begin{cases} B_{S_0} h & \text{for } B_{S_i} < B_{S_0} \\ B_{S_0}/h & \text{for } B_{S_i} > B_{S_0} \end{cases} \tag{C.3}$$

So it is possible to analyse coarser or finer meshes compared to the starting one. Then the uncertainty (U_D) can by estimated [41] by applying a safety factor (F_s) to the obtained error:

$$U_D = F_s \left| \delta_D \right| \tag{C.4}$$

Remembering equation (C.1), then the uncertainty of the numerical simulation (U_{SN}) becomes:

$$U_{SN} = U_D + U_I \approx U_D \tag{C.5}$$

On the other hand, also the data coming from the experimental test are subjected to an error (δ_E) and a relative uncertainty (U_E). For this reason also the experimental uncertainty should be determined, but once a detailed investigation is not possible because model test are not performed by the same parties, than the assumption and guidelines given by the dedicated comities for experimental test should be used. In case of towing tank experiments U_E has been selected equal to the 2.5% of the measured value, as averaged value given by the most important hydrodynamics institutes, however once test could be autonomously performed, uncertainty can be determined in more precise way [67]. Then the total uncertainty of the process (U_P) can be determined as:

$$U_P = \sqrt{U_{SN}^2 + U_E^2} \tag{C.6}$$

Having determined the total uncertainty of the process is then possible to compare it with the comparison error δ_C. It is also possible to avoid the calculation of U_P and evaluate directly the total error of the process (δ_P) in the following form [15]:

$$\delta_P = \delta_C - (\delta_{SN} - \delta_E) \tag{C.7}$$

However through this study this second option has not be applied, and the approach based on the uncertainty determination has been adopted. To establish whether a simulation can be considered validated with respect to experimental data, the following criterion has been applied:

$$\begin{cases} |\delta_C| > U_P & \text{not validated} \\ |\delta_C| < U_P & \text{validated} \end{cases} \tag{C.8}$$

In fact when U_P is much lower than δ_C, δ_{SN} is relatively too high, means that the problem modelling should be improved. On the other hand, when δ_C is lower than the total uncertainty, the problem modelling can be considered enough accurate and the calculation can be than considered validated.

On this purpose, some preliminary studies have been carried out on standard geometries where measured data were available in the literature, with the aim to identify suitable grids to analyse the current loads.

Series 58 for submerged bodies

As mentioned, the study is oriented to calculations neglecting free surface effects, implying the adoption of a double-body method. For such a reason, at first simple geometries of fully

Table C.1: Mesh sensitivity study on 4164 geometry at $Re = 1.2 \cdot 10^7$

Grid	cells	B_S	$R_{T_{NS}}$(N)	GCI
1	3870976	0.168L	53.39	-
2	2076984	0.210L	53.40	0.043
3	1118676	0.268L	53.44	0.085
4	581647	0.328L	53.57	0.266
5	328805	0.410L	53.84	0.654
6	181380	0.513L	53.94	0.837

Table C.2: Validation study on 4164 geometry (δ_C and U_P expressed as %R_T)

Re (-)	V (m/s)	R_T (N)	$R_{T_{NS}}$ (N)	$|\delta_C|$	U_P	validated
$8.0 \cdot 10^6$	2.546	25.05	24.80	1.008	3.420	YES
$1.2 \cdot 10^7$	3.819	53.40	54.27	1.603	3.468	YES
$1.6 \cdot 10^7$	5.093	91.47	92.83	1.465	3.465	YES
$2.0 \cdot 10^7$	6.366	138.87	140.78	1.357	3.463	YES
$2.4 \cdot 10^7$	7.639	195.35	198.63	1.651	3.469	YES

submerged bodies have been studied.

In this optic, the wider submerged body database is given by 58 Series [49], collecting a wider set of geometries. Here the results inherent to 4164 model are presented [87], regarding the GCI obtained from the sensitivity study (Table C.1) and the validation along a set of Reynolds numbers (Table C.2). In these tables, the longitudinal force on the body has been calculated with numerical simulations, i.e. the total resistance $R_{T_{NS}}$. The data are compared with experimental resistance values R_T. The mesh independence study has been carried out considering a constant refinement ratio 1.25, in such a way to respect the assumption necessary to determine the GCI. As it can be noticed, the calculations are validated for all the tested Re.

However, this simple case refers to a uniform flow with no vessel heading. For such a reason it is essential to further analyse other conditions to evaluate the behaviour in case of cross-flow.

DARPA SUBOFF

An enhanced example with respect to 58 series is given by the Defense Advanced Research Project Agency (DARPA) SUBOFF submarine hull form [52, 82]. For this geometry extensive
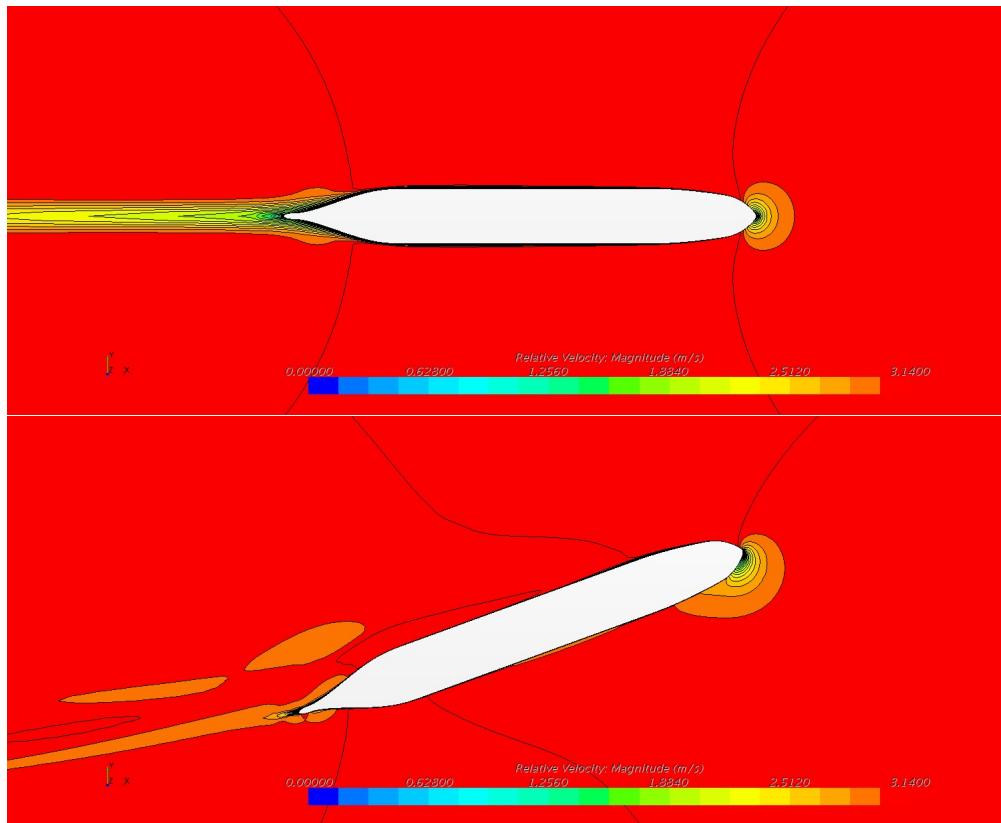
Figure C.2: DARPA SUBOFF AFF-1 velocity field at $\chi_c=0°$ (*upper*) and $\chi_c=18°$ (*lower*)

validation data is available, also for cross-flow conditions. The hull has been tested in several configurations, including different kind of appendages. Here the condition AFF-1 has been considered for the study, which is representative of a bare hull condition.

For the present case, the same initial conditions and discretisation have been used as per series 58 case. In addition, a grid study has been performed also for an incidence angle of 18 degrees, in which, of course, the whole domain is modelled. In this case a total of 4 different meshes has been studied, considering a standard refinement ratio of 1.25 between each one. In Table C.3 mesh sensitivity study is presented for the 18° case. In the table, the non dimensional forces and moments are refer to the following formulations:

$$X' = \frac{F_{x_c}}{\frac{1}{2}\rho_w L^2 V^2} \tag{C.9}$$

$$Y' = \frac{F_{y_c}}{\frac{1}{2}\rho_w L^2 V^2} \tag{C.10}$$

$$N' = \frac{M_{z_c}}{\frac{1}{2}\rho_w L^3 V^2} \tag{C.11}$$

that means the non-dimensional forces and moment are different from the coefficient used in the rest of the study, means they cannot be directly compared with data presented in Chapter

Table C.3: Mesh sensitivity study on SUBOFF AFF-1 geometry for $\chi_c=18°$

Grid	cells	B_S	$10^3 X'$	$10^3 Y'$	$10^3 N'$	GCI		
			-	-	-	X'	Y'	N'
1	7689456	0.168L	-0.7398	-7.0467	-2.9088	-	-	-
2	4234783	0.210L	-0.7437	-7.0558	-2.9123	0.242	0.127	0.052
3	2134639	0.268L	-0.7582	-7.0765	-2.9259	0.761	0.252	0.171
4	1234879	0.328L	-0.7601	-7.1098	-2.9623	0.137	0.941	0.643

3. From the data reported in Table C.3 it can be observed that mesh 2 can be adopted in order to ensure a low discretisation error for all the three considered quantities. The calculations have been performed for $Re = 1.4 \cdot 10^7$, in such a way to be comparable with experimental results provided in [124]. In Figure C.2 the velocity field at χ_c equal to 0° and 18° is presented. Here the huge differences in the flow can be observed once the body is no more aligned with the incoming flow. The validation process for $\chi_c=18°$ is represented in graphical form in Figure C.3. Considering the uncertainties levels evaluated per each of the considered quantities, it appears that the calculation can be validated for X' and N'. However, regarding the lateral force Y' the calculation is not validated, since the experimental value is outside the confidence interval, not satisfying the condition expressed by equation (C.8). The relatively excessive underestimation of Y' force, could be related to a wrong modelling of the physical problem, means that it could be possible that the turbulence model is not suitable to capture the flow behaviour when detachments occur. Another possible source of error could be the wake modelling behind the geometry. It could be possible that by considering a finer refinement in that area, a better estimation of the total forces may occur.

However, by comparing the obtained results with previous studies on the same geometry [136, 135], the accuracy level of the presented calculation is higher than the previously obtained data. This is mainly due to the adoption of a implicit unsteady approach instead of a fully steady one. Further improvements could be obtained by applying the above mentioned corrections, but all of them will led to an increased total calculation time.

Another consideration that should be stressed is regarding the experimental uncertainties. The essential differences in the total uncertainties evaluated for the present sensitivity study, is regarding the experimental value. Considering Y' and N' data, the published experimental results highlight an uncertainty of about 3% for Y' and 2.5% for N', however for X' force is
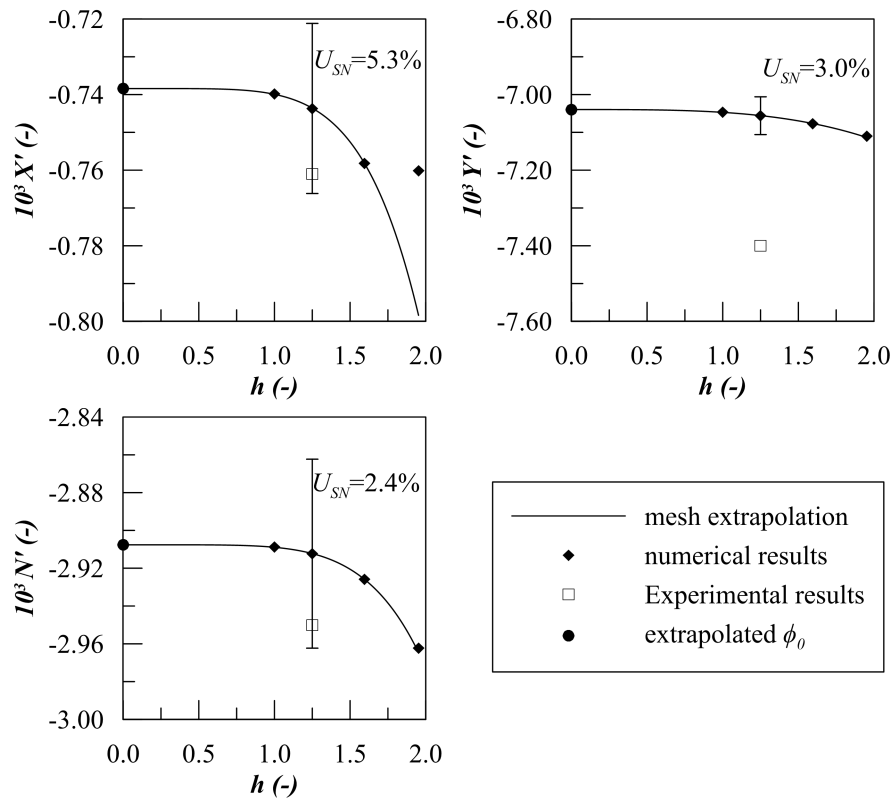
Figure C.3: DARPA SUBOFF AFF-1 mesh convergence study at $\chi_c=18°$

higher. This is quite strange, since it is reasonable that the uncertainty for the Y' force should be higher due to the non-stationary nature of the flow, with respect to X' force for such angle.

In any case, the obtained results can be considered satisfactory also for the evaluation of lateral forces on a submerged body. Further step will be the analysis of a surface vessel geometry.

KVLCC2

All the presented geometries were not representative of a surface vessel. On this purpose, the study has been extended on the KRISO Very Large Crude Carrier 2 (KVLCC2) hull form. The hull is representative of a 300000 t tanker of the 1997, fitted with a bulbous stern with U-shaped sections. This vessel has been used for a lot of reference study on ship manoeuvring, so data are available for different conditions, including cross-flow directions.

In this appendix, a sensitivity study is presented for an incidence angle $\chi_c=15°$, for a $Re = 3.27 \cdot 10^6$. Also in this case the meshes have been generated with a constant refinement ratio of 1.25 as per the previous cases. In Table C.4 the obtained data are presented, reporting te mesh dimensions and the obtained GCI. Also in this case it is possible to state that the mesh convergence is in-between grid 1 and 2, means also here the grid 2 has been selected as reference

Table C.4: Mesh sensitivity study on KVLCC2 geometry for χ_c=15°

Grid	cells	B_S	X'	Y'	N'	GCI		
			-	-	-	X'	Y'	N'
1	7823672	0.168L	-0.0160	-0.1020	-0.0301	-	-	-
2	4467021	0.210L	-0.0158	-0.1013	-0.0305	0.284	0.120	0.415
3	2321892	0.268L	-0.0145	-0.0956	-0.0325	1.527	0.791	1.705
4	1352609	0.328L	-0.0135	-0.0854	-0.0341	1.939	2.349	1.868

for the validation study.

The non-dimensional values reported in Table C.4 are different from the ones considered for the DARPA SUBOFF case. In fact, for the present application, to be compliant with the experimental data [138], the following non-dimensional coefficients are adopted:

$$X' = \frac{F_{x_c}}{\frac{1}{2}\rho_w L T_{DES} V^2} \tag{C.12}$$

$$Y' = \frac{F_{(y_c}}{\frac{1}{2}\rho_w L T_{DES} V^2} \tag{C.13}$$

$$N' = \frac{M_{z_c}}{\frac{1}{2}\rho_w L^2 T_{DES} V^2} \tag{C.14}$$

where T_{DES} is the draft and L the submerged body length. The results of the sensitivity study are presented in Figure C.4, for all three quantities related to the forces and moments in the horizontal plane. As it can be seen, in such a case all the three quantities can be considered validated for the presented χ_c angle, since the condition given by equation (C.8) is satisfied for all the cases. Also in this case the errors have been determined according to the presented procedure, however, the determination of the experimental error is still a matter of uncertainty. Compared to the studies presented in [138], here the values are validated also for Y' force, stating that the modelling can be considered satisfactory for such kind of incidence angle. A further improvements on the calculation accuracy may be introduced by modelling also the free surface, however, such kind of variation will led to a further increase of the computational effort needed to perform the calculations.

On the present geometry, calculations were carried out also at incidence angles above the standard ones tested in conventional manoeuvring benchmark tests. In Figure C.5 the pressure fields along the hull are presented for the incidence angles of 0° and 15°, being representative of a simple case without drift angle and of the case used for the mesh independence study,
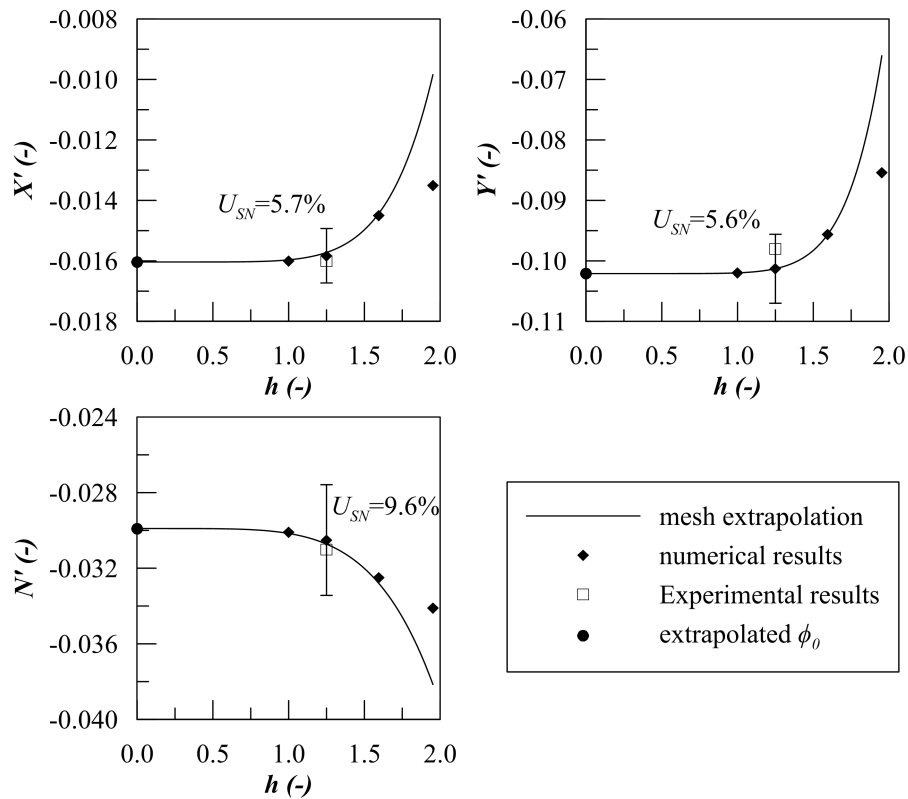
Figure C.4: KVLCC2 mesh convergence study at $\chi_c=15°$

respectively. It can be observed the strong variation of the pressure field especially in the bow and stern regions. In Fig. C.6, the pressure field is represented for a higher incidence angle ($\chi_c=60°$) and for a flow direction coming from $\chi_c=150$. These two cases cover a drift angle range outside the drift angles at which validation material is available in the literature. However, previous study performed on the same geometry by means of CFD calculations [137], highlights that the calculation results are in line with the proposed one up to an angle of 30°. In Fig. C.7 the comparison between the obtained coefficients, the previous study and the experimental ones is presented. It can be observed that the obtained values are in line with the experimental data and they have a validation level higher than the curves presented in [137]. For such a reason, it is reasonable to presume that calculations made with the presented physical modelling and meshes can be sufficiently accurate for current force estimation in early design stage.

C.3 Current loads calculations

By adopting meshes having the same refinements as per the presented validation studies, it is then possible to perform current forces calculation having a sufficient reliability level for bare
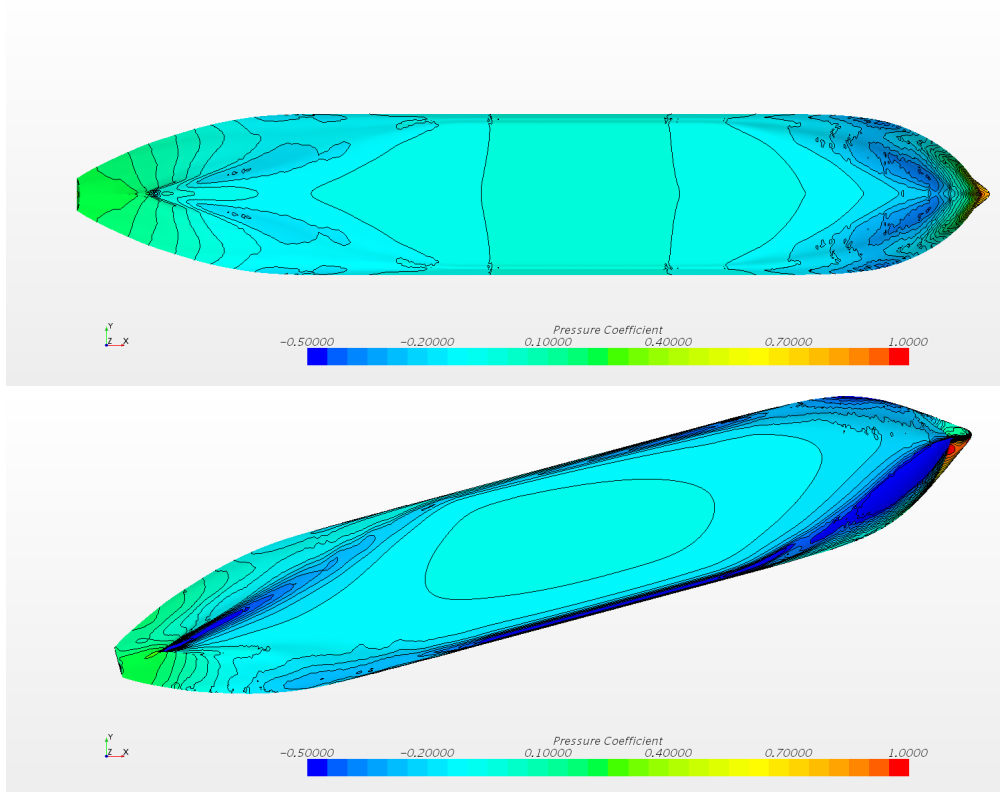
Figure C.5: KVLCC2 pressure field at χ_c=0° (*upper*) and χ_c=15° (*lower*)
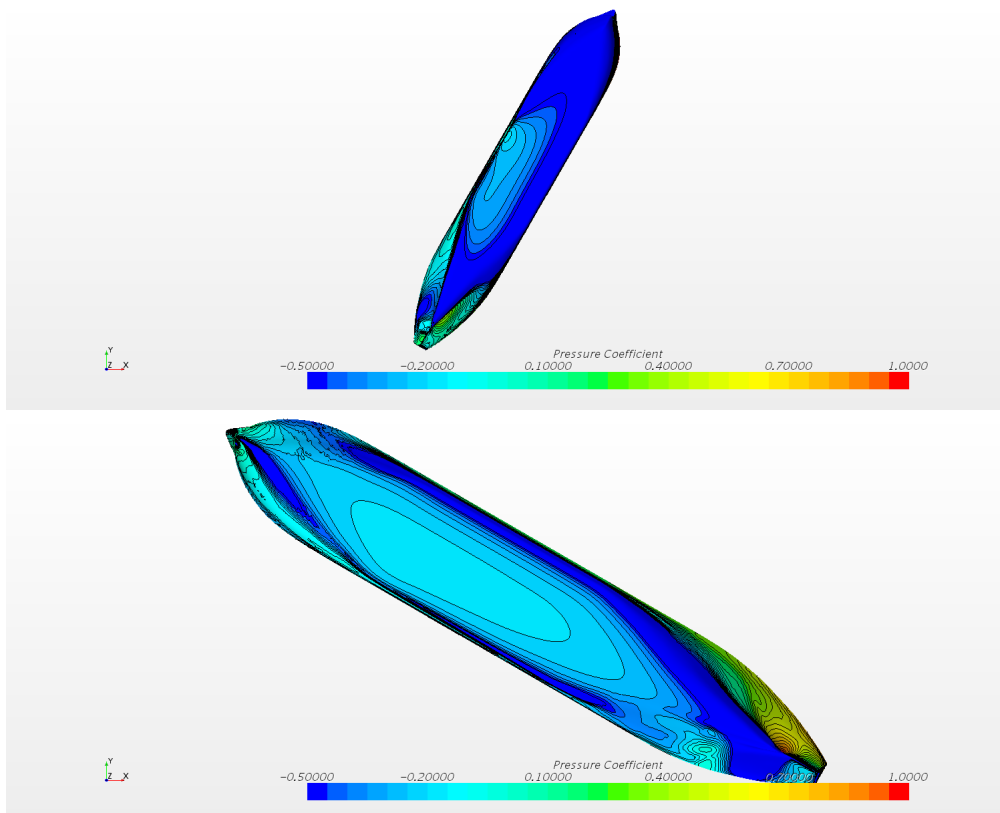
Figure C.6: KVLCC2 pressure field at χ_c=60° (*upper*) and χ_c=150° (*lower*)
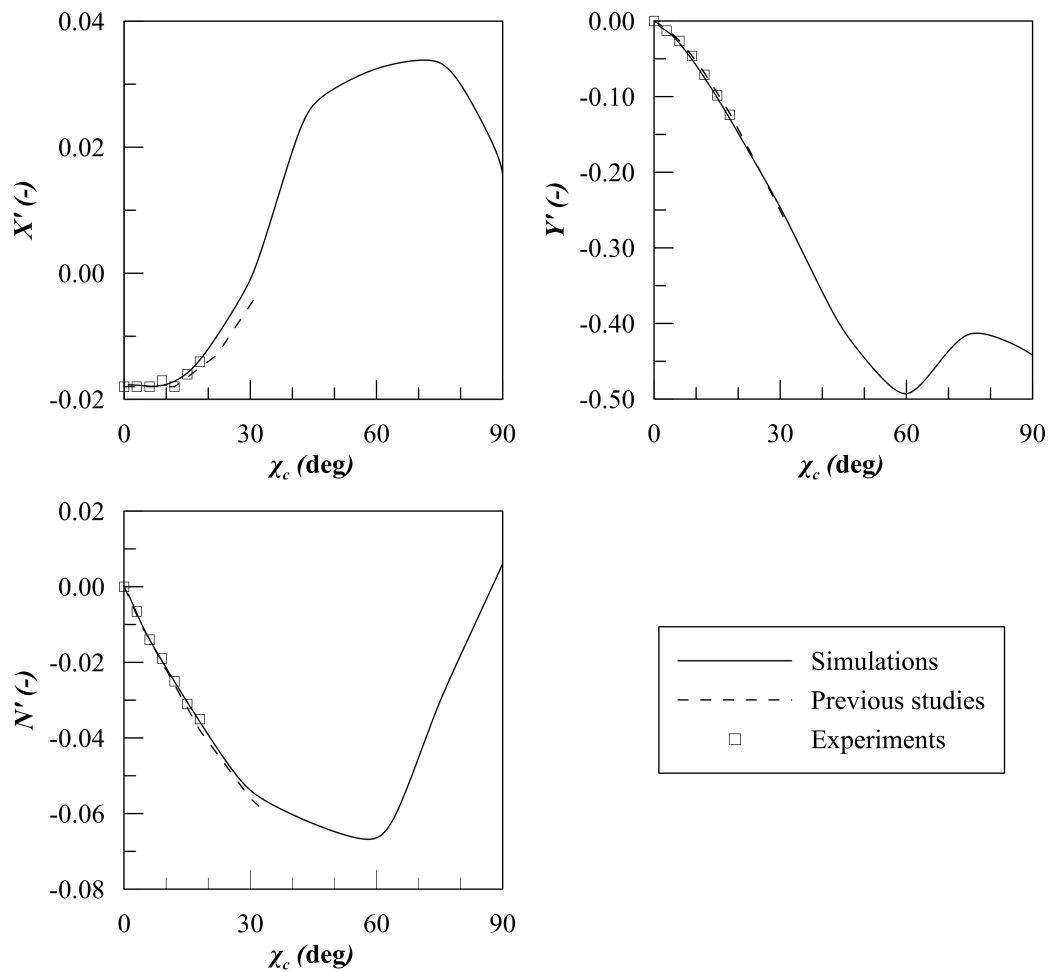
Figure C.7: Comparison of coefficients for KVLCC2 between different studies and experiments

hull geometry.

On this purpose, different hull forms have been tested, being representative of typical offshore vessels. In the specific, a drillship, a pipe-lay vessel and two supply vessels have been selected for the analysis. In this case the calculations have been performed with the same physical assumptions and mesh refinements of the KVLCC2 study. It must be also noticed that the adopted calculation geometry refers to bare-hull condition, means no appendages have been taken into account, except for the skeg fitted on the hull if present.

Since no asymmetry is present between starboard and port side of the analysed hulls, calculation have been performed from 0° and 180°. The results are presented in non-dimensional form, according to equations (C.12), (C.13) and (C.14). In Fig. C.8 the results obtained for four above mentioned vessels are reported for X' and Y' non dimensional forces and N' non dimensional moment. It can be easily observed that the coefficients have totally different trends. That means the hull shape is influencing a lot not only the magnitude of the current forces, but also their
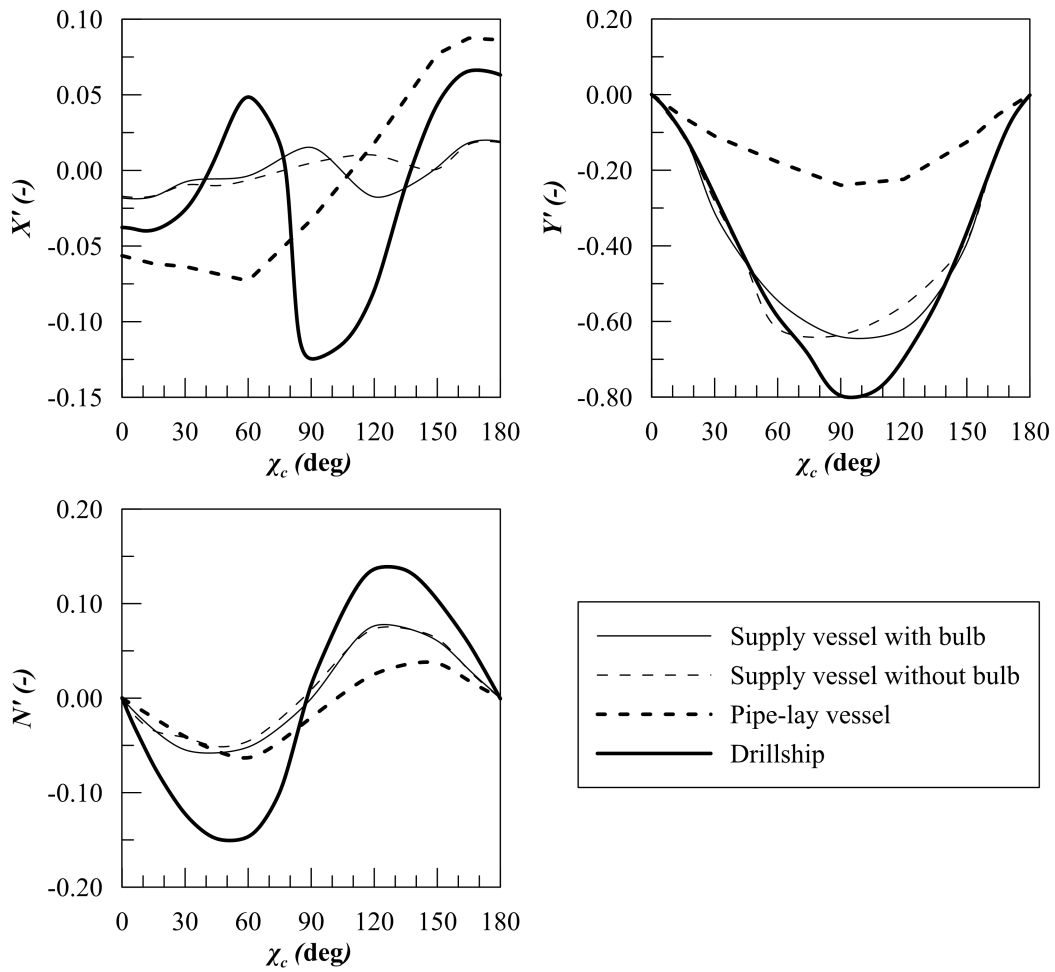
Figure C.8: Comparison between current loads on obtained by means of CFD calculations on different offshore hull types

distribution with the incoming flow angle. Compared to standard methods given by classification societies or specific associations, than it is clear that CFD calculation, done with proper validated meshes and settings, can be a suitable enhancement for the current load prediction on offshore vessel.

List of figures

List of tables

Curriculum vitae

The author was born on January 1, 1986, in Triest, Italy. After attending the secondary school from 1999 to 2004 at the "liceo scientifico", he studied naval architecture at the University of Trieste, completing in 2007 the Bachelor's (B.Sc.) Degree (experimental thesis on air cavity ships) and in 2009 the Master's (M.Sc.) Degree (thesis on dynamic positioning) with honours. After the Master degree he obtained a position at Altran consultancy company as software engineer for the development of military aircraft navigation models in collaboration with Selex Galileo Avionica (now Leonardo part of Finmeccanica Group). In 2011 he assumed a position at the Maritime Research Institute of Netherlands (MARIN) as a project manager in the ship department. Here he worked on different subjects related to hull form optimisation, full scale extrapolation procedures, added resistance in waves and marine engine simulations. Since 2015 he is employed as research fellow at the Engineering and Architecture Department of the University of Trieste, being also lecturer of Offshore Ship hydrodynamics and teaching assistant of Ship Propulsion at the Master's Degree program in Naval Architecture. His research activity covers a wide variety of subjects, from the conceptual ship design methodology to the development of simulation models for dynamic positioning of offshore vessels. Until now he authored more than 30 scientific papers published in international scientific journals and presented at international conferences. He is also supervisor and co-supervisor of more than 20 Master's and Bachelor's thesis in Naval Architecture at the University of Trieste.

List of publications

Scientific papers in peer reviewed journals

1. F. Mauro & R. Nabergoj. *Optimal thruster location on offshore DP vessels*, International Shipbuilding Progress, 66(2), 145-162, 2019.

2. F. Mauro, L. Braidotti & G. Trincas. *Determination of an optimal fleet for a CNG transportation scenario in the Mediterranean sea*, Brodogradnja 70(3) (online first), 1-23, 2019.

3. F. Mauro, L. Braidotti, U. la Monaca & R. Nabergoj. *Extreme loads determination on complex slender structures*, International Shipbuilding Progress, 66(1), 57-76, 2019.

4. C. Nasso, U. la Monaca, S. Bertagna, L. Braidotti, F. Mauro, G. Trincas, A. Marinò & V. Bucci. *Integrated design of an eco-friendly wooden passenger craft for inland navigation*, International Shipbuilding Progress, 66(1), 35-55, 2019.

5. L. Braidotti & F. Mauro. *A new calculation technique for onboard progressive floading simulations*, Ship Technology Research, 2018.

6. F. Mauro & R. Nabergoj. *An enhanced method for extreme loads analysis*, Brodogradnja 68(2), 79-92, 2017.

7. F. Mauro & R. Nabergoj. *Advantages and disadvantages of thrusters allocation procedures in preliminary dynamic positioning predictions*, Ocean Engineering 123, 96-102, 2016.

8. V. Bucci, F. Mauro & A. Marinò. *Performance prediction of a slender half-displacement passenger craft for inland navigation*, Annals of Dunarea de Jos University of Galati XI, 141-152, 2015.

Scientific papers in SCOPUS, CC, SCI and SCI-Expanded indexed Conference proceedings

1. F. Mauro, L. Braidotti & J. Prpić-Oršić. *Extreme loads estimation using genetic algorithm approach*, Proceedings of MARSTRUCT 2019, 6-8 May 2019, Dubrovnik, Croatia.

2. F. Mauro, G. Sorrenti, L. Bonfiglio & V. Bucci. *Integrated design of an eco-friendly luxury sailing super-yacht*, SNAME Maritime Convention, SMC 2018, Providence, United States, 24-27 October 2018.

3. F. Mauro, U. la Monaca, C. Nasso & V. Bucci. *An hybrid-electric solution for station-keeping and propulsion of a small coastal research vessel*, International Symposium on Power electronics, Electrical Drives, Automation and Motion SPEEDAM 2018, Amalfi, Italy, 20-22 June.

4. F. Mauro, U. la Monaca, C. Nasso & V. Bucci. *A simulation model for hybrid electric inland waterway passenger vessels*, 19th International Conference on Ship & Maritime Research NAV 2018, Trieste, Italy, 20-22 June 2018.

5. L. Braidotti, F. Mauro, L. Sebastiani, S. Bisiani & V. Bucci. *A ballast allocation technique to minimize fuel consumption*, 19th International Conference on Ship & Maritime Research NAV 2018, Trieste, Italy, 20-22 June 2018.

6. A. Bernardini, L. Cok, C. Baroni, C.M. Legittimo, A. Marinò, F. Mauro, C. Nasso & V. Bucci. *An innovative concept for inland waterway vessels*, 19th International Conference on Ship & Maritime Research NAV 2018, Trieste, Italy, 20-22 June 2018.

7. G. Scarpa, L. Braidotti, F. Mauro & G. Trincas. *The Bucintoro preliminary design: static and hydrodynamic assessment*, 19th International Conference on Ship & Maritime Research NAV 2018, Trieste, Italy, 20-22 June 2018.

8. F. Mauro, L. Braidotti & G. Trincas. *Effect of different propulsion systems on CNG ship fleet composition and economic effectiveness*, 19th International Conference on Ship & Maritime Research NAV 2018, Trieste, Italy, 20-22 June 2018.

9. F. Mauro & A. Dell'Acqua. *Vertical motions assessment of an offshore supply vessel in concept design stage*, 19th International Conference on Ship & Maritime Research NAV 2018, Trieste, Italy, 20-22 June 2018.

10. F. Mauro & F. Gaudiano. *Station-keeping in early design stage: two possible approaches*, 19th International Conference on Ship & Maritime Research NAV 2018, Trieste, Italy, 20-22 June 2018.

11. F. Mauro & M. Monacolli. *Evaluation of extreme wave loads for lender tubular structures*, 19th International Conference on Ship & Maritime Research NAV 2018, Trieste, Italy, 20-22 June 2018.

12. F. Mauro & E. Duranti. *Effect of propeller modelling on station-keeping thrust allocation strategy*, 19th International Conference on Ship & Maritime Research NAV 2018, Trieste, Italy, 20-22 June 2018.

13. G. Trincas, F. Mauro, L. Braidotti & V. Bucci. *Handling the path from concept to preliminary ship design*, Proceedngs of IMDC conference, Helsinki, Finland, 10-14 June 2018.

14. F. Mauro & R,. Nabergoj. *Determination of non-linear roll damping coefficients from model decay-test*, XXIII International Conference Engineering Mechanics EM 2016, Svratka, Czech Republic, 2017.

15. F. Mauro, P. Cerni & R. Nabergoj. *RANS calculations on submerged bodies*, XXIII International Conference Engineering Mechanics EM 2016, Svratka, Czech Republic, 2017.

16. V. Bucci, A. Marinò, F. Mauro, C. Sandron & G. Matiazzo. *Redesign of a wave energy converter in ferrocement*, XXIII International Conference Engineering Mechanics EM 2016, Svratka, Czech Republic, 2017.

17. V. Bucci, F. Mauro, A. Marinò, D. Bosich, A. Vicenzutti & G. Sulligoi. *Integrated design of a hybrid electric power system for coastal navigation multipurpose craft*, Proceedings of 12th International Conference on Ecological Vehicles and Renewable Energies EVER, 2017.

18. V. Bucci, A. Marinò & F. Mauro. *Quasi-steady determination of dynamic forces acting on tugs during escort operations*, Maritime Technology and engineering 3, 621-626, 2016.

19. V. Bucci, F. Mauro & A. Marinò. *A new concept design solution for pleasure sailing yachts*, Maritime Technology and engineering 3, 627-634, 2016.

20. V. Bucci, F. Mauro, A. Marinò, D. Bosich & G. Sulligoi. *An innovative hybrid-electric small passenger craft for sustainable mobility in the Venice lagoon*, International symposium SPEEDAM, Capri, italy, 2016.

21. V. Bucci, A. Marinò, F. Mauro, R. Nabergoj & C. Nasso. *On advanced ship evacuation analysis*, XXII International Conference Engineering Mechanics EM 2016, Svratka, Czech Republic, 2016.

22. F. Mauro & R. Nabergoj. *Extreme values calculation of multi-modal peaks distributions*, XXII International Conference Engineering Mechanics EM 2016, Svratka, Czech Republic, 2016.

23. F. Mauro & R. Nabergoj. *Integrated station-keeping and seakeeping predictions*, XVI International congress of the International Maritime Association of the Mediterranean IMAM 2015, Pula, Croatia, 2015.

24. F. Mauro & R. Nabergoj. *Smart thrust allocation procedures in early design stage dynamic positioning predictions*, XVIII International Conference on Ships and Shipping Research NAV 2015, Lecco, Italy, 2015.

Scientific papers in other peer-reviewed Conference proceedings

1. F. Mauro & R. Nabergoj. *Analysis of extreme loads with generalised Pareto distributions*, Proceedings of XII symposium Sorta, Trogir, Croatia, 2016.

2. F. Mauro, P. Cerni, I. Zotti & V. Bucci. *Numerical estimation of bare hull resistance on a sailing yacht*, Proceedings of XII symposium Sorta, Trogir, Croatia, 2016.

3. V. Bucci, A. Marinò, F. Mauro & C. Nasso. *Evacuation analysis for passenger ships: a new mandatory step for the early stage design*, Proceedings of XII symposium Sorta, Trogir, Croatia, 2016.

4. J. Dang, D. Chen, G. Dong, A. van der Ploeg, R. Hallman & F. Mauro. *An exploratory study on the working principle of energy saving devices (ESDs)*, symposium on Green Ship Technology GREENSHIP 2011, Wuxi, China, 2011.

INFORMATION ABOUT AUTHOR AND DOCTORAL THESIS

1. AUTHOR

First and last name: Francesco Mauro

Date and place of birth: January 1st, 1986., Triest, Italy

Name of the faculty, of the study and
year of completion of graduate study: Faculty of Engineering of the University of Trieste, Italy, Master's Degree in Naval Architecture, 2009.

Name of the faculty, of the module and
year of completion of postgraduate study: Faculty of Engineering of the University of Rijeka, Croatia, Design and building of ships, 2019.

Current employment: Research fellow

2. DOCTORAL THESIS

Title: Enhanced station keeping analysis in early design stage of offshore vessels

Number of pages, figures,
tables and references: 208, 90, 27, 155

Scientific area and branch: Naval Architecture, Ocean Engineering

Thesis supervisor: Prof. D.Sc. Jasna Prpić-Oršić

Place of the defense: Faculty of Engineering of the University of Rijeka, Croatia

3. DEFENCE AND EVALUATION

Date of registration of subject
of the thesis: March 26th, 2018.

Date of submission of the thesis: December 10th, 2018.

Date of the acceptance of the
evaluation of the thesis: April 27th, 2018.

Committee for the evaluation
of the thesis:
Prof. D. Sc. Roko Dejhalla
Prof. D. Sc. Nelida Črnjarić-Žic
Prof. D. Sc. Nastia Degiuli

Date of defense: July 2nd, 2019.

Committee for the defense
of the thesis:
Prof. D. Sc. Roko Dejhalla
Prof. D. Sc. Nelida Črnjarić-Žic
Prof. D. Sc. Nastia Degiuli

Degree conferred: _____